

TARGETED THERAPIES FOR MALIGNANT GLIOMAS:  
NOVEL AGENTS, SAME BARRIER

Fan Lin

The research described in this thesis was performed from January 2009 – January 2013 at the Division of Diagnostic Oncology, The Netherlands Cancer Institute/Antoni van Leeuwenhoek Hospital, Plesmanlaan 121, 1066CX Amsterdam, the Netherlands.

ISBN: 978-90-8891-582-6

Cover design: Jiyeon Kang  
Printed & Lay Out by: Proefschriftmaken.nl | | Uitgeverij BOXPress  
Published by: Uitgeverij BOXPress, 's-Hertogenbosch

Copyright © 2013 by Fan Lin, Amsterdam

Printing of this thesis was financial supported by the Netherlands Cancer Institute, Utrecht Institute for Pharmaceutical Sciences (UIPS) and to-BBB technologies BV.

# TARGETED THERAPIES FOR MALIGNANT GLIOMAS: NOVEL AGENTS, SAME BARRIER

Doelgerichte therapieën voor maligne gliomen:  
Nieuwe therapeutica, dezelfde barrière  
(met een samenvatting in het Nederlands)

Proefschrift

ter verkrijging van de graad van doctor aan de Universiteit Utrecht  
op gezag van de rector magnificus, prof.dr. G.J. van der Zwaan,  
ingevolge het besluit van het college voor promoties  
in het openbaar te verdedigen op vrijdag 1 maart 2013  
des middags te 2.30 uur

door Fan Lin  
geboren op 28 juni 1978 te Huzhou, China

Promotor: Prof. Dr. J.H.Beijnen

Co-promotor: Dr. O.van.Tellingen

Live, then, and be happy..., and never forget that  
until the day when God shall deign to reveal the  
future to man, all human wisdom is summed up  
in these two words, – ‘Wait and hope.’

‘The Count of Monte Cristo’ (1844)  
by Alexandre Dumas



# TABLE OF CONTENTS

## **CHAPTER 1: INTRODUCTION**

- 1.1 Targeting core (mutated) pathways of high-grade gliomas: challenges of intrinsic resistance and drug efflux transporters 11

## **CHAPTER 2: ANALYTIC ASSAYS FOR TARGETED THERAPEUTICS**

- 2.1 High-Performance Liquid Chromatography analysis of a novel small-molecule, anti-cancer drug, Palomid 529, in human and mouse plasma and in mouse tissue homogenates 47

- 2.2 Determination of NVP-BEZ235, a dual PI3K and mTOR inhibitor, in human and mouse plasma and in mouse tissue homogenates by reversed-phase high-performance liquid chromatography with fluorescence detection 67

## **CHAPTER 3: PHARMACOKINETICS AND THERAPEUTIC EFFECTS OF TARGETED THERAPIES IN MALIGNANT GLIOMAS**

- 3.1 Dual mTORC1 and mTORC2 inhibitor Palomid 529 penetrates the Blood-Brain Barrier without restriction by ABCB1 and ABCG2 89

- 3.2 High-grade glioma mouse models identify ABCB1, ABCG2 and PTEN as important factors for response to temozolomide and ABT-888 combination therapy 115

- 3.3 Optimizing the efficacy of PI3K/mTOR inhibitors against High-grade gliomas by selecting Blood-Brain Barrier permeable drugs 143

## **CHAPTER 4: COOPERATIVE BRAIN EFFLUX BY MULTIPLE DRUG EFFLUX TRANSPORTERS**

4.1 Abcc4 together with Abcb1 and Abcg2 form a robust co-operative drug efflux system that restricts the brain entry of camptothecin analogs	171
4.2 Sildenafil is not a useful modulator of ABCB1 and ABCG2 mediated drug resistance <i>in vivo</i>	197

## **CHAPTER 5**

Summary	212
Nederlandstalige samenvatting	217
List of publications	223
Curriculum Vitae	225
Acknowledgement	227



# CHAPTER 1

## INTRODUCTION



# Chapter 1.1

Targeting Core (Mutated) Pathways of High-grade Gliomas:  
Challenges of Intrinsic Resistance and Drug Efflux Transporters

Fan Lin, Mark C. De Gooijer, Diana Hanekamp, Dieta Brandsma, Jos H. Beijnen,  
Olaf Van Tellingen

Submitted for publication.

## ABSTRACT

High-grade gliomas are the most common type of primary brain tumors and are among the most lethal types of human cancers. Most patients with a high-grade glioma have a glioblastoma multiforme (GBM), the most malignant glioma subtype that is associated with a very aggressive course and short overall survival. Standard treatment of newly diagnosed GBM involves surgery followed by chemoradiation with temozolomide. However, despite this extensive treatment the mean overall survival is still only 14.6 months and more effective treatments are urgently needed. Although different types of GBMs are indistinguishable by histopathology, novel molecular pathological techniques allow the discrimination between four main GBM subtypes. Targeting the aberrations in the molecular pathways underlying these subtypes holds promise for improved therapies. Here, we will discuss the potential avenues and pitfalls of molecular targeted therapies for treatment of GBM.

## INTRODUCTION

High-grade gliomas are the most common type of primary brain tumors and are among the most lethal types of human cancers <sup>(1)</sup>. High-grade gliomas are classified by the World Health Organization (WHO) in grade III: anaplastic astrocytoma, anaplastic oligodendroglioma, and anaplastic oligoastrocytoma; and grade IV: gliosarcoma and glioblastoma multiforme (GBM) <sup>(2)</sup>. Unfortunately, the majority of high-grade glioma patients are diagnosed with GBM, the most malignant subtype that is associated with a very aggressive course and less than 3 months overall survival if left untreated <sup>(2)</sup>. Standard treatment of newly diagnosed GBM includes surgery, followed by radiotherapy (30x2 Gy) plus temozolomide (75 mg/m<sup>2</sup>, daily) for 6 weeks and adjuvant temozolomide courses (150-200 mg/m<sup>2</sup>, 5/28 days) during 6 months. However, despite this extensive treatment the mean overall survival is still only 14.6 months <sup>(3)</sup> and more effective treatments are thus urgently needed.

In contrast to conventional chemotherapies that work by interfering with DNA synthesis or cell metabolism, targeted therapies work by inhibition of the deregulated cell signaling pathways in cancer cells by small molecules or antibodies. The underlying concept is that these signaling pathways are more critical for survival and growth of cancer cells than for normal cells. Consequently, targeted therapy holds the promise of being effective with less toxicity than conventional chemotherapies. Despite the emerging success in some other tumor types; e.g. imatinib for chronic myelogenous leukemia <sup>(4)</sup> or vemurafenib in melanoma <sup>(5)</sup>, the development of molecular targeted therapy for gliomas appear to be extra challenging. Two small molecule inhibitors of epidermal growth factor receptor (EGFR) tyrosine kinase that received regulatory approval for the treatment of lung cancer, erlotinib (Tarceva<sup>®</sup>, OSI-774, Genentech, Inc, CA, USA) and gefitinib (Iressa<sup>®</sup>, ZD1839, AstraZeneca, DE, USA), have extensively been evaluated for GBM treatment with high expectations, since EGFR overexpression and EGFR mutations are common in GBM. The results of the first Phase I studies with erlotinib were exciting <sup>(6,7)</sup> and a phase II, a single institution study showed that erlotinib plus temozolomide before and after radiation significantly increased median survival of GBM patients to 19.3 months in comparison of 14.1 months in historical controls <sup>(8)</sup>. However, results of subsequent clinical trials with EGFR-inhibitors were all disappointing <sup>(9,10,11,12,13,14)</sup>. In particular, a randomised controlled phase II study carried out by the European Organisation for Research and Treatment of

Cancer (EORTC) demonstrated no clear benefit in progressive GBM patients treated with erlotinib compared to a control group receiving temozolomide or carmustine <sup>(10)</sup>.

The failures of targeted therapy in the treatment of GBM are not limited to EGFR inhibitors. Inhibitors of the mammalian target of rapamycin (mTOR) have also been regarded as a promising target for GBM as the frequently deregulated PI3K-AKT-mTOR signaling is considered to be a key mediator of GBM cell survival and growth. Rapamycin (sirolimus) and its analogues (rapalogs) temsirolimus (CCI-779) and everolimus (RAD001) are the three mTOR inhibitors that have undergone extensive clinical evaluation for their therapeutic effect in GBMs <sup>(15,16,17,18,19,20,21,22)</sup>. Similar to the EGFR inhibitors, most trials with mTOR inhibitors as a single agent in GBM, have failed to show any significant therapeutic benefit.

Despite these disappointing results, important lessons have been learned from translational studies with these agents. This review will focus on the recent development of targeted therapies on the core mutated pathways of GBM. Moreover several major putative resistance mechanisms of GBM to the earlier studied targeted therapies will be discussed.

# GENETIC ALTERATIONS AND CLASSIFICATION OF GBM

The majority of patients with GBM suffer from primary (or *de novo*) GBM. In comparison with secondary GBM that evolve from low-graded gliomas, primary GBM usually develops without pre-existing precursor lesions. Primary and secondary GBMs are histopathologically indistinguishable and are characterized by a high proliferative index, serpentine pseudopallisading necrosis and microvascular proliferation. Nevertheless, primary and secondary GBM are associated with differences in age of onset, clinical history, median survival and genetic changes (Table 1).

Primary and secondary GBMs develop as a result of multiple genetic alterations. that are distinct between the two types of GBM. Secondary GBM is more frequently a result of an early mutation of P53, whereas primary GBM much more often harbors mutations in the EGFR (Epidermal Growth Factor Receptor) gene, deletions within the CDKN2 (Cyclin-Dependent Kinase Inhibitor 2) locus that codes for p14<sup>Arf</sup>, p16<sup>Ink4a</sup> and p15<sup>Ink4b</sup> and a homozygous loss of chromosome 10q23, which houses the phosphatase and tensin homolog (PTEN) gene. Overall, loss of chromosome 10q, EGFR amplification and deletion of p16<sup>Ink4a</sup> have shown to be the most frequent genetic alterations in primary GBM <sup>(1,23,24,25,26)</sup>.

## The Cancer Genome Atlas project in GBMs

By implementation of large-scale multi-dimensional analytic platforms, a comprehensive characterization of the molecular basis of malignant gliomas recently became available. The Cancer Genome Atlas (TCGA) is a project aimed to catalogue genetic mutations responsible for cancer. In 2008, TCGA published the results of their first cancer project on the analysis of genomic abnormalities in human GBM (mostly primary GBM) <sup>(27)</sup>. This work not only confirmed the common genetic aberrations reported previously, but also provided new insight into the roles of some known tumor related genes as ERBB2/HER2 (Human Epidermal Growth Factor Receptor 2), NF1 (Neurofibromin 1) and P53, and uncovered new mutations. More importantly, it provided a network view of the pathways altered in the development of GBM which can be instructive for future therapeutic decisions and facilitate the searching for more efficacious targeted therapies. As shown in Fig. 1, frequent genetic alterations of GBM occur in three core pathways:

SUBTYPE	INCIDENCE	ORIGIN	ALTERATIONS	CLINICAL HISTORY	MEDIAN OVERALL SURVIVAL*
Classic classification	Primary or de novo GBM	95%;	LOH 10q (70%) EGFR Amplification (36%) P16INK4a Deletion (31%) TP53 Mutation (28%) PTEN Mutation (25%)	<3 months:68% <6 months 84%	4.7 months
	Secondary GBM	5%	LOH 10q (63%) EGFR Amplification (8%) P16INK4a Deletion (19%) TP53 Mutation (65%) PTEN Mutation (4%)	Low-grade astrocytoma origin: 5.1 years; Anaplastic astrocytoma: 1.9 years.	7.8 months
SUBTYPE	BIOMARKER	SIGNATURE	MAJOR ALTERATIONS	TREATMENT RESPONSE**	
TCGA classification	Classical	Neuro embryonic stemcell	Astrocytic	EGFR, CDKN2A/2B, PTEN	Good
	Mesenchymal	Mesenchymal markers	astroglial	NF1, PTEN, CHI3L1, MET	Modest
	Proneural	Oligodendrocytic development genes	Oligodendrocytic	TP53, PDGFRA or PI3KCA/PIK3RI, IDH1, PTEN	Poor or no response
	Neural	Neural markers	Neuronal and astrocytic	EGFR	Marginal

**Table 1.** The classic classification and the TCGA genomic classification of GBM. The classic classification includes primary and secondary GBM, distinguished by their lesion of origin whereas the TCGA classification includes four clinically relevant subtypes based on the genomic profiles of GBMs and their correlations with biomarker expression, cellular lineages, and response to standard chemoradiation.

\* median overall survival without treatment. \*\* Aggressive chemoradiation therapy



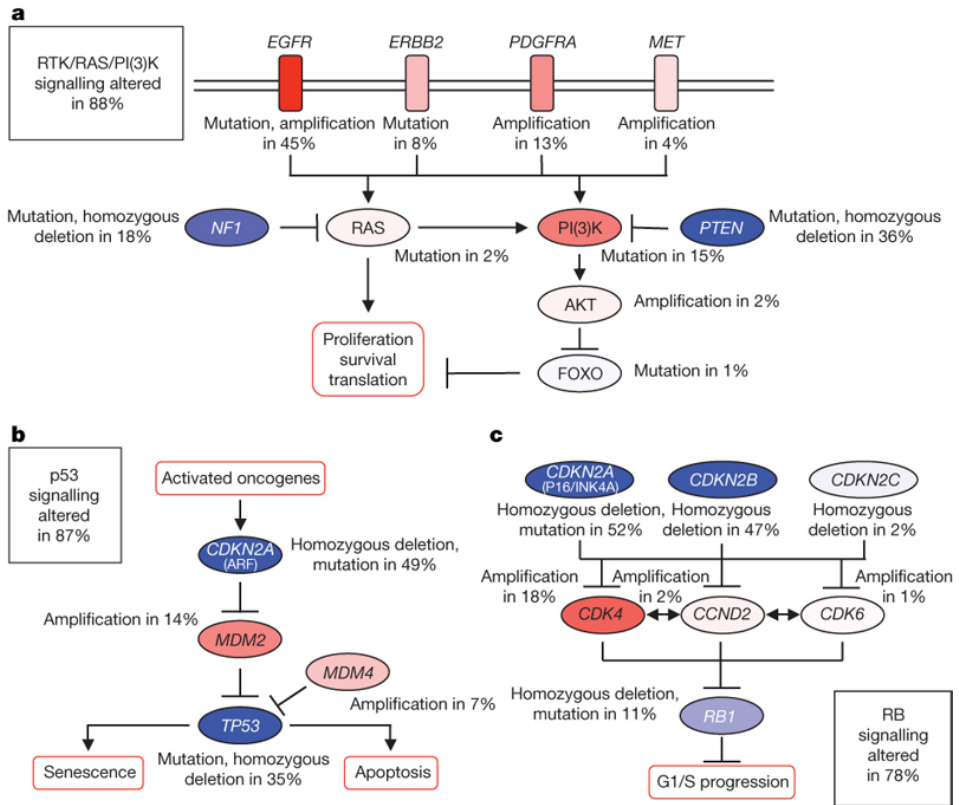


**Fig. 1.** Primary sequence alterations and significant copy number changes for components of the RTK/RAS/PI3K (a), P53 (b) and RB (c) signaling pathways are shown. Red indicates activating genetic alterations, with frequently altered genes showing deeper shades of red. Conversely, blue indicates inactivating alterations, with darker shades corresponding to a higher percentage of alteration. For each altered component of a particular pathway, the nature of the alteration and the percentage of tumors affected are indicated. Boxes contain the final percentages of GBMs with alterations in at least one known component gene of the designated pathway. Adopted from the TCGA publication <sup>(27)</sup>.

RTK/RAS/PI3K signaling and P53 and RB tumor suppressor pathway were mapped based on genetic analyses of 206 GBM samples.

Another important outcome of TCGA is the molecular classification of GBM <sup>(28)</sup>. Four GBM subtypes: proneural, neural, classical, and mesenchymal subtypes described in this study showed strong correlations with GBM cells of origin, clinical characteristics,

and response to standard chemoradiation. For example, the proneural subtype was associated with younger age and IDH1 (Isocitrate dehydrogenase 1) and P53 mutations, with a trend to longer survival for these patients. Intriguingly, however, patients with proneural type GBM did not have an improved survival when receiving aggressive treatment. On the contrary, the classical subtype GBM usually harboring EGFR amplification and homozygous deletion of the CDKN2 and PTEN had the greatest benefit from standard treatment among all subtypes (Table 1). Given the fact that each subtype harbors specific aberrations in molecular pathways, one may expect that targeting these pathways by specific inhibitors may provide new avenues for improved therapies.

## BLOOD-BRAIN BARRIER AND DRUG EFFLUX TRANSPORTERS

The brain is often referred to as a pharmacological sanctuary site since most drugs are unable to cross the Blood-Brain Barrier (BBB) <sup>(29,30,31)</sup>. The BBB represents one of the major challenges to the chemotherapy efficacy against GBM. The BBB is formed by endothelial cells that are closely linked by tight junctions disabling the paracellular movement of substances. Moreover, in contrast to most endothelial cells elsewhere in the body they lack fenestrae and have low endocytic activity. Consequently, entry of substances into the brain can only occur by transcellular passage of the endothelium. Moreover, the pericytes and astrocytes intimately surrounding the endothelial cells form a secondary lipid layer, which further enforces the impermeability of the BBB <sup>(32)</sup>. Entry of essential nutrients (e.g. glucose) is strictly regulated by a range of uptake transporters. Other substances can only enter the brain by passive diffusion across the BBB, and the ability to do so is determined by a series of molecular parameters such as sufficient lipid solubility (octanol:water partition coefficient), molecular weight, degree of ionization, plasma protein binding and tissue binding. Nevertheless, even compounds that comply with molecular characteristics in favor of passive diffusion demonstrate a much lower brain penetration than expected <sup>(31)</sup>, due to the activity of drug efflux transporters.

### **Drug efflux transporters**

ATP-binding cassette (ABC) drug transporters expressed at the BBB have well-known roles in the restriction of therapeutic agents into the brain <sup>(33)</sup>. Of all efflux transporters present in the BBB, two transporters are in particular responsible for the efflux of anticancer agents back into the blood capillaries. These proteins are ABCB1 (ATP-Binding Cassette transporter protein B1) and ABCG2 (ATP-Binding Cassette transporter G2) (see Fig. 2B).

### **ABCB1**

ABCB1 (also named Permeability-glycoprotein, P-gp, or Multidrug Resistance transporter protein 1, MDR1) is a 170-kDa membrane associated protein, expressed at high levels in normal human tissues, including the brain capillaries (see Fig. 2C). It was first discovered by its ability to confer multidrug resistance in cultured tumor cells <sup>(34)</sup>. ABCB1 is a highly

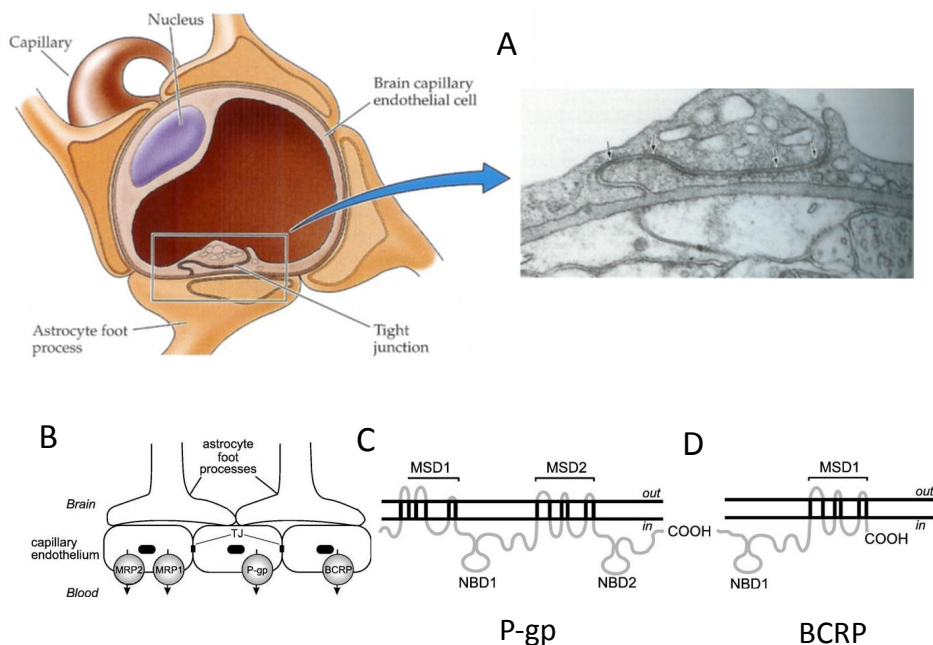


**Fig. 2.** Schematic and histological representation of the BBB and ABC drug efflux transporters at BBB (A and B). Arrows indicate tight junctions. Adopted from Purves *et al* <sup>(111)</sup>. C and D: Schematic representation of the secondary structures of respectively P-gp and BCRP. TJ = Tight Junction; MRP = Multidrug Resistance Protein. MSD = Membrane Spanning Domain; NBD, = Nucleotide Binding Domain. Adopted from Leslie *et al* <sup>(35)</sup>.

promiscuous transporter, recognizing an amazing range of drugs. Like all members of the ATP-binding cassette transporter superfamily, the energy for active transport of compound is provided by hydrolysis of ATP at the Nucleotide Binding Domains (NBDs) <sup>(35,31)</sup>.

Besides affecting cellular drug accumulation in tumor cells, ABC drug efflux transporters also actively affect the drug disposition by its expression at various barrier sites (BBB, intestinal epithelium. blood-testis barrier) <sup>(36,37,38,39,40)</sup>. ABCB1 was the first drug efflux transporter showing a remarkable impact on the brain delivery of substrate agents. Mice have two genes that are equivalent to ABCB1, namely *Abcb1a* and *Abcb1b* and. *Abcb1a* is the subtype that is expressed in the BBB and *Abcb1a* deficient mice demonstrate a dramatic sensitivity to the neurotoxic pesticide ivermectin and to the cytotoxic drug

vinblastine <sup>(41)</sup>. The role of ABCB1/Abcb1a in limiting drug brain penetration has been extended to a plethora of agents, including many novel targeted agents.

### **ABCG2**

ABCG2 (murine subtype *Abcg2*), also known as BCRP (Breast Cancer Resistance Protein) is a 72-kDa ABC transporter. Similar to ABCB1, it plays an important role in drug disposition and distribution in the body (Fig. 2D). ABCG2 is expressed in many tissues of the body including the apical side of the intestinal lumen, the bile canaliculus in liver hepatocytes, and the capillaries of the BBB. ABCG2 also transports a broad range of endogenous and exogenous compounds <sup>(31,35)</sup>. However, pharmacokinetic studies using *Abcg2* knockout mice showed little effect on the brain penetration of drugs, with a few exceptions, such as sorafenib <sup>(42)</sup>. The reason is that most drugs are substrates of both ABC transporters and the brain accumulation of these substances is limited by *Abcb1* that is still present in *Abcg2* knockout mice. The absence of both *Abcb1* and *Abcg2*, however, results in a profound increase in brain uptake compared with the absence of each transporter alone. Due to the extremely broad substrate specificities of these two transporters, the concerted action of ABCB1 and ABCG2 is not restricted to only a few drugs, but represents a common mechanism to limit the brain entry of many drugs and thus potentially conferring resistance to chemotherapies of brain tumors <sup>(43,44,45,46,47,48,49)</sup>. Other drug efflux transporters at the BBB, such as the Multidrug Resistance-associated Proteins (MRPs) may also contribute to this drug co-efflux system.

## TARGETING EGFR AND LESSONS LEARNED FROM ERLOTINIB TRIALS IN GBM

The EGFR (ERBB1) is a member of the ErbB family of trans-membrane receptor tyrosin kinases (RTK) and binds to at least six different ligands, including EGF (Epidermal Growth Factor) and TGF- $\alpha$  (Transforming Growth Factor- $\alpha$ ). After binding of a ligand, dimerization of EGFR takes place and the complex is activated and recruits phosphatidylinositol 3-kinase (PI3K). This activates the PI3K-AKT-mTOR pathway transducing a proliferation signal to the cell. In tumor cells EGFR amplification is often present as small fragments of extrachromosomal DNA (double minutes) and is often associated with structural mutations in the EGFR gene, of which several variants have been identified. EGFRvIII or  $\Delta$ EGFR is the most commonly occurring mutation in GBM derived by a non-random 801 bp in-frame deletion of exons 2-7, and codes for a truncated and constitutively activated protein<sup>(50,51,52)</sup>. Overall, EGFRvIII expression in the presence of EGFR amplification plays an important role in enhanced tumorigenicity and indicates a poor survival prognosis in GBM patients<sup>(53)</sup>.

Although EGFR amplification and mutation is considered to be an important factor, none of the currently tested EGFR inhibitors has shown any clinical efficacy against GBM. The contrast between the more successful application of EGFR inhibitors in other types of cancer such as lung cancer, and the failure in GBM has been extensively studied. These studies suggest that the lack of response to EGFR-inhibitors in GBM is multifactorial. A first issue is related to the drug delivery: *i.e.* can a therapeutic level of erlotinib be reached in the glioma tissue? Erlotinib is a substrate of both ABCB1 and ABCG2, and the two drug efflux transporters together resulted in a 7-fold reduction of brain-plasma ratio in wild-type compared to Abcb1;Abcg2 knockout mice<sup>(54,55)</sup>. Thus, the limited BBB penetration of erlotinib caused by ABCB1 and ABCG2 may at least be partly responsible for the resistance of GBM to erlotinib treatment. Unfortunately, the bare fact is that ABCB1 and ABCG2 have a long list of overlapping substrates, including most EGFR/tyrosin kinase inhibitors such as gefitinib<sup>(48)</sup>, sunitinib<sup>(56)</sup>, sorafenib<sup>(42)</sup>, dasatinib<sup>(49,57)</sup>, imatinib<sup>(43)</sup> and lapatinib<sup>(47)</sup> and the brain penetration of these compounds is also markedly restricted by these two transporters.

A second issue is that deregulated components downstream of EGFR could abolish the effects of EGFR inhibition. For example, Mellinghoff et al. reported that PTEN loss in GBM cells would be a cause of resistance to erlotinib <sup>(58)</sup>. However, this is not the only reason as the randomized EORTC study also found tumors with expression of PTEN and EGFR and/or EGFRvIII that responded poorly <sup>(10)</sup>. Only low levels of phosphorylated PKB/AKT appear to have a (weak) relation with outcome to erlotinib treatment. As we know, PTEN is not the only key factor controlling the signaling downstream of EGFR. Also PI3K mutation and AKT amplification can lead to activation of PI3K pathway. Furthermore, there is active crosstalk between the PI3K and RAS pathways <sup>(59,60)</sup> and activation of the RAS-RAF-MEK-ERK pathway is common in GBM <sup>(61)</sup>. This pathway activation can be caused by a mutation or deletion of NF1 or (more rarely) by mutation of RAS. Besides, mutation and amplification of other parallel receptor tyrosine kinases such as ERBB2, PDGFR and c-MET, could also activate signaling via the PI3K-mTOR and RAS pathway, thereby conferring resistance to EGFR-inhibition <sup>(62)</sup>. Last but not least, another explanation for the disappointing clinical activity of erlotinib in GBM versus lung cancer was delivered by a recent study of Vivanco et al. <sup>(63)</sup>. They showed that distinct types of EGFR mutations in lung cancer and GBMs responded differently to EGFR inhibitors. Importantly, they found that the first-generation EGFR inhibitor erlotinib effectively inhibits EGFR carrying mutations in the kinase domain, as found in lung cancer, whereas it performs very poorly against EGFR with mutations or deletions in the extracellular domain as in GBM <sup>(63)</sup>. The putative resistance of GBM to erlotinib caused by drug efflux transporters and/or intrinsic molecular mechanisms are illustrated in Fig. 3 A.

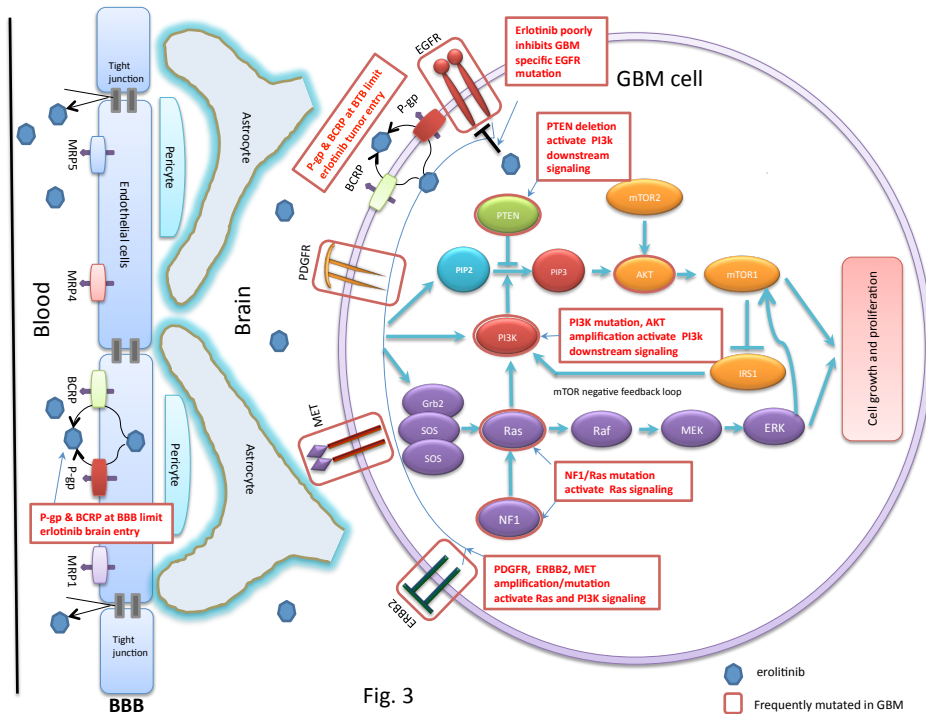


Fig. 3

Fig. 3. Schematic representation of several putative mechanisms of GBM resistance to erlotinib treatment.



## TARGETING THE PI3K-AKT-mTOR PATHWAY

The PI3K-AKT-mTOR pathway, activated by extracellular survival signaling factors via RTKs, is a major cell signaling pathway involved in regulating a variety of cellular processes including cell proliferation, survival, growth, glucose metabolism and protein synthesis<sup>(64)</sup>. The most frequent alteration responsible for the deregulation of this pathway in GBM is the loss of PTEN (36%). In addition, mutation of PI3KCA (15%) gene, and occasionally AKT amplification (2%) or FOXO mutation (1%) also contribute to the activation of the downstream signaling<sup>(65,66,27)</sup> (Fig. 1). Constitutive PI3K-AKT-mTOR pathway activation is a hallmark of GBM.

The class IA Phosphatidylinositol 3-kinase (PI3Ks) is a heterodimer composed of a 85 kDa regulatory subunit (P85 $\alpha$ ) and a 110 kDa catalytic subunit (P110 $\alpha$ ). Once RTK recruits PI3K to the cellular membrane, the PI3K subunit converts inactive PIP<sub>2</sub> (Phosphatidylinositol 4,5-bisphosphate) into active PIP<sub>3</sub> (phosphatidylinositol 3,4,5-trisphosphate). Next, PIP<sub>3</sub> recruits AKT to the membrane together with Phosphoinositide-Dependent Kinase 1 (PDK1). On the contrary, PTEN counteracts PI3K by converting PIP<sub>3</sub> back into PIP<sub>2</sub> and functions as a tumor suppressor. Unlike for other components of cellular pathways with multiple protein-family members, there is no PTEN related protein present in the cells that can compensate for its loss. Therefore, it is not surprising that the loss of PTEN function plays a pivotal role in tumorigenesis<sup>(67)</sup>.

### PI3K inhibitors

Due to the high mutation rates of PTEN and PI3KCA (the gene that encodes the catalytic subunit p110 $\alpha$  of PI3K) and the importance of this pathway in GBM, PI3K and especially its subunit P110 $\alpha$ , provides an attractive drug target. The first generation of PI3K inhibitors (LY294002 and wortmannin) showed *in vivo* antitumor efficacy, but were associated with poor stability or solubility, undesirable toxicities and cross-over inhibition of other lipid and protein kinases<sup>(68,69)</sup>. Therefore, clinical trials with these compounds have never been initiated. After the crystal structure of PI3K was elucidated, the development of new PI3K inhibitors has been accelerated. More selective PI3K inhibitors have been developed, with promising antitumor efficacy and low toxicity in preclinical research. For example, GDC-0941 is a potent and selective ATP-competitive PI3K inhibitor. It inhibits the PI3K p110 $\alpha$  subunit with an IC<sub>50</sub> < 10 nM and inhibits phosphorylation of AKT with

an  $IC_{50}$  value of 28 nM<sup>(70)</sup>. GDC-0941 treatment has led to an increase of apoptosis and inhibition of endothelial growth in a subset of tumor cell lines. *In vivo* antitumor activity with daily oral dosing at 150 mg/kg of GDC-0941 achieved 98% growth inhibition of subcutaneous U87MG xenografts<sup>(71,72)</sup>. Unfortunately, GDC-0941 is also a substrate of both ABCB1 and ABCG2. After intravenous or oral administration, the GDC-0941 brain-to-plasma ratio in *Abcb1;Abcg2*<sup>-/-</sup> knockout mice was about 30-fold higher than in the wild-type mice. The PI3K pathway was markedly inhibited as evidenced by a 60% suppression of the phosphorylated AKT in the brain of *Abcb1;Abcg2*<sup>-/-</sup> mice, whereas no inhibition was detected in the brain of wild-type mice<sup>(73)</sup>. Therefore, the potential efficacy of GDC-0941 as a targeted agent for treatment of GBM is limited due to ABCB1 and ABCG2.

AKT is a serine/threonine protein kinase which can be activated by phosphorylation at the Threonine-308 (T308) by PDK1, or Serine-473 (S473) by mTORC2 (mammalian Target of Rapamycin Complex 2). The mechanism by which the latter phosphorylation occurs is not fully understood but recent work suggested that activation of mTORC2 kinase activity is induced by EGFRVIII in GBM cells and that abnormal mTOR2 signaling can promote GBM growth and survival<sup>(74)</sup>. When phosphorylated, AKT in turn phosphorylates a variety of downstream effector proteins, of which mTORC1 (mammalian Target of Rapamycin complex 1) is one of the most important ones. There are very few trials with AKT inhibitors in GBM. The planned clinical trial with MK-2206 has been canceled by Merck due to a reprioritization within their oncology program (see ClinTrial.gov Identifier: NCT01249105).

### **mTORC1 and mTORC2 inhibitors**

mTORC1 is regarded as a central regulator of cell growth and has a critical role in tumor development. Via two major downstream targets S6K (p70 S6 kinases) and 4EBP1 (4E-Binding Protein), mTORC1 triggers the protein synthesis, which is essential for cell survival, growth and proliferation<sup>(75,76,77)</sup>. Mutations of the mTOR gene are rare in GBM, but frequently deregulated upstream signaling drives mTORC1 activation. Inhibition of mTORC1 by rapamycin or other rapalogs have shown efficacy in a subset of cancers<sup>(78,79)</sup>. However, rapamycin and other rapalogs only inhibit mTORC1 and not mTORC2<sup>(80)</sup>. This can lead to an activation of AKT via an mTORC2 driven positive feedback loop<sup>(81,82,78)</sup>. The novel generation of mTOR inhibitors are multi-targeting agents, which are capable of inhibiting dual targets in the PI3K pathway or even more targets, to more completely

block the feedback loop activation caused by inhibition of mTORC1. Dual mTORC1 and mTORC2 inhibitors that disrupt the downstream signaling of mTORC1 and at the same time inhibit the AKT activation by blocking the mTORC2 activity, thus are interesting candidates for evaluation of treatment efficacy in GBM. AZD8055, a dual mTORC1 and mTORC2 inhibitor, is a highly potent, ATP-competitive, and specific mTOR kinase inhibitor. *In vivo*, AZD8055 showed potent single-agent antitumor activity against a range of subcutaneous xenografts including U87 malignant glioma<sup>(83)</sup>. AZD8055 is currently evaluated in clinical trial in adults with recurrent glioma ((ClinicalTrail.gov Identifier: NCT01316809). Thus far no data has been presented in orthotopic brain tumor models, nor whether AZD8055 is able to cross the BBB. Like AZD8055, Palomid 529 is another dual mTORC1/mTOR2 inhibitor that markedly reduces the phosphorylation of AKT (S473-Akt) signaling by inhibition of both mTORC1 and mTORC2 activity. *In vivo* studies showed that Palomid 529 reduced angiogenesis, vascular permeability and tumor growth<sup>(84)</sup>. Moreover, Palomid 529 was shown to enhance the anti-proliferative effect of radiotherapy in GBM in an orthotopic model<sup>(85)</sup> as well as in prostate tumor models<sup>(86)</sup>. Another way to interrupt the mTORC2-PI3K positive feedback loop is by combined inhibition of mTORC1 and PI3K. Particularly, the imidazo[4,5-c]quinoline derivative NVP-BE2235 selectively inhibits both PI3K and mTOR kinase activity by binding the ATP-binding cleft of these enzymes, thus resulting into G1 arrest and autophagy in tumor cells. It displayed remarkable anti-tumor activity in U87MG GBM xenograft models with a dose dependent effect, and could further enhance the efficacy of temozolomide<sup>(87)</sup>. Further studies using U87 intracranial xenograft models again confirmed the anti-tumor potency of NVP-BE2235 in treatment of GBM<sup>(88)</sup>. NVP-BE2235 is not tested clinically against glioma, most likely because the company (Novartis) has prioritized NVP-BKM120 for development in glioma. BKM120 is a pan-Class 1 PI3K inhibitor but has no inhibitory activity against mTOR<sup>(89)</sup>. This compound is assumed to penetrate the BBB<sup>(90)</sup>.

### **TARGETING THE RAS-RAF-MEK-ERK PATHWAY**

The RAS-RAF-MEK-ERK (MAPK, Mitogen-Activated Protein Kinase) pathway is activated in the majority of GBMs via various ways, such as EGFR mutation or amplification (45%) or PDGFR amplification (13%) and deletion of NF1 (18%)<sup>(27)</sup>. Upon activation, the growth factor receptors generate binding sites for adaptor proteins like GRB2 (Growth factor Receptor-Bound protein 2) containing an SH2 domain. Next, GRB2 recruits SOS (Son of Sevenless) to the membrane, which in turn activate RAS through the replacement of

inactive GDP (guanosine diphosphate) with active GTP (guanosine triphosphate). As a result, RAS is able to recruit RAF kinases (A-RAF, B-RAF, C-RAF) to the plasma membrane, where they are being activated. RAF is able to phosphorylate and thereby activate MEK1 and MEK2 (mitogen-activated protein kinase kinase 1 and 2), which in turn activate ERK1 and ERK2 (extracellular-signal-regulated kinase 1 and 2). Activation of ERK leads to activation of a variety of nuclear and cytoplasmic substrates associated with gene regulation, cell cycle progression, differentiation and cell division <sup>(27,91,92)</sup>. Due to the important role in cell proliferation and survival, the MAPK pathway is frequently altered in a variety of tumors. K-RAS, one of the three RAS genes, is often mutated in leukemia, colon cancer, pancreatic cancer and lung cancer. Although human GBMs rarely show RAS mutations (2%), almost all malignant human gliomas show elevated levels of activated RAS as a result of other upstream molecular alterations.

### **MEK inhibitors**

Inhibition of MEK is an effective strategy to prevent the subsequent downstream signaling of the RAS pathway, and consequently induces tumor regression and/or stasis. A recent study by See et al. demonstrated that PD0325901 and AZD6244 as a single agent, suppressed the growth of NF1-deficient and MEK inhibitor-sensitive glioma cells both *in vitro* and *in vivo* <sup>(93)</sup>. Their findings indicate that a subset of NF1-deficient GBMs may be responsive to MEK inhibitors. Moreover, they found that NF1-deficient glioma cells that are intrinsically resistant to MEK inhibition were sensitized by the addition of the dual PI3K/mTOR inhibitor PI-103. Many commonly used MEK inhibitors are benzohydroxamate derivatives sharing many similarities in chemical structure. These inhibitors result in MEK-specific inhibition by binding to the hydrophobic pocket, adjacent to the ATP binding site of the MEK protein which keeps the kinase in a catalytically inactive state. This allosteric mechanism contributes to a high selectivity for MEK without affecting other protein kinases that have structurally similar ATP binding pockets. Therefore, MEK inhibitors are usually highly specific and non-ATP-competitive inhibitors. PD-0325901 was the first clinically tested MEK inhibitor. *In vivo* results demonstrated that PD-0325901 potently inhibits growth of human tumor xenografts bearing activating mutations of B-Raf, concomitant with suppression of ERK1/2 phosphorylation <sup>(94)</sup>. Interestingly, during the phase I and II clinical trials in advanced cancers anti-tumor activity was seen between 4 to 30 mg bidaily dosing <sup>(95,96)</sup>. However, besides the more common side effects like rash, diarrhea and fatigue, the drug also caused ocular and central nervous system

(CNS) toxicities at doses above 15 mg and Pfizer has suspended its further evaluation. Notably, a similar ocular toxicity has been observed with the MEK1 inhibitor AZD6244 (Selumetinib), albeit to a lesser extent than PD-0325901. Whether these CNS toxicities are a direct consequence of MEK inhibition in the brain or caused by off-target drug effects is still unclear; both are possible regarding the structural similarities of the MEK inhibitors tested so far. Clearly, these CNS toxicities suggest that MEK inhibitors like PD-0325901 are able to enter the CNS, which would qualify these as candidates for testing in GBM. However, MEK inhibitors are predominantly evaluated against non-CNS tumors and the selection of novel candidates is narrowed to those having a low BBB permeability, to avoid CNS toxicities. It should be noted that this strategy holds the risk that a complete class of targeted agents may become useless for treating GBM. The central role of an activated RAS pathway in GBM argues in favor of using MEK inhibitors, although it is obvious that finding the optimal dose level will be a challenging task.

## RB PATHWAY AND CDK INHIBITON

Deregulation of the G1/S checkpoint is very common in GBM. Cyclin-dependent kinases (CDKs) are serine/threonine protein kinases, whose activity depends on binding and activation by cyclin partners and they are required for cell cycle progression. CDK4 and CDK6, which are both under control of P16<sup>INK4a</sup> and P15<sup>INK4b</sup>, bind to cyclin D, phosphorylate the retinoblastoma protein (Rb), causing subsequent release of the transcription factor E2F and synthesis of proteins that are needed in S phase. The most common alteration of the Rb pathway in GBM (52% of cases) is a homozygous deletion of parts of the CDKN2 locus that codes for P16<sup>INK4a</sup> and P15<sup>INK4b</sup>. Other alterations include amplification and overexpression of CDK4 (15-20%) and homozygous deletion/mutation of the RB1 gene (~10%). Deletion of CDKN2A (or amplification of CDK4), CDKN2B and CDKN2C leads to loss of cell cycle control and increased cell proliferation. Co-deletion of CDKN2A and CDKN2C serves as a strong predictor of sensitivity to a selective inhibitor of CDK4/6<sup>(97)</sup>. Amplification of CDK6 and individual D-type cyclins, and homozygous deletion of CDKN2C encoding P18<sup>INK4c</sup> are less common<sup>(27)</sup>.

**CDK inhibitor PD0332991**

CDK4 is a logical target, taking into consideration that loss of CDKN2a/b or amplification of CDK4 is a frequent event in GBM. PD0332991 is an orally bio-available CDK inhibitor, which selectively inhibits cyclin-dependent kinases CDK4 and CDK6. Antiproliferative activity has been demonstrated in luminal breast cancer, myeloma and GBM cell lines<sup>(98,99)</sup>. As expected, RB1 deficient tumors were resistant to PD0332991. Michaud et al.<sup>(98)</sup> demonstrated that PD-0332991 was effective in suppressing the growth of intracranial U87MG tumors, including those that recurred after initial therapy with temozolomide. The combination of PD0332991 and radiation therapy resulted in a significantly increased survival compared with either therapy alone. Based on these results, it was argued that this compound can efficiently cross the blood-brain barrier<sup>(98)</sup>. It should be noted, however, that the BBB in U87MG tumors is very leaky<sup>(100)</sup>.

Two completed phase I trials showed that PD0332991 is generally well tolerated and neutropenia was the sole significant toxicity at maximum tolerated dose (125 mg once daily)<sup>(101,102)</sup>. A Phase II clinical study to test PD0332991 in patients with recurrent Rb positive GBM is currently ongoing (ClinTrials.gov Identifier: NCT01227434).

---

## FUTURE STRATEGIES FOR TARGETED THERAPY

As outlined above, at least three core signaling pathways (RAS-RAF-MEK-ERK, PI3K-AKT-mTOR and CDKN2-CDK4/6-RB1) are jointly activated in the majority of GBM's through different mechanisms and targeting just one of these components may be insufficient to achieve a meaningful effect on tumor progression. In addition, crosstalk between different molecules of two or more pathways increases the plasticity of tumor survival signaling and reduces the oncogene addiction<sup>(59)</sup>.

As depicted in Fig. 3, inhibition of EGFR will not be able to suppress the activation of PI3K and RAS pathways in case other oncogenic alterations in parallel (*e.g.* other RTK's) and/or downstream components (*e.g.* PI3K activation) have occurred. Similarly, as shown by the examples of mTOR inhibitors, treatment with an inhibitor of a single pathway may also not sufficiently block parallel signaling pathways to reach a significant anti-proliferative effect. For example, Di Nicolantonio et al. have shown that a number of human cancer cell lines carrying alterations in the PI3K pathway responded to everolimus, but only when there was no concomitant KRAS mutation<sup>(103)</sup>.

Although several studies with PI3K and RAS inhibitors, given as a single agent, have shown promising tumor growth inhibitory potencies by *in vitro* or *in vivo* models using established GBM cell lines such as U87-MG, it should be taken into account that these GBM cells have been cultured for many generations. When grown *in vivo*, they form homogenous non-invasive lesions with a relative stable genome, unlike the highly heterogeneous GBMs that are typically found in patients. This discrepancy may be a plausible explanation for their poor predictive value on the usefulness of these agents against GBM in the clinic.

The considerations above argue in favor of targeting multiple pathways simultaneously, by analogy with the poly-pharmacy that is commonly applied in anti-retroviral therapy. Ideally, this would include targeting all three core signaling pathways simultaneously. Although it will be a challenging task to achieve sufficient inhibition of these three core pathways simultaneously, this concept would have the intrinsic potential to be beneficial for a substantial fraction of GBM patients. A schematic overview of strategies to combine targeted inhibitors on the core pathways of GBM have been proposed in Fig. 4.

**Targeted therapy combined with drug efflux transporters inhibitors**

The important roles of ABCB1 and ABCG2 in drug resistance and in limiting the brain penetration of therapeutic drugs are well established. However, surprisingly little attention has been paid to this fact when designing clinical trials with targeted agents in GBM. Erlotinib, lapatinib and most other newly developed kinase inhibitors are substrates of ABCB1 and/or ABCG2 and as a consequence, their usefulness in treatment of GBM growth might be compromised by an inadequate brain penetration. The reality is that most targeted agents are in first place developed for treatment of major tumor types like lung and breast cancer, where good BBB penetration is irrelevant or considered undesirable (e.g. MEK inhibitors). Consequently, however, agents from this panel that are being considered for further evaluation in GBM may not be the best BBB permeable drugs.

Elacridar (GF120918) and tariquidar are both dual ABCB1 and ABCG2 inhibitors that have been developed in the 1990s to improve the treatment of ABCB1 mediated multidrug-resistant tumors. Due to the lack of success in this area, this concept is not receiving much attention nowadays. These same agents, however, have the potential to enhance the brain penetration of targeted therapies by blocking the efflux of drugs by these two transporters at the BBB, and perhaps also at the blood-tumor barrier. Co-administration of elacridar with a number of anti-cancer drugs have been proven to be an effective strategy to enhance the brain accumulation of these drugs including a range of potentially effective targeted therapeutics <sup>(45,56,57,104,48,105,106,107,108,109,110,49)</sup>. Therefore, the use of elacridar might represent a feasible strategy to improve the brain entry of potentially effective targeted therapeutics for GBM.



## CONCLUSIONS AND FUTURE PERSPECTIVES

The TCGA project and other collaborative research efforts have revealed how the oncogenetic processes of GBM are driven by multiple deregulated core signaling pathways and will provide new avenues for more effective targeted therapies in the treatment of GBM. Because the crosstalk between these molecular pathways fuels the plasticity of these processes, targeting a single, prevalent target that promotes and dominates GBM proliferation will -at best- provide only very short-lived effects.. Consequently, the next generation of targeted therapies should focus on multi-targeting agents or combinations of single-targeting agents against these core pathways.

Importantly, when selecting the most appropriate candidates of targeted therapeutics, the brain penetration of such candidates and in particular their interactions with the drug efflux transporters ABCB1 and ABCG2 should be taken into consideration. No matter how potent an agent is in inhibiting or activating its target, it has to reach that target at a therapeutic level, which is more difficult to achieve in the brain than in other tissues. Ideally, substances should be designed to have a low affinity for drug efflux transporters. Alternatively, co-administration of targeted agents together with inhibitors of these drug efflux transporters (*e.g.* elacridar) may be helpful and should also be considered.

The progress that has been made in the treatment of GBM during the last decades has been very modest. Therapies that are based on targeting core signaling pathways underlying the processes of malignant transformation is an emerging therapeutic strategy that hold great potential and receives a lot of attention. However, if we continue testing such agents against GBM one-by-one and without considering whether the candidate drugs are able to cross the BBB sufficiently, it is likely that again little progress will have been made in 5-10 years from now.

## OBJECTIVES AND OUTLINE OF THIS THESIS

The main objective of the research presented in this thesis was to investigate the roles of drug efflux transporters at BBB in limiting brain penetrations of novel agents as well as their impacts on the therapeutic effect against malignant gliomas. The candidate drugs we mainly focused on are the small molecular inhibitors which selectively inhibit the deregulated signaling pathway in cancer cells. To assess the pharmacokinetic behaviors of these targeted agents, rapid and sensitive analytic assays are needed. Therefore, we firstly developed and validated two sensitive analytic assays for determining Palomid 529, a dual mTORC1 and mTORC2 inhibitor, and NVP-BEZ235, a dual PI3K and mTOR inhibitor in murine and human plasma and tissue samples (Chapter 2). Furthermore, the roles of Abcb1 (P-glycoprotein) and Abcg2 (Bcrp1) in brain penetrations and anti-glioma therapeutic effects of several selected targeted agents have been investigated (Chapter 3). Two agents, Palomid 529 (Chapter 3.1) and ZSTK474 (PI3K inhibitor, Chapter 3.3) have been identified as non- or poor substrates of Abcb1 and Abcg2, so their brain penetrations have not been compromised by these transporters. We also found that Abcb1 and Abcg2 could cause severe impacts on the brain penetrations of agents which are substrates of one of them, like rapamycin and NVP-BEZ235 (Chapter 3.3); or both of them, like ABT-888 (PARP inhibitor, Chapter 3.2). However, co-administration of elacridar could reverse the drug efflux of Abcb1 and Abcg2 at both blood-brain barrier and at tumor cells, and consequently improve the therapeutic effect of targeted agents (Chapter 3.2). The last chapter describes an important role of another drug efflux transporters expressed at blood-brain barrier, ABCC4 (Mrp4) in brain pharmacokinetics of camptothecin analogs topotecan, gimatecan, irinotecan and SN-38 (Chapter 4.1); and also reports that sildenafil (viagra) is not a useful inhibitor of ABCB1 and ABCG2 mediated drug resistance in vivo (Chapter 4.2).

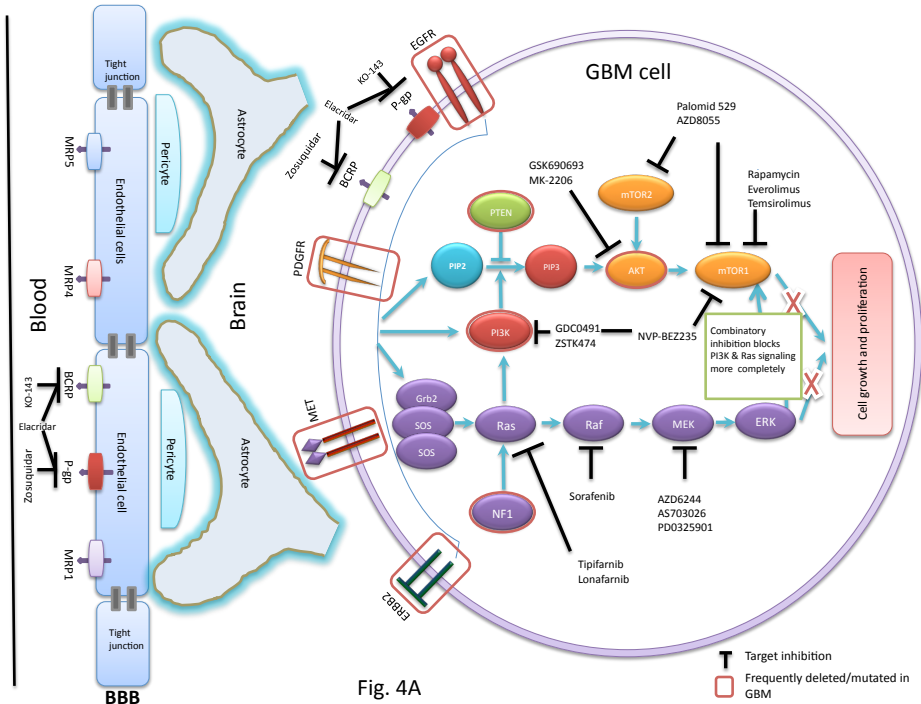
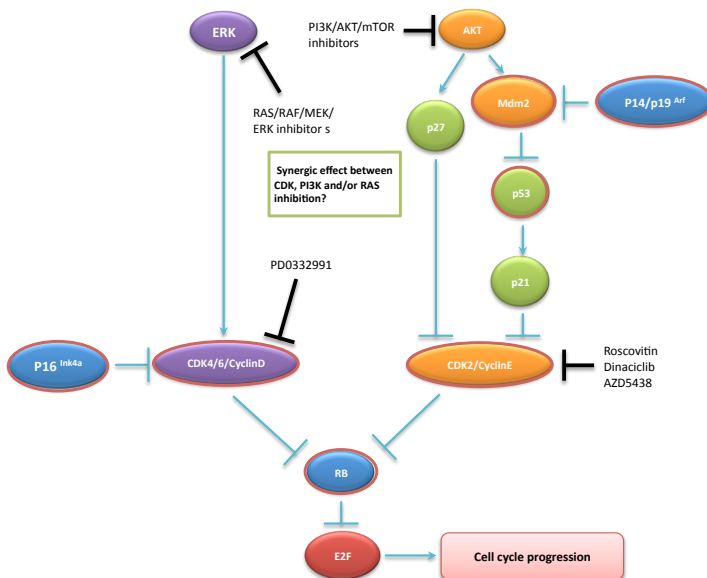


Fig. 4A



**Fig. 4.** Schematic overview of the core pathways involved in GBM: RTK-PI3K-AKT-mTOR and RTK-RAS-RAF-MEK-ERK pathways (A) and the Rb pathway (B) and a listing of some example drug that have been developed to inhibit these pathways. Several strategies to combine targeted inhibitors on the core pathways of GBM have been indicated in the figures.

## Reference List

1. Furnari FB, Fenton T, Bachoo RM *et al*: Malignant astrocytic glioma: genetics, biology, and paths to treatment. *Genes Dev.* 21(21), 2683-2710 (2007).
2. David N.Louis, Hiroko Ohgaki, Otmar D.Wiestler, Webster K.Cavenee. WHO Classification of Tumours of the Central Nervous System. In: IARC, 2007)
3. Stupp R, Mason WP, van den Bent MJ *et al*: Radiotherapy plus concomitant and adjuvant temozolomide for glioblastoma. *N.Engl.J Med.* 352(10), 987-996 (2005).
4. O'Brien SG, Guilhot F, Larson RA *et al*: Imatinib compared with interferon and low-dose cytarabine for newly diagnosed chronic-phase chronic myeloid leukemia. *N.Engl.J Med.* 348(11), 994-1004 (2003).
5. Sosman JA, Kim KB, Schuchter L *et al*: Survival in BRAF V600-mutant advanced melanoma treated with vemurafenib. *N.Engl.J Med.* 366(8), 707-714 (2012).
6. Prados MD, Lamborn KR, Chang S *et al*: Phase 1 study of erlotinib HCl alone and combined with temozolomide in patients with stable or recurrent malignant glioma. *Neuro.Oncol.* 8(1), 67-78 (2006).
7. Krishnan S, Brown PD, Ballman KV *et al*: Phase I trial of erlotinib with radiation therapy in patients with glioblastoma multiforme: results of North Central Cancer Treatment Group protocol N0177. *Int.J.Radiat.Oncol.Biol.Phys.* 65(4), 1192-1199 (2006).
8. Prados MD, Chang SM, Butowski N *et al*: Phase II study of erlotinib plus temozolomide during and after radiation therapy in patients with newly diagnosed glioblastoma multiforme or gliosarcoma. *J.Clin.Oncol.* 27(4), 579-584 (2009).
9. Brown PD, Krishnan S, Sarkaria JN *et al*: Phase I/II trial of erlotinib and temozolomide with radiation therapy in the treatment of newly diagnosed glioblastoma multiforme: North Central Cancer Treatment Group Study N0177. *J.Clin.Oncol.* 26(34), 5603-5609 (2008).
10. van den Bent MJ, Brandes AA, Rampling R *et al*: Randomized phase II trial of erlotinib versus temozolomide or carmustine in recurrent glioblastoma: EORTC brain tumor group study 26034. *J.Clin.Oncol.* 27(8), 1268-1274 (2009).
11. Peereboom DM, Shepard DR, Ahluwalia MS *et al*: Phase II trial of erlotinib with temozolomide and radiation in patients with newly diagnosed glioblastoma multiforme. *J.Neurooncol.* 98(1), 93-99 (2010).
12. Brandes AA, Franceschi E, Tosoni A, Hegi ME, Stupp R: Epidermal growth factor receptor inhibitors in neuro-oncology: hopes and disappointments. *Clin.Cancer Res.* 14(4), 957-960 (2008).
13. Franceschi E, Cavallo G, Lonardi S *et al*: Gefitinib in patients with progressive high-grade gliomas: a multicentre phase II study by Gruppo Italiano Cooperativo di Neuro-Oncologia (GICNO). *Br.J.Cancer* 96(7), 1047-1051 (2007).
14. Rich JN, Reardon DA, Peery T *et al*: Phase II trial of gefitinib in recurrent glioblastoma. *J.Clin.Oncol.* 22(1), 133-142 (2004).
15. Chang SM, Wen P, Cloughesy T *et al*: Phase II study of CCI-779 in patients with recurrent glioblastoma multiforme. *Invest New Drugs* 23(4), 357-361 (2005).

16. Galanis E, Buckner JC, Maurer MJ *et al*: Phase II trial of temsirolimus (CCI-779) in recurrent glioblastoma multiforme: a North Central Cancer Treatment Group Study. *J.Clin.Oncol.* 23(23), 5294-5304 (2005).
17. Chang SM, Kuhn J, Wen P *et al*: Phase I/pharmacokinetic study of CCI-779 in patients with recurrent malignant glioma on enzyme-inducing antiepileptic drugs. *Invest New Drugs* 22(4), 427-435 (2004).
18. Mason WP, Macneil M, Kavan P *et al*: A phase I study of temozolomide and everolimus (RAD001) in patients with newly diagnosed and progressive glioblastoma either receiving or not receiving enzyme-inducing anticonvulsants: an NCIC CTG study. *Invest New Drugs* (2011).
19. Sarkaria JN, Galanis E, Wu W *et al*: North Central Cancer Treatment Group Phase I trial N057K of everolimus (RAD001) and temozolomide in combination with radiation therapy in patients with newly diagnosed glioblastoma multiforme. *Int.J.Radiat.Oncol.Biol.Phys.* 81(2), 468-475 (2011).
20. Hainsworth JD, Shih KC, Shepard GC, Tillinghast GW, Brinker BT, Spigel DR: Phase II study of concurrent radiation therapy, temozolomide, and bevacizumab followed by bevacizumab/everolimus as first-line treatment for patients with glioblastoma. *Clin.Adv.Hematol.Oncol.* 10(4), 240-246 (2012).
21. Reardon DA, Desjardins A, Vredenburgh JJ *et al*: Phase 2 trial of erlotinib plus sirolimus in adults with recurrent glioblastoma. *J.Neurooncol.* 96(2), 219-230 (2010).
22. Cloughesy TF, Yoshimoto K, Nghiemphu P *et al*: Antitumor activity of rapamycin in a Phase I trial for patients with recurrent PTEN-deficient glioblastoma. *PLoS.Med.* 5(1), e8- (2008).
23. Ohgaki H, Dessen P, Jourde B *et al*: Genetic pathways to glioblastoma: a population-based study. *Cancer Res.* 64(19), 6892-6899 (2004).
24. Parsons DW, Jones S, Zhang X *et al*: An integrated genomic analysis of human glioblastoma multiforme. *Science* 321(5897), 1807-1812 (2008).
25. Lang FF, Miller DC, Koslow M, Newcomb EW: Pathways leading to glioblastoma multiforme: a molecular analysis of genetic alterations in 65 astrocytic tumors. *J Neurosurg.* 81(3), 427-436 (1994).
26. von Deimling A, von Ammon K, Schoenfeld D, Wiestler OD, Seizinger BR, Louis DN: Subsets of glioblastoma multiforme defined by molecular genetic analysis. *Brain Pathol.* 3(1), 19-26 (1993).
27. Cancer Genome Atlas Research Network.: Comprehensive genomic characterization defines human glioblastoma genes and core pathways. *Nature* 455(7216), 1061-1068 (2008).
28. Verhaak RG, Hoadley KA, Purdom E *et al*: Integrated genomic analysis identifies clinically relevant subtypes of glioblastoma characterized by abnormalities in PDGFRA, IDH1, EGFR, and NF1. *Cancer Cell* 17(1), 98-110 (2010).
29. Agarwal S, Sane R, Oberoi R, Ohlfest JR, Elmquist WF: Delivery of molecularly targeted therapy to malignant glioma, a disease of the whole brain. *Expert Rev Mol Med* 13, e17- (2011).

30. Muldoon LL, Soussain C, Jahnke K *et al*: Chemotherapy delivery issues in central nervous system malignancy: a reality check. *Journal of Clinical Oncology* 25(16), 2295-2305 (2007).
31. de Vries NA, Beijnen JH, Boogerd W, van Tellingen O: Blood-brain barrier and chemotherapeutic treatment of brain tumors. *Expert.Rev.Neurother.* 6(8), 1199-1209 (2006).
32. Urquhart BL, Kim RB: Blood-brain barrier transporters and response to CNS-active drugs. *Eur.J.Clin.Pharmacol.* 65(11), 1063-1070 (2009).
33. Deeken JF, Loscher W: The blood-brain barrier and cancer: transporters, treatment, and trojan horses. *Clinical Cancer Research* 13(6), 1663-1674 (2007).
34. Juliano RL, Ling V: A surface glycoprotein modulating drug permeability in Chinese hamster ovary cell mutants. *Biochim.Biophys.Acta* 455(1), 152-162 (1976).
35. Leslie EM, Deeley RG, Cole SP: Multidrug resistance proteins: role of P-glycoprotein, MRP1, MRP2, and BCRP (ABCG2) in tissue defense. *Toxicol.Appl.Pharmacol.* 204(3), 216-237 (2005).
36. Dietrich CG, Geier A, Oude Elferink RP: ABC of oral bioavailability: transporters as gatekeepers in the gut. *Gut* 52(12), 1788-1795 (2003).
37. Szakacs G, Varadi A, Ozvegy-Laczka C, Sarkadi B: The role of ABC transporters in drug absorption, distribution, metabolism, excretion and toxicity (ADME-Tox). *Drug Discov. Today* 13(9-10), 379-393 (2008).
38. Ayrton A, Morgan P: Role of transport proteins in drug absorption, distribution and excretion. *Xenobiotica* 31(8-9), 469-497 (2001).
39. Schinkel AH, Jonker JW: Mammalian drug efflux transporters of the ATP binding cassette (ABC) family: an overview. *Adv.Drug Deliv.Rev.* 55(1), 3-29 (2003).
40. Enokizono J, Kusuhara H, Ose A, Schinkel AH, Sugiyama Y: Quantitative investigation of the role of breast cancer resistance protein (Bcrp/Abcg2) in limiting brain and testis penetration of xenobiotic compounds. *Drug Metab Dispos.* 36(6), 995-1002 (2008).
41. Schinkel AH, Smit JJ, van Tellingen O *et al*: Disruption of the mouse *mdr1a* P-glycoprotein gene leads to a deficiency in the blood-brain barrier and to increased sensitivity to drugs. *Cell* 77(4), 491-502 (1994).
42. Lagas JS, van Waterschoot RA, Sparidans RW, Wagenaar E, Beijnen JH, Schinkel AH: Breast cancer resistance protein and P-glycoprotein limit sorafenib brain accumulation. *Mol. Cancer Ther.* 9(2), 319-326 (2010).
43. Zhou L, Schmidt K, Nelson FR, Zelesky V, Troutman MD, Feng B: The effect of breast cancer resistance protein and P-glycoprotein on the brain penetration of flavopiridol, imatinib mesylate (Gleevec), prazosin, and 2-methoxy-3-(4-(2-(5-methyl-2-phenyloxazol-4-yl)ethoxy)phenyl)propanoic acid (PF-407288) in mice. *Drug Metab Dispos.* 37(5), 946-955 (2009).
44. Mittapalli RK, Vaidhyanathan S, Sane R, Elmquist WF: Impact of P-glycoprotein (ABCB1) and Breast Cancer Resistance Protein (ABCG2) on the Brain Distribution of a novel B-RAF Inhibitor: Vemurafenib (PLX4032). *J.Pharmacol.Exp.Ther.* (2012).

45. de Vries NA, Zhao J, Kroon E, Buckle T, Beijnen JH, van Tellingen O: P-glycoprotein and breast cancer resistance protein: two dominant transporters working together in limiting the brain penetration of topotecan. *Clin Cancer Res* 13(21), 6440-6449 (2007).
46. Iusuf D, Teunissen SF, Wagenaar E, Rosing H, Beijnen JH, Schinkel AH: P-glycoprotein (ABCB1) transports the primary active tamoxifen metabolites endoxifen and 4-hydroxytamoxifen and restricts their brain penetration. *J.Pharmacol.Exp.Ther.* 337(3), 710-717 (2011).
47. Polli JW, Olson KL, Chism JP *et al*: An unexpected synergist role of P-glycoprotein and breast cancer resistance protein on the central nervous system penetration of the tyrosine kinase inhibitor lapatinib (N-{3-chloro-4-[(3-fluorobenzyl)oxy]phenyl}-6-[5-{{[2-(methylsulfonyl)ethyl]amino }methyl}-2-furyl]-4-quinazolinamine; GW572016). *Drug Metab Dispos.* 37(2), 439-442 (2009).
48. Agarwal S, Sane R, Gallardo JL, Ohlfest JR, Elmquist WF: Distribution of gefitinib to the brain is limited by P-glycoprotein (ABCB1) and breast cancer resistance protein (ABCG2)-mediated active efflux. *J.Pharmacol.Exp.Ther.* 334(1), 147-155 (2010).
49. Chen Y, Agarwal S, Shaik NM, Chen C, Yang Z, Elmquist WF: P-glycoprotein and breast cancer resistance protein influence brain distribution of dasatinib. *J.Pharmacol.Exp.Ther.* 330(3), 956-963 (2009).
50. Aldape KD, Ballman K, Furth A *et al*: Immunohistochemical detection of EGFRvIII in high malignancy grade astrocytomas and evaluation of prognostic significance. *J.Neuropathol. Exp.Neurol.* 63(7), 700-707 (2004).
51. Frederick L, Wang XY, Eley G, James CD: Diversity and frequency of epidermal growth factor receptor mutations in human glioblastomas. *Cancer Res.* 60(5), 1383-1387 (2000).
52. Wong AJ, Ruppert JM, Bigner SH *et al*: Structural alterations of the epidermal growth factor receptor gene in human gliomas. *Proc.Natl.Acad.Sci.U.S.A* 89(7), 2965-2969 (1992).
53. Shinjima N, Tada K, Shiraishi S *et al*: Prognostic value of epidermal growth factor receptor in patients with glioblastoma multiforme. *Cancer Res.* 63(20), 6962-6970 (2003).
54. Kodaira H, Kusuhara H, Ushiki J, Fuse E, Sugiyama Y: Kinetic analysis of the cooperation of P-glycoprotein (P-gp/Abcb1) and breast cancer resistance protein (Bcrp/Abcg2) in limiting the brain and testis penetration of erlotinib, flavopiridol, and mitoxantrone. *J.Pharmacol. Exp.Ther.* 333(3), 788-796 (2010).
55. de Vries NA, Buckle T, Zhao J, Beijnen JH, Schellens JH, van TO: Restricted brain penetration of the tyrosine kinase inhibitor erlotinib due to the drug transporters P-gp and BCRP. *Invest New Drugs* 30(2), 443-449 (2012).
56. Tang SC, Lagas JS, Lankheet NA *et al*: Brain accumulation of sunitinib is restricted by P-glycoprotein (ABCB1) and breast cancer resistance protein (ABCG2) and can be enhanced by oral elacridar and sunitinib coadministration. *Int.J Cancer* 130(1), 223-233 (2012).
57. Lagas JS, van Waterschoot RA, van Tilburg VA *et al*: Brain accumulation of dasatinib is restricted by P-glycoprotein (ABCB1) and breast cancer resistance protein (ABCG2) and can be enhanced by elacridar treatment. *Clin.Cancer Res.* 15(7), 2344-2351 (2009).
58. Mellinghoff IK, Wang MY, Vivanco I *et al*: Molecular determinants of the response of glioblastomas to EGFR kinase inhibitors. *N.Engl.J.Med.* 353(19), 2012-2024 (2005).

59. Mendoza MC, Er EE, Blenis J: The Ras-ERK and PI3K-mTOR pathways: cross-talk and compensation. *Trends Biochem.Sci.* 36(6), 320-328 (2011).
60. To MD, Perez-Losada J, Mao JH, Balmain A: Crosstalk between Pten and Ras signaling pathways in tumor development. *Cell Cycle* 4(9), 1185-1188 (2005).
61. Jeuken J, van den Broecke C, Gijsen S, Boots-Sprenger S, Wesseling P: RAS/RAF pathway activation in gliomas: the result of copy number gains rather than activating mutations. *Acta Neuropathol.* 114(2), 121-133 (2007).
62. Stommel JM, Kimmelman AC, Ying H *et al*: Coactivation of receptor tyrosine kinases affects the response of tumor cells to targeted therapies. *Science* 318(5848), 287-290 (2007).
63. Vivanco I, Robins HI, Rohle D *et al*: Differential sensitivity of glioma- versus lung cancer-specific EGFR mutations to EGFR kinase inhibitors. *Cancer Discov.* 2(5), 458-471 (2012).
64. Cheng CK, Fan QW, Weiss WA: PI3K signaling in glioma--animal models and therapeutic challenges. *Brain Pathol.* 19(1), 112-120 (2009).
65. Vivanco I, Sawyers CL: The phosphatidylinositol 3-Kinase AKT pathway in human cancer. *Nat.Rev.Cancer* 2(7), 489-501 (2002).
66. Courtney KD, Corcoran RB, Engelman JA: The PI3K pathway as drug target in human cancer. *J.Clin.Oncol.* 28(6), 1075-1083 (2010).
67. Bader AG, Kang S, Zhao L, Vogt PK: Oncogenic PI3K deregulates transcription and translation. *Nat.Rev.Cancer* 5(12), 921-929 (2005).
68. Yap TA, Garrett MD, Walton MI, Raynaud F, de Bono JS, Workman P: Targeting the PI3K-AKT-mTOR pathway: progress, pitfalls, and promises. *Curr.Opin.Pharmacol.* 8(4), 393-412 (2008).
69. Carnero A, Blanco-Aparicio C, Renner O, Link W, Leal JF: The PTEN/PI3K/AKT signalling pathway in cancer, therapeutic implications. *Curr.Cancer Drug Targets.* 8(3), 187-198 (2008).
70. Folkes AJ, Ahmadi K, Alderton WK *et al*: The identification of 2-(1H-indazol-4-yl)-6-(4-methanesulfonyl-piperazin-1-ylmethyl)-4-morpholin-4-yl-t hieno[3,2-d]pyrimidine (GDC-0941) as a potent, selective, orally bioavailable inhibitor of class I PI3 kinase for the treatment of cancer. *J Med.Chem.* 51(18), 5522-5532 (2008).
71. Yap TA, Garrett MD, Walton MI, Raynaud F, de Bono JS, Workman P: Targeting the PI3K-AKT-mTOR pathway: progress, pitfalls, and promises. *Curr.Opin.Pharmacol.* 8(4), 393-412 (2008).
72. Raynaud FI, Eccles SA, Patel S *et al*: Biological properties of potent inhibitors of class I phosphatidylinositide 3-kinases: from PI-103 through PI-540, PI-620 to the oral agent GDC-0941. *Mol.Cancer Ther.* 8(7), 1725-1738 (2009).
73. Salphati L, Lee LB, Pang J, Plise EG, Zhang X: Role of P-glycoprotein and breast cancer resistance protein-1 in the brain penetration and brain pharmacodynamic activity of the novel phosphatidylinositol 3-kinase inhibitor GDC-0941. *Drug Metab Dispos.* 38(9), 1422-1426 (2010).
74. Tanaka K, Babic I, Nathanson D *et al*: Oncogenic EGFR signaling activates an mTORC2-NF-kappaB pathway that promotes chemotherapy resistance. *Cancer Discov.* 1(6), 524-538 (2011).



75. Shor B, Gibbons JJ, Abraham RT, Yu K: Targeting mTOR globally in cancer: thinking beyond rapamycin. *Cell Cycle* 8(23), 3831-3837 (2009).
76. Samuels Y, Wang Z, Bardelli A *et al*: High frequency of mutations of the PIK3CA gene in human cancers. *Science* 304(5670), 554- (2004).
77. Petroulakis E, Mamane Y, Le Bacquer O, Shahbazian D, Sonenberg N: mTOR signaling: implications for cancer and anticancer therapy. *Br J Cancer* 94(2), 195-199 (2006).
78. Abraham RT , Gibbons JJ: The mammalian target of rapamycin signaling pathway: twists and turns in the road to cancer therapy. *Clin Cancer Res* 13(11), 3109-3114 (2007).
79. Easton JB , Houghton PJ: mTOR and cancer therapy. *Oncogene* 25(48), 6436-6446 (2006).
80. Sarbassov DD, Guertin DA, Ali SM, Sabatini DM: Phosphorylation and regulation of Akt/PKB by the rictor-mTOR complex. *Science* 307(5712), 1098-1101 (2005).
81. Phung TL, Eyah-Mensah G, O'Donnell RK *et al*: Endothelial Akt signaling is rate-limiting for rapamycin inhibition of mouse mammary tumor progression. *Cancer Res* 67(11), 5070-5075 (2007).
82. O'Reilly KE, Rojo F, She QB *et al*: mTOR inhibition induces upstream receptor tyrosine kinase signaling and activates Akt. *Cancer Res* 66(3), 1500-1508 (2006).
83. Chresta CM, Davies BR, Hickson I *et al*: AZD8055 is a potent, selective, and orally bioavailable ATP-competitive mammalian target of rapamycin kinase inhibitor with in vitro and in vivo antitumor activity. *Cancer Res.* 70(1), 288-298 (2010).
84. Xue Q, Hopkins B, Perruzzi C, Udayakumar D, Sherris D, Benjamin LE: Palomid 529, a novel small-molecule drug, is a TORC1/TORC2 inhibitor that reduces tumor growth, tumor angiogenesis, and vascular permeability. *Cancer Res* 68(22), 9551-9557 (2008).
85. Cerna D, Carter D, Flaherty S, Cal L, Sherris D, and Yoo SS. Palomid 529, a PI3K/Akt/mTOR dual TORC1/2 inhibitor, is a radiosensitizer with effect in both subcutaneous and orthotopic U251 glioblastoma tumor xenograft models [abstract]. *AACR 2010:2506* (2010)
86. Diaz R, Nguewa PA, Diaz-Gonzalez JA *et al*: The novel Akt inhibitor Palomid 529 (P529) enhances the effect of radiotherapy in prostate cancer. *Br J Cancer* 100(6), 932-940 (2009).
87. Maira SM, Stauffer F, Brueggen J *et al*: Identification and characterization of NVP-BEZ235, a new orally available dual phosphatidylinositol 3-kinase/mammalian target of rapamycin inhibitor with potent in vivo antitumor activity. *Mol.Cancer Ther.* 7(7), 1851-1863 (2008).
88. Liu TJ, Koul D, LaFortune T *et al*: NVP-BEZ235, a novel dual phosphatidylinositol 3-kinase/mammalian target of rapamycin inhibitor, elicits multifaceted antitumor activities in human gliomas. *Mol.Cancer Ther.* 8(8), 2204-2210 (2009).
89. Bendell JC, Rodon J, Burris HA *et al*: Phase I, dose-escalation study of BKM120, an oral pan-Class I PI3K inhibitor, in patients with advanced solid tumors. *J Clin Oncol* 30(3), 282-290 (2012).
90. Wen PY, Lee EQ, Reardon DA, Ligon KL, Alfred Yung WK: Current clinical development of PI3K pathway inhibitors in glioblastoma. *Neuro.Oncol* 14(7), 819-829 (2012).
91. Rodriguez-Viciana P, Tetsu O, Oda K, Okada J, Rauen K, McCormick F: Cancer targets in the Ras pathway. *Cold Spring Harb.Symp.Quant.Biol.* 70, 461-467 (2005).
92. Peyssonnaud C , Eychene A: The Raf/MEK/ERK pathway: new concepts of activation. *Biol. Cell* 93(1-2), 53-62 (2001).

93. See WL, Tan IL, Mukherjee J, Nicolaidis T, Pieper RO: Sensitivity of Glioblastomas to Clinically Available MEK Inhibitors Is Defined by Neurofibromin 1 Deficiency. *Cancer Res.* 72(13), 3350-3359 (2012).
94. Solit DB, Garraway LA, Pratilas CA *et al*: BRAF mutation predicts sensitivity to MEK inhibition. *Nature* 439(7074), 358-362 (2006).
95. Haura EB, Ricart AD, Larson TG *et al*: A phase II study of PD-0325901, an oral MEK inhibitor, in previously treated patients with advanced non-small cell lung cancer. *Clin Cancer Res.* 16(8), 2450-2457 (2010).
96. LoRusso PM, Krishnamurthi SS, Rinehart JJ *et al*: Phase I pharmacokinetic and pharmacodynamic study of the oral MAPK/ERK kinase inhibitor PD-0325901 in patients with advanced cancers. *Clin Cancer Res.* 16(6), 1924-1937 (2010).
97. Wiedemeyer WR, Dunn IF, Quayle SN *et al*: Pattern of retinoblastoma pathway inactivation dictates response to CDK4/6 inhibition in GBM. *Proc.Natl.Acad.Sci.U.S.A* 107(25), 11501-11506 (2010).
98. Michaud K, Solomon DA, Oermann E *et al*: Pharmacologic inhibition of cyclin-dependent kinases 4 and 6 arrests the growth of glioblastoma multiforme intracranial xenografts. *Cancer Res.* 70(8), 3228-3238 (2010).
99. Konecny GE, Winterhoff B, Kolarova T *et al*: Expression of p16 and retinoblastoma determines response to CDK4/6 inhibition in ovarian cancer. *Clin Cancer Res.* 17(6), 1591-1602 (2011).
100. Kemper EM, Leenders W, Kusters B *et al*: Development of luciferase tagged brain tumour models in mice for chemotherapy intervention studies. *Eur.J Cancer* 42(18), 3294-3303 (2006).
101. Schwartz GK, LoRusso PM, Dickson MA *et al*: Phase I study of PD 0332991, a cyclin-dependent kinase inhibitor, administered in 3-week cycles (Schedule 2/1). *Br.J Cancer* 104(12), 1862-1868 (2011).
102. Flaherty KT, LoRusso PM, Demichele A *et al*: Phase I, dose-escalation trial of the oral cyclin-dependent kinase 4/6 inhibitor PD 0332991, administered using a 21-day schedule in patients with advanced cancer. *Clin Cancer Res.* 18(2), 568-576 (2012).
103. Di NF, Arena S, Tabernero J *et al*: Deregulation of the PI3K and KRAS signaling pathways in human cancer cells determines their response to everolimus. *J Clin Invest* 120(8), 2858-2866 (2010).
104. Bihorel S, Camenisch G, Lemaire M, Scherrmann JM: Modulation of the brain distribution of imatinib and its metabolites in mice by valsopodar, zosuquidar and elacridar. *Pharm.Res.* 24(9), 1720-1728 (2007).
105. Sane R, Agarwal S, Elmquist WF: Brain distribution and bioavailability of elacridar after different routes of administration in the mouse. *Drug Metab Dispos.* 40(8), 1612-1619 (2012).
106. Oostendorp RL, Buckle T, Beijnen JH, van TO, Schellens JH: The effect of P-gp (Mdr1a/1b), BCRP (Bcrp1) and P-gp/BCRP inhibitors on the in vivo absorption, distribution, metabolism and excretion of imatinib. *Invest New Drugs* 27(1), 31-40 (2009).

107. Minocha M, Khurana V, Qin B, Pal D, Mitra AK: Co-administration strategy to enhance brain accumulation of vandetanib by modulating P-glycoprotein (P-gp/Abcb1) and breast cancer resistance protein (Bcrp1/Abcg2) mediated efflux with m-TOR inhibitors. *Int.J Pharm.* 434(1-2), 306-314 (2012).
108. Lee YJ, Kusahara H, Jonker JW, Schinkel AH, Sugiyama Y: Investigation of efflux transport of dehydroepiandrosterone sulfate and mitoxantrone at the mouse blood-brain barrier: a minor role of breast cancer resistance protein. *J Pharmacol.Exp.Ther.* 312(1), 44-52 (2005).
109. Breedveld P, Pluim D, Cipriani G *et al*: The effect of Bcrp1 (Abcg2) on the in vivo pharmacokinetics and brain penetration of imatinib mesylate (Gleevec): implications for the use of breast cancer resistance protein and P-glycoprotein inhibitors to enable the brain penetration of imatinib in patients. *Cancer Res.* 65(7), 2577-2582 (2005).
110. Agarwal S, Mittapalli RK, Zellmer DM *et al*: Active efflux of dasatinib from the brain limits efficacy against murine glioblastoma: broad implications for the clinical use of molecularly-targeted agents. *Mol.Cancer Ther.* (2012).
111. Purves D, Augustine GJ, Fitzpatrick D *et al*. Neuroscience. In: Sinauer Associates, 2008)



# CHAPTER 2

## ANALYTIC ASSAYS FOR TARGETED THERAPEUTICS



# Chapter 2.1

High-Performance Liquid Chromatography analysis of a novel small-molecule, anti-cancer drug, Palomid 529, in human and mouse plasma and in mouse tissue homogenates

Fan Lin, David Sherris, Jos H. Beijnen, Olaf Van Tellingen

## ABSTRACT

Palomid 529 (8-(1-Hydroxy-ethyl)-2-methoxy-3-(4-methoxy-benzyloxy)-benzo[c]chromen-6-one), is a novel non-steroidal small-molecule drug, which inhibits both mTORC1 and mTORC2 assembly, and elicits both anti-angiogenic and direct anti-tumor effects in vivo. We have developed and validated a sensitive and selective method for the quantification of Palomid 529 in human and mouse plasma and in a range of mouse tissue samples. Sample pretreatment involved liquid-liquid extraction with *tert*-butyl methyl ether yielding a recovery of >75%. Palomid 529 and the internal standard Palomid 545 were separated using a GraceSmart RP18 column (2.1×150mm) packed with 5 μm C-18 material and a mobile phase comprised of 50% (v/v) acetonitrile and 50% (v/v) water delivered at a flow rate of 0.2 ml/min, and were detected by UV absorbance at a wavelength of 315 nm. Within the linear range of the calibration curve (10 to 10,000 ng/ml), acceptable accuracy and precision was achieved for all tested matrices. The validation results show that the method was selective and reproducible. Palomid 529 was stable in plasma upon 3 repeated freeze-thaw cycles and during storage for up to 24 h at ambient temperature. However, pre-treated samples waiting for HPLC analyses need to be kept under dimmed light conditions at ambient temperature since a significant degradation of both Palomid 529 and Palomid 545 was observed when exposed to light. A pilot pharmacokinetic study in mice demonstrated the applicability of this method for pharmacokinetic purposes. Even at a low dose of 5.4 mg/kg this assay was still sensitive enough to determine the drug concentration in plasma samples obtained up to 24 h after administration.

**Keywords:** Palomid 529; Palomid 545; HPLC; mTOR inhibitor; photosensitivity



## INTRODUCTION

PI3K-mTOR signalling pathway plays a critical role in tumour development. Mutation of upstream genes in this signaling pathway results into hyperactivation of mammalian target of rapamycin complex-1 (mTORC1), a central regulator of cell growth, and in turn triggers on the protein synthesis which is essential for cell growth and survival [1-3]. Inhibition of mTOR complex1 by its natural inhibitor rapamycin or other rapalogs have shown clinical efficacy in a subset of cancers [4,5]. However, effect of rapamycin and current rapalogs is solely on the mTORC1 but not on the mTORC2 [6]. This can lead to a hyper-activation of the kinase AKT via inhibition on the mTORC1 negative feedback loop while not inhibiting the mTORC2 positive feedback to AKT [5, 7, 8]. Thus the antitumor potential of mTOR targeting in tumor may not been fully exploited. Recently, Palomid 529 (8-(1-Hydroxy-ethyl)-2-methoxy-3-(4-methoxy-benzyloxy)-benzo[c]chromen-6-one; Fig. 1 A), a nonsteroidal small molecular compound synthesized by modification of dibenzo[c]chromen-6-one antiestrogen derivatives has shown to be an inhibitor of both the mTORC1 and mTORC2 [9]. In vivo studies showed that Palomid 529 reduced angiogenesis, vascular permeability and tumor growth. In addition, Palomid 529 was reported for its ability to sensitize the effect of radiotherapy in prostate cancer by targeting on multiple pathways [10].

To assess the pharmacokinetic behavior of Palomid 529 in preclinical models and later in patients, a rapid, sensitive and selective method is required. In this article we report, for the first time, a reversed-phase high-performance liquid chromatographic assay for determination of the Palomid 529 levels in human and mouse plasma and in mouse tissue homogenates.

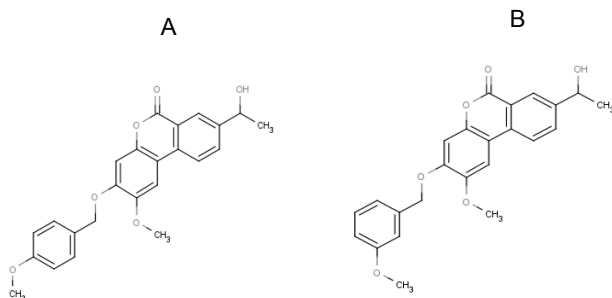


**Fig.1.** Structure of Palomid 529 and internal standard.

## EXPERIMENTAL

### *Materials and reagents*

Palomid 529 and Palomid 545 were provided by Paloma Pharmaceuticals Inc. (Jamaica Plain, MA, USA). Acetonitrile was purchased from Biosolve (Valkenswaard, The Netherlands). Water was purified by the Milli-Q Plus system (Millipore, Milford, USA). Drug-free human plasma was obtained from healthy donors from the Central Laboratory of the Blood Transfusion Service (Sanquin, Amsterdam, The Netherlands).

### *Instrumentation and Chromatographic Condition*

The chromatographic system consisted of a model SRD-3600 Solvent Racks (with in-line degasser), a model DGP-3600A pump, a model WPS-3000TSL autosampler (Dionex, Sunnyvale, CA, USA), and a model SF757 UV/VIS detector (Kratos, Ramsey, NJ, USA) operating at a wavelength of 315 nm. Some experiments were carried out using a UV-photodiode array (UV-PDA) detector (Waters, Milford, MA, USA). Chromatographic separations were performed using a stainless steel analytical GraceSmart RP18 column (2.1×150mm) packed with 5 µm C-18 material. A guard column holding an AJ0-A286 C18 cartridge (Phenomenex, Torrance, CA, USA) was installed in front of the column to protect it from retained impurities. The mobile phase was prepared by mixing 500 ml of acetonitrile with 500 ml Milli-Q water. The mobile phase was delivered at a flow rate of 0.2 ml/min. Peak detection and integration was performed with a Chromeleon data system version 6.8 (Dionex, Sunnyvale, CA, USA).

### *Collection of blank murine specimens.*

Mice were housed and handled according to institutional guidelines complying with Dutch legislation. Animals were kept in a temperature-controlled environment with a 12-hour light/12-hour dark cycle and received a standard diet (AM-II, Hope Farms, Woerden, The Netherlands) and acidified water *ad libitum*. Female FVB mice (9–15 weeks of age) were anesthetized with isoflurane flow and whole blood samples were obtained by cardiac puncture and collected in heparinized tubes. Next, the mice were killed by cervical dislocation and the following tissues were dissected: brain, liver, kidney, lung, spleen and heart. Blood was centrifuged (5 min, 14,000 rpm, 4°C) to separate the plasma fraction and both plasma and tissue samples were stored at –20°C. Frozen mouse tissues were thawed at 4°C and homogenized (Polytron PT1200, Kinematica AG, Littau,

Switzerland) in 1 % (w/v) bovine serum albumin (BSA) in water (3 ml for brain, liver, kidneys and 2 ml for other tissues, respectively). Homogenized samples were stored at -20°C until analysis.

#### *Drug stock solutions and internal standard*

Approximately 10 mg of Palomid 529 powder was accurately weighed and dissolved in dimethyl sulfoxide (DMSO) to yield a final concentration of 1.00 mg/ml. This stock solution was used to prepare a 10,000 ng/ml calibration stock standard in blank human plasma. Palomid 545, an analog of P529, was used as internal standard (IS) and 2.00 mg/ml Palomid 545 stock solution was prepared with the same methods described above for Palomid 529 stock solution. A working solution of IS was prepared in advance by 500-fold diluting the IS stock in acetonitrile-water (30:70, v/v), to yield a final concentration of 4,000 ng/ml Palomid 529. Calibration stock and IS stock solution were aliquoted and stored at -20 °C.

#### *Calibration standards and quality control samples.*

Fresh calibration standards 10, 20, 50, 100, 200, 500, 1,000, 2,000, 5,000, 10,000 ng/ml were prepared in blank human plasma for each analytical run in duplicate. Quality control samples in plasma were prepared by appropriate dilution of a stock solution in human plasma to final concentrations of 50 ng/ml, 500 ng/ml and 5,000 ng/ml and in mouse plasma to final concentrations of 50 ng/ml, 500 ng/ml and 5,000 ng/ml.

#### *Sample pretreatment.*

Liquid-liquid extraction principle was applied for Palomid 529 extraction from samples. A volume of 100 µl of plasma or tissue homogenate was pipetted into a 2 ml polypropylene tube (Eppendorf, Hamburg, Germany). Volumes of 50 µl of internal standard stock solution and 1 ml *tert*-butyl-methyl ether were added. After vigorously mixing for 5 minutes, the samples were centrifuged for 2 minutes at 14,000 rpm to separate the aqueous and organic layers. The aqueous layer was frozen by placing the vial in a dry ice/ethanol bath. The upper organic layer was decanted into a 1.5 ml micro tube (Brand, Wertheim, Germany). After evaporation in a Speed-Vac SC210A (Savant, Farmingdale, NY, USA) at 43 °C, the residue was reconstituted in 100 µl acetonitrile-water (30:70, v/v) by vigorous vortexing for 10 seconds and sonication for 5 minutes. The sample was then briefly vortexed again and centrifuged and placed in the HPLC autosampler.

*Assay validation.*

Validation of the assay including the determination of the linearity, precision, accuracy, selectivity, lower limit of quantification, recovery and stability were performed in human plasma and murine biological matrices (including plasma, brain, liver, kidney, lung, spleen and heart). The statistical analysis was done with the software package SPSS (SPSS Statistics Release 17.0, Chigago, IL, USA).

*Linearity and sensitivity.*

Calibration curves were calculated by linear regression analysis of the peak area ratios of Palomid 529 to IS versus the concentration of Palomid 529. We first established the most appropriate weight factor as  $1/x^2$  (reciprocal of the square of the concentration). The F-test for lack of fit ( $\alpha = 0.05$ ) was used to evaluate the linearity of the calibration curves.

*Precision and accuracy.*

To assess the accuracy, within-day precision and between-day precision of the assay, we performed replicate measurements of the quality control samples in human plasma in 50, 500, and 5,000 ng/ml in 3 different analytical runs. We also assessed the accuracy and within-day precision of the assay in murine matrices, namely, mouse plasma and tissue homogenates spiked with 200, 1,000, 5,000 ng/ml Palomid 529 in triplicate for each spiked concentration in one analytical run.

The between-groups mean square ( $MS_{\text{between-day}}$ ), within-groups mean square ( $MS_{\text{within-day}}$ ) and the grand mean (GM) of the observed concentrations across runs were calculated using SPSS. The Stand Deviation each run ( $SD_{\text{run}}$ ), BDP% (between-day precision) and the WDP% (within-day precision) were calculated using the formulas:

$SD_{\text{run}} = [(MS_{\text{between}} - MS_{\text{within}})/n]^{1/2}$  ( n represents the number of replicates within each run).

$$BDP\% = [SD_{\text{run}}/GM]*100\%$$

$$WDP\% = [(MS_{\text{within-day}}^{1/2})/GM]*100\%$$

The accuracy was expressed as the mean percentage deviation (%DEV) calculated by:

$$DEV\% = [(GM(\text{observed concentration} - \text{nominal concentration})/\text{nominal concentration})*100$$

Values within  $\pm 15\%$  for precision and accuracy were considered acceptable, except for concentrations at the lower limit of quantitation (LLQ), where 20% was accepted.

### *Selectivity.*

To assess the selectivity of the assay, drug-free human plasma from six healthy donors and mouse plasma and tissues from untreated mice were processed and analyzed to determine whether endogenous peaks co-eluted with Palomid 529 or the internal standard. We also checked for potential interferences by analyzing plasma samples from 30 randomly selected cancer patients. To further characterize the selectivity of this assay, we selected 14 commonly used medications, namely, acetylsalicylic acid, phenytoin, valproate, diazepam, warfarin, ondansetron, simvastatin, pravastatin, triamcinolone acetonide, buprenorphine, fentanyl, fluanisone, sildenafil, streptomycin and prepared them in acetonitrile-water (30:70, v/v) as test solutions (20 µg/ml). All prepared solutions were directly analyzed under the chromatographic condition described above.

### *Determination of the lower limit of quantification.*

Lower limit of quantitation was defined as the peak height that was five times larger than baseline signal-to-noise. To validate the LLQ, human and mouse plasma spiked with 2 different concentrations (5 and 10 ng/ml) of Palomid 529 was processed and analyzed. The LLQ was accepted when the deviation of accuracy (DEV%) and precision were within the ±20% range.

$$\text{DEV\%} = \left( \frac{|\text{GM}(\text{observed concentration}) - \text{GM}(\text{nominal concentration})|}{\text{nominal concentration}} \right) * 100$$

### *Stability.*

The stability of Palomid 529 and Palomid 545 (internal standard) was examined in human plasma and murine matrices subjected to 0-3 freeze-thaw cycles, and in acetonitrile-water (30:70, v/v) after sample pretreatment staying at room temperature for 0-24 hours. Furthermore, we examined the stability and photosensitivity of Palomid 529 and Palomid 545 in a longer duration up to 72 hours in 4 different conditions: in room temperature with or without light, in 4 °C without light, in -20 °C without light. Stability was assessed by comparing the Palomid 529 concentrations with those in freshly prepared and analyzed spiked samples.

### *Recovery.*

The recovery of sample pretreatment was calculated by comparing the peak area from spiked human plasma with those prepared from drug stock diluted in acetonitrile-water

(30:70, v/v) at the same concentrations. Six samples at low and high concentration (50 and 5,000 ng/ml) were analyzed.

#### *Long-term reproducibility*

We used this assay to analyze animal Palomid 529 pharmacokinetic samples after validation. Reproducibility was established taking the results of 10 runs over a period of about eight months. Inter-day and between-day precision were calculated using a one-way ANOVA test (see above) for the quality control samples assayed in triplicate at 3 concentrations of 5,000, 500 and 5 ng/ml within each analytical run.

#### *In vivo applicability.*

To demonstrate the applicability of this assay for preclinical pharmacokinetic study purposes, we analyzed a series of murine plasma samples from an in vivo experiment. Palomid 529 in micronized formulation was administered i.v. at a high dose of 54 mg/kg and a low dose of 5.4 mg/ml. Blood sampling from the tip of the tail was performed at time points: 30 minutes, 2, 4, 6, 12 and 24 hours from five FVB female mice (9–15 weeks of age) after administration. After tail sampling for 24 hours, the blood samples were processed and stored as described in the section *Collection of blank murine specimens*. For a more practical manipulation of the small sample volumes obtained from tail bleedings, the plasma samples were accurately weighed and mixed with 250 µl blank human plasma. Dilution factor for each sample was recorded and processed by the Chromeleon data system. Furthermore, the applicability of this assay for murine tissue homogenates was assessed. An FVB female mouse was sacrificed by cervical dislocation and brain, liver, kidney, lung, spleen and heart tissues were dissected after one hour intravenously administration of 54 mg/kg Palomid 529. Tissues collected were homogenized using a polytron (Polytron PT1200, Kinematica AG, Littau, Switzerland) in 1 % (w/v) bovine serum albumin (BSA) (3 ml for brain, liver, kidneys and 2 ml for other tissues, respectively). The homogenized samples were stored at –20°C until analysis.

## RESULTS AND DISCUSSION

### *Detection and Chromatography*

Ultraviolet and visible (UV absorbance) scanning between wavelengths ranging from 200 to 400 nm demonstrated 3 absorption maxima for Palomid 529 (Fig. 2). To reduce the impact of interfering substances that are present in biological specimens, we selected 315 nm as operating wavelength.

We tested several different columns and mobile phase conditions. We found that the relatively economic GraceSmart PR18 column (2.1×150mm) packed with 5 µm C-18 material combining with a flow of 0.2 ml/min acetonitrile-water (50:50, v/v) gave a satisfactory chromatographic profile for Palomid 529. Next, Palomid 545 was tested as candidate for internal standard because of its high structural similarity with Palomid 529 (Fig. 1 B). Under these conditions there is one-minute difference between the retention times of Palomid 529 and Palomid 545, yielding sufficient resolution between the two peaks even if the concentrations of Palomid 529 was low (Fig. 3. D). The peak areas of both Palomid 529 and Palomid 545 were comparable when injected at equal concentration, suggesting similar molar extinction coefficients. The peak resolution of P529 and P545 is about 2. From a series of calibration standard samples measured in an analytic run the peak resolution of P529 and P545 is  $2,113 \pm 0,046$  (calculated by Chromeleon data system).

### *Sample pretreatment*

Extraction using *tert*-butyl methyl ether was chosen for sample pretreatment after comparing several organic solvents. Mean extraction recoveries from spiked human plasma were 75% at low concentration (50 ng/ml) and 76.2% at high concentration (5,000 ng/ml). Furthermore, *tert*-butyl methyl ether extracted blank human and mouse plasma were free of endogenous substances that co-eluted with Palomid 529 or Palomid 545 (Fig. 3 A and B), as were all mouse tissue homogenates (data not shown). Representative chromatograms of all spiked tissue homogenates (brain, heart, kidney, liver, lung and spleen) are shown in Fig. 4. In addition, chromatograms of 30 randomly selected patients' plasma samples after extraction did not show peaks of exogenous substances interfering with Palomid 529 or Palomid 545. We further assessed the selectivity of this assay by testing 16 commonly used medications. No interference to Palomid 529 or Palomid 545

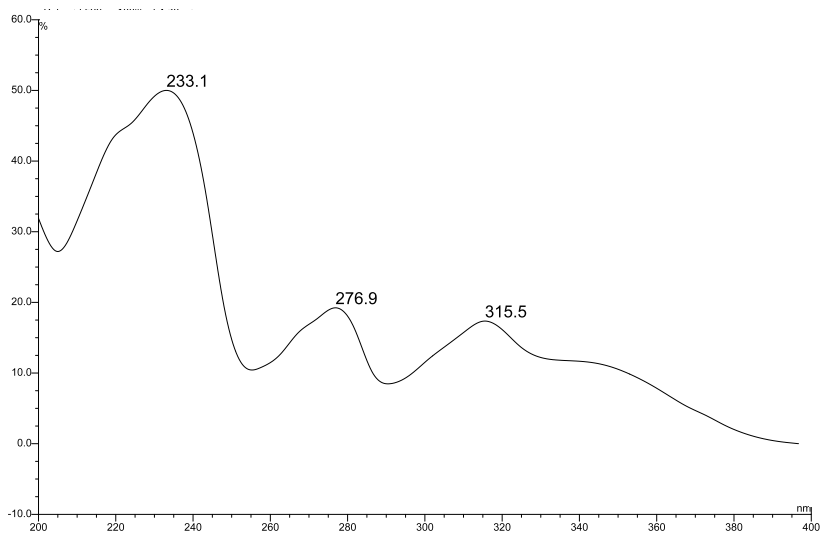


**Fig. 2.** UV spectrum of Palomid 529.

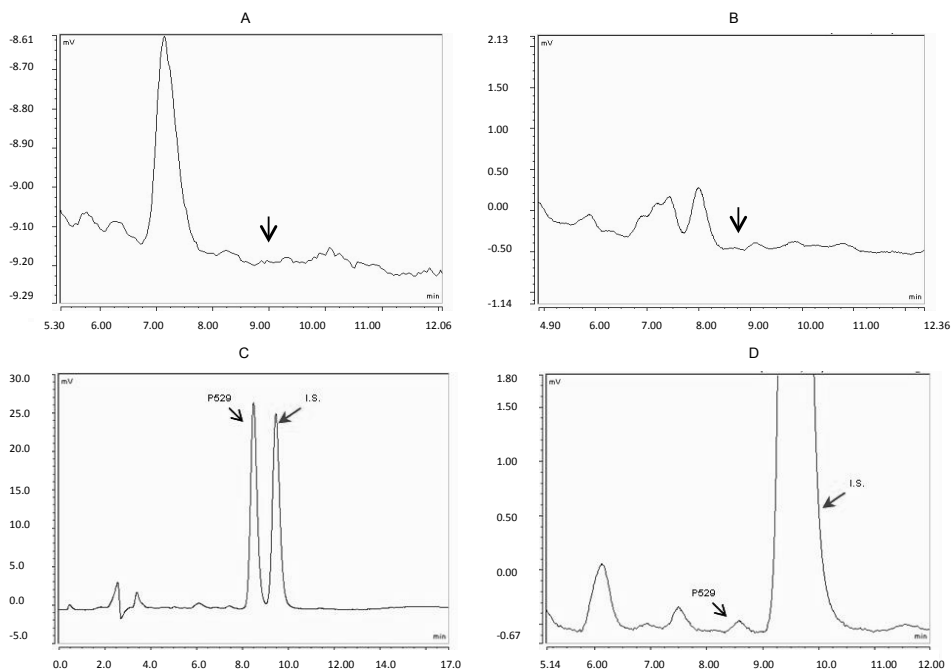


**Fig. 3.** Representative HPLC chromatograms for Palomid 529. HPLC chromatograms of A: blank human plasma and B: blank mouse plasma. C and D: Calibration standard of 2,000 ng/ml (C) and 10 ng/ml (D) spiked human plasma showing two elution peaks of Palomid 529 and Palomid 545 as internal standard. The black arrows indicate the Palomid 529 peaks or where Palomid 529 peak supposed to present at and the arrows indicate the Palomid 545 peaks.



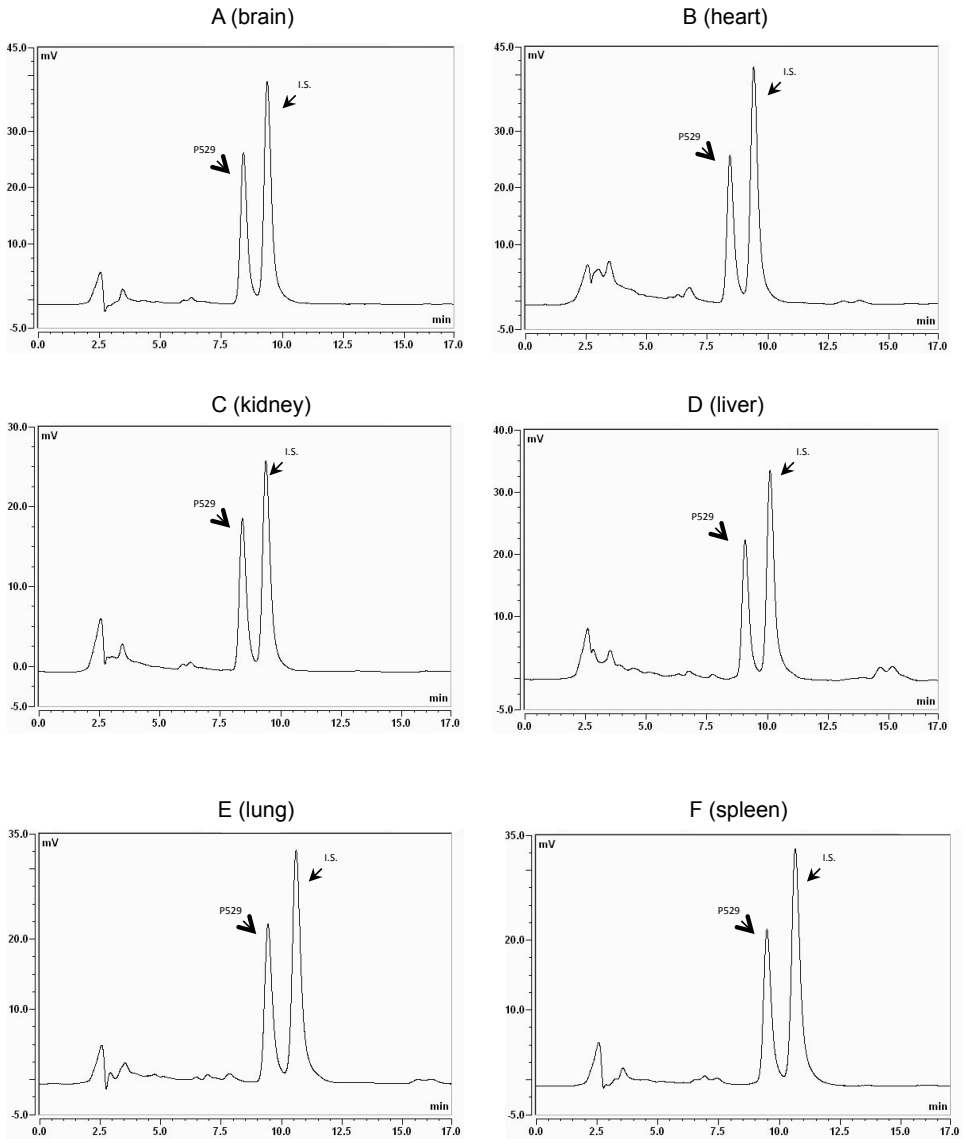


**Fig. 4.** Representative chromatograms of 1,000 ng/ml Palomid 529 spiked in 6 mouse tissue homogenates A: brain, B: heart, C: kidney, D: liver, E: lung, F: spleen. The black arrows indicate the Palomid 529 peaks or where Palomid 529 elutes and the arrows indicate the Palomid 545 peaks.

elution was observed from these substances, except for 20 µg/ml ondansetron which gave a distortion of the baseline from seven minutes onwards after injection. However, ondansetron was well separated from Palomid 529 and 545 when a human plasma spiked with a clinically relevant concentration (200 ng/ml) of ondansetron was extracted and analyzed using this assay. All together these observations suggest a good selectivity of this assay even when it is applied in clinical settings.

#### *Accuracy and precision*

The within-day and between-day precision and accuracy were analyzed using spiked blank human plasma assayed in three separate runs, as we used this matrix for preparing the calibration curve and it is available in relatively large quantities compared to matrices from laboratory animals such as mice. As Table 1 showed, the accuracy ranged from 96.8% to 103.8% and inter-day and between-day precision was ≤ 15.0%, thus fulfilling accepted criteria for accuracy and precision of a bioanalytical assay. We further assessed the accuracy and precision of this assay in mouse plasma and 6 mouse tissue homogenates spiked at 3 concentrations with Palomid 529 analyzed in a singular analytical run. Both the deviation of accuracy (DEV%) and precision were in an acceptable range, with the highest value in 1,000 ng/ml spiked heart homogenate but less than 15% (Table 2).

The LLQ was established by spiking blank human plasma with two low concentrations of Palomid 529: 5 ng/ml and 10 ng/ml. Only the accuracy and precision at 10 ng/ml met the requirement, making this the LLQ of the assay (Table 3). Calibration curves from 10 ng/ml to 10,000 ng/ml were linear based on linearity tests on three calibration curves obtained from three random analytical runs. The optimum weight factor for curve fitting was  $1/x^2$  (reciprocal of the square of the concentration).

#### *Long-term reproducibility.*

Accuracy, within-day precision, and between-day precision were determined for the triplicate quality control samples containing three concentrations of 5,000, 500 and 5 ng/ml from 10 analytical runs with a total time span around eight months. The quality control samples were freshly prepared and randomly inserted into each analytical run during the routine use of this assay. Repeatability, which is equivalent to within-day precision here of three concentrations 5,000, 500 and 5 ng/ml, was 5.3, 4.4 and 11.0%

Specimen	Nominal concentration (ng/ml)	Grand Mean	Accuracy(%)	Within-day precision (%)	Between-day precision (%)
Human plasma	5000	5000	100	3,9	4,0
	500	519	104	3,3	4,2
	50,0	48,4	96.8	10,4	9,6

**Table 1.** Accuracy, within-day precision, and between-day precision of P529 in blank human plasma using three concentrations used in quality control samples. Data was determined using three different analytical runs with triplicate samples assayed in each run.

Specimen	Nominal concentration (ng/ml)	Measured concentration (ng/ml)	Accuracy (%)	Within-day precision (%)
Mouse plasma	5000	5070	101,5	1,1
	1000	1080	108,1	1,0
	200	210	104,9	2,7
Human plasma	5000	5080	101,6	3,0
	1000	1120	112,0	3,4
	200	203	101,7	2,3
Brain	5000	5010	100,2	2,3
	1000	1030	102,8	1,9
	200	221	110,6	1,5
Liver	5000	4830	96,7	5,4
	1000	962	96,2	7,7
	200	212	105,9	4,9
Kidney	5000	5160	103,1	2,0
	1000	1030	102,6	1,4
	200	206	103,1	3,5
Lung	5000	4750	95,0	1,7
	1000	1030	102,5	1,7
	200	206	103,3	1,1
Spleen	5000	5070	101,4	2,4
	1000	1070	107,2	2,4
	200	202	101,3	3,8
Heart	5000	5060	101,2	8,4
	1000	891	89,1	11,4
	200	207	103,5	2,3

**Table 2.** Accuracy and within-day precision of P529 in murine matrices. Results presented were based on triplicate freshly prepared tissue homogenate samples spiked at three different concentrations.

Specimen	Nominal concentration (ng/ml)	Measured concentration (ng/ml)	Accuracy (%)	Within-day precision (%)
Human plasma	10,0	11,0	109,6	11,6
	5,00	9,02	180,4	7,1

**Table 3.** Validation and determination of the lower limit of quantification (LLQ). Accuracy and within-day precision were assessed in human plasma spiked at two low concentration: 5 and 10 ng/ml.

Specimen	Nominal concentration (ng/mL)	Cycle 0 (Mean±SD)	Cycle 3 (Mean±SD)	DEV% <sup>1</sup>	DEV% <sup>2</sup>
Human plasma (low)	100	104±3	96,5±7,1	-3,6	-7,5
Human plasma (high)	5000	4420±470	4550±80	-9,0	3,1
Mouse plasma	1000	1050±30	995±12	-0,5	-5,7
Brain	1000	985±2	963±49	-3,7	-2,2
Liver	1000	958±18	882±44	-11,8	-7,9
Kidney	1000	958±3	920±24	-8,0	-4,0
Lung	1000	1010±10	962±23	-3,8	-4,7
Spleen	1000	963±5	869±3	-13,1	-9,8
Heart	1000	989±8	932±15	-6,8	-5,8

**Table 4.** Freeze-thaw stability of P529 in spiked human and mouse matrices. The stability was expressed as the mean percentage deviation (DEV%).

1. DEV% was calculated as the difference between the observed concentration and the nominal concentration.  $DEV\%^1 = (\text{Cycle } 3_{\text{conc.}} - \text{Nominal}_{\text{conc.}}) / \text{Nominal}_{\text{conc.}}$
2. DEV% was calculated as the difference between the observed concentration and concentration of those freshly prepared and analyzed samples.  $DEV\%^2 = (\text{Cycle } 3_{\text{conc.}} - \text{Cycle } 0_{\text{conc.}}) / \text{Cycle } 0_{\text{conc.}}$

respectively. Reproducibility which is equivalent to between-day precision here was 1.1, 3.4 and 6.9%, respectively. These results were all in acceptable range (within 15%), suggesting both repeatability and reproducibility of this assay were acceptable for the tested concentrations range.

#### *Stability and photosensitivity*

We assessed the stability of the Palomid 529 in plasma after three freeze-thaw cycles and upon storage for 24 hour at room temperature. Comparing both the nominal concentration and the concentration of freshly prepared and analyzed samples to that of 3-cycle freeze-thawed samples, the deviations observed of all samples are less than 15% (Table 4). This demonstrates that the stability of Palomid 529 spiked in human plasma and mouse plasma and tissue homogenates is not affected by repeated freeze-thaw cycles. Concentrations of pretreated samples stored at room temperature for 24 hour also did not change notably (Table 5. All values were less than 15% except the liver homogenate sample). However, while we were using this assay for pharmacokinetic studies, we found a trend that most of the observed concentrations of QC samples that were in the autosampler for longer periods were slightly higher than those of freshly prepared and analyzed QC samples. As this trend can not be caused by an increase in the concentration of Palomid 529, we investigated the stability of the internal standard Palomid 545 in these pretreated samples.

For this purpose, we did a stability test for a longer duration under four different conditions. Table 6 shows that up to 3 days in the dark, the recovery of both Palomid 529 and Palomid 545 were acceptable independent from temperature. However, a marked degradation of Palomid 545 was observed in a condition with light after 72 hours, suggesting photosensitivity of this compound. Loss of Palomid 529 in samples exposed to light was also observed but the difference was not significant compared to the freshly analyzed samples. Apparently, Palomid 529 is also photosensitive but the photo degradation rate is slower than for Palomid 545. Together, a long-term exposure of pretreated samples under light could cause overestimation of Palomid 529 concentration using this assay. Consequently, samples should be stored protected from light following sample pretreatment.

#### *In vivo applicability*

To investigate the applicability of this assay *in vivo*, a relatively high dose of 54 mg/kg and low dose of 5.4 mg/kg were given to mice by i.v. injection. Even for the low dose, this assay was still sensitive enough to determine the drug concentration in plasma samples up to 24 h after administration (Fig. 5). In addition, we have collected brain, heart, liver, kidney, lung and spleen from an FVB mouse which received 54 mg/kg Palomid 529 intravenously and analyzed the tissue homogenates using this assay. No endogenous

Specimen	Nominal concentration (ng/mL)	0hr (Mean±SD)	RT 24 hr (Mean±SD)	DEV% <sup>1</sup>	DEV% <sup>2</sup>
Human plasma (low)	100	91,6±14,2	101±1	0,8	10,1
Human plasma (high)	5000	4580±110	4930±30	-1,5	7,6
Mouse plasma	1000	1010±10	1060±0	5,6	4,9
Brain	1000	920±34	1020±40	2,0	10,9
Liver	1000	966±66	1150±40	14,7	18,7
Kidney	1000	996±8	1090±100	8,7	9,1
Lung	1000	954±22	1030±30	3,0	8,0
Spleen	1000	923±9	981±6	-1,9	6,3
Heart	1000	956±6	978±63	-2,2	2,3

**Table 5.** Stability of P529 in spiked human and mouse matrices stored at room temperature. The stability was expressed as the mean percentage deviation (DEV%).

- DEV% was calculated as the difference between the observed concentration and the nominal concentration.  $DEV\%^1 = (24hr_{conc.} - Nominal_{conc.}) / Nominal_{conc.}$
- DEV% was calculated as the difference between the observed concentration and concentration of those freshly prepared and analyzed samples.  $DEV\%^2 = (24hr_{3_{conc.}} - 0hr_{conc.}) / Cycle 0_{conc.}$

500 ng/ml P529		P545 (Area <sup>1</sup> )	Recovery % <sup>2</sup>	Sig, (compare 0 hour)	P529 (Area <sup>1</sup> )	Recovery % <sup>2</sup>	Sig, (compare 0 hour)
0 hour	Reference	14,9±1,1			3,7±0,3		
72 hour	-20°C dark	14,9±0,0	99,7	0,940	3,8±0,0	102	0,653
	4°C dark	13,9±0,6	93,4	0,159	3,6±0,3	97,4	0,647
	RT dark	14,2±0,5	95,4	0,271	4,0±0,3	108	0,181
	RT light	10,6±0,6	71,3	0,001	3,3±0,3	89,6	0,152

**Table 6.** Stability of 500 ng/ml P529 spiked in human and mouse matrices stored in four different conditions for 72 hours.

- Area under the P529 peak were measured and compared.
- Recovery was expressed as the ratio of observed concentration versus concentration of freshly prepared and analyzed samples.

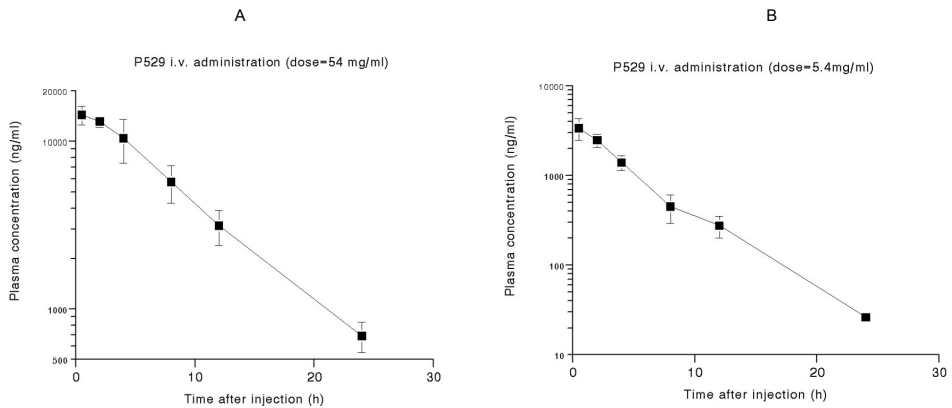


**Fig. 5.** Plasma concentration versus time curve from 0.5 to 24 hours after i.v. administration of A: 54 mg/ml; B: 5.4 mg/ml Palomid 529. Data are shown as the mean  $\pm$  SE, n=5.

interfering peaks have been observed in chromatograms of all tissue homogenates (Fig. 6). Therefore, this assay can be applied for the mouse, the most important preclinical model. Given the results of the validation in human plasma, we expect that the assay is also suitable for human pharmacokinetic studies.

### Acknowledgements

This project is supported by the foundation of The Netherlands Laboratory for Anticancer Drug Formulation (NLADF). We thank Mark de Gooijer for critical reading of the manuscript.

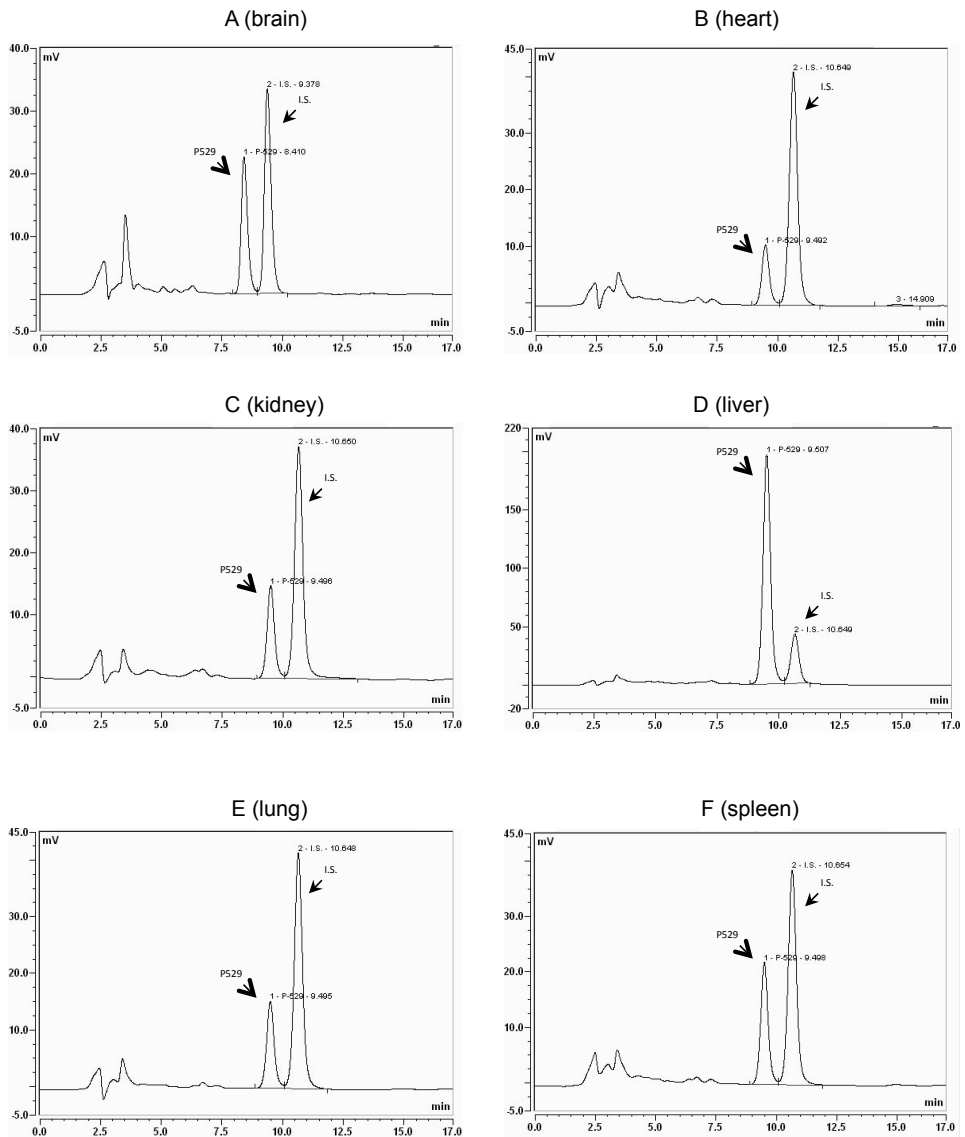


**Fig. 6.** Representative chromatograms of 6 mouse tissue homogenates obtained from an FVB mouse received 54 mg/kg Palomid 529 intravenously. The mouse was sacrificed one hour after administration and tissues were then collected. The black arrows indicate the Palomid 529 peaks or where Palomid 529 elutes and the arrows indicate the Palomid 545 peaks.



## Reference

- [1] B.Shor, J.J.Gibbons, R.T.Abraham and K.Yu, *Cell Cycle*, 8 (2009) 3831.
- [2] Y.Samuels, Z.Wang, A.Bardelli, N.Silliman, J.Ptak, S.Szabo, H.Yan, A.Gazdar, S.M.Powell, G.J.Riggins, J.K.Willson, S.Markowitz, K.W.Kinzler, B.Vogelstein and V.E.Velculescu, *Science*, 304 (2004) 554.
- [3] E.Petroulakis, Y.Mamane, O.Le Bacquer, D.Shahbazian and N.Sonenberg, *Br J Cancer*, 94 (2006) 195.
- [4] J.B.Easton and P.J.Houghton, *Oncogene*, 25 (2006) 6436.
- [5] R.T.Abraham and J.J.Gibbons, *Clin Cancer Res*, 13 (2007) 3109.
- [6] D.D.Sarbassov, D.A.Guertin, S.M.Ali and D.M.Sabatini, *Science*, 307 (2005) 1098.
- [7] T.L.Phung, G.Eyiah-Mensah, R.K.O'Donnell, R.Bieniek, S.Shechter, K.Walsh, C.Kuperwasser and L.E.Benjamin, *Cancer Res*, 67 (2007) 5070.
- [8] K.E.O'Reilly, F.Rojo, Q.B.She, D.Solit, G.B.Mills, D.Smith, H.Lane, F.Hofmann, D.J.Hicklin, D.L.Ludwig, J.Baselga and N.Rosen, *Cancer Res*, 66 (2006) 1500.
- [9] Q.Xue, B.Hopkins, C.Perruzzi, D.Udayakumar, D.Sherris and L.E.Benjamin, *Cancer Res*, 68 (2008) 9551.
- [10] R.Diaz, P.A.Nguewa, J.A.Diaz-Gonzalez, E.Hamel, O.Gonzalez-Moreno, R.Catena, D.Serrano, M.Redrado, D.Sherris and A.Calvo, *Br J Cancer*, 100 (2009) 932.



## Chapter 2.2

Determination of NVP-BEZ235, a dual PI3K and mTOR inhibitor, in human and mouse plasma and in mouse tissue homogenates by reversed-phase high-performance liquid chromatography with fluorescence detection

Fan Lin, Gayathri Chandrasekaran, Mark C. de Gooijer, Jos H. Beijnen,  
Olaf van Tellingen

## ABSTRACT

NVP-BEZ235 is a novel dual inhibitor of PI3K/mTOR and currently undergoing phase I/II clinical trials for advanced solid tumors. We developed a sensitive and selective reversed-phase high-performance liquid chromatographic (HPLC) assay with fluorometric detection for quantification of NVP-BEZ235 in biological matrices. Liquid-liquid extraction with tert-butyl methyl ether was used for sample pre-treatment, yielding a recovery of >84%. Chromatographic separation of NVP-BEZ235 and the internal standard (IS) NVP-BBD130 was achieved on a GraceSmart C-18 column by isocratic elution with a mobile phase which consisted of acetonitrile, methanol, and milliQ water adjusted with acetic acid to pH 3.7 (20:36:44, v/v/v). Fluorescence detection using excitation and emission wavelengths of 270 and 425nm, respectively, provided a selectivity and sensitivity allowing quantification down to 1 ng/ml in human plasma and linear calibration curves within a range of 1 to 1000 ng/ml.

The assay was validated for human plasma, mouse plasma and a range of tissues. The accuracy, within-day and between-day precision for all matrices were within the generally accepted 15% range. NVP-BEZ235 was stable for 72 h in pretreated samples in reconstitution mixture (acetonitrile-water (30:70, v/v)), but unstable in mouse tissue homogenates upon repeated freeze-thaw cycles or long term storage ( $\geq 24$  hrs) at room temperature. A pilot pharmacokinetic study in mice demonstrated the applicability of this method for pharmacokinetic purposes. Overall, this assay is suitable for the pharmacokinetic studies of NVP-BEZ235 in mice and in human plasma.

## INTRODUCTION

The phosphatidylinositol 3-kinase (PI3K)/Akt/mammalian target of rapamycin inhibitor (mTOR) pathway is frequently deregulated in human malignancies [1, 2]. The addiction of tumor cells on the oncogenic state of this pathway provides promising opportunities for anticancer therapeutic intervention. NVP-BE235, an imidazo[4,5-c]quinoline derivative (Fig. 1), efficiently blocks the dysfunctional activation of the PI3K/mTOR pathway in cellular and *in vivo* settings, thus inhibiting the growth and proliferation of various cancer cells. Compared to the earlier generation of PI3K/mTOR inhibitors, NVP-BE235 has a much better inhibition potency and specificity. Moreover, as a dual PI3K/mTOR inhibitor, NVP-BE235 has been reported to have a better antiproliferative activity than the combination of PI3K and mTOR inhibitor [3]. NVP-BE235 is currently in phase I/II clinical trials for breast cancer, renal cancer and advanced solid tumors, either as a single agent or in combination with paclitaxel, trastuzumab, BKM120 or BKM162 [4]. To support the clinical and preclinical studies with this targeted therapeutic drug, a bio-analytical method for determining NVP-BE235 levels is required. To date, only a very brief description of an HPLC-UV assay for NVP-BE235 without validation has been reported by Maira et al. [5]. Moreover, we found that UV absorption at 340 nm did not provide satisfactory sensitivity for this agent. Based on our finding that NVP-BE235 has excellent fluorescence properties we now present a novel validated bio-analytical assay for NVP-BE235 in human and mouse plasma and in mouse tissue homogenates.

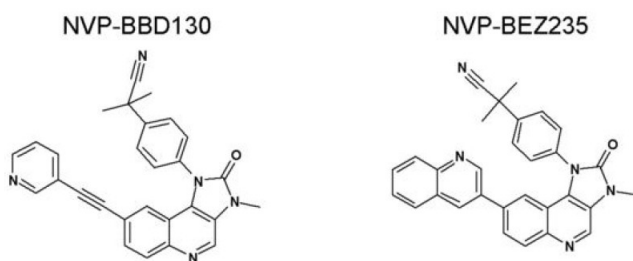


**Fig. 1.** Structures of NVP-BE235 and NVP-BBD130 (internal standard).

## EXPERIMENTAL

### Materials

#### *Materials and reagents*

NVP-BEZ235 was purchased from LC Laboratories (Woburn, USA). NVP-BBD130 was purchased from Axon Medchem (Groningen, The Netherlands). Acetonitrile originated from Biosolve (Valkenswaard, The Netherlands). Water was purified by the Milli-Q Plus system (Millipore, Milford, USA). Drug-free human plasma was obtained from healthy donors from the Central Laboratory of the Blood Transfusion Service (Sanquin, Amsterdam, The Netherlands). All other chemicals were purchased from Merck (Darmstadt, Germany).

### Experimental Procedures

#### *Instrumentation and Chromatographic Conditions*

The chromatographic system consisted of a model SRD-3600 Solvent Racks (with in-line degasser), a model DGP-3600A pump, a model WPS-3000TSL autosampler (Dionex, Sunnyvale, CA, USA), and a model FP-1520 fluorescence detector (Jasco, Hachioju City, Japan) operating at excitation and emission wavelengths 270 and 425 nm, respectively. Chromatographic separations were performed using a stainless steel analytical GraceSmart column (2.1×150mm) packed with 5 µm C-18 material, preceded by a guard column holding an AJ0-A286 C18 cartridge (Phenomenex, Torrance, CA, USA). The mobile phase consisted of acetonitrile, methanol, and milliQ water adjusted with glacial acetic acid to pH 3.7 (20:36:44, v/v/v). The mobile phase was delivered at a flow rate of 0.2 ml/min. Peak detection and integration was done with a Chromeleon data system version 6.8 (Dionex, Sunnyvale, CA, USA).

#### *Collection of blank murine specimens*

Experiments involving laboratory animals were approved by the animal experiment committee of the Netherlands Cancer Institute. Mice were housed and handled according to institutional guidelines complying with Dutch legislation. Animals were kept in a temperature-controlled environment with a 12-hour light/12-hour dark cycle and received a standard diet (AM-II, Hope Farms, Woerden, The Netherlands) and acidified water *ad libitum*. Female FVB mice (9–15 weeks of age) were anesthetized with isoflurane flow and whole blood samples obtained by cardiac puncture were collected

in heparinized tubes. Next, the mice were killed by cervical dislocation and the following tissues were dissected: brain, liver, kidney, lung, spleen and heart. Blood samples were centrifuged (5 min, 14,000 rpm, 4°C) to separate the plasma fraction and both plasma and tissue samples were stored at -20°C.

#### *Drug stock solutions and internal standard*

The analytes NVP-BEZ235 and NVP-BBD130 were dissolved in dimethyl sulfoxide (DMSO) to yield stock solutions with concentrations of 1.00 mg/ml. The NVP-BEZ235 stock solution was used to prepare a 10,000 ng/ml calibration stock standard in blank human plasma. The NVP-BBD130 stock solution was diluted in acetonitrile-water (30:70, v/v) to yield an internal standard (IS) working solution with concentration of 250 ng/ml. Calibration stock and IS working solution were aliquoted and stored at -20°C.

#### *Calibration standards and quality control samples.*

NVP-BEZ235 calibration standards with concentrations of 1, 2, 5, 10, 20, 50, 100, 200, 500, 1,000 ng/ml were prepared in blank human plasma for each analytical run in duplicate. Quality control (QC) samples in plasma were prepared by appropriate dilutions of an independently prepared stock solution in human and mouse plasma to final concentrations of 5 ng/ml, 50 ng/ml and 500 ng/ml. QC's were aliquoted and stored at -20°C.

#### *Sample pre-treatment*

Frozen mouse tissues were thawed at 4°C and homogenized (Polytron PT1200, Kinematica AG, Littau, Switzerland) in 1 % (w/v) bovine serum albumin (BSA) in water (3 ml for brain, liver, kidneys and 2 ml for other tissues, respectively). A volume of 50 µl of IS working solution and 1 ml *tert*-butyl-methyl ether was added to 100 µl plasma or tissue homogenate sample. After vigorously mixing for 5 min, the samples were centrifuged at 20,000 g for 2 min to separate the aqueous and organic layers. Next, the lower aqueous layer was frozen by placing the vial in a dry ice/ethanol bath and the upper organic layer was decanted into a 1.5 ml micro tube (Brand, Wertheim, Germany). The organic solvent was evaporated in a Speed-Vac SC210A (Savant, Farmingdale, NY, USA) at 43°C and the residue was reconstituted in 100 µl acetonitrile-water (30:70, v/v). After brief vortexing and sonication (5 min) the sample was transferred to an HPLC autosampler vial and a volume of 50 µl was injected into an HPLC system.

### *Selectivity*

To assess the selectivity of this analytical assay, drug-free human plasma from six healthy donors and mouse plasma and tissues (brain, liver, kidney, lung, spleen and heart) from untreated mice were processed and analyzed to determine whether endogenous peaks co-eluted with NVP-BEZ235 or the IS. To further characterize the selectivity of this assay, we selected 14 commonly used medications including acetylsalicylic acid, phenytoin, valproate, diazepam, warfarin, ondansetron, simvastatin, pravastatin, triamcinolone acetonide, buprenorphine, fentanyl, fluanisone, sildenafil, and streptomycin, prepared in acetonitrile-water (30:70, v/v) as test solutions (20 µg/ml). All prepared solutions were directly analyzed under the chromatographic condition described above.

### *Determination of the lower limit of quantification (LLQ)*

To determine the LLQ, human plasma spiked with 1, 2, 5 and 10 ng/ml of NVP-BEZ235 was processed and analyzed in 3-fold. The LLQ was accepted when the %DEV of samples with the lowest nominal concentration was within  $\pm 20\%$ .

### *Recovery of sample pre-treatment*

The recovery of the sample pre-treatment procedure was calculated by dividing the peak area of NVP-BEZ235 of spiked human plasma sample (5, 50, 500 ng/ml) with these of samples prepared from drug stock solution diluted in acetonitrile-water (30:70, v/v) at the same concentrations.

### *Linearity and sensitivity*

Calibration curves were calculated by weighted linear regression analysis of the peak area ratios of NVP-BEZ235-to-IS versus the concentration of NVP-BEZ235. We first established the most appropriate weight factor as  $1/x^2$  (reciprocal of the square of the concentration). The F-test for lack of fit ( $\alpha = 0.05$ ) was used to evaluate the linearity of the calibration curves.

### *Precision and accuracy*

To assess the accuracy, within-day precision and between-day precision of the assay, we performed replicate measurements of the QC samples in human plasma in 5, 50, and 500 ng/ml in six different analytical runs. We also assessed the accuracy and within-day



precision of the assay in murine matrices, namely, mouse plasma and tissue homogenates spiked with 5, 50, 500 ng/ml NVP-BEZ235 in triplicate for each spiked concentration in one analytical run.

The between-day (BDP) and within-day precision (WDP) was calculated by one-way analysis of variance (ANOVA) for each control sample using the software package SPSS for windows (version 17.0; SPSS, Chicago, IL, USA). The day of analytic runs performed was used as the classification variable. The between-groups mean square ( $MS_{\text{between-day}}$ ), within-groups mean square ( $MS_{\text{within-day}}$ ) and the grand mean (GM) of the observed concentrations across runs were used. The standard deviation of each run ( $SD_{\text{run}}$ ), BDP% (between-day precision) and the WDP% (within-day precision) were calculated using the following formulas:

$$SD_{\text{run}} = [(MS_{\text{between}} - MS_{\text{within}})/n]^{1/2}$$

(n represents the number of replicates within each run).

$$BDP\% = [SD_{\text{run}}/GM] * 100\%$$

$$WDP\% = [(MS_{\text{within-day}})^{1/2}/GM] * 100\%$$

The accuracy was calculated by dividing the observed concentration and the nominal concentration and multiplied by 100%. The mean percentage deviation (DEV%) was calculated by:

$$DEV\% = [(GM(\text{observed concentration} - \text{nominal concentration})/\text{nominal concentration}] * 100\%$$

Values within  $\pm 15\%$  for precision (BDP%, WDP%) and  $100 \pm 15\%$  for accuracy were considered acceptable, except for concentrations at the lower limit of quantitation (LLQ), where  $100 \pm 20\%$  for accuracy was accepted [6].

#### *Long-term reproducibility*

Reproducibility was further established taking the results of QC samples measured in five analytical runs that were performed for the analysis of study samples over a period of about three months. Within-day and between-day precisions were calculated as described based on the one-way ANOVA analysis of 50 and 500 ng/ml QC samples assayed in triplicate within each analytical run for five runs.

### *Stability of NVP-BEZ235*

We examined the stability of NVP-BEZ235 and NVP-BBD130 in pretreated plasma samples reconstituted in acetonitrile-water (30:70, v/v) to assess the appropriate storage conditions while waiting for injection. For this purpose, human plasma was spiked with 500 ng/ml of NVP-BEZ235 and pretreated. The reconstituted samples were pooled and, next, re-aliquoted in sets of triplicates that were analyzed after storage for 72 hours at: room temperature with ambient light, room temperature (dark), 4°C (dark) and at -20°C (dark).

The stabilities of NVP-BEZ235 and NVP-BBD130 were examined in human plasma samples spiked with 500 and 10 ng/ml of NVP-BEZ235, and murine plasma and tissues samples spiked with 500 ng/ml of NVP-BEZ235. These samples were subjected to 1 or 3 freeze-thaw cycles and analyzed in one run. In addition, the stability of NVP-BEZ235 in human plasma and murine plasma and tissues was checked in samples kept for 0, 4 or 24 hours at room temperature or for 4 hours at 4°C before analysis.

Moreover a similar set of pre-treated spiked plasma and tissue samples reconstituted in acetonitrile-water (30:70, v/v) were subjected to direct pre-treatment and analysis (t=0 hr) or kept at room temperature for an additional 24 hours prior to injection to confirm the stability of NVP-BEZ235 in pretreated tissue samples while waiting for injection.

### *In vivo applicability*

To assess the applicability of this assay for preclinical pharmacokinetic study purposes, we analyzed murine plasma and tissue samples from mice receiving NVP-BEZ235. A solution of 1 mg/ml of NVP-BEZ235 formulated in DMSO-PEG400 (1:4, v/v) was given orally to an FVB female mouse by oral gavage at dose of 10 mg/kg. After one hour, cardiac blood and brain, liver, kidney, lung, spleen and heart of this mouse were collected as described in the section "*Collection of blank murine specimens*". Plasma collection, tissue homogenization, sample storage and pre-treatment were executed as described.

## RESULTS AND DISCUSSION

### *Detection and Chromatography*

Ultraviolet (UV) and visible absorbance scanning between wavelengths ranging from 200 to 400 nm showed that NVP-BEZ235 has absorption maxima at wavelengths 220 and 270 nm. Since this is in the range where many endogenous compounds absorb UV light, we anticipated that it would be difficult to develop a selective assay using UV detection. We found, however, that NVP-BEZ235 also exhibits strong fluorescence properties, which markedly increased the selective capacity to separate NVP-BEZ235 from endogenous interferences in biological samples. An emission wavelength at 425 nm with excitation wavelength at 270 nm was found to be the optimal for detection.

Next, an appropriate column, mobile phase composition and IS for NVP-BEZ235 chromatographic separation were explored. NVP-BBD130 was selected as IS because of its structural similarity with NVP-BEZ235 (Fig. 1). After some round of optimization we established a mobile phase comprised of acetonitrile, methanol and water buffered with glacial acetic acid to pH 3.7 (20:36:44, v/v/v). This mobile phase could successfully separate NVP-BEZ235 and IS from some minor endogenous peaks found in blank plasma and tissue specimens using the relatively economic GraceSmart 5  $\mu$ m RP18 column (2.1 $\times$ 150mm). Under these conditions, the retention times of NVP-BEZ235 and IS were around 16 and 21 min, respectively. Next, we compared the sensitivity of fluorescence detection vs. UV detection. When using UV detection at a wavelength of 340 nm, the peak area of a sample containing 50 ng/ml of NVP-BEZ235 in acetonitrile-water (30:70, v/v) was 120-fold lower than by fluorescence detection. A concentration of 5 ng/ml of NVP-BEZ235 was below the detection limit of UV detection (Fig. 2) but still detectable by fluorescence.

### *Sample pre-treatment*

Liquid-liquid extraction of NVP-BEZ235 using *tert*-butyl methyl ether, yielded high recoveries, ranging from 84.3% to 94.7% for spiked human plasma containing 5, 50, 500 ng/ml NVP-BEZ235. In addition, *tert*-butyl methyl ether extracted blank human and mouse plasma were free of endogenous substances that co-eluted with NVP-BEZ235 or IS (Fig. 3A and B), as were all mouse tissue homogenates (data not shown). Representative chromatograms of all spiked tissue (brain, heart, kidney, liver, lung and

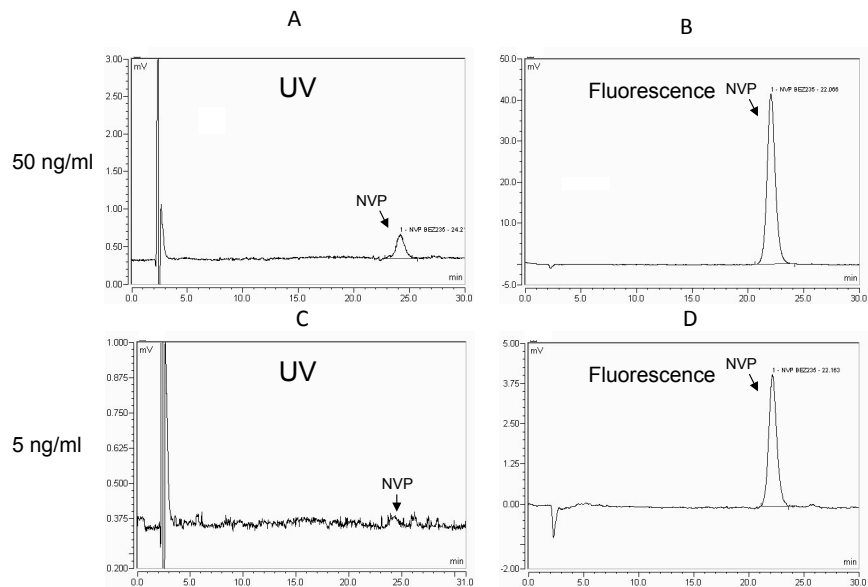


**Fig. 2.** HPLC chromatograms of 5 and 50 ng/ml NVP-BEZ235 dissolved in acetonitrile-water (30:70, v/v) and detected with UV detection (340 nm, A and C) and fluorescent detection (Ex: 270 nm; Em: 425 nm, B and D).

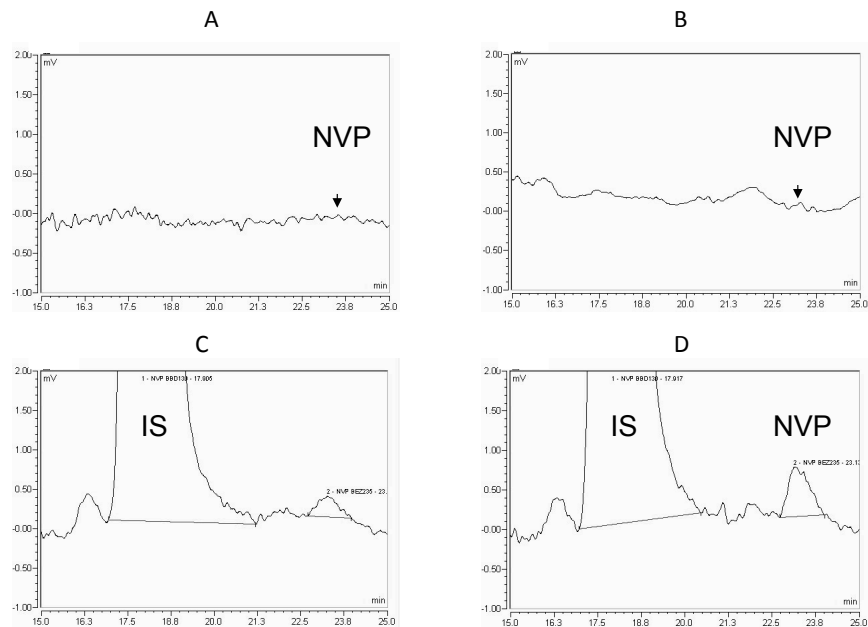


**Fig. 3.** Representative HPLC chromatograms of blank human plasma (A) and blank mouse plasma (B), human plasma spiked with 1 ng/ml (C) and 2 ng/ml of NVP-BEZ235 (D).

spleen) homogenates are shown in Fig. 4. We further assessed the selectivity of this assay by testing 14 commonly used medications. No interferences to NVP-BE2235 or IS elution were observed from above substances.

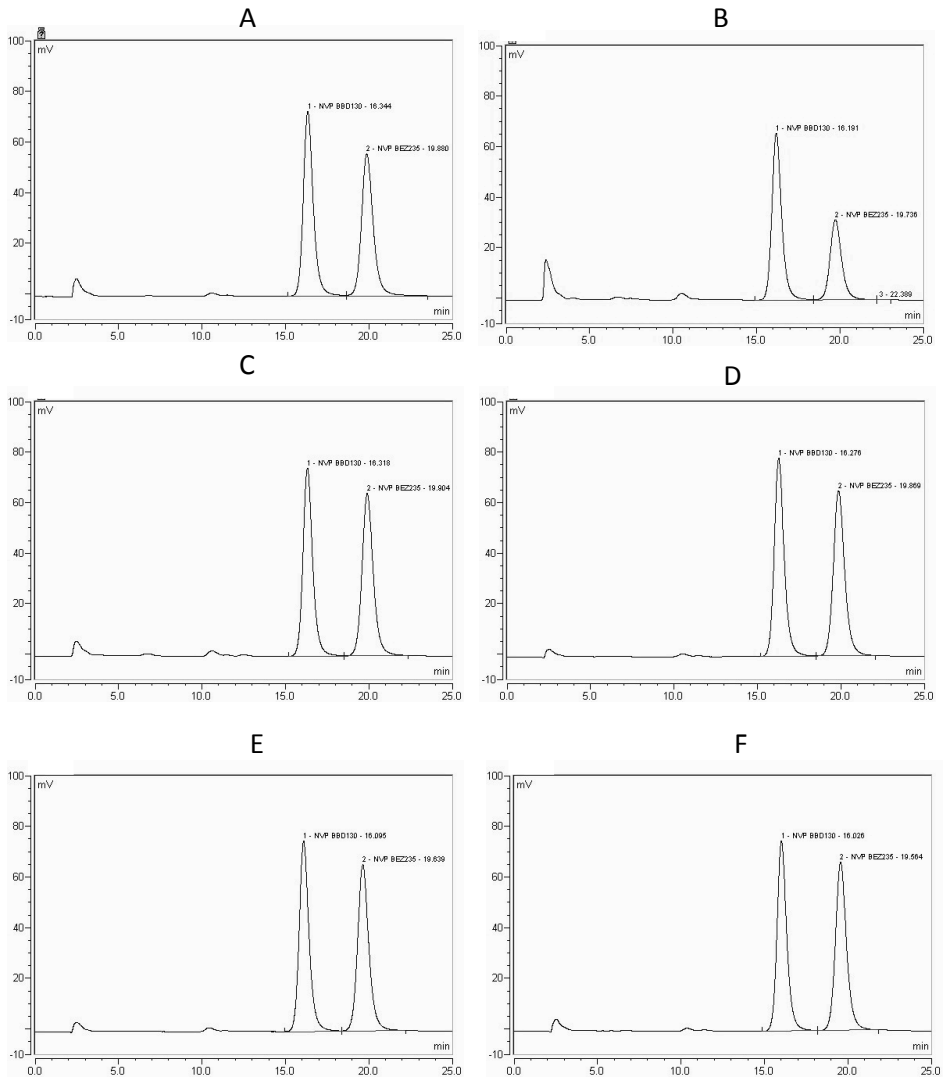


**Fig. 4.** Representative chromatograms of mouse tissue homogenates spiked with 50 ng/ml of NVP-BE2235. A: brain, B: liver, C: kidney, D: lung, E: spleen, F: heart.

### *Assay validation*

To establish the LLQ, we analyzed human plasma spiked at four levels of NVP-BEZ235: 1, 2, 5 and 10 ng/ml. The accuracy and precision of measurements at all these concentrations met the requirements (Table 1) and 1 ng/ml was accepted as the LLQ of this assay. The peak height of NVP-BEZ235 at 1 ng/ml was close to 5 times of that of noise level (Fig. 3 C and D)..

Calibration curves from 1 ng/ml to 1000 ng/ml were linear based on lack-of fit tests on three calibration curves obtained from three random analytical runs. The optimum weighting factor for curve fitting was  $1/x^2$  (reciprocal of the square of the concentration). The  $r^2$  of the calibration curves was always better than 0.99.

For assay validation, we determined the within-day and between-day precisions and accuracy of this analytical assay using spiked blank human plasma. As Table 2 shows, the accuracies were in the range of  $100\pm 15\%$  and within-day and between-day precisions were  $\leq 15.0\%$ , thus fulfilling accepted criteria for accuracy and precision of a bio-analytical assay. Next, the accuracy and precision of this assay were assessed in mouse and human plasma and in six mouse tissue homogenates spiked at three concentrations of NVP-BEZ235 and analyzed the same day in a singular analytical run. As a result, both the accuracy and precision were within the acceptable range, with the highest value in 5 ng/ml spiked kidney homogenate but still less than 15% (Table 3). All the above results of accuracy and precision were within the generally accepted ranges for bioanalytical assays [6].

To assess the reproducibility during routine use of this assay, results from the QC samples randomly inserted into five analytical run were analyzed. The repeatability, namely, the within-day precision of QC 500, and QC 50, was 5.8% and 3.8% respectively. The results of the ANOVA analysis indicated that no statistically significant additional variation was introduced when samples were measured in subsequent runs. Therefore, both repeatability and reproducibility of this assay were acceptable.

### *Drug stability*

We investigated the stability of NVP-BEZ235 and IS in pretreated samples kept under three different conditions, namely, room temperature with ambient light, room

Specimen	Nominal concentration (ng/ml)	Measured concentration (ng/ml)	Accuracy (%)	Within-run Precision (%)
Human plasma	10.0	10.4	104	5.11
	5.00	5.50	110	8.84
	2.00	1.87	93.6	6.62
	1.00	0.87	86.7	11.6

**Table 1.** Validation and determination of the lower limit of quantification (LLQ). Accuracy and within-day precision were assessed in human plasma spiked at four low concentrations: 1. 2. 5 and 10 ng/ml.

Specimen	Nominal concentration (ng/ml)	Grand Mean	Accuracy (%)	Within-day precision (%)	Between-day precision (%)
Human plasma	500	509	102	1.75	0.96
	50.0	51.2	102	1.66	0.47
	5.00	5.05	101	4.64	2.78

**Table 2.** Accuracy, within-day precision, and between-day precision of NVP-EZ235 in blank human plasma using three concentrations used in quality control samples. Data was determined using six different analytical runs with triplicate samples assayed in each run.

temperature in dark, 4 °C in dark for 72 hours. As a result, relative to the same samples analyzed immediately the peak areas of NVP-BEZ235 and IS from all sample groups were not different, confirming both of the two compounds are stable under these conditions. Daily laboratory analytical practice requires (repeated) freeze-thawing of samples and/or handling and storage of samples at room temperature for some time prior to analysis. To assess the stability of NVP-BEZ235 under these conditions, we analyzed NVP-BEZ235 spiked human plasma and murine matrices after one and three freeze-thaw cycles. The importance of such checks is demonstrated by the fact that freeze-thawing resulted in deviations that exceeded the acceptable range (Table 4). Although still within the acceptable  $\pm 15\%$  range, even after one freeze-thaw cycle the concentration in the homogenates was already considerably below the nominal value. After three freeze-thaw cycles, only plasma (human and mouse) and brain were within the acceptable range,

Specimen	Nominal concentration (ng/ml)	Measured concentration (ng/ml)	Accuracy (%)	Within-day Precision (%)
Human plasma	5	5.37	107	3.28
	50	49.7	99.4	2.68
	500	509	102	3.29
Mouse plasma	5	5.13	103	5.09
	50	51.2	102	5.78
	500	527	105	1.94
Brain	5	5.29	106	3.71
	50	53.4	107	10.2
	500	542	108	5.04
Liver	5	4.89	97.8	5.88
	50	52.1	104	0.89
	500	520	104	2.30
Kidney	5	5.32	106	13.9
	50	53.6	107	3.27
	500	487	97.3	9.66
Lung	5	5.36	107	3.54
	50	51.2	102	4.45
	500	513	103	3.14
Spleen	5	5.21	104	10.7
	50	52.4	105	0.96
	500	531	106	3.95
Heart	5	5.28	106	3.65
	50	53.5	107	0.36
	500	518	104	6.71

**Table 3.** Accuracy and within-day precision of NVP-BEZ235 in murine matrices. Results presented were based on triplicate freshly prepared tissue homogenate samples spiked at three different concentrations.



Specimen	Nominal concentration (ng/ml)	Measured concentration (ng/ml)		DEV <sup>1</sup> (%)	DEV <sup>1</sup> (%)
		Cycle 1 (Mean±SD)	Cycle 3 (Mean±SD)		
Human plasma (high)	500	458 ± 49	480 ± 22	-8.5	-4.0
Human plasma (low)	10.0	9.60 ± 0.10	9.66 ± 0.37	-4.0	-3.4
Mouse plasma	500	496 ± 75	523 ± 180	-0.9	4.7
Brain	500	434 ± 79	529 ± 76	-13.2	5.7
Liver	500	426 ± 22	346 ± 86	-14.8	-30.7
Kidney	500	428 ± 44	344 ± 15	-14.5	-42.3
Lung	500	463 ± 76	289 ± 19	-7.5	-31.3
Spleen	500	501 ± 56	307 ± 11	0.2	-38.6
Heart	500	517 ± 61	251 ± 44	3.5	-49.8

**Table 4.** Freeze-thaw stability of NVP-BEZ235 in spiked human and mouse matrices in triplicate. The stability was expressed as the mean percentage deviation (DEV%).

1. **DEV<sup>1</sup> (%)** was calculated as the difference between the concentration of the observed concentration and the nominal concentration.  $DEV\%^1 = \frac{(\text{Observed}_{\text{conc.}} - \text{Nominal}_{\text{conc.}})}{\text{Nominal}_{\text{conc.}}}$

whereas the levels in liver, kidney, lung, spleen and heart were reduced by 30% or more. No additional peaks emerged in the chromatograms. Thus, NVP-BEZ235 appears to be unstable in mouse tissue homogenates upon repeated free-thaw cycles. The reason for this instability in tissue homogenates is not clear, but we have observed similar results with topotecan in heart homogenates [7]. Obviously, repeated freeze-thawing should be avoided by storing aliquots for one-time use rather than storing the sample as a whole.

To assess whether drug degradation also happens during handling for sample pre-treatment, we further tested the stability of NVP-BEZ235 in bio-matrices stored at 4 °C or room temperature for long or short durations prior to analysis. As shown in Table 5, all samples stored both at 4 °C and in room temperature for 4 hours did not show substantial decay of the NVP-BEZ235 level with all deviations within the acceptable ranges, though a trend towards declining drug concentrations in tissue homogenate

samples stored at room temperature was noted. However, at 24 hour, kidney, lung and heart homogenate samples stored at room temperature showed unacceptable loss of NVP-BEZ235. Consequently, these stability issues demand that samples should be kept on ice during handling to prevent unacceptable degradation.

In line with the finding that NVP-BEZ235 is stable in pretreated plasma samples we also found that NVP-BEZ235 was stable in pretreated tissue samples while waiting for injection into the HPLC system. Leaving these samples at room temperature for an additional 24h did not notably change the observed concentration. (Table 5). Thus, the instability of NVP-BEZ235 in tissue homogenates might be due to degradation catalyzed by enzymes or other factors present in murine tissues but not due to chemical instability.

Specimen	Nominal concentration (ng/ml)	Measured concentration (ng/ml)				DEV <sup>1</sup> (%)		DEV <sup>2</sup> (%)	
		T=0 hr	T=4 hr 4 °C	T=4 hr RT	T=24 hr RT	T=0 hr	T=4 hr 4 °C	T=4 hr RT	T=24 hr RT
Human plasma (high)	500	578±10	538±12	545±8	582±6	15.65	-7.0	-5.7	0.7
Human plasma (low)	10.0	11.2±0.3	10.7±0.1	10.9±0.5	11.3±0.4	12.17	-4.9	-2.9	1.0
Mouse plasma	500	578±10	542±8	546±13	549±11	10.48	-1.9	-1.2	-0.7
Brain	500	526±1	516±7	540±4	533±31	5.27	-2.1	2.6	1.3
Liver	500	487±13	496±8	435±5	448±56	-2.57	1.9	-10.7	-8.0
Kidney	500	512±21	490±7	489±10	363±24	2.42	-4.3	-4.5	-29.0
Lung	500	531±6	516±13	470±2	361±10	6.19	-2.8	-11.6	-32.0
Spleen	500	550±12	538±7	540±21	534±9	10.06	-2.3	-1.9	-3.0
Heart	500	517±61	471±19	440±22	364±62	3.48	-9.0	-14.9	-29.6

**Table 5.** Stability of NVP-BEZ235 in spiked human and mouse matrices in triplicate stored at 4 °C for 4 hr, or at room temperature for 4 and 24 hr. The stability was expressed as the mean percentage deviation (DEV%).

1. **DEV<sup>1</sup> (%)** was calculated as the difference between the concentration of those freshly prepared and analyzed samples and the nominal concentration.  $DEV^1 = (0 \text{ hr}_{\text{conc.}} - \text{Nominal}_{\text{conc.}}) / \text{Nominal}_{\text{conc.}}$
2. **DEV<sup>2</sup> (%)** was calculated as the difference between the observed concentration and concentration of those freshly prepared and analyzed samples.  $DEV^2 = (4 \text{ or } 24 \text{ hr}_{\text{conc.}} - 0 \text{ hr}_{\text{conc.}}) / 0 \text{ hr}_{\text{conc.}}$

*In vivo applicability*

To test the applicability of this assay *in vivo*, we analyzed brain, liver, kidney, lung, spleen, heart and plasma samples from an FVB mouse which received 10 mg/kg NVP-BEZ235 orally. No endogenous interfering peaks have been observed in chromatograms of plasma and all tissue homogenates (Fig. 5). The concentrations of NVP-BEZ235 of all samples were within the dynamic range of the calibration curve.

In conclusion, we have developed and validated a sensitive and selective fluorometric HPLC method to quantify the levels of NVP-BEZ235 in human plasma and mouse plasma and tissue homogenates. We observed that the stability of NVP-BEZ235 in mouse tissues brain, liver, kidney, lung, spleen and heart can be compromised by repeated freeze-thaw cycles and by storage at room temperature for several hours, indicating that frequent freeze-thaw cycles should be avoided during storage, and pre-treatment or handling of these samples should be performed at 4 °C. Given the results of the validations in human plasma and mouse matrices, this assay is expected to be suitable for preclinical and clinical pharmacokinetic studies.

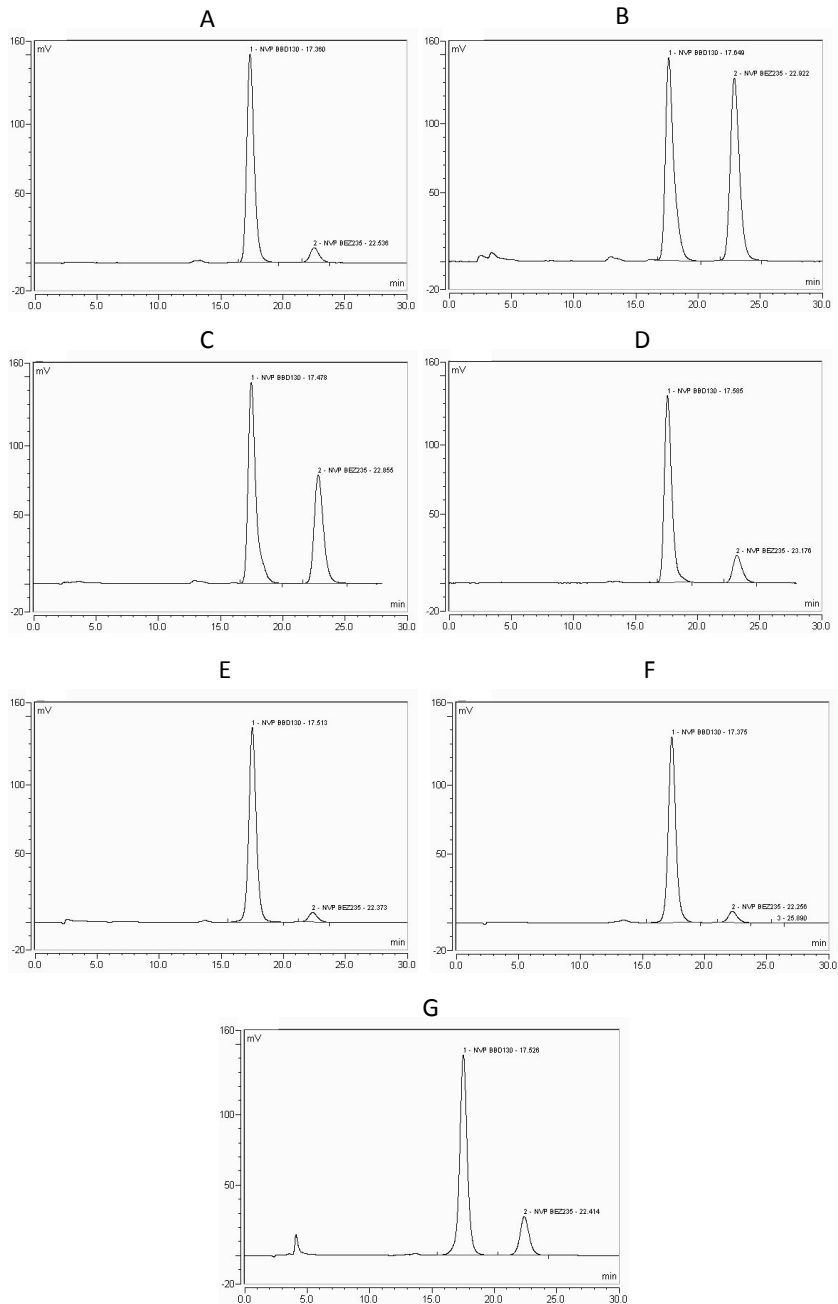


**Fig. 5.** Representative chromatograms of mouse tissue homogenates obtained from an FVB mouse receiving 10 mg/kg of NVP-BE2235 orally. The mouse was sacrificed one hour after administration and plasma and tissues were collected. A: brain, B: liver, C: kidney, D: lung, E: spleen, F: heart, G: plasma.

Specimen	Nominal concentration (ng/mL)	Measured concentration (ng/ml)		DEV <sup>1</sup> (%)	DEV <sup>2</sup> (%)
		t=0 hr (Mean±SD)	t=24 hr (Mean±SD)		
Human plasma (high)	500	502 ± 19	532 ± 42	0.3	6.0
Human plasma (low)	10.0	10.2 ± 2.3	9.83 ± 1.28	1.8	-3.4
Mouse plasma	500	467 ± 10	454 ± 4	-6.7	-2.7
Brain	500	433 ± 60	475 ± 74	-13.5	9.7
Liver	500	460 ± 17	476 ± 31	-7.9	3.4
Kidney	500	450 ± 44	465 ± 64	-10.1	3.4
Lung	500	434 ± 34	435 ± 10	-13.3	0.3
Spleen	500	469 ± 72	498 ± 69	-6.13	6.16
Heart	500	441 ± 37	422 ± 18	-11.8	-4.2

**Table 6.** Stability of NVP-BEZ235 in spiked human and mouse matrices after pretreatment stored at room temperature for 24 hours. The stability was expressed as the mean percentage deviation (DEV%).

1. **DEV<sup>1</sup> (%)** was calculated as the difference between the concentration of those freshly prepared and analyzed samples and the nominal concentration.  $DEV\%^1 = (0hr_{conc.} - Nominal_{conc.}) / Nominal_{conc.}$
2. **DEV<sup>2</sup> (%)** was calculated as the difference between the observed concentration and concentration of those freshly prepared and analyzed samples.  $DEV\%^2 = (24hr_{conc.} - 0hr_{conc.}) / 0hr_{conc.}$

## Reference List

- [1] J.A.Engelman, J.Luo and L.C.Cantley, *Nat Rev Genet*, 7 (2006) 606.
- [2] K.Inoki, M.N.Corradetti and K.L.Guan, *Nat Genet*, 37 (2005) 19.
- [3] R.Marone, D.Erhart, A.C.Mertz, T.Bohnacker, C.Schnell, V.Cmiljanovic, F.Stauffer, C.Garcia-Echeverria, B.Giese, S.M.Maira and M.P.Wymann, *Mol Cancer Res*, 7 (2009) 601.
- [4] D.Benjamin, M.Colombi, C.Moroni and M.N.Hall, *Nat Rev Drug Discov*, 10 (2011) 868.
- [5] S.M.Maira, F.Stauffer, J.Brueggen, P.Furet, C.Schnell, C.Fritsch, S.Brachmann, P.Chene, P.A.De, K.Schoemaker, D.Fabbro, D.Gabriel, M.Simonen, L.Murphy, P.Finan, W.Sellers and C.Garcia-Echeverria, *Mol Cancer Ther*, 7 (2008) 1851.
- [6] V.P.Shah, K.K.Midha, J.W.Findlay, H.M.Hill, J.D.Hulse, I.J.McGilveray, G.McKay, K.J.Miller, R.N.Patnaik, M.L.Powell, A.Tonelli, C.T.Viswanathan and A.Yacobi, *Pharm Res*, 17 (2000) 1551.
- [7] N.A.de Vries, M.Ouwehand, T.Buckle, J.H.Beijnen and O.van Tellingen, *Biomed Chromatogr*, 21 (2007) 1191.

# **CHAPTER 3**

## **PHARMACOKINETICS AND THERAPEUTIC EFFECTS OF TARGETED THERAPIES IN MALIGNANT GLIOMAS**





# Chapter 3.1

Dual mTORC1 and mTORC2 inhibitor Palomid 529 penetrates the Blood-Brain Barrier without restriction by ABCB1 and ABCG2

Fan Lin, Levi Buil, David Sherris, Jos H. Beijnen, and Olaf van Tellingen

International Journal of Cancer, 2013, In press

## ABSTRACT

Palomid 529, a novel dual mTORC1/2 inhibitor has displayed interesting activities in experimental models and is a candidate for clinical evaluation. We have assessed the interaction of Palomid 529 with ATP-binding cassette (ABC) drug efflux transporters ABCB1 (P-gp/P-glycoprotein) and ABCG2 (BCRP/Breast Cancer Resistant Protein) by *in vitro* transwell assays, and their effects on the brain penetration using drug disposition analysis of i.v. and oral Palomid 529 in wild-type (WT) and Abcb1 and/or Abcg2 knockout (KO) mice. Palomid 529 lacked affinity for these transporters *in vitro*, in contrast to GDC-0941, a small molecule PI3K inhibitor, which we used as control substance for *in vitro* transport. The plasma AUC<sub>i.v.</sub> of micronized and DMSO formulated Palomid 529 was similar in WT and KO mice. Importantly, the brain and brain tumor concentration of Palomid 529 at a high dose (54 mg/kg) was also similar in both strains, whereas a less than 1.4-fold difference ( $p < 0.05$ ) was found at the low (5.4 mg/kg) dose. Due to poor solubility, the oral bioavailability of micronized Palomid 529 was only 5%. Olive oil or spray-dried formulation greatly improved the bioavailability up to 50%. Finally, Palomid 529 effectively inhibits the orthotopic U87 glioblastoma growth. In summary, Palomid 529 is the first mTOR targeting drug lacking affinity for ABCB1/ABCG2 and having good brain penetration. This warrants further evaluation of Palomid 529 for treatment of high-grade gliomas and other intracranial malignancies.

## INTRODUCTION

The oncogenic activation of the phosphatidylinositol 3-kinase (PI3K)/AKT/mammalian target of rapamycin (mTOR) pathway is considered to be crucial for tumorigenesis and tumor development in most cancer types (1-3). This is also the case for glioblastoma multiforme (GBM), the most common and lethal primary central nervous tumor. In GBM, activation of this pathway occurs by amplification and/or mutation of EGFR gene, mutation and/or deletion of the PTEN gene and mutations of the PIK3CA gene (rare cases) (4). Taken together, activation of the PI3K-mTOR pathway takes place in up to 82% of patients (5). Recently, several major components in this pathway have shown to be promising targets for small molecular inhibitors. In particular, mTORC2 may have a special role in promoting GBM growth or mediating chemotherapy resistance (6). Palomid 529 (8-(1-Hydroxy-ethyl)-2-methoxy-3-(4-methoxy-benzyloxy)-benzo[c]chromen-6-one;) markedly reduces the phosphorylation of Akt (S473-Akt) signaling through inhibition of both mTOR-raptor and mTOR-riCTOR association and accordingly inhibits the mTORC1 and mTORC2 activity. *In vivo* studies showed that Palomid 529 reduced angiogenesis, vascular permeability and tumor growth (7). Moreover, it has been reported that Palomid 529 enhances the anti-proliferative effect of radiotherapy in glioblastoma in an orthotopic model (8) as well as in prostate tumor models (9), and more recently, this dual mTORC1 and mTORC2 inhibitor has exhibited its effect to sensitize the chemotherapy in hormone refractory prostate tumors (10).

The brain is a pharmacological sanctuary site due to the inability of many drugs to cross the blood-brain barrier (BBB) in a therapeutic meaningful dose. The BBB is formed by the brain micro-vascular endothelial cells that are closely linked by tight-junctions, lack fenestrations and exhibit low pinocytotic activity (11). Consequently, the entry of substances into the brain requires trans-endothelial trafficking, which is tightly regulated by a set of influx transporters (*e.g.* Glut1 for glucose). BBB penetration of agents that lack such an influx carrier is contingent on passive diffusion, which depends on the lipophilicity of the compound (12). However, even lipophilic substances may not reach into the brain as a further obstacle to BBB penetration is mediated by a set of ATP-binding cassette (ABC) drug efflux transporters that are expressed at the luminal side of the brain micro-vascular endothelial cells. In particular, ABCB1 (P-glycoprotein, P-gp, Mdr1) and ABCG2 (Breast Cancer Resistance Protein, BCRP), two dominant drug efflux

transporters highly expressed at the murine and human BBB, are known to limit brain accumulation of many lipophilic anti-cancer agents as well as small molecule inhibitors (13-15). Although brain tumors tend to cause a disruption of the BBB, it remains a major obstacle as this disruption occurs only in a part of the tumor and in particular many cells that have invaded into the normal surrounding brain are far away from this leaky area (11). Palomid 529 is a lipophilic substance, but whether it is a substrate for the ABC-transporters and if these would impede the drug delivery of Palomid 529 to the brain is yet unknown. In this study, we have explored the pharmacokinetic properties of this compound. We have assessed the affinity of Palomid 529 for ABCB1 and ABCG2, which are implicated in drug-drug interactions and drug resistance and that are known to limit the oral bioavailability and brain penetration of substrate drugs. Our results from both *in vitro* and *in vivo* models clearly suggest that unlike most of anti-cancer drugs, the interactions of Palomid 529 and ABCB1 or ABCG2 are minimal and that they do not restrict the brain penetration of Palomid 529.

## MATERIALS AND METHODS

### *Reagents*

Palomid 529 (MW=406.4) was provided by Paloma Pharmaceuticals Inc. (Jamaica Plain, MA USA) and was received as a micronized formulation suspended in Alcon Balanced Salt Solution containing 0.2% tyloxapol (prepared by AMRI, Burlington, MA), as a spray dried formulation (prepared by Bend Research, Bend, OR, USA) and as pure (>98% purity) powder. GDC-0941 (MW=513.2) was purchased from Chemdea (Ridgewood, NJ, USA). Modified Eagles medium (MEM), L-glutamine, non-essential amino acids, MEM vitamins penicillin-streptomycin, fetal calf serum, trypsin-EDTA and other reagents for cell culture were purchased from Invitrogen (Invitrogen Corporation, Carlsbad, CA, USA). Blank human plasma was obtained from healthy donors from the Central Laboratory of the blood Transfusion Service (Sanquin, Amsterdam, The Netherlands). All other chemicals were purchased from Merck (Darmstadt, Germany).

### *Drug analytical method*

A high-performance liquid chromatography assay was developed and validated for the quantification of Palomid 529 in human and mouse plasma and in mouse tissue samples for the *in vivo* pharmacokinetic studies (16). In short, sample pretreatment involved liquid-liquid extraction with *tert*-butyl methyl ether. Palomid 529 and the internal standard Palomid 545 were chromatographically separated using a GraceSmart 5  $\mu$ m RP18 column (2.1 $\times$ 150mm) and a mobile phase comprised of 50% (v/v) acetonitrile and 50% (v/v) milliQ water delivered at a flow speed 0.2 ml/min and were detected by a UV detector set at a wavelength of 315 nm.

### *In vitro transport experiments*

The parental LLC pig-kidney cell line (LLC-PK1) and sub-lines transduced with murine Abcb1a (LLC-Mdr1a) or human ABCB1 (LLC-MDR1) were used to determine whether Palomid 529 was a substrate of murine Abcb1a (Mdr1a) or human ABCB1 (MDR1). The parental Madine Darby Canine Kidney (MDCK) type II cell line (MDCKII-parental) and murine Abcg2 (MDCKII-Bcrp1) or human ABCG2 transduced sub-lines (MDCKII-BCRP) were used to determine whether Palomid 529 was a substrate of murine Abcg2 or human ABCG2. Cells were used for a maximum of 13 passages after thawing. Complete medium prepared from MEM medium containing L-glutamine, non-essential amino acids, MEM vitamins penicillin-streptomycin, and 10% v/v fetal calf serum was used throughout. For transport studies, cells were seeded on Transwell microporous polycarbonate membrane filters (3.0  $\mu\text{m}$  pore size, 24 mm diameter; Costar Corning, NY, USA) at a density of  $2 \times 10^6$  cells per well in 2 ml complete medium. Cells were incubated at 37°C in 5%  $\text{CO}_2$  for three days. Both the conventional bi-directional transport assay (17;18) and the more recently described concentration equilibrium transport assay (19) were utilized. Briefly, 2 ml of complete MEM medium containing 5  $\mu\text{g/ml}$  Palomid 529 was applied to either apical or basolateral compartments in the conventional bi-directional transport experiments, or to both the apical and basolateral compartments in the concentration equilibrium transport experiments. Zosuquidar (LY335979, 5  $\mu\text{M}$ ) was added to the medium to inhibit endogenous canine ABCB1 when doing all experiments with MDCK cell lines, and in one experiment of GDC-0941 with LLC-PK1 cell lines. [ $^{14}\text{C}$ ]-inulin (approximately  $1.59 \times 10^6$  DPM/ml) was added to check the integrity of the membrane. Samples of 50  $\mu\text{l}$  were taken at 60, 120, 180 and 240 min and used for drug analysis by HPLC, whereas at the same time points 20  $\mu\text{l}$  samples were collected only from apical side for radioactivity counting. Wells showing leakiness in excess of 1.5 % per hour were excluded. Control experiments with 0.5  $\mu\text{M}$  of GDC-0941 were run in parallel. GDC-0941 is a small molecule PI3K inhibitor, which is a typical substrate for both ABCB1 and ABCG2 (20).

### *Animals*

Mice were housed and handled according to institutional guidelines complying with Dutch legislation. All experiments with animals were approved by the animal experiment committee of the institute. The animals used for pharmacokinetics studies in non-tumor bearing animals were female wild-type (WT), Abcb1a/1b<sup>-/-</sup>, Abcg2<sup>-/-</sup>, and Abcb1a/1b<sup>-/-</sup>;Abcg2<sup>-/-</sup> mice, all of a >99% FVB genetic background, between 9 and 14 weeks of age.

Animals injected with tumor cells used for the efficacy study or for pharmacokinetics studies in tumor bearing animals were athymic (nude) mice of FVB background with WT or *Abcb1a/1b<sup>-/-</sup>;Abcg2<sup>-/-</sup>* genotype. These latter *Abcb1a/1b<sup>-/-</sup>;Abcg2<sup>-/-</sup>* nude mice have been obtained by intercrossing of FVB nude mice with *Abcb1a/1b<sup>-/-</sup>;Abcg2<sup>-/-</sup>* mice and will be described in detail elsewhere (manuscript in preparation). The animals were kept in a temperature-controlled environment with a 12-hr dark/ 12-hr light cycle and received a standard diet (AM-II, Hope Farm B.B., Woerden, The Netherlands) and acidified water *ad libitum*.

*Plasma and brain pharmacokinetics of Palomid 529 in non-tumor bearing mice*

FVB WT and/or *Abcb1a/b<sup>-/-</sup>;Abcg2<sup>-/-</sup>* mice (n = 5 for each group) received Palomid 529 as a solution of 54 mg/ml in DMSO at a dose of 54 mg/kg (1  $\mu$ l of DMSO per gram body weight) or as a micronized formulation of 18 mg/ml or 1.8 mg/ml at a dose of 54 mg/kg or 5.4 mg/kg by i.v. (intravenous) or i.p. (intraperitoneal) injection into the tail vein. Next, about 50  $\mu$ l blood samples were collected from the tip of the tail at time points 0.5, 2, 4, 8, 12 and 24 hr after dosing using heparinized capillaries (Oxford labware, St. Louis, USA). At 24 hr blood was also sampled by cardiac puncture and the mice were sacrificed by cervical dislocation. To investigate the brain distribution of Palomid 529, two studies have been performed with DMSO dissolved drug or micronized formulated Palomid 529, both administered i.v. at a dose of 54 mg/kg to wild-type and *Abcb1a/b<sup>-/-</sup>;Abcg2<sup>-/-</sup>* mice (n = 5 for each group). To further assess the role of *Abcb1* and *Abcg2* in limiting the brain distribution of Palomid 529, a dose of 5.4 mg/kg of micronized Palomid 529 was administered i.v. to WT and *Abcb1a/b<sup>-/-</sup>*, *Abcg2<sup>-/-</sup>* and *Abcb1a/b<sup>-/-</sup>;Abcg2<sup>-/-</sup>* mice (n = 6, 6, 5 and 9 for above group, respectively). At 1 and 4 hr after administration animals were anesthetized with isoflurane and blood was collected by cardiac puncture. Next, the mice were immediately sacrificed by cervical dislocation and brain, liver, kidney, lung, spleen and heart tissues were dissected. Blood samples from all experiments were centrifuged (10 min, 5000 rpm, 4°C) and the plasma fractions in supernatant were transferred into clean vials. Tissues collected were weighed and homogenized using a polytron (Polytron PT1200, Kinematica AG, Littau, Switzerland) in a solution of 1% (w/v) bovine serum albumin (BSA) in water. We used 3 ml for brain, liver, and kidneys and 2 ml for the other tissues. Both plasma and homogenized tissue samples were stored at -20°C until analysis.

*Oral drug formulation and administration*

Oral formulations included an olive oil formulation (2 mg/ml), a micronized formulation (5.4 mg/ml) and a spray dried formulation (2 mg/ml). The olive oil formulation, micronized formulation and spray dried formulation (suspended in 0.5% (w/v) methyl cellulose) were orally administered by gavage to FVB WT mice at dose of 20 mg/kg, 20 mg/kg and 54 mg/kg, respectively (n = 5 for each group). The preparation of above formulations was described in supplementary materials. Sampling of tail blood and sample processing were performed as described above.

*Brain and tumor distribution and in vivo efficacy in intracranial GBM model*

We used FVB or *Abcb1a/b<sup>-/-</sup>;Abcg2<sup>-/-</sup>* nude mice with orthotopic grafted U87 GBM to investigate the Palomid 529 tumor distribution and its effect of GBM growth inhibition. To establish tumors, 100,000 U87-luc cells in 2  $\mu$ l were injected stereotactically in the right forebrain (caudate nucleus) of mice as described previously (21). Mice with U87-luc tumors were used for the drug distribution study when the bioluminescence signal exceeded  $10^8$  photons per second by bioluminescence imaging using an IVIS 200 camera (Caliper Life Science, Alameda, CA, USA). The micronized formulated of Palomid 529 was administered i.v. at a dose of 54 mg/kg (n=4 or 5 for each group). At 1 and 4 hr after administration, whole blood was collected by cardiac puncture. The U87 tumors were collected together with the tumor-free left forebrains. Sample homogenization, pretreatment and analysis were performed the same as in the pharmacokinetic studies.

For *in vivo* efficacy study, the tumor load was established for each animal after seven days by bioluminescence imaging, and the animals were stratified, according to the bioluminescence signal, into a control group receiving no therapy and a treatment group receiving micronized Palomid 529 i.p. at a dose of 54 mg/kg per day (n = 8 or 9 for each group, respectively). Bioluminescence imaging was repeated twice every 3 to 4 days to establish the efficacy of the therapy. The amount of bioluminescence in each animal was calculated relative to the first measurement when therapy was initiated (arbitrarily set at 100%).

*Pharmacokinetic calculations and statistical analysis*

Pharmacokinetic parameters were calculated using an add-in program for Microsoft Excel PKSolver (22). The area under the plasma concentration-time curve (AUC) was



calculated using the computing area under curve function of GraphPad Prism 5.01 (GraphPad Software, Inc., La Jolla, CA, USA). The oral bioavailability (F) was calculated as the dose-corrected area under the plasma concentration-time curve after oral dosing ( $AUC_{p.o.}$ ) divided by the dose-corrected AUC after intravenous dosing  $AUC_{i.v.}$  of the corresponding drug formulations using the following formula:

$$F = [AUC_{p.o.} * Dose_{i.v.} / AUC_{i.v.} * Dose_{p.o.}] * 100\%$$

$AUC_{p.o.}$  of micronized formulation is compared with  $AUC_{i.v.}$  of micronized formulation;  $AUC_{p.o.}$  of olive oil formulation and spray dried formulation are compared with  $AUC_{i.v.}$  of free drug dissolved in DMSO.

We applied the GLM (General linear model) repeated measures procedure to analyze the results of concentration equilibrium transport experiments using SPSS (v17.0; SPSS Inc, Chicago, IL, USA). The differences of the percentage ratio of peak area of the measured samples to the reference (medium sampled at time=0) between apical and basolateral compartments were considered as the observed values from repeated measurements. They were grouped by defining 4 sampling time points (1, 2, 3 and 4 hr) as a 4-level within-subjects factor. Simple contrast was selected to compare the differences between the mean observed values of 2, 3 and 4 hr and 1 hr. Then, the multivariate significance tests were performed to determine whether the apical-basolateral differences of the Palomid 529 levels were significantly increased by the factor of time.

For *in vivo* pharmacokinetic experiments in which only WT and *Abcb1a/b*<sup>-/-</sup>; *Abcg2*<sup>-/-</sup> mice were involved, the two-tailed student's t-test was used to determine the significance between two groups. For the experiment in which more than two strains were included, one-way analysis of variance (ANOVA) and post-hoc Bonferroni was performed. Difference were considered statistically significant when  $P < 0.05$ . For *in vivo* efficacy study, the two-tailed student's t-test was used to determine the significance between tumor growth ratios of control and treated group.

## RESULTS

### ***In vitro* transport of Palomid 529**

We first determined whether Palomid 529 is a substrate of Abcb1 and Abcg2 using LLC-Mdr1a and MDCK-Bcrp1 cell lines in a conventional bi-directional setup, with apical-to-basolateral and basolateral-to-apical transport. After 4 hr, about 25% to 30% of Palomid 529 was recovered at the opposite side of the membrane, showing that this compound has appropriate cell membrane permeable properties (Fig. 1A and B). Overexpression of Abcb1 or Abcg2 did not cause vectorial basolateral-to-apical translocation of Palomid 529 in LLC-Mdr1a and MDCK-Bcrp1 cells. Since it has been reported that the conventional bi-directional transport assay may be less suitable to identify weak Abcb1 substrates, we have used the more recently described concentration equilibrium transport assay (19) for all subsequent experiments. The concentration equilibrium transport system showed good sensitivity when we tested the translocation of GDC-0941, a PI3 kinase inhibitor that is a good substrate of Abcb1 and Abcg2 (23) (Fig. 1C, F, I, J and L). With this setting, we were even able to detect translocation of GDC-0941 in the LLC-PK1 cell line that is most likely mediated by the low level of endogenously expressed porcine Abcb1 in these LLC-PK1 cells, because this translocation was attenuated by the specific P-gp inhibitor zosuquidar (Fig. 1F vs. G). Despite the sensitivity of this setup, there was still no basolateral-to-apical translocation of Palomid 529 by Abcb1a or ABCB1 (Fig. 1D and E), suggesting that this compound is indeed not a substrate of Abcb1a. We found a small albeit significant ( $p=0.028$ , Fig. 1J and M) increase of the apical to basolateral translocation of Palomid 529 in murine Abcg2 overexpressing cells over time, but not in MDCK-parent cells, suggesting that this compound is a very weak Abcg2 substrate. Furthermore, we used the same setup to test translocation of Palomid 529 in corresponding cell lines that over-express human ABCB1 and ABCG2, but we did not observe any basolateral-to-apical directed translocation of Palomid 529 in both cell lines, indicating that Palomid 529 is not a substrate of human ABCB1 or ABCG2 (Fig. 1E and K).

### **Plasma pharmacokinetics of Palomid 529 in mice**

Next, we evaluated whether Abcb1a/b and/or Abcg2 have an impact on the plasma pharmacokinetics of Palomid 529 by using WT and Abcb1a/b<sup>-/-</sup>;Abcg2<sup>-/-</sup> (Abcb1a/b and Abcg2 deficient) mice. We measured the plasma concentration following i.v. administration of the micronized formulation and of Palomid 529 dissolved in DMSO

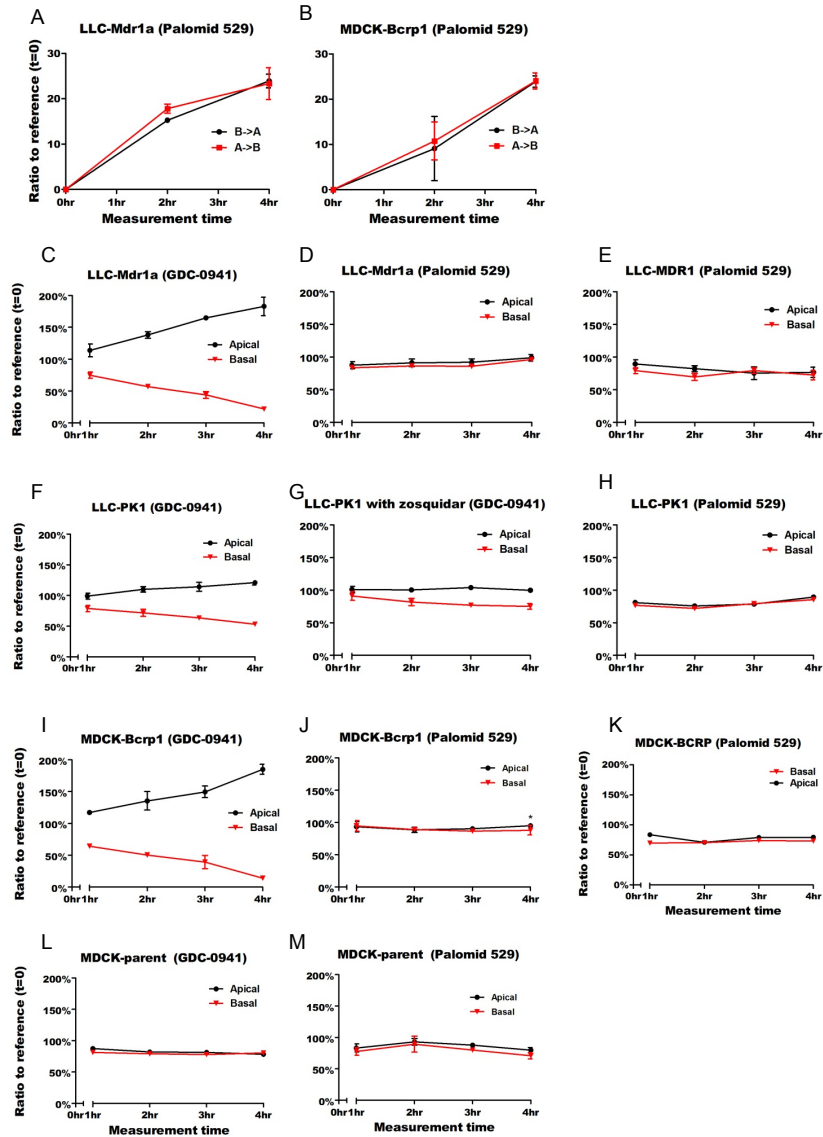


**Fig. 1.** Transepithelial translocation of GDC-0941 and Palomid 529 were assessed either using parental LLC-PK1 cells (F, G and H) and cells transduced with mouse Abcb1a (LLC-Mdr1a, C and D) or human ABCB1 (LLC-MDR1, E), or parental MDCKII cells (MDCK-parent, L and M) and cells transduced with mouse Abcg2 (MDCK-Bcrp1, I and J) or human ABCG2 (MDCK-BCRP, K). The setup was either a conventional bi-directional transwell setting (A and B) or a concentration equilibrium setting (C-M). Translocation of GDC-0941, a dual substrate of Abcb1 and Abcg2, was used as positive control. Zosuquidar (5  $\mu$ M) was added to LLC-PK1 cells to inhibit the transport mediated by endogenous porcine Abcb1 of LLC parent cells (G). Results are presented as the ratio of observed concentration to reference concentration.

at a dose of 54 mg/kg for up to 24 hr. There was no statistically significant difference in the  $AUC_{0-24}$  between WT and *Abcb1a/b<sup>-/-</sup>;Abcg2<sup>-/-</sup>* mice (Fig. 2A and B and table 1). To check whether drug clearance was dose-independent, we also tested a 10-fold lower dose level of 5.4 mg/kg of Palomid 529 (Fig. 2C). All results demonstrate that *Abcb1a/b* and *Abcg2* have no impact on the plasma clearance of Palomid 529. We also checked the plasma pharmacokinetics of Palomid 529 when it was administered i.p. at a dose of 54 mg/kg and found that the pharmacokinetic parameters were similar to those of WT mice receiving i.v. Palomid 529 (Table 1 and Fig. 2D). Due to the convenience of i.p. administration, it provides a less stressful manner for tumor growth intervention study, which requires daily repeated drug administration.

The formulation of Palomid 529, however, did have some effect on the plasma concentration time curve. At the first sampling point of 30 min after i.v. dosing the plasma concentration with the micronized formulation was about 2 to 3-fold lower than when Palomid 529 was dissolved in DMSO. On the other hand, the half-life of micronized Palomid 529 was longer, but overall the AUC (and plasma clearance) between the two formulations was similar. Most likely, a fraction of the relatively large micronized particles (0.8  $\mu$ m) is removed from the circulation during their passage through tissues of the mononuclear phagocyte system and is retained there. Next, redistribution occurs as Palomid 529 is (slowly) released from the particles and re-enters the blood circulation. This hypothesis is supported by the finding of much higher Palomid 529 levels in liver and spleen at 24 hour, whereas the levels in brain and kidney follow the plasma level (Fig. 2E).

### **Role of *Abcb1* and *Abcg2* in brain penetration of Palomid 529**

Because both ABCB1 and ABCG2 are very efficient in keeping substances out of the brain, we first used FVB WT versus *Abcb1a/b<sup>-/-</sup>;Abcg2<sup>-/-</sup>* mice lacking both *Abcb1a/b* and *Abcg2* to evaluate the impact of *Abcb1* and *Abcg2* on brain penetration of Palomid 529. In line with the previous results from tail blood samples, the plasma concentration of Palomid 529 does not differ significantly between these two genotypes at both 1 and 4 hr after i.v. administration of 54 mg/kg micronized or DMSO solubilized Palomid 529 (Fig. 3A and B). Moreover, the brain penetration of Palomid 529 after administration of micronized Palomid 529 was not higher in *Abcb1a/b<sup>-/-</sup>;Abcg2<sup>-/-</sup>* mice at 1 and 4 hours. Administration of Palomid 529 in DMSO resulted in a very modest 1.33-fold higher brain-plasma ratio in *Abcb1a/b<sup>-/-</sup>;Abcg2<sup>-/-</sup>* mice compared with WT mice at 1 hr ( $p=0.036$ ) and a non-significant

**Table 1.** Plasma pharmacokinetic parameters from FVB wild type and/or Abcb1a/b;Abcg2<sup>-/-</sup> mice after i.v. or i.p. administration of Palomid 529 using different dose levels and formulations. Data except *p*-values are mean ± SD, n = 5. Students t-test was performed to evaluate the difference in AUC values between wild type and Abcb1a/b;Abcg2<sup>-/-</sup> mice. We also established the pharmacokinetic parameters after i.p dosing because this route was used for daily dosing during the efficacy study. Abbreviations: AUC, area under plasma concentration-time curve; C<sub>max</sub>, maximum plasma concentration; T<sub>1/2</sub>, el, elimination half-life, calculated from 1-2 hr; Cl, clearance.

Strain	WT	Abcb1a/b;Abcg2 <sup>-/-</sup>	WT	Abcb1a/b;Abcg2 <sup>-/-</sup>	WT	Abcb1a/b;Abcg2 <sup>-/-</sup>	WT
Dose, mg/kg	5.4	5.4	54	54	54	54	54
Admin.	i.v.	i.v.	i.v.	i.v.	i.v.	i.v.	i.p.
Formulation	Micronized	Micronized	Micronized	Micronized	DMSO	DMSO	Micronized
AUC(0-24h) ng/mL*h	15690±2340	14600±985	120980±20410	132690±25830	119330±5250	146360±41180	132002±13362
<i>P</i>	0.89		0.77		0.99		N/A
C <sub>max</sub> ng/mL	3390±920	3590±300	15090±1090	15270±1300	37020±3770	50890±12670	15358±2041
T <sub>1/2</sub> h	3.33±0.25	3.30±0.380	5.22±0.40	4.80±1.27	2.42±0.08	2.63±0.24	5.15±0.49
Cl, l/hr.kg	0.36±0.06	0.38±0.03	0.45±0.07	0.42±0.11	0.49±0.02	0.44±0.19	0.39±0.02

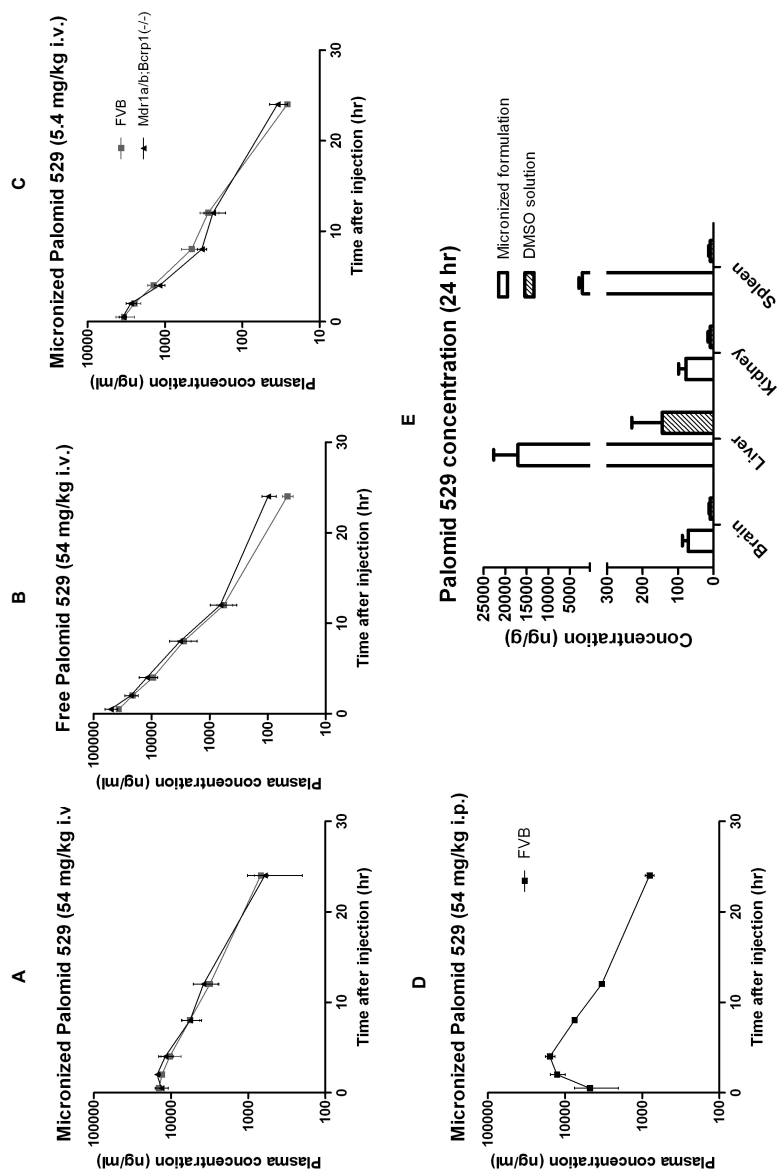


**Fig.2.** Mean plasma concentration time curves of Palomid 529 in WT mice and *Abcb1;Abcg2*<sup>-/-</sup> mice after i.v. administration of 54 mg/kg micronized Palomid 529 (A) or Palomid 529 dissolved in DMSO (B), and 5.4 mg/kg micronized Palomid 529 (C), or after i.p. administration of 54 mg/kg micronized Palomid 529 (D). Palomid 529 tissue concentrations in WT mice collected at 24 hr following i.v. administration of 54 mg/kg micronized and DMSO formulated Palomid 529 indicate a longer retention of micronized formulated Palomid 529 in liver and spleen (E). Data are presented as means  $\pm$  SD, n = 4 or 5 animals per group.

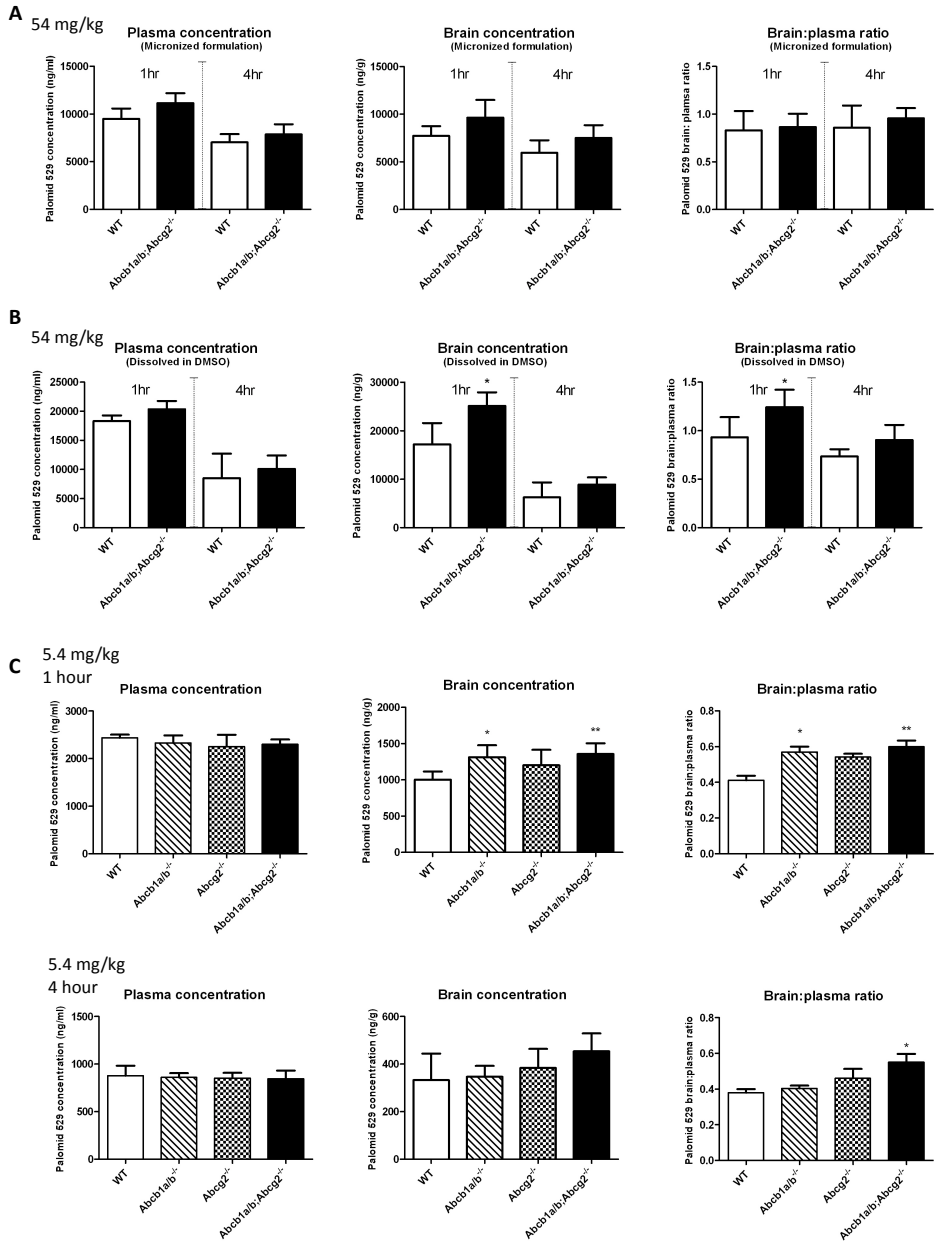


**Fig. 3.** Palomid 529 plasma concentration, brain concentration, brain-to-plasma ratio at 1 and 4 hr following i.v. administration of a high dose of 54 mg/kg (A and B) or a low dose of 5.4 mg/kg (C). C upper: 1 hr; lower panel: 4hr. At 54 mg/kg, Palomid 529 was administrated in a micronized formulation (A) or a free compound form dissolved in DMSO (B). Data are presented as means  $\pm$  SD, n = 5 animals per group for studies of A and B and n = 6, 6, 5, 9 for C. \* P < 0.05, \*\* P < 0.01. Statistical significance was determined by comparison of values of knockout with WT mice.

1.22-fold higher ratio at 4 hr after drug administration ( $p=0.059$ ). Thus, it shows that Abcb1 and/or Abcg2 play only a very minor role in limiting the brain penetration of Palomid 529.

In order to identify which transporter contributes mainly to the small increase of brain penetration of Palomid 529 in the compound knockout mice, and to check whether Abcb1 and Abcg2 may be more important at lower plasma concentrations, we have performed an additional experiment with Palomid 529 at a dose of 5.4 mg/kg. We have also included single Abcb1a/b<sup>-/-</sup> and Abcg2<sup>-/-</sup> animals, next to WT and Abcb1a/b<sup>-/-</sup>;Abcg2<sup>-/-</sup> mice in this analysis. In line with results from the high-dose study, a significant increase (1.45-fold,  $p=0.001$ ) of the brain-plasma ratio of Palomid 529 was observed in Abcb1a/b<sup>-/-</sup>;Abcg2<sup>-/-</sup> mice relative to WT mice at 1 hr after administration (Fig. 3C). We also observed a 1.38-fold increase ( $p=0.015$ ) of the brain-plasma ratio of Abcb1a/b<sup>-/-</sup> mice relative to WT mice whereas that of Abcg2<sup>-/-</sup> mice was 1.31-fold higher but this difference relative to WT mice did not reach statistical significance ( $p=0.081$ ). At 4 hr, the brain concentration and brain-plasma ratio of Palomid 529 was also 1.45-fold higher in Abcb1a/b<sup>-/-</sup>;Abcg2<sup>-/-</sup> mice relative to WT but not significantly higher in any of the single knockout mice. Thus, overall only a very moderate restriction of the brain entry of Palomid 529 is noted, which appears to be caused by a concerted action of Abcb1 and Abcg2.

### **Bioavailability of Palomid 529 is improved by an optimized oral formulation**

Chronic treatment period is usually required for targeted therapeutics such as mTOR inhibitors, thus a convenient p.o. application form with acceptable oral availability is certainly a preferred feature for such drugs. To investigate the bioavailability of Palomid 529, we first tested the micronized formulation of Palomid 529 in FVB WT mice at a dose of 54 mg/kg and monitored the plasma concentration of Palomid 529 for up to 24 hr after administration. Unfortunately the bioavailability was only 4.8% (Fig. 4 and Table 2). To assess whether the poor bioavailability might be due to a slow dissolution rate of Palomid 529 from the micronized form or due to poor penetration and uptake by the intestinal epithelium, we switched to a more solubilized drug formulation in olive oil. In order to minimize the possibility of drug precipitation in the gut as a possible source of low oral bioavailability, we started with a lower dose level of 20 mg/kg. As shown in table 2, the oral bioavailability of mice receiving 20 mg/kg of Palomid 529 formulated in olive



**Table 2.** Plasma pharmacokinetic parameters from WT mice after oral administration of Palomid 529 at different doses and in different formulations. Data are mean  $\pm$  SD, n = 5/6. Abbreviations: AUC, area under plasma concentration-time curve;  $C_{max}$ , maximum plasma concentration;  $T_{1/2}$ , el, elimination half-life, calculated from 1-2 hr; Cl, plasma clearance. F, oral bioavailability, calculated as the dose-corrected AUC<sub>p.o.</sub> divided by AUC<sub>i.v.</sub> of corresponding drug formulations.

	Micronized formulation (Dose=54 mg/kg)	Olive oil formulation (Dose=20 mg/kg)	Olive oil formulation (Dose=54 mg/kg)	Spray dried formulation (Dose=20mg/kg)
<b>AUC(0-24h)</b>	5800 $\pm$ 3660	23880 $\pm$ 3020	22224 $\pm$ 4422.09	14250 $\pm$ 3660
<b><math>C_{max}</math>, ng/mL</b>	1100 $\pm$ 240	4820 $\pm$ 1330	2710 $\pm$ 810	2540 $\pm$ 670
<b><math>T_{1/2}</math>, h</b>	2.87 $\pm$ 1.15	3.12 $\pm$ 0.45	3.51 $\pm$ 0.32	2.76 $\pm$ 0.88
<b>Cl, l/hr.kg</b>	9.67 $\pm$ 2.9	0.84 $\pm$ 0.19	2.70 $\pm$ 0.54	1.49 $\pm$ 0.45
<b>F(%)</b>	4.9 $\pm$ 1.0%	54.0 $\pm$ 6.8%	17.8 $\pm$ 3.7	32.2 $\pm$ 8.3%

oil was 54.0%, indicating that the low oral bioavailability with the micronized form was probably due to a slow dissolution rate of Palomid 529 *in vivo*. When we increased the concentration of Palomid 529 in olive oil formulation to deliver a dose of 54 mg/kg, the plasma AUC did not increase (Table 2). Since Palomid 529 is a very poorly water-soluble compound, this might be due to a more extensive precipitation of Palomid 529 occurring when the more concentrated drug solution in oil is being mixed with the aqueous gastric fluids of the animal. Still, the oral bioavailability of 54 mg/kg of Palomid 529 in the oily formulation was about 18% and therefore much better than using the micronized formulation. In order to explore a more clinically acceptable drug formulation, we performed a pilot study with administration of a spray-dried formulation of Palomid 529. At a dose of 20 mg/kg, we found a bioavailability of 32.2% (Fig. 4 and table 2). With this formulation, a further increase of the dose may be feasible without compromising the bioavailability. The results obtained from the latter two formulations, particularly the spray-dried formulation, suggested that despite of a poor solubility of Palomid 529, a relatively acceptable bioavailability could be achieved with further optimization of the formulation.

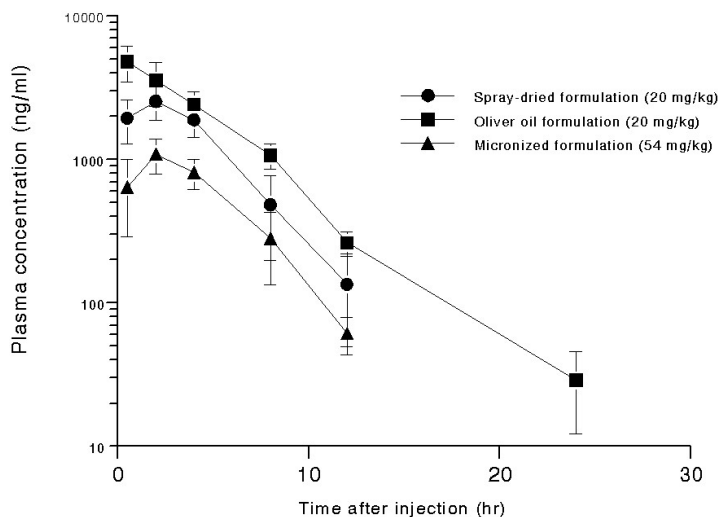


**Fig. 4.** Plasma concentration-time curves of Palomid 529 in WT after oral administration of 20 mg/kg Palomid 529 in spray dried formulation (●) and 20 mg/kg Palomid 529 in olive oil formulation (■) or 54 mg/kg Palomid 529 in micronized formulation (▲). n = 5 animals per group.

#### Palomid 529 tumor distribution and *in vivo* efficacy in intracranial GBM model

To investigate the roles of Abcb1 and Abcg2 in the tumor distribution of Palomid 529, we performed a pharmacokinetic analysis using the FVB nude mice bearing an intracranial U87 GBM tumor. In line with our previous experiments using non-tumor bearing FVB mice, the Palomid 529 concentrations in plasma and left (tumor free) brain hemisphere of Abcb1a/1b<sup>-/-</sup>;Abcg2<sup>-/-</sup> vs. WT mice were similar at 1 and 4 hour after administration of micronized formulation. Similarly, Abcb1 and Abcg2 also do not affect the Palomid 529 tumor distribution since the tumor concentrations in WT and Abcb1a/1b<sup>-/-</sup>;Abcg2<sup>-/-</sup> mice were also not significantly different (Fig. 5A, B and C). Interestingly, the Palomid 529 concentrations in plasma, brain and tumor were very similar, suggesting this agent has excellent brain permeability. Overall, we noted that the Palomid 529 concentrations in plasma and brain were about 2-fold lower than in the previous studies (Fig 3 and Fig. 5). This difference in clearance may be strain (FVB nude mice vs FVB) and/or tumor related.

Lastly, we evaluated the efficacy of Palomid 529 in the same GBM model. Treatment composed of daily i.p. administration of micronized Palomid 529 at a dose of 54 mg/kg was well tolerated and significantly inhibited orthotopic U87 tumor growth relative to untreated mice (Fig. 5 D).

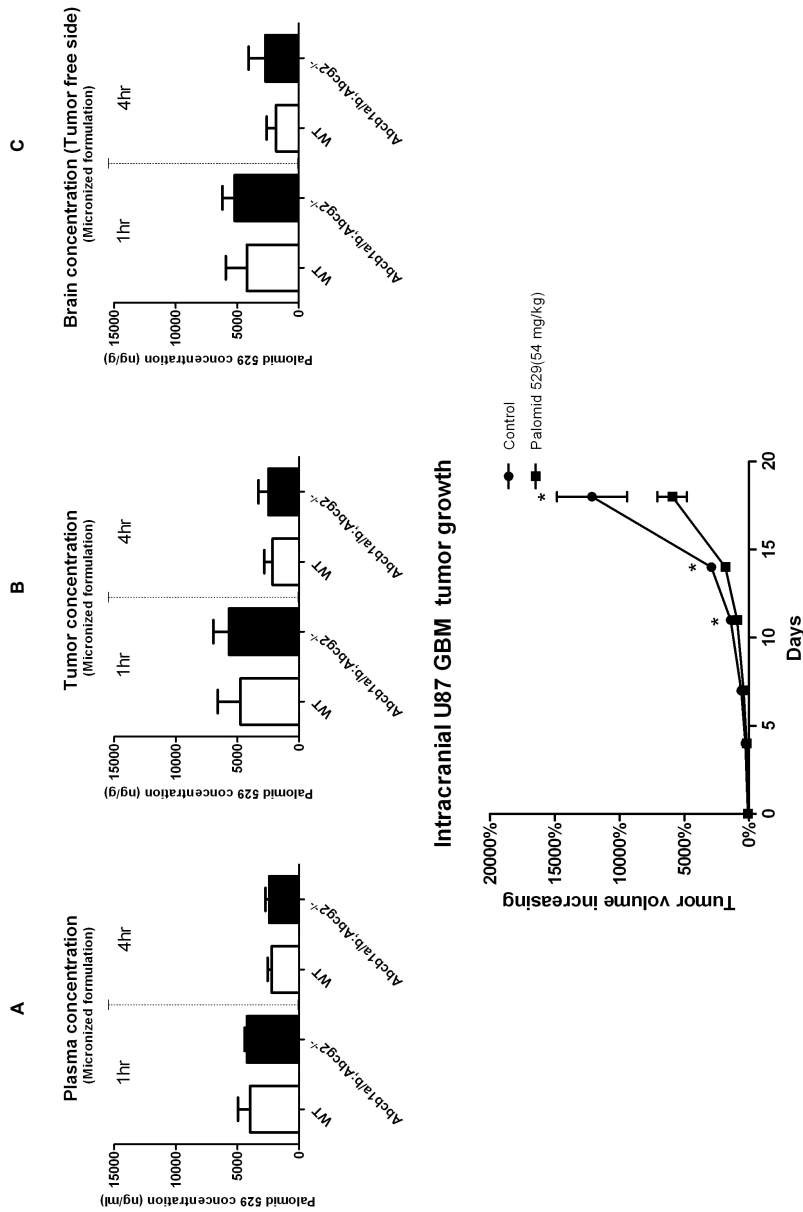


**Fig. 5.** Plasma, intracranial tumor (U87 GBM) and brain (tumor free) concentration of Palomid 529 at 1 and 4 hr after i.v. administration of 54 mg/kg micronized drug (A, B and C). *In vivo* tumor growth ratios in WT FVB nude mice bearing orthotopic U87 GBM (D). Control group animals receiving no treatment vs. 54 mg/kg micronized formulated Palomid 529 q.d. Data are presented as means  $\pm$  SD, n = 4 or 5 animals per group for tumor and brain distribution study and n=8 (control group) or 9 (treatment group) for the efficacy study. \* P < 0.05.

## DISCUSSION

In the present study we show that Palomid 529 is not or just a very weak substrate of Abcb1 and/or Abcg2 and accordingly its systemic availability and brain and brain tumor delivery is hardly affected by these two transporters. This is an interesting finding given the broad substrate ranges of these two ABC transporters that alone or together severely limit the brain entry of many substances. This pharmacokinetic feature of Palomid 529 provides a unique advantage for potential application of this drug against intracranial tumors as also demonstrated in a U87 orthotopic GBM model. Oral application of this drug will be possible, as we found that an acceptable oral availability (>50%) could be achieved by optimization of the formulation.

ABCB1 and ABCG2 are two of the most important ABC drug transporters frequently being associated with drug resistance. This includes expression at the cell membrane of tumor cells as well as expression at barrier sites to build pharmacological sanctuary sites where tumor cells can flourish. ABCB1 and ABCG2 have well-established roles in cooperatively limiting the brain penetration of many cytotoxic anticancer drugs such as topotecan (14), but also for novel targeted agents. In recent years, a series of small molecular inhibitors including erlotinib (24-26), gefitinib (13), sunitinib (27), sorafenib (28), dasatinib (29;30), imatinib (31), tamoxifen (32), lapatinib (15), GDC-0941 (23), vemurafenib (33) have been identified as substrates of Abcb1 and/or Abcg2 and the brain penetrations of these compounds are markedly restricted by these two transporters.

Despite that Abcb1 transports a wide variety of substrates, Palomid 529 was not translocated by murine and human Abcb1, even when using a concentration equilibrium setup, which was claimed as an appropriate and more sensitive assay for highly cell membrane permeable drugs (19). Similarly, we found that Palomid 529 was not transported by human ABCG2, and that murine Abcg2 might transport Palomid 529 only at a marginal level. Due to the poor aqueous solubility of Palomid 529, 10% fetal calf serum was added to the medium of the apical and basolateral compartments in both models to avoid loss of drug by precipitation and/or adsorption. With about 25% translocation of Palomid 529 in the classical Transwell assay, it is shown here that Palomid 529 can still freely cross the cell-monolayer in the presence of serum proteins. Consequently, the absence of directional transport of Palomid 529 in both ABC-transporter transduced

LLC and MDCK cell lines can only be due the fact that the affinity of Palomid 529 for both ABC-transporters is weak. We, next, confirmed these findings by using *Abcb1a/b<sup>-/-</sup>;Abcg2<sup>-/-</sup>* mice.

*Abcb1* was the first ABC transporter being identified as an important factor limiting the brain penetration of substances (34) and usually it is the most dominant efflux transporter restricting the brain delivery of many chemotherapeutics. Only for some drugs, e.g. sorafenib (28), its brain accumulation is predominantly limited by *Abcg2* instead of *Abcb1*. In many cases, however, the absence of both transporters results in a more than proportional increase in brain uptake compared to the absence of each transporters alone (13-15;30-33). The marked potency of *Abcb1* to limit the brain entry of substances is also observed to some extent with Palomid 529. Although the *in vitro* transwell experiments for Palomid 529 was not capable to show transport by *Abcb1*, the brain concentration was still significantly, albeit only very moderately, increased in *Abcb1* deficient mice. In contrast, the absence of *Abcg2* alone did not statistically change the brain concentration and brain-plasma of Palomid 529 ratio in comparison with WT mice. Besides the differences in substrate affinities, the expression of *Abcg2* in mouse BBB is also lower than that of *Abcb1* as demonstrated by a proteomic based quantitative analysis of protein expression of transporters expressed in human and murine BBB, where *Abcg2* expression was only 31.3% of *Abcb1* expression in mouse brain microvessels (35). Expression of ABCG2 in human BBB is 1.85-fold higher than in mouse BBB, but due to the fact that Palomid 529 is not or just a very weak substrate of human ABCG2, it is probably not a limiting factor in the brain distribution in humans as well. Moreover, the effect of ABCB1 in human brain might also be smaller than in mouse brain, because ABCB1 expression in human brain microvessels was only 43.0% of its mouse counterparts (35). Consequently, ABCB1 and ABCG2 are not expected to exert a meaningful impact on the brain penetration of Palomid 529 in humans, making this compound potentially useful for treatment of intracranial tumors. Notably, at a therapeutically useful dose of 50 mg/kg (7), the transport capacity of *Abcb1* and *Abcg2* might be saturated. Therefore we included a lower dose of 5.4 mg/kg to further determine the role of transporters. Indeed, the difference in the brain concentration of Palomid 529 between WT and *Abcb1a/b<sup>-/-</sup>;Abcg2<sup>-/-</sup>* mice became more evident at the lower dose. Nevertheless, the brain-to-plasma ratio was about 2-fold higher at the 54 mg/kg dose compared to 5.4

mg/kg in both WT and *Abcb1a/b<sup>-/-</sup>;Abcg2<sup>-/-</sup>* strains, which may implicate saturation of another, unknown efflux system, independent of *Abcb1* and *Abcg2*.

Besides the BBB, ABCB1 and ABCG2 are also expressed on the blood tumor barrier (BTB). In fact, overexpression of ABCB1 and ABCG2 on tumor cells often confers multidrug resistance (MDR) and are linked clinically to poor prognosis (36;37). This is presumably due to a reduction of cellular drug accumulation caused by ABC-transporter mediated drug efflux. For drugs that are excellent substrates of *Abcb1* such as doxorubicin, even a moderate increase of expression of *Abcb1* in tumors is sufficient to confer resistance (17). In addition, ABC-transporter mediated acquired drug resistance is less likely when non/poor-substrate drugs are applied. Consequently, it may be preferred to use active substances that are not or only very weak substrates of ABCB1 and ABCG2. This may be even more valid for targeted agents that need to be administered chronically, as prolonged exposure increases the chance to cause an upregulation of expression of ABC-transporters. Using mice bearing orthotopic U87 tumor, we were able to show that both *Abcb1* and *Abcg2* did not impair the Palomid 529 distribution in tumor.

A major obstacle of the current standard of care of patients with malignant gliomas is that after surgical resection of the bulk tumor mass, there are still many tumor cells remaining that have invaded into the normal surrounding brain. Due to the protection by an intact BBB, these tumor cells are poorly accessible by most commonly used chemotherapeutic agents and can escape from therapy. Interestingly, other drugs, which poorly penetrate the BBB demonstrate a much more profound accumulation into brain tumor tissue relative to normal brain because of the leakiness of the vessels in those tumors. Consequently, the antitumor efficacy of these agents results from the fact that these experimental tumors are exposed to a very high drug concentration. For example, the brain tumor accumulation of vincristine was 10-fold higher compared to normal brain as shown by Wang et al (38). In contrast, the concentration of Palomid 529 in brain and brain tumor was similar, despite the fact that U87 tumors also possess a leaky vasculature (21). These results strongly suggest that this agent will also be delivered at pharmacologically active levels to the invading GBM cells residing in normal brain with functional BBB.

High-grade glioma is a disease with a very dismal prognosis. Although the PI3K-mTOR signaling pathway is very frequently activated in this disease, it is not very likely that a single agent directed against this pathway by itself can exert a potent anti-proliferative effect. In this respect, however, Palomid 529 has been shown to synergize with radiation in experimental models including orthotopic gliomas (8;9). Importantly, in the present study we demonstrate that pharmacologically active levels of Palomid 529 can be delivered throughout the brain, which is important as this drug is being considered for clinical evaluation in high-grade glioma.

In short, Palomid 529 has an advantageous pharmacokinetic feature as being not or just a very weak substrate of Abcb1/ABCB1 and/or Abcg2/ABCG2. This feature enables Palomid 529 to enter the brain more easily than most other anti-cancer drugs whose brain penetrations are severely limited by Abcb1 and Abcg2. Consequently, pharmacologically active levels are reached throughout the brain. The systemic exposure of Palomid 529 is not affected by ABC-transporters and the availability of an orally applicable spray-dried dosing formulation allows convenient employment of this drug. Together, these preclinical results warrant further clinical testing of this drug.

### **Acknowledgments**

We gratefully acknowledge the statistical advice of Dr. Marta Lopez Yurda and Dr. Catharina M. Korse. This work was supported by a grant of the foundation StopHersentumoren to OvT

## Reference List

- (1) Inoki K, Corradetti MN, Guan KL. Dysregulation of the TSC-mTOR pathway in human disease. *Nat Genet* 2005 Jan;37(1):19-24.
- (2) Shaw RJ. Ras, PI(3)K and mTOR signalling controls tumour cell growth. 2006 May 25.
- (3) Vivanco I, Sawyers CL. The phosphatidylinositol 3-Kinase AKT pathway in human cancer. *Nat Rev Cancer* 2002 Jul;2(7):489-501.
- (4) Mueller W, Mizoguchi M, Silen E, D'Amore K, Nutt CL, Louis DN. Mutations of the PIK3CA gene are rare in human glioblastoma. *Acta Neuropathol* 2005 Jun;109(6):654-5.
- (5) Cancer Genome Atlas Research Network. Comprehensive genomic characterization defines human glioblastoma genes and core pathways. *Nature* 2008 Oct 23;455(7216):1061-8.
- (6) Tanaka K, Babic I, Nathanson D, Akhavan D, Guo D, Gini B, Dang J, Zhu S, Yang H, de JJ, Amzajerdi AN, Zhang Y, et al. Oncogenic EGFR signaling activates an mTORC2-NF-kappaB pathway that promotes chemotherapy resistance. *Cancer Discov* 2011 Nov 1;1(6):524-38.
- (7) Xue Q, Hopkins B, Perruzzi C, Udayakumar D, Sherris D, Benjamin LE. Palomid 529, a novel small-molecule drug, is a TORC1/TORC2 inhibitor that reduces tumor growth, tumor angiogenesis, and vascular permeability. *Cancer Res* 2008 Nov 15;68(22):9551-7.
- (8) Cerna D, Carter D, Flaherty S, Cal L, Sherris D, Yoo SS. Palomid 529, a PI3K/Akt/mTOR dual TORC1/2 inhibitor, is a radiosensitizer with effect in both subcutaneous and orthotopic U251 glioblastoma tumor xenograft models [AACR abstract:P21-2506]. 2010.
- (9) Diaz R, Nguewa PA, Diaz-Gonzalez JA, Hamel E, Gonzalez-Moreno O, Catena R, Serrano D, Redrado M, Sherris D, Calvo A. The novel Akt inhibitor Palomid 529 (P529) enhances the effect of radiotherapy in prostate cancer. *Br J Cancer* 2009 Mar 24;100(6):932-40.
- (10) Gravina GL, Maramon F, Petini F, Biordi L, Sherris D, Jannini EA, Tombolini V, Festuccia C. The TORC1/TORC2 inhibitor, Palomid 529, reduces tumor growth and sensitizes to docetaxel and cisplatin in aggressive and hormone-refractory prostate cancer cells. *Endocr Relat Cancer* 2011 Aug;18(4):385-400.
- (11) de Vries NA, Beijnen JH, Boogerd W, van Tellingen O. Blood-brain barrier and chemotherapeutic treatment of brain tumors. *Expert Rev Neurother* 2006 Aug;6(8):1199-209.
- (12) Muldoon LL, Soussain C, Jahnke K, Johanson C, Siegal T, Smith QR, Hall WA, Hynynen K, Senter PD, Peereboom DM, Neuwelt EA. Chemotherapy delivery issues in central nervous system malignancy: a reality check. *J Clin Oncol* 2007 Jun 1;25(16):2295-305.
- (13) Agarwal S, Sane R, Gallardo JL, Ohlfest JR, Elmquist WF. Distribution of gefitinib to the brain is limited by P-glycoprotein (ABCB1) and breast cancer resistance protein (ABCG2)-mediated active efflux. *J Pharmacol Exp Ther* 2010 Jul;334(1):147-55.
- (14) de Vries NA, Zhao J, Kroon E, Buckle T, Beijnen JH, van Tellingen O. P-glycoprotein and breast cancer resistance protein: two dominant transporters working together in limiting the brain penetration of topotecan. *Clin Cancer Res* 2007 Nov 1;13(21):6440-9.
- (15) Polli JW, Olson KL, Chism JP, John-Williams LS, Yeager RL, Woodard SM, Otto V, Castellino S, Demby VE. An unexpected synergist role of P-glycoprotein and breast cancer resistance



- protein on the central nervous system penetration of the tyrosine kinase inhibitor lapatinib (N-{3-chloro-4-[(3-fluorobenzyl)oxy]phenyl}-6-[5-{{2-(methylsulfonyl)ethyl}amino}methyl]-2-furyl]-4-quinazolinamine; GW572016). *Drug Metab Dispos* 2009 Feb;37(2):439-42.
- (16) Lin F, Sherris D, Beijnen JH, van Tellingen O. High-performance liquid chromatography analysis of a novel small-molecule, anti-cancer drug, Palomid 529, in human and mouse plasma and in mouse tissue homogenates. *J Chromatogr B Analyt Technol Biomed Life Sci* 2011 Dec 15;879(32):3823-31.
- (17) Pajic M, Iyer JK, Kersbergen A, van der Burg E, Nygren AO, Jonkers J, Borst P, Rottenberg S. Moderate increase in Mdr1a/1b expression causes in vivo resistance to doxorubicin in a mouse model for hereditary breast cancer. *Cancer Res* 2009 Aug 15;69(16):6396-404.
- (18) Ueda K, Okamura N, Hirai M, Tanigawara Y, Saeki T, Kioka N, Komano T, Hori R. Human P-glycoprotein transports cortisol, aldosterone, and dexamethasone, but not progesterone. *J Biol Chem* 1992 Dec 5;267(34):24248-52.
- (19) Luna-Tortos C, Fedrowitz M, Loscher W. Several major antiepileptic drugs are substrates for human P-glycoprotein. *Neuropharmacology* 2008 Dec;55(8):1364-75.
- (20) Salphati L, Lee LB, Pang J, Plise EG, Zhang X. Role of P-glycoprotein and breast cancer resistance protein-1 in the brain penetration and brain pharmacodynamic activity of the novel phosphatidylinositol 3-kinase inhibitor GDC-0941. *Drug Metab Dispos* 2010 Sep;38(9):1422-6.
- (21) Kemper EM, Leenders W, Kusters B, Lyons S, Buckle T, Heerschap A, Boogerd W, Beijnen JH, van Tellingen O. Development of luciferase tagged brain tumour models in mice for chemotherapy intervention studies. *Eur J Cancer* 2006 Dec;42(18):3294-303.
- (22) Zhang Y, Huo M, Zhou J, Xie S. PKSolver: An add-in program for pharmacokinetic and pharmacodynamic data analysis in Microsoft Excel. *Comput Methods Programs Biomed* 2010 Sep;99(3):306-14.
- (23) Salphati L, Lee LB, Pang J, Plise EG, Zhang X. Role of P-glycoprotein and breast cancer resistance protein-1 in the brain penetration and brain pharmacodynamic activity of the novel phosphatidylinositol 3-kinase inhibitor GDC-0941. *Drug Metab Dispos* 2010 Sep;38(9):1422-6.
- (24) Marchetti S, de Vries NA, Buckle T, Bolijn MJ, van Eijndhoven MA, Beijnen JH, Mazzanti R, van Tellingen O, Schellens JH. Effect of the ATP-binding cassette drug transporters ABCB1, ABCG2, and ABCC2 on erlotinib hydrochloride (Tarceva) disposition in in vitro and in vivo pharmacokinetic studies employing Bcrp1-/-/Mdr1a/1b-/- (triple-knockout) and wild-type mice. *Mol Cancer Ther* 2008 Aug;7(8):2280-7.
- (25) Kodaira H, Kusuhara H, Ushiki J, Fuse E, Sugiyama Y. Kinetic analysis of the cooperation of P-glycoprotein (P-gp/Abcb1) and breast cancer resistance protein (Bcrp/Abcg2) in limiting the brain and testis penetration of erlotinib, flavopiridol, and mitoxantrone. *J Pharmacol Exp Ther* 2010 Jun;333(3):788-96.
- (26) de Vries NA, Buckle T, Zhao J, Beijnen JH, Schellens JH, van Tellingen O. Restricted brain penetration of the tyrosine kinase inhibitor erlotinib due to the drug transporters P-gp and BCRP. *Invest New Drugs* 2010 Apr 1;30(2):443-9.

- (27) Tang SC, Lagas JS, Lankheet NA, Poller B, Hillebrand MJ, Rosing H, Beijnen JH, Schinkel AH. Brain accumulation of sunitinib is restricted by P-glycoprotein (ABCB1) and breast cancer resistance protein (ABCG2) and can be enhanced by oral elacridar and sunitinib coadministration. *Int J Cancer* 2012 Jan 1;130(1):223-33.
- (28) Lagas JS, van Waterschoot RA, Sparidans RW, Wagenaar E, Beijnen JH, Schinkel AH. Breast cancer resistance protein and P-glycoprotein limit sorafenib brain accumulation. *Mol Cancer Ther* 2010 Feb;9(2):319-26.
- (29) Lagas JS, van Waterschoot RA, van Tilburg VA, Hillebrand MJ, Lankheet N, Rosing H, Beijnen JH, Schinkel AH. Brain accumulation of dasatinib is restricted by P-glycoprotein (ABCB1) and breast cancer resistance protein (ABCG2) and can be enhanced by elacridar treatment. *Clin Cancer Res* 2009 Apr 1;15(7):2344-51.
- (30) Chen Y, Agarwal S, Shaik NM, Chen C, Yang Z, Elmquist WF. P-glycoprotein and breast cancer resistance protein influence brain distribution of dasatinib. *J Pharmacol Exp Ther* 2009 Sep;330(3):956-63.
- (31) Zhou L, Schmidt K, Nelson FR, Zelesky V, Troutman MD, Feng B. The effect of breast cancer resistance protein and P-glycoprotein on the brain penetration of flavopiridol, imatinib mesylate (Gleevec), prazosin, and 2-methoxy-3-(4-(2-(5-methyl-2-phenyloxazol-4-yl)ethoxy)phenyl)propanoic acid (PF-407288) in mice. *Drug Metab Dispos* 2009 May;37(5):946-55.
- (32) Iusuf D, Teunissen SF, Wagenaar E, Rosing H, Beijnen JH, Schinkel AH. P-glycoprotein (ABCB1) transports the primary active tamoxifen metabolites endoxifen and 4-hydroxytamoxifen and restricts their brain penetration. *J Pharmacol Exp Ther* 2011 Jun;337(3):710-7.
- (33) Mittapalli RK, Vaidhyanathan S, Sane R, Elmquist WF. Impact of P-glycoprotein (ABCB1) and Breast Cancer Resistance Protein (ABCG2) on the Brain Distribution of a novel B-RAF Inhibitor: Vemurafenib (PLX4032). *J Pharmacol Exp Ther* 2012 Mar 27.
- (34) Schinkel AH, Smit JJ, van Tellingen O, Beijnen JH, Wagenaar E, van DL, Mol CA, van der Valk MA, Robanus-Maandag EC, te Riele HP, . Disruption of the mouse *mdr1a* P-glycoprotein gene leads to a deficiency in the blood-brain barrier and to increased sensitivity to drugs. *Cell* 1994 May 20;77(4):491-502.
- (35) Uchida Y, Ohtsuki S, Katsukura Y, Ikeda C, Suzuki T, Kamiie J, Terasaki T. Quantitative targeted absolute proteomics of human blood-brain barrier transporters and receptors. *J Neurochem* 2011 Apr;117(2):333-45.
- (36) Szakacs G, Paterson JK, Ludwig JA, Booth-Genthe C, Gottesman MM. Targeting multidrug resistance in cancer. *Nat Rev Drug Discov* 2006 Mar;5(3):219-34.
- (37) Kusuvara H, Sugiyama Y. ATP-binding cassette, subfamily G (ABCG family). *Pflugers Arch* 2007 Feb;453(5):735-44.
- (38) Wang F, Zhou F, Kruh GD, Gallo JM. Influence of blood-brain barrier efflux pumps on the distribution of vincristine in brain and brain tumors. *Neuro Oncol* 2010 Oct;12(10):1043-9.

## Chapter 3.2

High-grade glioma mouse models identify ABCB1, ABCG2 and PTEN as important factors for response to temozolomide and ABT-888 combination therapy

Fan Lin, Mark C. De Gooijer, Eloy Moreno Roig, Susan Christner, Jan H. Beumer, Jos H. Beijnen, Olaf van Tellingen

To be submitted

## ABSTRACT

Glioblastoma (GBM) is among the most lethal types of human cancer. Despite aggressive multi-modality treatment, including surgery, radiotherapy and temozolomide (TMZ) chemotherapy, the prognosis remains dismal and novel therapeutics are urgently needed.

PARP inhibitors such as ABT-888 enhance the activity of DNA damaging therapies by impeding the base excision repair pathway, and represent a potential strategy to improve the efficacy of chemoradiation. However, using an intracranial P53;Ink4a/Arf;K-Ras<sup>v12</sup> GBM allograft model, which resembles many features of human GBM, no significant therapeutic benefit was obtained from TMZ and ABT-888 treatment relative to single TMZ treatment. Further investigation revealed that ABT-888 is a good substrate of both Abcb1 and Abcg2, two important drug efflux transporters that are abundantly expressed at the blood-brain barrier (BBB) and may be expressed by tumor cells. Indeed, Abcb1 and Abcg2 impaired the *in vitro* anti-proliferative effect of ABT-888 and TMZ in cell cultures, but also caused a 4.9-fold reduction of the brain penetration. These effects could be reversed by the dual Abcb1 and Abcg2 inhibitor elacridar. Efficacy studies against this P53;Ink4a/Arf;K-Ras<sup>v12</sup> GBM cell line injected into WT or Abcb1a/1b<sup>-/-</sup>;Abcg2<sup>-/-</sup> recipients and co-administration of elacridar suggest that Abcb1 and Abcg2 at both the BBB and in tumor cells limit the efficacy of TMZ and ABT treatment. In a spontaneous P53;Ink4a/Arf;K-Ras<sup>v12</sup> GBM model, elacridar also successfully improved the efficacy of TMZ and ABT-888 combination treatment. Moreover, we found that the PTEN;Ink4a/Arf;K-Ras<sup>v12</sup>;LucR GBM cells (harboring PTEN instead of P53 deficiency) were much more sensitive to TMZ and ABT-888 treatment *in vitro*, which is likely due to a failure of the homologous recombination DNA repair pathway. Despite that the intracranial Pten;Ink4a/Arf;K-Ras<sup>v12</sup> GBM model is more aggressive, the animals benefited significantly TMZ and ABT treatment.

In conclusion, the efficacy of TMZ and ABT-888 combination therapy in GBM is limited by Abcb1, Abcg2 and dependent on the PTEN status. These findings suggest that clinical benefit might be achieved by co-administration of elacridar together with TMZ and ABT-888 therapy. Moreover, a subgroup analysis of patients whose tumors are deficient in PTEN should be performed when analyzing the data from ongoing Phase II trials as these patients may benefit most from this treatment.

## INTRODUCTION

Glioblastoma multiforme (GBM) is the most common and aggressive primary brain tumor. Unlike many other types of cancers, there are very few chemotherapeutic agents available that exert a meaningful response against this disease. The current standard-of-care is surgery plus chemoradiation (a combination of the DNA-alkylating agent temozolomide and radiotherapy). This DNA damaging treatment modality significantly increases the overall median survival to 14.6 months after diagnosis [1]. However, even with this aggressive treatment regimen the prognosis of GBM patients remains dismal. Therefore, novel therapeutics are urgently needed.

PARP inhibitors enhance the activity of DNA damaging therapies, due to the critical function of PARP-1 and PARP-2 in base excision repair [2, 3]. Several preclinical studies suggest that PARP inhibitors enhance the efficacy of TMZ in both sensitive and resistant tumors [4, 5]. Moreover, their activity in sensitizing GBM cells to TMZ treatment and reversing the TMZ resistance has been reported [6-8]. ABT-888 is a potent poly (ADP-ribose) polymerase (PARP) inhibitor and is currently in Phase 2 clinical trials. The combination of ABT-888 with chemo-radiation therapies for the treatment of various tumors is receiving considerable interest because this combination has shown promise in preclinical models, including intracranial models [9, 10]. However, a potential weakness of the commonly used preclinical intracranial tumor models is that those cell lines have lost many of their characteristics, because they have been cultured in serum containing media for generations [11]. Moreover, many of the intracranial models also possess leaky blood vessels, rendering it relatively easy for any drug to reach into the tumor cells. Therefore, these models may not be stringent enough to evaluate the efficacy of potential therapies for GBM. In GBM patients, the tumors are believed to contain a subset of cells (so-called glioma initiating cells) that harbor features such as indefinite self-renewal potential and resistance to radiotherapy and chemotherapy [12]. In addition, tumor cells, which have infiltrated surrounding normal brain tissue, are perfused by the pre-existing brain vasculature and are thus protected by the BBB [13, 14]. Consequently, intrinsic resistance of GBM cells and the protection by the BBB are potential obstacles for any (targeted) therapeutic agent.

ATP-binding cassette (ABC) drug efflux transporters expressed at the BBB have well-known roles in restricting the entry of therapeutic agents into the brain [15]. Of all efflux transporters present in the BBB, ABCB1 (ATP-Binding Cassette transporter protein B1, P-glycoprotein or MDR1) and ABCG2 (ATP-Binding Cassette transporter G2 or BCRP) are the most dominant transporters responsible for the efflux of therapeutic agents back into the systemic circulation. Both of these two transporters recognize a wide range of substrates including a many of the small molecule inhibitors that are currently under (clinical) investigation for brain cancer. Most likely, the brain penetrations of these compounds are markedly restricted by these two transporters. Moreover, ABCB1 and ABCG2 are also expressed at the membrane of tumor cells and may confer chemoresistance to GBMs [16].

We have previously developed Cre-LoxP conditional transgenic mouse models of GBM for chemotherapy intervention studies [17]. In the present study, we found that a cell line derived from a spontaneous P53;Ink4a/Arf;K-Ras<sup>v12</sup> GBM and re-injected into nude mice did not respond to ABT-888 and temozolomide combination therapy. We investigated the reasons underlying this lack of efficacy in this clinically relevant model. We assessed the affinity of ABT-888 for ABCB1 and ABCG2, and investigated the sensitivity of GBM cells with different genotypes to this therapy in various *in vitro* and *in vivo* models.

## MATERIALS AND METHODS

### **Reagents**

The PARP-inhibitor ABT-888 was purchased from Selleck Chemicals (Houston, TX, USA). Temozolomide (TMZ) for *in vitro* experiments, Poly-L-Ornithine hydrobromide, laminin were purchased from Sigma-Aldrich (St Louis, MO, USA). TMZ for *in vivo* studies was purchased from Schering Plough BV (Utrecht, The Netherlands). Elacridar was kindly provided by GlaxoSmithKline (Research Triangle Park, NC, USA). Zosuquidar (LY335979) was kindly provided by Eli Lilly (Indianapolis, IN, USA). Modified Eagles medium (MEM), L-glutamine, non-essential amino acids, MEM vitamins penicillin-streptomycin, fetal calf serum, trypsin-EDTA and other reagents for cell culture were purchased from Invitrogen (Carlsbad, CA, USA). All other chemicals were purchased from Merck (Darmstadt, Germany).

### **Animals**

Mice were housed and handled according to institutional guidelines complying with Dutch legislation. All experiments with animals were approved by the animal experiment committee of the institute. The animals used for pharmacokinetics studies were female wild-type (WT), *Abcb1a/1b*<sup>-/-</sup>, *Abcg2*<sup>-/-</sup>, and *Abcb1a/1b*<sup>-/-</sup>;*Abcg2*<sup>-/-</sup> mice of FVB genetic background, between 9 and 14 weeks of age. *Ink4a/Arf*;*K-Ras*<sup>v12</sup>;*LucR*, *Pten*;*Ink4a/Arf*;*K-Ras*<sup>v12</sup>;*LucR*, *P53*;*Ink4a/Arf*;*K-Ras*<sup>v12</sup>;*LucR* and *P53*;*Pten*;*Ink4a/Arf*;*K-Ras*<sup>v12</sup>;*LucR* conditional mice for efficacy studies were genotyped as described previously (1). Recipient animals for orthotopic injection of primary GBM cells generated from the above mentioned conditional mouse models and cultured under neurosphere conditions were athymic (nude) WT and *Abcb1a/1b*<sup>-/-</sup>;*Abcg2*<sup>-/-</sup> mice of FVB background. The animals were kept in a temperature-controlled environment with a 12-hr dark/ 12-hr light cycle and received a standard diet (AM-II, Hope Farm B.B., Woerden, The Netherlands) and acidified water *ad libitum*.

### ***In vitro* transport experiments**

To determine whether ABT-888 is a substrate of murine *Abcb1a* (*Mdr1a*) or human ABCB1 (*MDR1*), we analyzed the translocation of ABT-888 (0.5  $\mu$ M) in a concentration equilibrium setting using the parental LLC pig-kidney cell line (LLC-PK1) and sub-lines transduced with murine *Abcb1a* (LLC-*Mdr1a*) or human ABCB1 (LLC-*MDR1*). Similarly,

the parental Madine Darby Canine Kidney (MDCK) type II cell line (MDCKII-parental) and murine Abcg2 (MDCKII-Bcrp1) or human ABCG2 transduced sub-lines (MDCKII-BCRP) were used to determine whether ABT-888 was a substrate of murine Abcg2 or human ABCG2. Cells were seeded on Transwell microporous polycarbonate membrane filters (3.0  $\mu\text{m}$  pore size, 24 mm diameter; Costar Corning, NY, USA) at a density of  $2 \times 10^6$  cells per well in 2 ml OPTI-MEM medium. Zosuquidar (5  $\mu\text{M}$ ) was added to the medium to inhibit endogenous canine ABCB1 in all experiments with MDCK cell lines, and to inhibit the endogenous or exogenous ABCB1/Abcb1 activity in experiments with LLC cell when necessary. Elacridar was added to the medium to inhibit the endogenous or exogenous ABCG2/Abcg2 (and ABCB1/Abcb1) activity. [ $^{14}\text{C}$ ]-inulin (approximately  $1.59 \times 10^6$  DPM/ml) was added to check the integrity of the membrane. Samples of 50  $\mu\text{l}$  were taken at 30, 120, 180 and 240 min and used for drug analysis.

#### ***Plasma and brain pharmacokinetics***

ABT-888 was dissolved in DMSO and further diluted in 0.9% saline to 1 and 2 mg/ml for p.o. (per os) and i.v. (intravenous) administration, respectively. Mice (n=5 for each group) were administered p.o. or by i.v. injection into the tail vein at a dose of 10 mg/kg. Elacridar prepared as described earlier (2) was given p.o. at a dose of 100 mg/kg 15 min prior to ABT-888. For plasma pharmacokinetics blood sampling was performed either by collecting tail vein blood at time points 15min, 1, 2 and 4 hr after dosing or by cardiac puncture in an end point. Brains were dissected after mice were sacrifice and were homogenized in 3 ml 1% (w/v) bovine serum albumin (BSA). Both plasma and brain homogenates were stored at  $-20^\circ\text{C}$  until analysis.

#### ***Drug analytical method***

ABT-888 in the transwell samples was analyzed by HPLC-UV at 295 nm using a 10 min gradient running from 4% to 40% of methanol in 0.1% formic acid in water delivered at a flow rate of 0.2 ml/min. Detection was done using a UV at 295 nm. ABT-888 pharmacokinetic samples were analyzed in an LC-MS system under previously described conditions [18].

#### ***Stereotactic intracranial injections and bioluminescence imaging***

The detailed procedures of stereotactic intracranial injection and bioluminescence imaging are described previously (3). In short, Pten;Ink4a/Arf;K-Ras<sup>v12</sup>;LucR and



P53;Ink4a/Arf;K-Ras<sup>v12</sup>;LucR mice were anaesthetized and placed in a stereotact, and 2  $\mu$ l of CMV-Cre virus suspension was injected 2 mm lateral and 1 mm anterior to the bregma, 3 mm below the skull. For orthotopic transplantation models, 2  $\mu$ l of cell suspension containing 5.000 cells was injected in athymic WT and Abcb1a/1b<sup>-/-</sup>;Abcg2<sup>-/-</sup> mice. Tumor development was monitored 2 to 3 times weekly by bioluminescence using the IVIS 200 Imaging system (Xenogen, Corporation, Alameda, CA, USA). Mice were sacrificed when clear neurological symptoms occurred or weight loss ( $\geq 20\%$ ) was observed. Brain tissue was fixed in an ethanol-glacial acetic acid mixture containing 4% formaldehyde (EAF), embedded in paraffin and cut into coronal slice of 4  $\mu$ m. Sections were H&E stained for verification of tumor growth.

#### ***Drug formulation and treatment regime***

TMZ for the efficacy studies was prepared freshly (less than 1 hr before the administration) by dissolving the contents of a temozolomide capsule containing 100 mg of active substance in 2 ml ethanol and 18 ml saline to yield a solution of 5.0 mg/ml. For all efficacy studies, TMZ was p.o. administered at a dose 100 mg/kg q.d. for 5 days. Elacridar was p.o. administered at a dose of 100 mg/kg 15 min prior to ABT-888 or TMZ administration for q.d. or b.i.d. for 5 days (q.d. for graft model and b.i.d. for spontaneous model). ABT-888 was prepared by dissolving the drug in DMSO and diluted in saline to yield a solution of 1.0 mg/ml (DMSO:saline=10:90; v/v) and was p.o. administered at a dose of 10 mg/kg q.d. or b.i.d. for 5 days (q.d. for graft model and b.i.d. for spontaneous model).

#### ***Establishment of GBM cell culture, anti-proliferation assay and Western blotting***

GBM cells lines have been created from tumors generated in Ink4a/Arf;KRasv12;LucR, Pten;Ink4a/Arf;K-Rasv12;LucR, P53;Ink4a/Arf;K-Rasv12;LucR and P53;Pten;Ink4a/Arf;K-Ras<sup>v12</sup>;LucR conditional mice after lentiviral infection. Small amounts of tumor tissue were transferred in ice-cold CA<sup>2+</sup> and Mg<sup>2+</sup> free HBSS (Gibco) and subsequently triturated mechanically. Cell suspensions prepared in ultra low binding 6 well plates (Corning) in serum-free MHM (Medium Hormone-Mix) medium (DMEM-F12 supplemented with modified N2 medium composed of 100 mg/L apo-transferrin, 25 mg/L recombinant human insulin, 100  $\mu$ M putrescine, 20 nM progesterone, and 30 nM sodium selenite, 2 mM glutamine, 6 mg/ml glucose, 14 mM NaHCO<sub>3</sub> and 5mM HEPES) containing 20 ng/ml EGF and bFGF as described previously [19].

For the proliferation assays, cells from the above established GBM culture were seeded in laminin coated 96-well black-well/clear-bottom plate (Greiner Bio-One, Alphen, the Netherlands) at a density of 2,000 cells/well in MHM medium. Treatment was started after one to two days when about 3-5% cell confluence was reached. Next, the medium was replaced by MHM medium containing 0.1% DMSO as a control, or 100  $\mu$ M TMZ alone, or in combination with increasing concentrations of ABT-888 (0.3  $\mu$ M to 30  $\mu$ M). For inhibition of Abcb1 and/or Abcg2, 1  $\mu$ M of elacridar was added. Cell density/viability was determined on day 0 (treatment start) and day 5 using bioluminescence imaging on an IVIS Lumina II Imaging System (Xenogen, Corporation, Alameda, CA, USA) with 150  $\mu$ g/ml of luciferin in each well.

For Western blotting, GBM cells were cultured on laminin as in anti-proliferation assay in 6 well plates and drugs were added during 4 h when 80-90% cell confluence was reached. Next, Cells were lysed with complete RIPA buffer, containing phosphatase inhibitors. Cell lysate was processed for Western blotting as described elsewhere [20, 21]. Primary antibodies used in this study are rabbit anti-PAR (1:1000, Trevigen) and mouse anti- $\beta$ -tubulin isotype III (1:1000, Sigma, Saint Louis, MO). Enhanced chemiluminescence (ECL) was used for detection using Molecular imaged ChemiDoc™ XRS+ system (Bio-Rad). Data were analyzed using ImageLab software (version 2.0.1) from Bio-Rad laboratories.

### ***Pharmacokinetic calculations and statistical analysis***

We applied the GLM (General linear model) repeated measures procedure to analyze the results of concentration equilibrium transport experiments using SPSS (v17.0; SPSS Inc, Chicago, IL, USA). The differences of the percentage ratio of peak area of the measured samples to the reference (medium sampled at time=0) between apical and basolateral compartments were considered as the observed values from repeated measurements. They were grouped by defining 4 sampling time points (1, 2, 3 and 4 hr) as a 4-level within-subjects factor. Simple contrast was selected to compare the differences between the mean observed values of 2, 3 and 4 hr and 1 hr. Then, the multivariate significance tests were performed to determine whether the apical-basolateral differences of the ABT-888 levels were significantly increased by the factor of time.

For *in vivo* pharmacokinetic experiments, pharmacokinetic parameters were calculated using an add-in program for Microsoft Excel PKSolver [22]. To determine the differences

of brain and plasma concentrations among multiple strains, one-way analysis of variance (ANOVA) and post-hoc Bonferroni was performed. Differences were considered statistically significant when  $P < 0.05$ .

Survival fractions were calculated using Kaplan-Meier method by GraphPad Prism 5.01 (GraphPad Software, Inc., La Jolla, CA, USA). The log-rank test was used to compare survival of groups. Differences between groups were analyzed using ANOVA protected least significant difference for comparing groups.

## RESULTS

### ***P53;Ink4a/Arf;K-Rasv12 GBM are resistant to TMZ or TMZ and ABT-888 treatment in vivo***

Traditionally established GBM cell lines grown in serum containing media have lost important characteristics of GBM, including subpopulations of tumor stem cells, and thus may not recapitulate the *in vivo* biology and/or actual therapeutic responsiveness of human GBM [11]. For example, U87MG, a frequently used GBM cell lines for the evaluation of therapeutic agents, responds dramatically to temozolomide (TMZ) treatment [23] even at low doses (supplementary Fig. 1). Similar tumor sensitivity to TMZ has been observed in other models [20, 21]. Taking into account the much more modest activity of TMZ in combination with radiotherapy in GBM patients, these models might not be accurate for evaluating the efficacy of agents that may potentiate TMZ chemotherapy. We took advantage of our previously established conditional mouse models of GBM [17] to generate GBM cell lines, which harbor all of the most frequently activated pathways of human GBM [24]. The GBM652457 cells were isolated from the tumors of P53;Ink4a/Arf;K-Rasv12;LucR mice and cultured in serum-free MHM media. Tumors that developed after intracranial injection into nude mice resemble many pathological features of human high-grade gliomas [17]. Mice were stratified based on the bioluminescence readings and received either no treatment (control), single treatment with 100 mg/kg TMZ q.d. or combined with 10 mg/kg ABT-888 b.i.d. for 5 days. Although there was a slight delay in tumor growth in the treatment groups (Fig. 1), no significant differences of survival have been found between treated groups and control group ( $P = 0.37$ ), or between two treated groups ( $P = 0.22$ ). Since these mice received only one cycle 5-day treatment, this lack of efficacy reflects innate and not acquired resistance to the TMZ and/or ABT-888 combination therapy.

### ***ABT-888 is an excellent substrate of both Abcb1 and Abcg2***

It is well established that the drug efflux transporters Abcb1 and Abcg2 can severely impair the brain penetration of therapeutic agents. In addition, Abcb1 is known to be a major determinant of the response of tumor cells to the PARP inhibitor olaparib [25, 26]. To determine whether ABT-888 is also a substrate of Abcb1 and/or Abcg2, we assessed the translocation ratio of ABT-888 by the concentration equilibrium transport assay in murine Abcb1 and Abcg2 or human ABCB1 and ABCG2 transduced cell relative

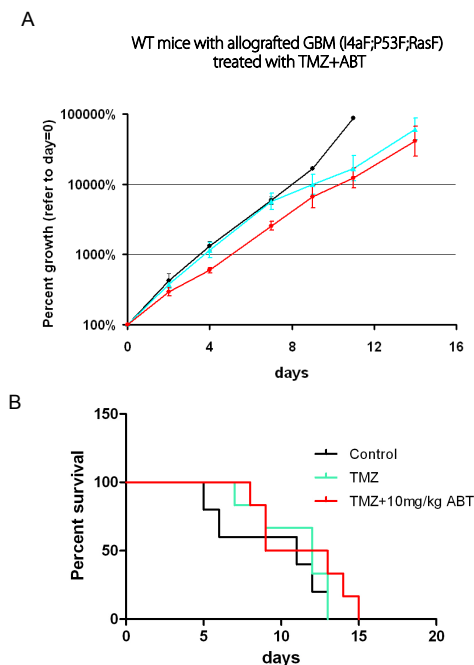


**Fig. 1.** Efficacy of ABT-888 in combination with TMZ in P53;Ink4a/Arf;K-Rasv12 GBM652457 allografts implanted intracranially in WT immunodeficient mice. TMZ was administered p.o. at 100 mg/kg q.d. alone or with ABT-888 at 10 mg/kg b.i.d. for 5 days. A, Tumor growth curves of mice in control (no treatment received), TMZ treatment and TMZ combined with ABT-888 treatment groups, calculated as the ratio of bioluminescence in time vs the initial assessment. B, Kaplan-Meier analysis for GBM related survival. Data are means  $\pm$  SD. n= 5, 6 and 6 for mice in control, TMZ and TMZ+ABT treated group, respectively.

to corresponding controls. As shown in Fig.2 A, a significant basolateral to apical translocation of ABT-888 during 4 hours was caused by both the endogenously expressed porcine *Abcb1* in the LLC-PK1 cells and exogenous *Abcb1*, because the translocation of ABT-888 either in LLC-PK1 or LLC-Mdr1a was completely blocked by the specific P-gp inhibitor zosuquidar. Similarly, a significant directional translocation of ABT-888 was observed in MDCK-Bcrp1 cells. This was exclusively due to *Abcg2* since there was no translocation of ABT-888 in MDCK-parent cells and this translocation was inhibited by the *Abcb1* and *Abcg2* inhibitor elacridar (Fig.2 B). Therefore, ABT-888 is transported both by *Abcb1* and *Abcg2*. Furthermore, we tested translocation of ABT-888 in corresponding cell lines that over-express human ABCB1 and ABCG2, and we observed that the average basolateral to apical ratio of ABT888 in LLC-MDR1 cells was higher (at 4 hour: 67.8% of original concentration) than that in LLC-PK1 cells (28.9%), indicating that ABCB1 also transport ABT-888 (Fig. 2 C). ABT-888 appears to be a weaker substrate of ABCG2 since there was only a trend towards basolateral-to-apical translocation of ABT-888 in MDCK-BCRP cells. However, it must be noted that we commonly find that the translocation of a substrate drug is much more efficient in MDCK-Bcrp1 cells than in MDCK-BCRP cells,

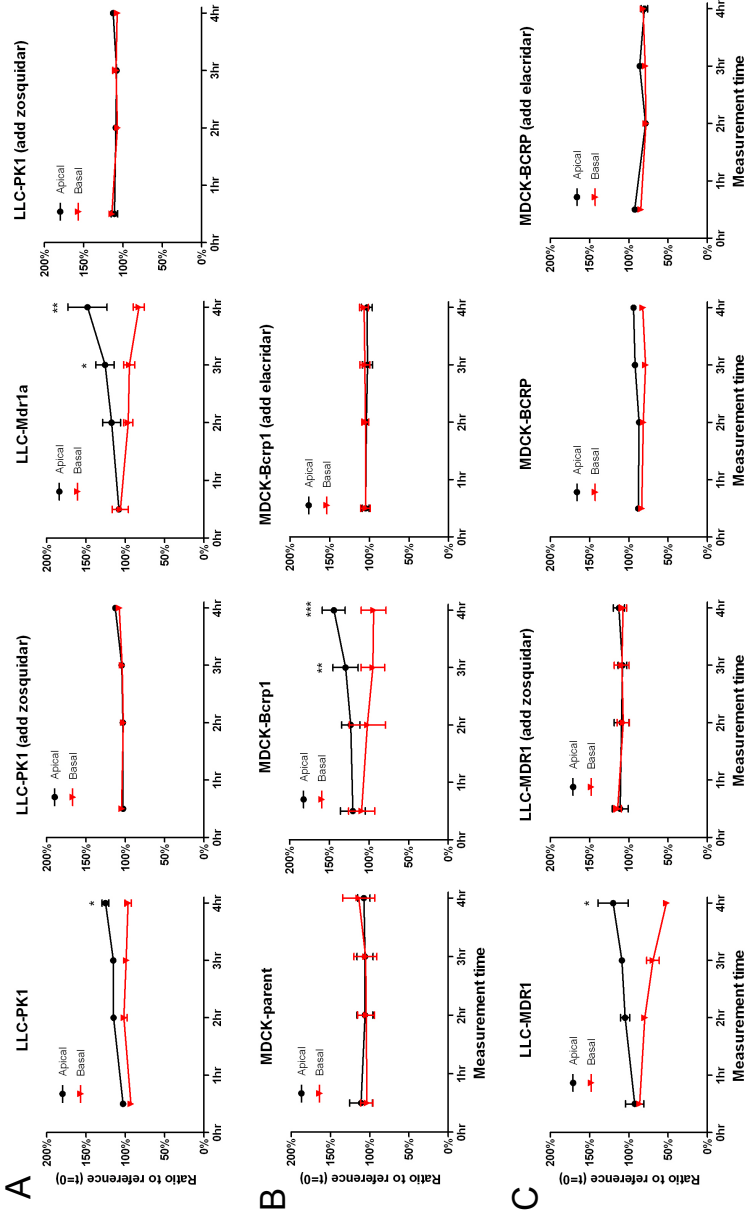


**Fig. 2.** Transcriptional translocation of ABT-888 was assessed using (A and C) parental LLC-PK1 cells and cells transduced with mouse Abcb1a (LLC-Mdr1a) or human ABCB1 (LLC-MDR1), or (B and C) parental MDCKII cells (MDCK-parent) and cells transduced with mouse Abcg2 (MDCK-Bcrp1) or human ABCG2 (MDCK-BCRP). The setup was a concentration equilibrium assay, starting with an equal drug concentration in apical and basal compartment: Zosuquidar (5  $\mu$ M) in MDCK-BCRP cells to inhibit the transport mediated by Abcg2/ABCG2. Results are presented as the ratio of ABCB1. Elacridar (5  $\mu$ M) in MDCK-BCRP1 or MDCK-BCRP cells to inhibit the transport mediated by Abcb1/ABCB1. Data are means  $\pm$  SD; n = 6 per experiment. \* P < 0.05, \*\* P < 0.01, \*\*\* P < 0.001.

suggesting a more general difference in the transport properties between the two cell lines.

**Elacridar enhances the anti-proliferative effect of TMZ and ABT-888 treatment in GBM cells in vitro**

Both Abcb1 and Abcg2 have established roles in conferring resistance to anticancer drugs by limiting their cellular accumulation [27, 28]. As we have found that ABT-888 is a substrate of both Abcb1 and Abcg2, it is of interest to assess the impact of these two transporters on in vitro growth inhibition of the GBM cell lines by TMZ and ABT-888 treatment. As shown in Fig. 3 A, 1  $\mu\text{M}$  of ABT-888 alone or with elacridar did not affect the proliferation of p53;Ink4a/Arf;K-Rasv12;LucR GBM652457 cells. However, inhibition of Abcb1 or Abcb1 plus Abcg2 by elacridar increased the efficacy of ABT-888 to synergize with 100  $\mu\text{M}$  of TMZ. Elacridar also enhanced the target inhibitory effect of ABT-888, as shown by the reduced PAR level by combined treatment with elacridar in the same GBM cell lines (Fig. 3 B). The effect was lost at concentrations of 10  $\mu\text{M}$  of ABT-888 or higher.

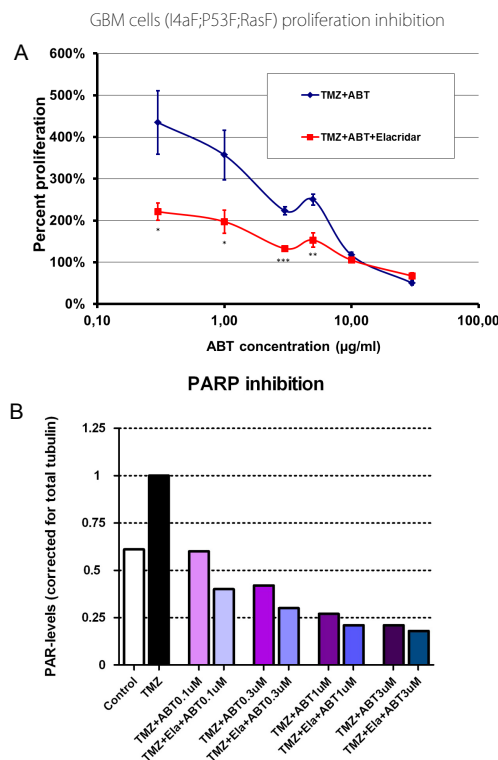


**Fig. 3.** P53;Ink4a/Arf;K-Rasv12 GBM652457 cell proliferation ratio after exposure to TMZ at a fixed concentration of 100  $\mu\text{M}$  and ABT-888 at concentrations of 0.3, 1, 3, 5, 10, 30  $\mu\text{M}$  with/without presence of elacridar. Cell growth was monitored using bioluminescence at day 0 and 5 after adding drugs. A, Statistical analysis of the difference of cell proliferation among the different treatments. Data are means  $\pm$  SE; n = 4 per treatment. \* P < 0.05, \*\* P < 0.01. \*\*\* P < 0.001. Elacridar vs controls. B, Quantification of Poly ADP-ribose (PAR) Western Blotting results of GBM cell lysates after ABT-888 treatment with/without elacridar.

Most likely it is due to Abcb1 and/or Abcg2 are no longer capable to keep the intracellular accumulation of ABT-888 below a pharmacologically active level (supplementary Fig. 4).

***Brain penetration of AB-888 is restricted by Abcb1 and Abcg2 and can be enhanced by oral elacridar administration***

Next, we evaluated whether Abcb1a/1b and/or Abcg2 have an impact on the plasma and brain pharmacokinetics of ABT-888 by using WT, Abcb1a/1b<sup>-/-</sup>, Abcg2<sup>-/-</sup>, and Abcb1a/1b<sup>-/-</sup>;Abcg2<sup>-/-</sup> mice. Following i.v. administration of 10 mg/kg of ABT-888, the plasma AUC<sub>i.v.</sub> did not differ significantly among the various strains although there was a slight difference in the ABT-888 plasma concentration at 1 hr (Fig. 4 A). Consequently, Abcb1 and Abcg2 are not likely to play critical roles in the systemic clearances of ABT-888. In contrast, the brain AUC<sub>i.v.</sub> of both Abcb1a/1b<sup>-/-</sup> and Abcb1a/1b<sup>-/-</sup>;Abcg2<sup>-/-</sup> mice were significantly higher than that of WT mice (3.8 and 4.9-fold higher, respectively), demonstrating that Abcb1 expressed at BBB severely impairs the brain entry of ABT-888. Although the brain AUC<sub>i.v.</sub> of WT and Abcg2<sup>-/-</sup> mice were similar, the additional deletion of the Abcg2 gene in Abcb1a/1b<sup>-/-</sup>;Abcg2<sup>-/-</sup> mice caused a further 1.3-fold increase of the brain AUC<sub>i.v.</sub> of ABT-888 relative to Abcb1a/1b<sup>-/-</sup> mice, indicating that Abcg2 is also restricting the brain entry of ABT-888. Interestingly, the lack of Abcb1a/b leads to continuously increasing brain-to-plasma ratio of ABT-888 in Abcb1a/1b<sup>-/-</sup> and Abcb1a/1b<sup>-/-</sup>;Abcg2<sup>-/-</sup> mice in a time course of 4 hr. This implies that the clearance from the brain does not keep up with the systemic clearance, demonstrating the important role of Abcb1 in brain ABT-888 clearance. In addition, Abcc4, another relevant drug efflux transporters expressed at BBB, is not likely to be involved in brain penetration/accumulation of ABT-888 since we did not find any difference of brain concentration, brain-to-plasma ratio and brain distribution of ABT-888 between Abcb1a/1b<sup>-/-</sup>;Abcg2<sup>-/-</sup> and Abcb1a/1b<sup>-/-</sup>;Abcg2<sup>-/-</sup>;Abcc4<sup>-/-</sup> mice at 1 hr (Supplementary Fig 2).

Next, we evaluated whether pharmacologic inhibition of Abcb1 and Abcg2 by elacridar could also increase the brain accumulation of ABT-888. Since oral administration is the route of administration in patients, ABT-888 was p.o. administrated to WT and Abcb1a/1b<sup>-/-</sup>;Abcg2<sup>-/-</sup> mice with or without co-administration of elacridar 15 min prior to ABT-888. By using a dose of 10 mg/kg we achieved maximum plasma levels that are in line with those observed in patients [29] (Fig. 4 B). Moreover, co-administration of elacridar did not lead to major changes in the plasma concentration in 4 hr. There was



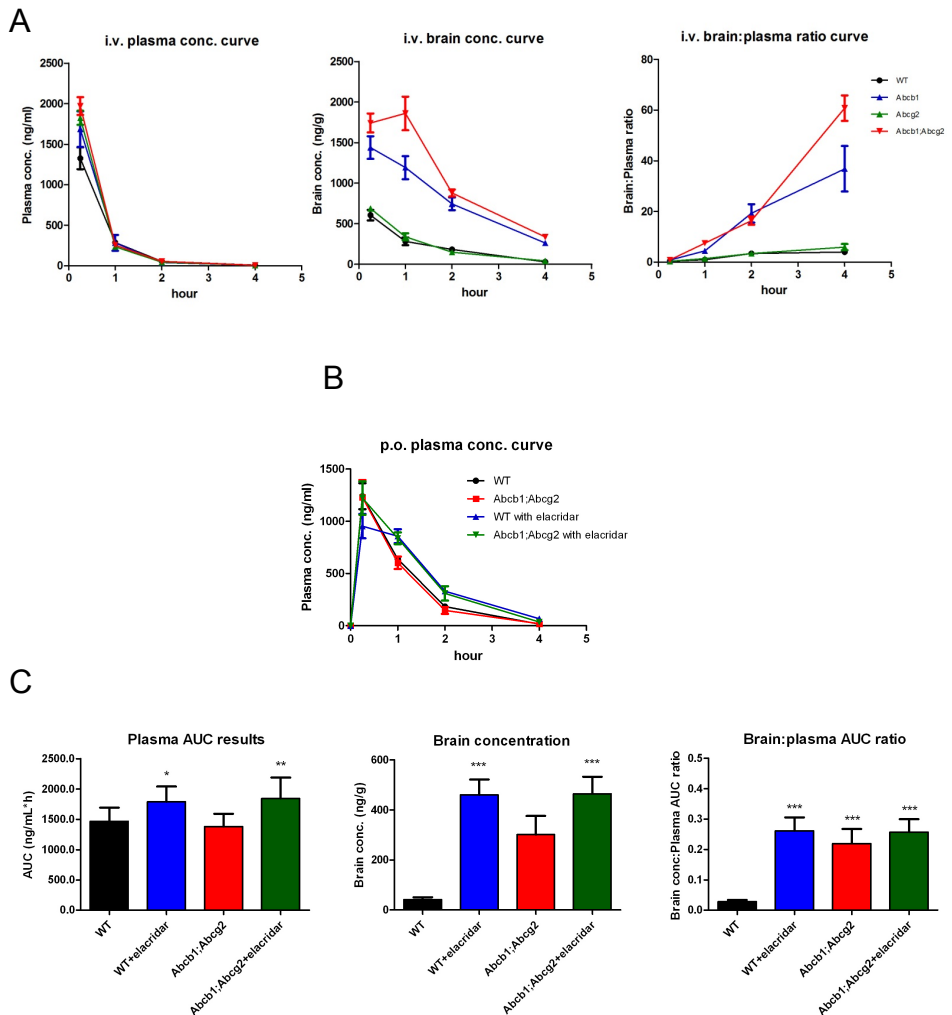


**Fig. 4.** ABT-888 plasma concentrations, brain concentrations and brain-to-plasma ratios following i.v. or p.o. administration of 10 mg/kg of ABT-888. A, ABT-888 was i.v. administrated to WT, Abcb1a/1b<sup>-/-</sup>, Abcg2<sup>-/-</sup>, and Abcb1a/1b<sup>-/-</sup>;Abcg2<sup>-/-</sup> mice and plasma and brain samples were collected at 15 min, 1, 2 and 4 hr. B, ABT-888 was p.o. administrated to WT and Abcb1a/1b<sup>-/-</sup>;Abcg2<sup>-/-</sup> mice with co-administration of 100 mg/kg elacridar. Plasma samples were collected from tail blood at 15 min, 1, 2 and 4 hr. Brain samples for analysis of ABT-888 concentration were collected 4 hr after drug administration. Data are presented as means ± SD, n = 5 animals per group. \* P < 0.05, \*\* P < 0.01. \*\*\* P < 0.001. Statistical significance was determined by comparison of values of knockout with WT mice.

a trend towards a higher plasma AUC<sub>p.o.</sub> of ABT-888 with elacridar, but since this effect was also seen in *Abcb1a/1b<sup>-/-</sup>;Abcg2<sup>-/-</sup>* mice receiving elacridar this is most likely due to off-target effects (e.g. inhibition other drug elimination pathways) (Fig. 4 C). Importantly, elacridar caused an 11-fold increased brain concentration of ABT-888 in WT mice.

Elacridar also increased the brain concentration of ABT-888 in *Abcb1a/1b<sup>-/-</sup>;Abcg2<sup>-/-</sup>* mice, but this was due to the higher plasma level of ABT-888 in this group. When we normalized the brain levels to the plasma AUC in each cohort the brain-to-plasma AUC<sub>p.o.</sub> ratio of *Abcb1a/1b<sup>-/-</sup>;Abcg2<sup>-/-</sup>* mice receiving elacridar was similar to that of *Abcb1a/1b<sup>-/-</sup>;Abcg2<sup>-/-</sup>* mice whereas brain-to-plasma ratio of WT mice receiving elacridar was 9-fold higher than WT controls. Together, oral administration of elacridar significantly enhances the brain accumulation of ABT-888 and this effect is mainly due to its inhibition of *Abcb1* and *Abcg2* at BBB.

#### ***Co-administration of elacridar enhances the efficacy of TMZ and ABT-888 against GBM***

Since the absence of *Abcb1* and *Abcg2* at BBB significantly increased the brain penetration of ABT-888, we investigated whether this elevated brain accumulation of ABT-888 would result in an improved efficacy of TMZ and ABT-888 treatment. For this purpose, we repeated the *in vivo* efficacy experiment with P53;Ink4a/Arf;K-Rasv12;LucR GBM652457 cells but now injected into *Abcb1a/1b<sup>-/-</sup>;Abcg2<sup>-/-</sup>* nude mice instead of WT nude mice. As shown in Fig 5 A, we observed an overall better response to TMZ and ABT-888 treatment in *Abcb1a/1b<sup>-/-</sup>;Abcg2<sup>-/-</sup>* mice than in WT mice, reflected by the fact that both the tumor growth and survival curves between TMZ treated and TMZ plus ABT treated groups are diverged more pronounced. The mice receiving ABT-888 had significantly prolonged survival than mice in control group (median survival 15 vs 9 day;  $P = 0.004$ ), which was not observed previously in WT mice. The difference in survival between the TMZ only vs the TMZ + ABT888 treated groups is not significant (median survival is 11 vs 15 day, respectively;  $P = 0.17$ ), probably due to the lack of sufficient number of mice.

Besides the presence of *Abcb1* and *Abcg2* at BBB, their presence at the cell membrane of tumor cells may also hinder ABT-888 to reach its intercellular target. This impact on cellular accumulation of ABT-888 can be reversed by elacridar, as demonstrated *in vitro*. We found that intracranial GBM652457 cells express *Bcrp1* (S. Fig. 5) To investigate whether *Abcb1* and *Abcg2* presence in tumor cells also limit the efficacy of TMZ and

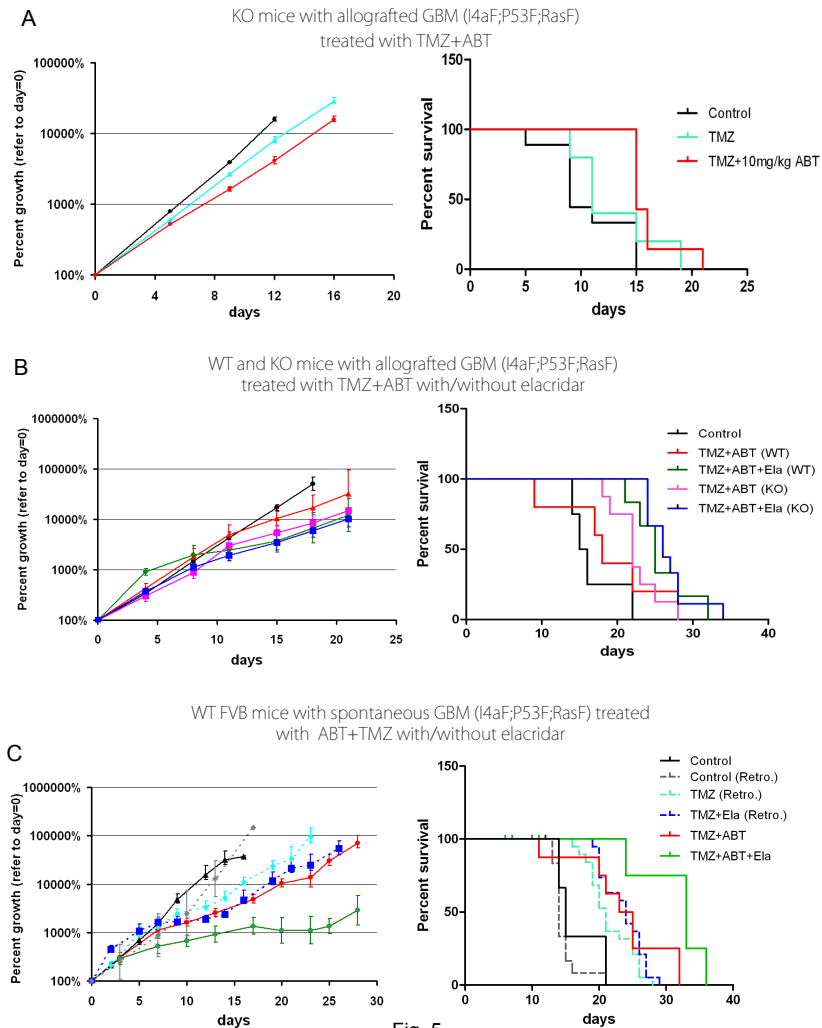


Fig. 5

**Fig. 5.** Efficacy of TMZ and ABT-888 treatment in combination with elacridar against P53;Ink4a/Arf;K-Ras<sup>v12</sup> GBM652457 cells injected intracranially into WT or *Abcb1a/1b*<sup>-/-</sup>;*Abcg2*<sup>-/-</sup> mice or against spontaneous P53;Ink4a/Arf;K-Ras<sup>v12</sup> tumors induced by intracranial injection of lenti-Cre virus [22]. TMZ was p.o. administrated at 100 mg/kg q.d. alone, or concurrently with p.o. ABT-888 at 10 mg/kg b.i.d., and/or p.o. elacridar at 100 mg/kg q.d. 15 min prior to TMZ for 5 days. A B and C left panels, tumor growth ratio curves. A B and C right panels, Kaplan-Meier analysis for GBM related survival. Data are means  $\pm$  SD. A, n= 6, 7 and 9 for mice in control, TMZ and TMZ+ABT treated group, respectively. B, n=3, 5, 6, 8, 8 for mice in control, TMZ+ABT (WT mice), TMZ+ABT+elacridar (WT mice), TMZ+ABT (KO mice), TMZ+ABT+elacridar (KO mice) treated group, respectively. C, n=15 (mice from previous and current studies), 19 (previous study), 22 (previous study), 8, 8 for mice in control, TMZ, TMZ+elacridar, TMZ+ABT, TMZ+ABT+elacridar treated group, respectively.

ABT-888 *in vivo*, we administrated elacridar together with TMZ and ABT-888 to both WT and *Abcb1a/1b<sup>-/-</sup>;Abcg2<sup>-/-</sup>* mice bearing orthotopic P53;Ink4a/Arf;K-Ras<sup>v12</sup>;LucR GBM652457 to compare with their counterparts receiving only TMZ and ABT-888 but not elacridar. Indeed, *Abcb1* and *Abcg2* in tumor cells also impair the effect of TMZ and ABT-888 because the *Abcb1a/1b<sup>-/-</sup>;Abcg2<sup>-/-</sup>* mice receiving elacridar survived significantly longer than mice of same strain receiving only TMZ and ABT-888 (Median survival 26.5 vs 22 days, Fig. 5 B). WT mice receiving elacridar in combination with TMZ and ABT-888 responded as similarly good as *Abcb1a/1b<sup>-/-</sup>;Abcg2<sup>-/-</sup>* mice, suggesting that elacridar effectively inhibited *Abcb1* and *Abcg2* both at BTB/BBB and in tumor cells. Overall, elacridar enhanced the tumor inhibitory effect and significantly prolonged the survival of WT mice received TMZ and ABT treatment (median survival is 25 vs 18 day for WT mice received TMZ+ABT+elacridar vs TMZ+ABT, respectively.  $P = 0.039$ ).

Next, we used our recently established spontaneous high-grade glioma model induced by lentivirus in LoxP conditional P53;Ink4a/Arf;K-Ras<sup>v12</sup>;LucR mice [17] to evaluate the therapeutic effect of TMZ and ABT-888 with or without co-administration of elacridar. For comparison, we included data from a previous study where animals were treated with TMZ or TMZ + elacridar (Fig. 5 C).

These studies demonstrate that TMZ does have an effect on the survival in this model and that elacridar enhances the efficacy of TMZ in this model, because TMZ is a (weak) substrate of *Abcb1* and *Abcg2* (de Vries et al., submitted). When TMZ was combined with ABT-888 the response was only marginally better (median survival is 24 vs 21 day for mice received TMZ+ABT vs TMZ, respectively.  $P = 0.156$ ). However, when we used elacridar together with TMZ and ABT the response was significantly improved (median survival is 33 vs 24 day for mice received TMZ+ABT+elacridar vs TMZ+ABT, respectively.  $P = 0.023$ ), which supports the idea that *Abcb1* and *Abcg2* at BBB/BTB and in tumor cells restricts the efficacy.

### ***PTEN deficiency renders GBM sensitive to TMZ and ABT-888 treatment in vitro and in vivo***

McEllin and colleagues recently showed that PTEN-null astrocytes have a compromised homologous recombination DNA repair pathway, which makes them more sensitive to treatment with TMZ and the PARP inhibitor ABT-888 due to synthetic lethality [30].

Since these data are based on *in vitro* experiments only, we now investigated whether PTEN deficiency is also important to determine the *in vivo* response to TMZ and ABT-888 treatment in our GBM models. First, we compared cell lines established from spontaneous tumors in Ink4a/Arf;K-Ras<sup>v12</sup>;LucR mice and equivalents harboring additional PTEN and/or P53 deletions. Western blotting using anti-PAR antibody showed that PARP inhibition by ABT-888 at concentrations ranging from 0.1 to 3  $\mu$ M among all cell lines is similar (supplementary Fig. 4). In presence of TMZ, the Pten;Ink4a/Arf;K-Ras<sup>v12</sup>;LucR GBM cells indeed were much more sensitive to ABT-888, because about 70% cell growth was inhibited even at the lowest concentration of ABT-888 (0.3  $\mu$ M) relative to those in TMZ only medium, and this ratio dropped remarkably with increasing concentrations of ABT-888 (Fig. 6 A). In contrast, P53;Ink4a/Arf;K-Ras<sup>v12</sup>;LucR GBM652457 cells appeared to be much more resistant to combination treatment with ABT-888. Moreover, combined P53;PTEN-null GBM707263 cells also responded better to ABT-888 than the P53-null;PTEN-proficient GBM652457 cells but not as good as the P53-proficient;PTEN-null GBM696677 cells. This result has been confirmed in at least one other GBM cell line of the same genotype (except for the Ink4a/Arf;K-Ras<sup>v12</sup>;LucR genotype) and similar results were obtained (supplementary Fig. 3).

Next, we treated both WT and Abcb1a/1b<sup>-/-</sup>;Abcg2<sup>-/-</sup> mice orthotopically injected with Pten;Ink4a/Arf;K-Ras<sup>v12</sup>;LucR GBM696677 cells with TMZ and ABT-888. These mice survived relatively short due to the aggressive growth of these cells *in vivo*. Control group mice bearing this cell line experienced a 100-fold increase relative to the initial tumor bioluminescence within 5 days, relative to about 10 to 14 days for the P53;Ink4a/Arf;K-Ras<sup>v12</sup>;LucR GBM control group animals, thus leaving only a short time windows for drug intervention. Nevertheless, a clear benefit from TMZ+ABT-888 treatment was achieved for WT mice bearing PTEN-null GBM696677 tumors relative to control group or single TMZ treated animals (median survival is 10, 8 and 7 days for mice treated with TMZ+ABT-888, single TMZ and no treatment, respectively. TMZ+ABT vs TMZ:  $P = 0.044$  ; TMZ+ABT vs control:  $P = 0.0004$ ). Because such a therapeutic benefit of ABT-888 was not found in the WT mice bearing P53-null;PTEN-proficient GBM as was shown above (Fig. 1), this indicates that PTEN deficiency also sensitize GBM to TMZ and ABT-888 treatment *in vivo*. Importantly, Abcb1a/1b<sup>-/-</sup>;Abcg2<sup>-/-</sup> mice even benefited more from the TMZ and ABT-888 treatment regarding the bigger difference between these mice treated with additional ABT-888 or not (median survival is 12 vs 9 day for KO mice received

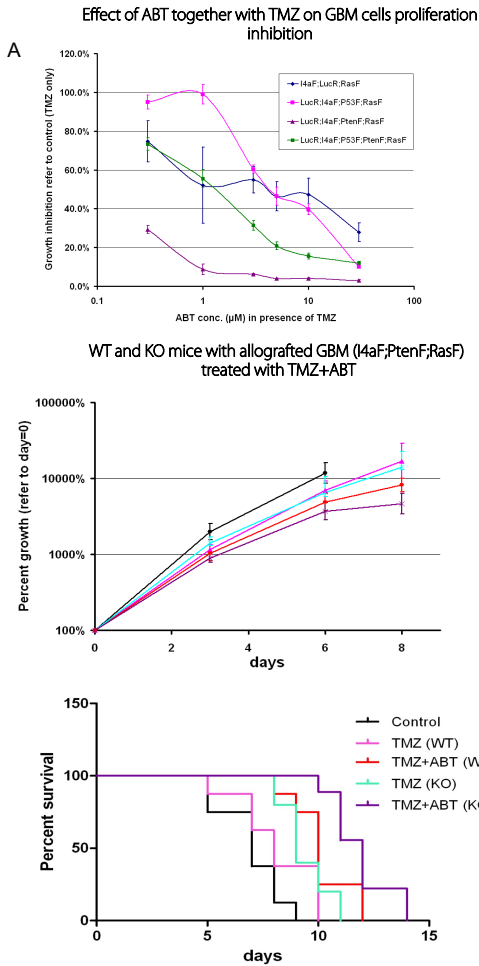


**Fig. 6.** GBM cells established from different genetic backgrounds were exposed to TMZ 100  $\mu$ M and increasing concentrations of ABT-888 and demonstrate that Pten deficient cells were the most sensitive (A). We here show the result in the GBM696677 cell line, but this was confirmed in another Pten deficient cell line. Data as percentage relative to treatment with TMZ only are means  $\pm$  SE;  $n = 4$  per treatment.. Next, the efficacy of ABT-888 in combination with TMZ against Pten;Ink4a/Arf;K-Ras<sup>v12</sup> GBM696677 cells injected intracranially into WT or Abcb1a/1b<sup>-/-</sup>;Abcg2<sup>-/-</sup> mice was investigated. TMZ was p.o. administrated at 100 mg/kg q.d. alone, or concurrently with ABT-888 at 10 mg/kg b.i.d. for 5 days. (B), Tumor growth ratio curves of mice in control (no treatment received), TMZ treatment and TMZ combined with ABT-888 treatment group. B, Kaplan-Meier analysis for GBM696677 related survival. Data are means  $\pm$  SD.  $n = 5, 6$  and  $6$  for mice in control, TMZ and TMZ+ABT treated group, respectively.

TMZ+AB vs TMZ, respectively.  $P = 0.0006$ ). This suggests that the roles of Abcb1 and Abcg2 at BBB and BTB become even more critical for those GBMs being sensitive to TMZ and ABT-888 treatment.

## DISCUSSION

This study, using clinically relevant *in vivo* high grade glioma mouse models, shows that the PARP inhibitor ABT-888 may improve the efficacy of TMZ chemotherapy against high-grade gliomas. However, we have also identified two important factors that may determine the outcome of this combination treatment. Firstly, the ABC-transporters ABCB1 and ABCG2 restrict the penetration of ABT-888 through the BBB and the entry into tumor cells. Secondly, therapeutic benefit in WT mice was only significant in PTEN deficient tumors. Importantly, responses were observed at dose levels of ABT-888 that provide a systemic exposure, which is clinically achievable. Based on these results we propose that GBM patients entered into clinical trial should be stratified according to the PTEN status of their tumor. Moreover, concomitant inhibition of ABCB1 and ABCG2 by elacridar may further improve the efficacy of ABT-888, so that PTEN proficient tumors may also become responsive to ABT-888.

P53, PTEN and Ink4a/Arf are among the most frequently mutated or deleted genes in GBM [18]. We have previously developed high-grade gliomas models using transgenic mice carrying these genes between loxP sites that are deleted in brain cells following intracranial injection of Lenti-Cre virus. The tumors that develop in these mice, as well as tumors from cell lines derived from these spontaneous tumors and reinjected back into recipient mice, resemble many features that are characteristic for human GBM [31]. In the present study, we have used these models to evaluate the efficacy of ABT-888 to potentiate the activity of TMZ against high-grade glioma. Chemoradiation following surgical resection is the standard therapy for GBM and by its ability to interfere with DNA repair, PARP inhibitors such as ABT-888 are expected to further enhance the efficacy of DNA-damaging therapies. However, the first trial using WT mice injected with P53;Ink4a/Arf;K-Ras<sup>v12</sup> GBM652457 cells, demonstrated only a very minor response to this combination therapy. Further investigation to the reasons that may be responsible for the poor response demonstrated that ABT-888 is a good substrate of two drug efflux transporters Abcb1 and Abcg2 that are expressed at the BBB. Indeed, we observed a more favorable response when repeating this experiment with the GBM652457 cell line injected into our Abcb1a/1b<sup>-/-</sup>;Abcg2<sup>-/-</sup> mice, which do not express these transport proteins at the BBB. Immuno-staining revealed that Bcrp1 was present in the tumor vessels (s. Fig. 5). This staining was specific, because it was not found in tumor vessels of

Bcrp1 deficient *Abcb1a/1b<sup>-/-</sup>;Abcg2<sup>-/-</sup>* mice. Importantly, Bcrp1 was also found in tumor cells, albeit that this staining was not uniform throughout the tumors. Considering that BCRP is a marker of early progenitor or stem cells, these Bcrp1 positive regions may reflect the areas of the tumor enriched for tumor initiating cells. Subsequently we successfully used elacridar in combination with TMZ and ABT-888 to increase the efficacy, which may indicate that also these cells were targeted more efficiently (Fig. 5B).

Clearly, the response for ABT-888 that is observed in our high-grade glioma models is not as profound as reported previously [9,10] using other intracranial models. There are several reasons that may explain this discrepancy. Firstly, the intracranial models in the previous studies have leaky vessels. Because of this the tumors are well accessible for drugs, which may lead to over-prediction of their efficacy. In fact, the accessibility is limited due to the BBB. Although high grade gliomas are heterogeneous, with leaky centers, they also comprise invasive regions with more intact BBB properties. Moreover, the bulk mass of tumor that contains the more leaky vessels is usually resected by surgery, whereas the invasive GBM cells that have migrated to more distant areas in the brain are shielded by an intact BBB.

Secondly, the GBM cell lines used for the classical models have been maintained on serum containing media for many generations, which is known to cause loss of critical characteristics contained within tumor stem cells. Importantly, these include chemotherapy resistance profiles such as expression of several ABC transporters, active DNA-repair capacity, and resistance to apoptosis [12, 32]. Most likely, the high-grade models (allograft and spontaneous) used in this study are a much more stringent models for drug testing.

Finally, in this study we used a dose of 10 mg/kg throughout all *in vivo* studies since this dose results in a clinically relevant systemic exposure of ABT-888. Recent clinical trials report a peak plasma level of 500 ng/ml with an AUC of 3500 ng/ml\*h [33]. Previous preclinical studies have been using much higher doses of up to 50 mg/kg. Further increasing of the dose in patients to improve the efficacy, will probably result into unacceptable toxicity. Interestingly co-administration of elacridar hardly affected the systemic exposure of ABT-888 (Table 1), but elevated the brain concentration of ABT-888 substantially (11-fold increase at 4 hr). Consequently, this combination may allow



improved local drug delivery to the brain, without increased systemic exposure and toxicity.

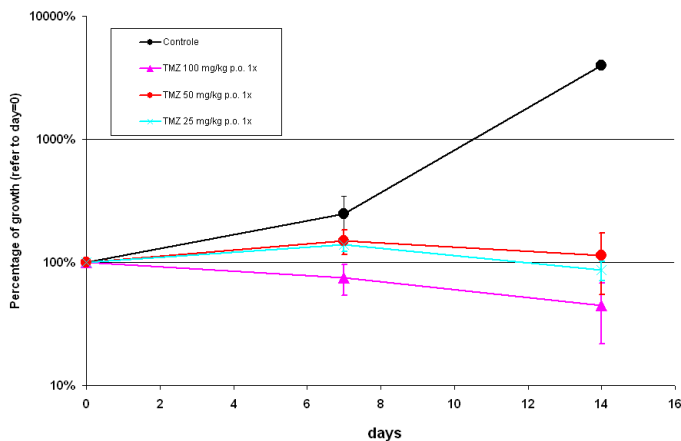
When exploring the efficacy of ABT-888 in our panel of spontaneous high-grade glioma derived cell lines, we also found that cell lines that are deficient in PTEN but not in P53 were much more sensitive to TMZ and ABT-888 treatment than those deficient in P53 or proficient PTEN. Our results support the *in vitro* data reported by McEllin et al [30] showing that PTEN-null astrocytes have a disturbance in the homologous recombination DNA repair pathway and this causes a synthetic lethality when the base excision repair activity is inhibited by a PARP inhibitor. Next, we took advantage of the fact that we could further explore this concept using our *in vivo* high-grade glioma models. Both WT and *Abcb1a/1b*<sup>-/-</sup>;*Abcg2*<sup>-/-</sup> mice bearing tumors from *Pten;Ink4a/Arf;K-Ras*<sup>v12</sup> GBM696677 responded better to the TMZ and ABT-888 treatment than the mice bearing P53-null; PTEN proficient GBM652457 tumors. Notably, however, although the PTEN deficient GBM696677 cell line is more sensitive to TMZ and ABT-888 treatment, the effect of this combination on the tumor growth *in vivo* was not as dramatic as might have been hoped for based on the results obtained *in vitro*. This finding on one hand reminds us that the tumor environment of GBM cells proliferating *in vivo* can help these cells to escape from the lethal effects of drugs. On the other hand, it highlights the importance of using the appropriate preclinical models to evaluate the drug efficacy objectively.

Obviously, these preclinical findings needed to be validated / confirmed in patients. With respect to the currently ongoing clinical trial with ABT-888 in glioma patients, it would seem a plausible strategy to include a subgroup analysis in patients whose tumor harbors a PTEN deletion (about 40% of GBM's), since there is now reasonable evidence that this may be the subgroup of patients receiving the greatest benefit of PARP inhibitors. Moreover, we have shown that the efficacy of ABT-888 and TMZ combination therapy may be improved by inhibitors of ABCB1 and ABCG2.

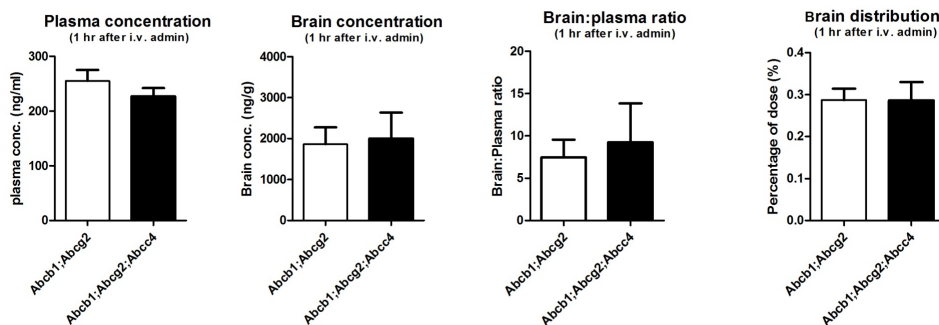
#### **Acknowledgements.**

This work has been supported by a grant of the foundation “www.StopHersentumoren.nl”.

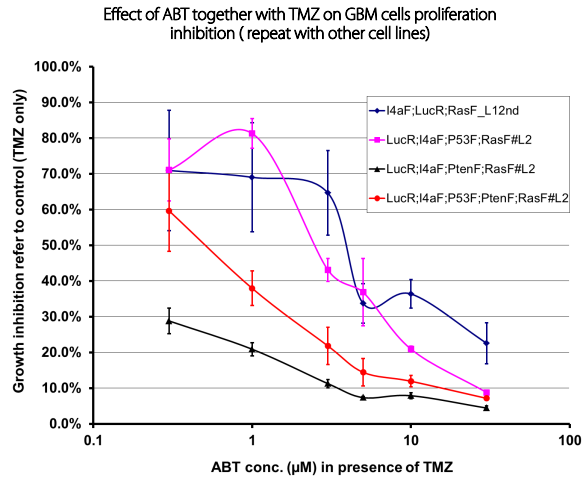
## WT mice with xenografted U87 treated with TMZ



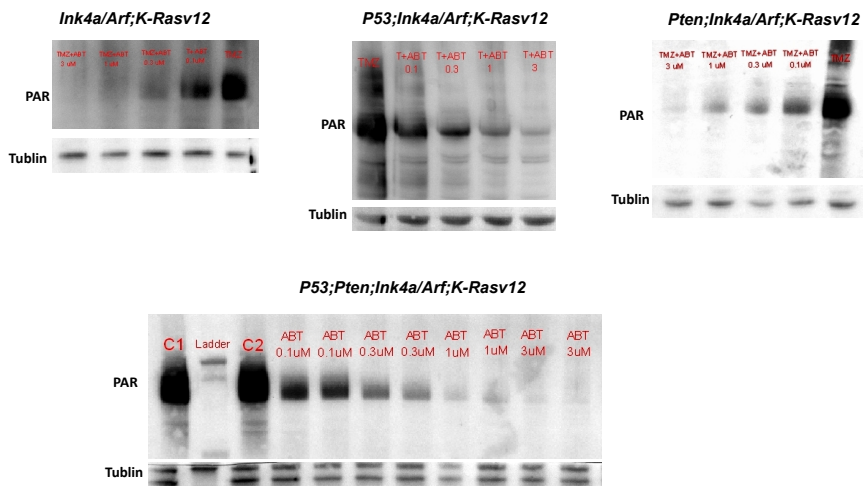
**S. Fig. 1.** Efficacy of TMZ in U87Luc GBM xenografts injected intracranially into WT nude mice. TMZ was p.o. administrated at 25, 50 and 100 mg/kg for once only. Tumor growth ratios of mice in control (no treatment received) and TMZ treated groups were calculated as the ratio of bioluminescence from day 7 and 14 vs initial assessment. The U87 cells were extremely sensitive to TMZ treatment.



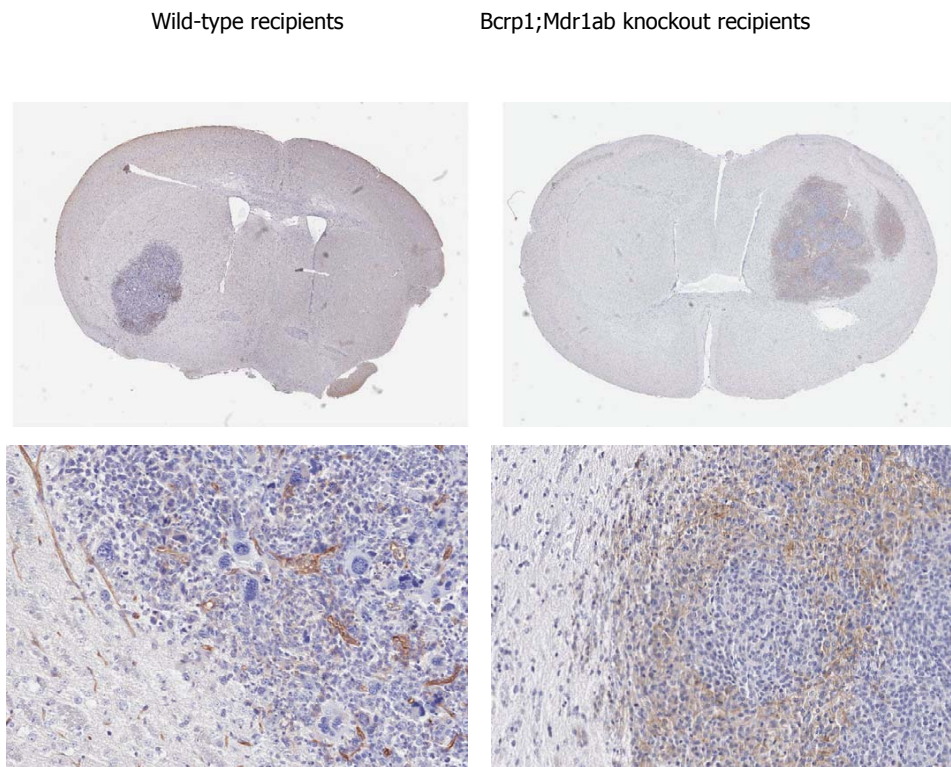
**S. Fig. 2.** ABT-888 plasma concentrations, brain concentrations and brain-to-plasma ratio and brain distribution (percentage dose of ABT-888 in brain) following i.v. administration of a dose of 10 mg/kg of ABT-888. ABT-888 administrated to *Abcb1a/1b<sup>-/-</sup>;Abcg2<sup>-/-</sup>* and *Abcb1a/1b<sup>-/-</sup>;Abcg2<sup>-/-</sup>;Abcc4<sup>-/-</sup>* mice and plasma and brain samples were collected after 1 hr.



**S. Fig. 3.** Repetition of experiment in Fig. 6A with cell lines derived from another mouse of each lineage (Pten;Ink4a/Arf;K-Ras<sup>v12</sup>;LucR GBM910330, P53;Ink4a/Arf;K-Ras<sup>v12</sup>;LucR GBM652449, P53;Ink4a/Arf;K-Ras<sup>v12</sup>;LucR GBM 707251). The same (Ink4a/Arf;K-Ras<sup>v12</sup>;LucR) GBM763663 was used, because an independent line was not available. GBM cells growth inhibition upon continuous exposure to TMZ (100 μM) and ABT-888 at increasing concentration. Data are means ± SE; n = 4 per treatment.



**S. Fig. 4.** Poly ADP-ribose (PAR) Western Blotting results of GBM cell lysates after ABT-888 treatment. GBM cells were exposed to TMZ (100 μM) alone, or together with ABT-888 at concentrations of 0.1, 0.3, 1 and 3 μM for 4 hr and then PAR levels in cell lysates were determined by immunoblotting with anti-PAR antibody.



**S. Fig. 5.** Bcrp1 expression in P53;Ink4a/Arf;K-Rasv12;LucR GBM652457 tumors in WT and Abcb1a/1b<sup>-/-</sup>;Abcg2<sup>-/-</sup> nude mice. In WT mice Bcrp1 is expressed at the BBB, in blood vessels throughout the tumor (BTB) as well as on tumor cells. The presence of Bcrp1 in tumor cells is even better visualized in the Bcrp1 deficient Abcb1a/1b<sup>-/-</sup>;Abcg2<sup>-/-</sup> recipients. Notably, the expression in tumor cells is not uniform. Unfortunately, we were not successful in doing similar immunostainings for P-glycoprotein. The C-219 antibody on frozen sections, as used previously (Schinkel et al, Cell 1994) gave at best only a weak signal, which was also present in vessels of Abcb1a/b deficient mice. Other antibodies that were tested didn't work at all.

## Reference List

- [1] Stupp R, Mason WP, van den Bent MJ, et al. Radiotherapy plus concomitant and adjuvant temozolomide for glioblastoma. 352 ed. 2005. p. 987-96.
- [2] Alexander BM, Pinnell N, Wen PY, D'Andrea A. Targeting DNA repair and the cell cycle in glioblastoma. 107 ed. 2012. p. 463-77.
- [3] Jagtap P, Szabo C. Poly(ADP-ribose) polymerase and the therapeutic effects of its inhibitors. 4 ed. 2005. p. 421-40.
- [4] Calabrese CR, Almassy R, Barton S, et al. Anticancer chemosensitization and radiosensitization by the novel poly(ADP-ribose) polymerase-1 inhibitor AG14361. 96 ed. 2004. p. 56-67.
- [5] Curtin NJ, Wang LZ, Yiakouvaki A, et al. Novel poly(ADP-ribose) polymerase-1 inhibitor, AG14361, restores sensitivity to temozolomide in mismatch repair-deficient cells. 10 ed. 2004. p. 881-9.
- [6] Cheng CL, Johnson SP, Keir ST, et al. Poly(ADP-ribose) polymerase-1 inhibition reverses temozolomide resistance in a DNA mismatch repair-deficient malignant glioma xenograft. 4 ed. 2005. p. 1364-8.
- [7] Miknyoczki SJ, Jones-Bolin S, Pritchard S, et al. Chemopotential of temozolomide, irinotecan, and cisplatin activity by CEP-6800, a poly(ADP-ribose) polymerase inhibitor. 2 ed. 2003. p. 371-82.
- [8] Miknyoczki S, Chang H, Grobelny J, et al. The selective poly(ADP-ribose) polymerase-1(2) inhibitor, CEP-8983, increases the sensitivity of chemoresistant tumor cells to temozolomide and irinotecan but does not potentiate myelotoxicity. 6 ed. 2007. p. 2290-302.
- [9] Palma JP, Wang YC, Rodriguez LE, et al. ABT-888 confers broad in vivo activity in combination with temozolomide in diverse tumors. 15 ed. 2009. p. 7277-90.
- [10] Donawho CK, Luo Y, Luo Y, et al. ABT-888, an orally active poly(ADP-ribose) polymerase inhibitor that potentiates DNA-damaging agents in preclinical tumor models. 13 ed. 2007. p. 2728-37.
- [11] Lee J, Kotliarova S, Kotliarov Y, et al. Tumor stem cells derived from glioblastomas cultured in bFGF and EGF more closely mirror the phenotype and genotype of primary tumors than do serum-cultured cell lines. 9 ed. 2006. p. 391-403.
- [12] Liu G, Yuan X, Zeng Z, et al. Analysis of gene expression and chemoresistance of CD133+ cancer stem cells in glioblastoma. 5 ed. 2006. p. 67.
- [13] de Vries NA, Beijnen JH, Boogerd W, van Tellingen O. Blood-brain barrier and chemotherapeutic treatment of brain tumors. 6 ed. 2006. p. 1199-209.
- [14] Agarwal S, Sane R, Oberoi R, Ohlfest JR, Elmquist WF. Delivery of molecularly targeted therapy to malignant glioma, a disease of the whole brain. 13 ed. 2011. p. e17.
- [15] Deeken JF, Loscher W. The blood-brain barrier and cancer: transporters, treatment, and trojan horses. 13 ed. 2007. p. 1663-74.
- [16] Decleves X, Amiel A, Delattre JY, Scherrmann JM. Role of ABC transporters in the chemoresistance of human gliomas. 6 ed. 2006. p. 433-45.

- [17] de Vries NA, Bruggeman SW, Hulsman D, et al. Rapid and robust transgenic high-grade glioma mouse models for therapy intervention studies. 16 ed. 2010. p. 3431-41.
- [18] Parise RA, Shawaqfeh M, Egorin MJ, Beumer JH. Liquid chromatography-mass spectrometric assay for the quantitation in human plasma of ABT-888, an orally available, small molecule inhibitor of poly(ADP-ribose) polymerase. 872 ed. 2008. p. 141-7.
- [19] Bruggeman SW, Valk-Lingbeek ME, van der Stoop PP, et al. Ink4a and Arf differentially affect cell proliferation and neural stem cell self-renewal in Bmi1-deficient mice. 19 ed. 2005. p. 1438-43.
- [20] Clarke MJ, Mulligan EA, Grogan PT, et al. Effective sensitization of temozolomide by ABT-888 is lost with development of temozolomide resistance in glioblastoma xenograft lines. 8 ed. 2009. p. 407-14.
- [21] Palma JP, Wang YC, Rodríguez LE, et al. ABT-888 confers broad in vivo activity in combination with temozolomide in diverse tumors. 15 ed. 2009. p. 7277-90.
- [22] Zhang Y, Huo M, Zhou J, Xie S. PKSolver: An add-in program for pharmacokinetic and pharmacodynamic data analysis in Microsoft Excel. 99 ed. 2010. p. 306-14.
- [23] Kemper EM, Leenders W, Kusters B, et al. Development of luciferase tagged brain tumour models in mice for chemotherapy intervention studies. 42 ed. 2006. p. 3294-303.
- [24] Cancer Genome Atlas Research Network. Comprehensive genomic characterization defines human glioblastoma genes and core pathways. 455 ed. 2008. p. 1061-8.
- [25] Rottenberg S, Jaspers JE, Kersbergen A, et al. High sensitivity of BRCA1-deficient mammary tumors to the PARP inhibitor AZD2281 alone and in combination with platinum drugs. 105 ed. 2008. p. 17079-84.
- [26] Jaspers JE, Kersbergen A, Boon U, et al. Loss of 53BP1 causes PARP inhibitor resistance in BRCA1-mutated mouse mammary tumors. 2012.
- [27] Szakacs G, Paterson JK, Ludwig JA, Booth-Genthe C, Gottesman MM. Targeting multidrug resistance in cancer. 5 ed. 2006. p. 219-34.
- [28] Kusuvara H, Sugiyama Y. ATP-binding cassette, subfamily G (ABCG family). 453 ed. 2007. p. 735-44.
- [29] Kummar S, Ji J, Morgan R, et al. A phase I study of veliparib in combination with metronomic cyclophosphamide in adults with refractory solid tumors and lymphomas. 18 ed. 2012. p. 1726-34.
- [30] McEllin B, Camacho CV, Mukherjee B, et al. PTEN loss compromises homologous recombination repair in astrocytes: implications for glioblastoma therapy with temozolomide or poly(ADP-ribose) polymerase inhibitors. 70 ed. 2010. p. 5457-64.
- [31] de Vries NA, Beijnen JH, van Tellingen O. High-grade glioma mouse models and their applicability for preclinical testing. 35 ed. 2009. p. 714-23.
- [32] Dean M, Fojo T, Bates S. Tumour stem cells and drug resistance. 5 ed. 2005. p. 275-84.
- [33] Kummar S, Ji J, Morgan R, et al. A phase I study of veliparib in combination with metronomic cyclophosphamide in adults with refractory solid tumors and lymphomas. 18 ed. 2012. p. 1726-34.

# Chapter 3.3

Optimizing the efficacy of PI3K/mTOR inhibitors against high-grade gliomas by selecting blood-brain barrier permeable drugs

Fan Lin, Mark C. De Gooijer, Diana Hanekamp, Gayathri Chandrasekaran, Ruud Weijer, Levi Buil, Rolf Sparidans, Jos H. Beijnen, Olaf van Tellingen

To be submitted

## ABSTRACT

Activation of PI3K occurs in most cancers including glioblastoma (GBM), the most common primary brain tumor. Inhibition of this pathway may result in either direct reduction of tumor proliferation and/or in sensitizing tumor cells to conventional chemotherapy and radiotherapy. Therefore small molecule inhibitors targeting this pathway may provide a new basis for treatment of high-grade gliomas. Several clinical trials with PI3K inhibitors have been conducted but, unfortunately, the results are disappointing. Various reasons maybe responsible for this lack of response. Due to the protection by the BBB, many drugs may fail to reach the target tumor tissue in sufficient amounts. ABCB1/Abcb1 (P-glycoprotein, MDR1) and ABCG2/Abcg2 (BCRP) are two dominant efflux transporters that restrict the brain penetration of many exogenous compounds.

In this project, we used *in vitro* models and *in vivo* pharmacological models to evaluate the impacts of Abcb1 and Abcg2 on the brain penetration of rapamycin, the prototype inhibitor of mTOR, and two more novel PI3K/mTOR inhibitors NVP-BEZ235 and ZSTK474. Furthermore, the anti-proliferative properties of these latter two agents were assessed on stem-like GBM cells *in vitro* and further *in vivo* in a spontaneous high-grade gliomas mouse model.

The *in vitro* transport assays showed that rapamycin is a good Abcb1 substrate, whereas NVP-BEZ235 and ZSTK474 were not substrates of Abcb1. Abcg2 is able to transport NVP-BEZ235 but not ZSTK474 or rapamycin. Pharmacokinetic studies in WT and Abcb1 and/or Abcg2 knockout mice confirmed that Abcb1 severely impaired the brain penetration of rapamycin with more than 10-fold higher brain concentrations in the knockout mice. In line with the *in vitro* data, the brain penetration of ZSTK474 was not impaired by Abcb1 and/or Abcg2. However, in spite of the *in vitro* data, the brain penetration was to some extent impaired by Abcb1 (about 2-fold difference in brain-to-plasma ratio), whereas Abcg2 had no effect. Both NVP-BEZ235 and ZSTK474 efficiently inhibited the PI3K/mTOR signaling pathway and proliferation in GBM cells with different genotypes *in vitro*. In a clinical relevant spontaneous GBM model, ZSTK474 (200 mg/kg q.d., p.o) delayed the tumor onset and prolonged the overall survival, although the tumor proliferation rate in more advanced tumors was not suppressed.



In conclusion, PI3K/mTOR inhibitors with a low affinity for the ABC transporters have a more favorable brain penetration and this may be a requirement for a drug that should be active against GBM. ZSTK474 had a good brain penetration and inhibited the PI3K/mTOR pathway *in vitro* and *in vivo*. ZSTK474 delayed the tumor onset and improved the survival of transgenic mice developing spontaneous GBM. However, continued treatment of more advanced tumors had little effect. These data indicate that ZSTK474 is able to cross the BBB in pharmacologically relevant amounts, but that treatment of advanced tumors by a single agent targeting PI3K will not be sufficient for a meaningful response.

## INTRODUCTION

Malignant gliomas, particularly the glioblastoma multiform (GBM, WHO Grade IV), is the most common primary brain tumor with a median survival of only 14.6 months following multimodality treatment with surgery and chemo-radiation. The most common mutations of GBM include overexpression of the oncogenes EGFR and PDGFR, gain-of-function mutations of PI3K or deletions/mutation of tumor suppressor genes PTEN [1, 2]. These alterations lead to constitutive activation of PI3K and accordingly its downstream effectors such as mTOR (mammalian target of rapamycin) which are crucial for tumor cell growth, proliferation, and survival. Preclinical studies suggest that blockage of this pathway results in either direct inhibition of tumor growth or in sensitizing the cells to conventional chemotherapy and radiotherapy. Therefore, many small molecules inhibiting the PI3K-mTOR pathway are currently being explored for treatment of GBM (Clinicaltrials.gov). However, many of the PI3K inhibitors have been developed for more common types of solid cancer and are tested against glioma for more opportunistic reasons.

Unfortunately, the outcomes of clinical studies with agents that target the PI3K pathway in GBM have been disappointing so far. Typically, the prototype inhibitor of mTOR rapamycin (sirolimus) and its analogs temsirolimus and everolimus have been regarded as promising targeted agents for GBM, but a number of Phase I and II trials applying them either as monotherapy or in combination with EGFR kinase inhibitor failed to demonstrate meaningful clinical efficacy in recurrent GBM [3-6]. A variety of possible explanations for this lack of efficacy have been proposed, such as the fact that rapalogs do not inhibit mTORC2 [7] and other feedback loops of mTOR inhibition that lead to increased upstream signaling of Akt [8, 9], or whether that PTEN is deficient [10]. These possible explanations, which are focusing on the cellular or molecular level of PI3K-mTOR signaling, will certainly contain elements responsible for lack of responsiveness. However, another critical issue to be addressed is related to the basic pharmacokinetic – pharmacodynamic principle that sufficient drug should be delivered to tumor cells in order to elicit a meaningful effect. Especially the residual GBM cells that have escaped surgical resection because they had migrated to more distant parts of brain will be shielded by an intact blood-brain barrier (BBB). In this respect, it is important to realize that many preclinical evaluations of potential therapeutic agents for GBM may have

given too optimistic results, since these were usually performed in classical xenograft models which often contain leaky vessels throughout the lesion and/or lost many critical characteristics due to culturing in serum containing media [11].

As a fact, the intact BBB restricts the brain entry of the majority of xenobiotics by its unique structure [12]. In particular, the drug efflux transporters expressed at BBB play a very important role in limiting the brain penetration of a wide variety of compounds including frequently used chemotherapeutics and novel targeted agents. Two well established drug efflux transporters, ABCB1 (P-glycoprotein, P-gp, Mdr1) and ABCG2 (Breast Cancer Resistance Protein, BCRP) abundantly expressed the human and murine BBB, restrict most newly developed kinase inhibitors such as erlotinib, lapatinib, etc. [13, 14]. As a consequence, their usefulness in treatment of GBM growth might be compromised by an inadequate brain penetration.

In the present study, we have compared the affinity for ABCB1 and ABCG2 as well as their impacts on brain pharmacokinetics of the prototype mTOR inhibitor rapamycin with two novel PI3K/mTOR inhibitors ZSTK474 and NVP-BEZ235, as both of them have been implicated in treatment of GBM [15, 16]. Moreover, we have evaluated the anti-proliferative effect of the PI3K inhibitors using stem-like GBM cells which were harvested from spontaneous high-grade glioma models harboring mutations that are relevant for GBM. Finally, we used the PI3K inhibitor with optimized brain penetration as a single agent to evaluate its efficacy in a spontaneous GBM model [17].

## MATERIALS AND METHODS

### **Reagents**

The PI3K inhibitors rapamycin and ZSTK474 were purchased from LC Laboratories (Woburn, MA, USA). NVP-BEZ235 was purchased from Selleck Chemicals (Houston, TX, USA). These compounds were dissolved in dimethyl sulfide (DMSO, Sigma) to yield 10 nM and 4 nM working solutions and were stored at 4°C. Elacridar was kindly provided by GlaxoSmithKline (Research Triangle Park, NC, USA). Zosuquidar (LY335979) was kindly provided by Eli Lilly (Indianapolis, IN, USA). Modified Eagles medium (MEM), Opti-MEM (reduced serum medium), HBSS (Hank's Balanced Salt Solution), L-glutamine, non-essential amino acids, MEM vitamins penicillin-streptomycin, fetal calf serum, trypsin-EDTA and other reagents for cell culture were purchased from Invitrogen (Carlsbad, CA, USA). All other chemicals were purchased from Merck (Darmstadt, Germany).

### **Animals**

Mice were housed and handled according to institutional guidelines complying with Dutch legislation. All experiments with animals were approved by the animal experiment committee of the institute. The animals used for pharmacokinetics studies were female wild-type (WT), *Abcb1a/1b*<sup>-/-</sup>, *Abcg2*<sup>-/-</sup>, and *Abcb1a/1b*<sup>-/-</sup>;*Abcg2*<sup>-/-</sup> mice of FVB genetic background, between 9 and 14 weeks of age. *Ink4a/Arf*;K-Ras<sup>v12</sup>;LucR, *Pten*;*Ink4a/Arf*;K-Ras<sup>v12</sup>;LucR, *P53*;*Ink4a/Arf*;K-Ras<sup>v12</sup>;LucR and *P53*;*Pten*; *Ink4a/Arf*;K-Ras<sup>v12</sup>;LucR conditional mice for generation of GBM cell lines and efficacy studies were genotyped as described previously (1). The animals were kept in a temperature-controlled environment with a 12-hr dark/ 12-hr light cycle and received a standard diet (AM-II, Hope Farm B.B., Woerden, The Netherlands) and acidified water *ad libitum*.

### **In vitro transport experiments**

To determine whether Rapamycin, NVP-BEZ235 and ZSTK474 are substrates of murine *Abcb1a* (*Mdr1a*) or human *ABCB1* (*MDR1*), we analyzed the translocation of these compounds in a concentration equilibrium setting using the parental LLC pig-kidney cell line (LLC-PK1) and sub-lines transduced with murine *Abcb1a* (LLC-*Mdr1a*) or human *ABCB1* (LLC-*MDR1*). Similarly, the parental Madine Darby Canine Kidney (MDCK) type II cell line (MDCKII-parental) and murine *Abcg2* (MDCKII-*Bcrp1*) or human *ABCG2* transduced sub-lines (MDCKII-BCRP) were used to determine whether ABT-888 was a

substrate of murine Abcg2 or human ABCG2. Cells were seeded on Transwell microporous polycarbonate membrane filters (3.0  $\mu\text{m}$  pore size, 24 mm diameter; Costar Corning, NY, USA) at a density of  $2 \times 10^6$  cells per well in 2 ml MEM medium. When confluency was reached, we started the transport experiment by replacing the drug free medium with Opti-MEM medium containing 0.5  $\mu\text{M}$  Rapamycin, or MEM medium containing 0.5  $\mu\text{M}$  ZSTK474 or NVP-BEZ235. Zosuquidar (5  $\mu\text{M}$ ) was added to the medium to inhibit endogenous canine ABCB1 in all experiments with MDCK cell lines, and to inhibit the endogenous or exogenous Abcb1 activity in experiments with LLC cell when necessary. [ $^{14}\text{C}$ ]-inulin (approximately  $1.59 \times 10^6$  DPM/ml) was added to check the integrity of the membrane. Samples of 50  $\mu\text{l}$  were taken at 30, 120, 180 and 240 min and used for drug analysis.

#### ***Drug formulations and treatment regime***

For pharmacokinetic studies, rapamycin was first dissolved in 100% ethanol and further diluted in HBSS to yield a solution of 0.05 mg/ml. For p.o. administration, ZSTK474 was mixed with water and sonicated, suspended in a mixture of hydroxypropyl methylcellulose (4%, v/v) and Tween 80 (polysorbate 80; 0.75%, v/v) to yield a drug suspension of 20 mg/ml. For i.v. administration, ZSTK474 was dissolved in DMSO to yield a solution of 1 mg/ml. NVP-BEZ235 was dissolved in DMSO (using a hot water bath) to yield a solution of 5 mg/ml and further mixed with PEG400 to yield a solution of 1 mg/ml. For the efficacy study, a suspension containing 20 mg/ml of ZSTK474 was prepared in the same formulation as used for the pharmacokinetic studies. Animals received a dose of 200 mg/kg q.d. starting 3 days after lentiviral injection until the day of sacrifice.

#### ***Plasma and brain pharmacokinetics***

The prepared solutions were administered to WT and Abcb1a/b;Abcg2<sup>-/-</sup> mice and/or Abcb1a/b<sup>-/-</sup> and Abcg2<sup>-/-</sup> mice. Rapamycin at a dose of 1.5 mg/kg, i.p; NVP-BEZ235, 10 mg/kg, p.o. and ZSTK474 10 mg/kg i.v. and 200 mg/kg p.o. Elacridar prepared as described earlier (2) was given p.o. at a dose of 100 mg/kg 15 min prior to Rapamycin. Blood sampling was performed either by collecting tail vein blood or by cardiac puncture at different time points. Brains were dissected after mice were sacrificed and were homogenized in 3 ml 1% (w/v) bovine serum albumin (BSA). Both plasma/blood and brain homogenates were stored at  $-20^\circ\text{C}$  until analysis.

***Drug analytical method***

Rapamycin samples were measured using LC-ESI-MS/MS with tacrolimus as internal standard and protein precipitation with methanol for sample pretreatment. Samples of 5  $\mu$ l were injected onto an Atlantis C18 column (Waters, Milford, USA) coupled with a Polaris 3 C18-A pre-column (Middelburg, The Netherlands). The gradient elution of methanol ranged from 65% to 100% (v/v) in 1% (v/v) formic acid allowed elution of the rapamycin (MRM 936.6/409.2) and tacrolimus (826.5/616.2) at 2.8 and 2.7 min, respectively. Spray voltage was set to 3900 V, capillary temperature to a 400°C and argon collision pressure to 2.0 mTorr. Collision energy was at 54 and 36 V, respectively.

For quantification of ZSTK474 in plasma and brain samples, a reversed-phase high-performance liquid chromatographic (HPLC) assay with fluorometric detection was used. ZSTK474 and its internal standard NVP-BE2235 were chromatographically separated using XBridge BEH130 C18 column (Waters, Milford, MA, USA) by isocratic elution with a mobile phase which consisted of acetonitrile, and 0.1% triethylamine adjusted with hydrochloric acid to pH 9.5 (50:50, v/v). Fluorescence detection was used with excitation and emission wavelengths of 240 and 425 nm, respectively. NVP-BE2235 concentration in biological samples was measured using the HPLC assay as described previously [18].

***Stereotactic intracranial injections and bioluminescence imaging***

The detailed procedures of stereotactic intracranial injection and bioluminescence imaging are described previously (3). In short, Ink4a/Arf;KRasv12;LucR, Pten;Ink4a/Arf;K-Rasv12;LucR, P53;Ink4a/Arf;K-Rasv12;LucR and P53;Pten;Ink4a/Arf;K-Ras<sup>v12</sup>;LucR mice were anaesthetized and placed in a stereotactic frame, and 2  $\mu$ l of CMV-Cre lentivirus suspension was injected 2 mm lateral and 1 mm anterior to the bregma, 3 mm below the skull. After the initial tumor load was established, tumor development was monitored by bioluminescence using the IVIS 200 Imaging system (Xenogen, Corporation, Alameda, CA, USA). Mice were sacrificed when clear neurological symptoms occurred or weight loss ( $\geq 20\%$ ) was observed. Brain tissue was fixed in an ethanol-glacial acetic acid mixture containing 4% formaldehyde (EAF), embedded in paraffin and cut into coronal slice of 4  $\mu$ m. Sections were H&E stained for verification of tumor growth.

***Establishment of GBM cell culture, anti-proliferation assay and Western blotting***

GBM cells lines have been created from tumors generated in Ink4a/Arf;KRasv12;LucR, Pten;Ink4a/Arf;K-Rasv12;LucR, P53;Ink4a/Arf;K-Rasv12;LucR and P53;Pten;Ink4a/Arf;K-

Ras<sup>v12</sup>;LucR conditional mice after lentiviral injection into the brain. Small amounts of tumor tissue were transferred in ice-cold CA<sup>2+</sup> and Mg<sup>2+</sup> free HBSS and subsequently triturated mechanically. Cell suspensions prepared in ultra low binding 6 well plates (Corning) in serum-free MHM (Medium Hormone-Mix) medium (DMEM-F12 supplemented with modified N2 medium composed of 100 mg/L apo-transferrin, 25 mg/L recombinant human insulin, 100 µM putrescine, 20 nM progesterone, and 30 nM sodium selenite, 2 mM glutamine, 6 mg/ml glucose, 14 mM NaHCO<sub>3</sub> and 5mM HEPES) containing 20 ng/ml EGF and bFGF as described previously [19].

For the proliferation assays, cells from the above established GBM culture were seeded in laminin coated 96-well black-well/clear-bottom plate (Greiner Bio-One, Alphen, the Netherlands) at a density of 2,000 cells/well in MHM medium. Treatment was started after one to two days when about 3-5% cell confluence was reached. Next, the medium was replaced by MHM medium containing 0.1% DMSO as a control, ZSTK474 at concentrations of 100, 500, 1000 or 2000 nM, or NVP-BEZ235 at concentrations of 1, 10, 100 and 1000 nm. Cell density/viability was determined on day 0 (treatment start) and day 2 using bioluminescence imaging on an IVIS Lumina II Imaging System (Xenogen, Corporation, Alameda, CA, USA) with 150 µg/ml of luciferin in each well.

For Western blotting, GBM cells were cultured in 6 well plates under the same conditions as used in anti-proliferation assays and drugs were added during 4 h when 80-90% cell confluence was reached. Next, Cells were lysed with complete RIPA buffer, containing phosphatase inhibitors. Cell lysate was processed for Western blotting as described elsewhere [20, 21]. Primary antibodies used in this study are pErk1/2(Thr202/Tyr204) Erk1 (C16) (Santa Cruz Biotechnology; Santa Cruz, CA, USA) and pAkt (Ser473), Akt and pS6(Ser235/236) Ribosomal protein (Cell Signaling Technology (Danvers, MA, USA), and mouse β-tubulin isotype III (Sigma, Saint Louis, MO).

### ***Pharmacokinetic calculations and statistical analysis***

The General linear model repeated measures procedure (as previously described in the Palomid 529 pharmacokinetics paper) was used to determine whether the basolateral-to-apical differences of the drugs levels were significantly increased by the factor of time and at which time point(s) these difference became significant.

For *in vivo* pharmacokinetic experiments, pharmacokinetic parameters were calculated using an add-in program for Microsoft Excel PKSolver [22]. To determine the differences of brain and plasma concentrations among multiple strains, one-way analysis of variance (ANOVA) with post-hoc Bonferroni was performed. Differences were considered statistically significant when  $P < 0.05$ .

Survival fractions were calculated using Kaplan-Meier method by GraphPad Prism 5.01 (GraphPad Software, Inc., La Jolla, CA, USA). The log-rank test was used to compare survival of groups. Differences between groups were analyzed using ANOVA protected least significant difference for comparing groups.



## RESULTS

### ***Abcb1 severely impairs the brain penetration of rapamycin***

We first performed a series of experiments using concentration equilibrium transport assay [23] in murine *Abcb1* and *Abcg2* transduced cells and their corresponding parent lines as controls to determine whether rapamycin is a substrate of *Abcb1* and *Abcg2*. As shown in Fig.1 A, rapamycin was significantly translocated in LLC-PK1 cells in 4 hr, and this translocation can be blocked by adding zosuquidar, a specific *Abcb1* inhibitor. Therefore, it might result from the endogenously expressed porcine *Abcb1*. The translocation of rapamycin in *Abcb1* overexpressed LLC-Mdr1a cells was more pronounced and was also completely inhibited by zosuquidar, confirming that rapamycin is an good substrate of *Abcb1*. However, rapamycin is not transported by *Abcg2* since no translocation has been observed in both MDCK-parent and MDCK-Bcrp1 cells.

Next, we assessed the impacts of *Abcb1* and *Abcg2* on drug levels in plasma and brain and some other tissues using WT, *Abcb1a/b*<sup>-/-</sup>, *Abcg2*<sup>-/-</sup> and *Abcb1a/b;Abcg2*<sup>-/-</sup> mice. Surprisingly, blood levels of rapamycin in all knockout mice receiving rapamycin at a dose of 1.5 mg/kg were much higher than in WT mice, resulting to 35 to 52-fold higher AUC values compared to WT mice. However, no difference of rapamycin levels between WT and knockout mice was found in well perfused organs such as the kidney or any of the other tissues (*e.g.* liver), where drug levels are usually well equilibrated with levels in blood or plasma. In the brain, *Abcb1* is clearly the only dominant factor that determines the brain penetration of rapamycin because the brain AUC of *Abcb1a/b*<sup>-/-</sup> and *Abcb1a/b;Abcg2*<sup>-/-</sup> are at least 10-fold higher than that of WT mice. In fact, the levels in brain samples of WT mice were below the limit of quantification (LLQ) of the assay. The levels in brain samples from *Abcg2*<sup>-/-</sup> mice taken at the early time points were just above the LLQ (Fig 1B), but this was probably due to the higher levels of rapamycin in blood of these mice. No significant difference was found between the *Abcb1a/b*<sup>-/-</sup> and *Abcb1a/b;Abcg2*<sup>-/-</sup> mice, suggesting *Abcg2* is not involved in eliminating rapamycin in brain. To further investigate if *Abcb1* and/or *Abcg2* mediated transport is responsible for the differences of plasma and brain levels between WT and knockout mice, the dual *Abcb1* and *Abcg2* inhibitor elacridar was co-administrated to WT mice 30 min prior to i.p. administration of rapamycin. Moreover, the LC-MS assay was adapted to improve the LLQ to allow quantification in brain samples of WT mice. Interestingly, elacridar

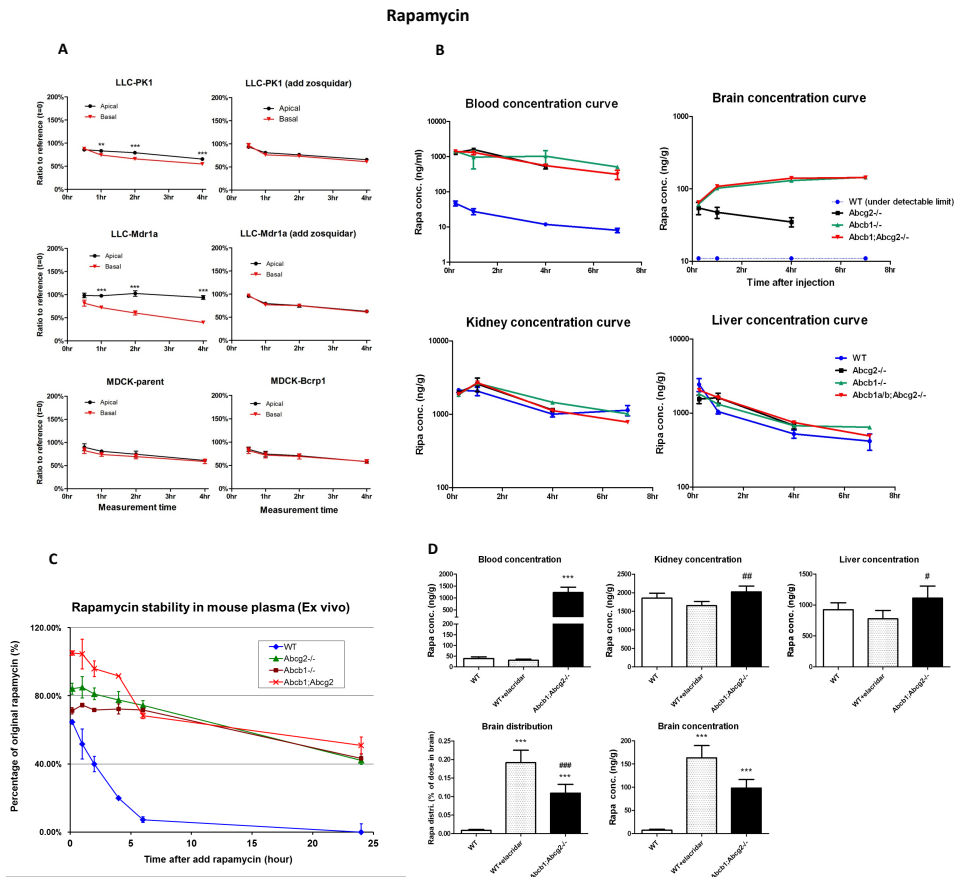


**Fig. 1.** *In vitro* Transport, *in vivo* pharmacokinetics and *ex vivo* stability of rapamycin.

**A**, Transepithelial translocation of rapamycin was assessed using parental LLC-PK1 cells and cells transduced with mouse *Abcb1a* (LLC-Mdr1a), or MDCK-parent cells and MDCK cells transduced with mouse *Abcg2* (MDCK-Bcrp1). The setup was a concentration equilibrium setting. Zosuquidar (5  $\mu$ M) was added to LLC-PK1 and LLC-Mdr1a cells to inhibit the transport mediated by endogenous and/or exogenous *Abcb1* in these LLC lines. Results are presented as the ratio of observed concentration to reference concentration. Data are means  $\pm$  SD;  $n = 6$  per experiment. \*  $P < 0.05$ ; \*\*  $P < 0.01$ ; and \*\*\*  $P < 0.001$ , comparing the difference of apical vs basolateral drug concentrations at a certain time point with that at the initial time point (30 min). **B**, Rapamycin levels in blood, brain, kidney and liver of WT, *Abcb1a/1b<sup>-/-</sup>*, *Abcg2<sup>-/-</sup>*, and *Abcb1a/1b<sup>-/-</sup>; Abcg2<sup>-/-</sup>* mice at 15 min, 1, 4 and 7 hr following i.p. administration of rapamycin at a dose of 1.5 mg/kg. **C**, Percentage of unchanged rapamycin as a function of time incubated at 37  $^{\circ}$ C in plasma of WT, *Abcb1a/1b<sup>-/-</sup>*, *Abcg2<sup>-/-</sup>*, and *Abcb1a/1b<sup>-/-</sup>; Abcg2<sup>-/-</sup>* mice. Rapamycin. **D**, 100 mg/kg elacridar was p.o. administered to WT mice 15 min prior to rapamycin i.p. administration. Plasma and brain samples were collected at 1 hr. Data are presented as means  $\pm$  SD,  $n = 5$  animals per group. \*\*\*  $P < 0.001$ , compared to WT mice without elacridar. #  $P < 0.05$ ; ##  $P < 0.01$ . compared with WT mice with elacridar

enhanced the brain concentration and brain distribution of rapamycin in WT mice by about 23-fold, but did not cause any alteration of rapamycin levels in blood and kidney (Fig.1 C). Together, these results suggest that Abcb1 at BBB indeed severely impairs the accumulation of rapamycin into the brain. However, transport by Abcb1 and/or Abcg2 is unlikely responsible for the difference in the systemic clearance of the rapamycin in WT mice.

Because the rapamycin levels in the kidney and liver were not different between WT and knockout mice, and because it has previously been reported that rapamycin is unstable in plasma and whole blood of human, rabbit and rat [24], we have investigated the stability of rapamycin in murine whole blood and plasma. We observed a much more rapid degradation in plasma of WT compared to knockout mice. After 6 hr incubation of rapamycin with freshly collected plasma from mice of different knockout strains, we observed that more than 65% of the added rapamycin was recovered in plasma of Abcb1a/b<sup>-/-</sup>, Abcg2<sup>-/-</sup> and Abcb1a/b;Abcg2<sup>-/-</sup> mice, but was less than 10% in plasma of WT mice (Fig.1 D). We speculate that the higher blood level of rapamycin in knockout mice is caused by avid binding of rapamycin to an (unknown) serum factor that is (more abundantly) present in plasma of knockout mice. Due to this avid binding, only a small fraction of rapamycin is available for degradation and for distribution. This hypothesis is currently being explored.

***NVP-BEZ235 is a substrate of Abcg2 but its brain penetration is mainly limited by Abcb1 in vivo***

Similarly, we performed *in vitro* transport experiments with NVP-BEZ235. We did not observe significant basolateral-to-apical translocation of NVP-BEZ235 in LLC-PK1 and LLC-Mdr1a cells, suggesting that NVP-BEZ235 is not transported by Abcb1. In contrast, significant basolateral-to-apical translocation was found in MDCK-Bcrp1 cells, but not in MDCK-parent cells, and this was inhibited by adding elacridar, indicating that NVP-BEZ235 is transported by Abcg2. We also used the same setup to test translocation of NVP-BEZ235 in corresponding cell lines that over-express human ABCB1 and ABCG2, but there was no basolateral-to-apical translocation of NVP-BEZ235 in these cell lines, indicating that NVP-BEZ235 is not a substrate of human ABCB1 or ABCG2.

Next, we evaluated the roles of Abcb1 and Abcg2 in the brain penetration of NVP-BEZ235 using WT and Abcb1a/b;Abcg2<sup>-/-</sup> mice. We first tried i.v. administration of NVP-BEZ235 by tail vein injection, but mice receiving only 5 to 10  $\mu$ l of 0.5 mg/ml NVP-BEZ235 dissolved in DMSO from tail vein died immediately, probably due to the very low solubility of the compound (1.33mg/ml in DMSO with warming). We therefore switched to oral administration of NVP-BEZ235 formulated in mixture of DMSO and PEG400 at a dose of 10 mg/kg. As shown in Fig.2 B, both plasma and brain levels of NVP-BEZ235 were significantly higher in Abcb1a/b;Abcg2<sup>-/-</sup> mice than those in WT mice at multiple time points. Moreover, the brain-to-plasma ratio of Abcb1a/b;Abcg2<sup>-/-</sup> mice was 2.0 and 1.6-fold higher than that of WT mice at 1 and 4 hr, respectively, suggesting that the higher brain level of NVP-BEZ235 was not only a consequence of higher plasma level in Abcb1a/b;Abcg2<sup>-/-</sup> mice, but also due to the absence of the active brain efflux of NVP-BEZ235 mediated by Abcb1 and/or Abcg2. In order to identify which transporter contributes to the increased brain penetration of NVP-BEZ235 in the compound knockout mice, we have performed an additional experiment using single Abcb1a/b<sup>-/-</sup> and Abcg2<sup>-/-</sup> animals, next to WT and Abcb1a/b;Abcg2<sup>-/-</sup> mice. Interestingly, despite the *in vitro* finding that NVP-BEZ235 is a substrate of Abcg2, the brain penetration is dominantly determined by Abcb1 because the brain concentration and brain-plasma ratio of NVP-BEZ235 in WT mice was 3.6 and 1.7-fold lower than those of Abcb1a/b<sup>-/-</sup> mice and 4.5 and 2.0-fold lower than those of Abcb1a/b;Abcg2<sup>-/-</sup> mice, but were similar as Abcg2<sup>-/-</sup> mice. We have found similar discrepancies between *in vitro* and *in vivo* observations for other drugs, which clearly indicate the need to confirm substrate-transporter results by *in vivo* models.

#### **ZSTK474 brain penetration is not restricted by Abcb1 and Abcg2**

As shown in Fig.3 A, although a minor apical and basolateral difference of ZSTK474 was observed at 4 hr in MDCK-Bcrp1 cells (The asterisk at 4 hr indicates that the difference between the apical and basolateral levels at 4 hr was significantly greater than at 30 min), it did not lead to significant difference in overall basolateral-to-apical translocation. No significant directional translocation of ZSTK474 was found in other cell lines including LLC-Mdr1a and LLC-MDR1 and LLC-BCRP cells (Fig.3 A), indicating that ZSTK-474 is not transported by murine and human Abcb1/ABCB1 and Abcg2/ABCG2.

We first investigated the roles of Abcb1 and Abcg2 on the brain and plasma pharmacokinetics of this compound *in vivo* by p.o. administration of ZSTK474 to WT and

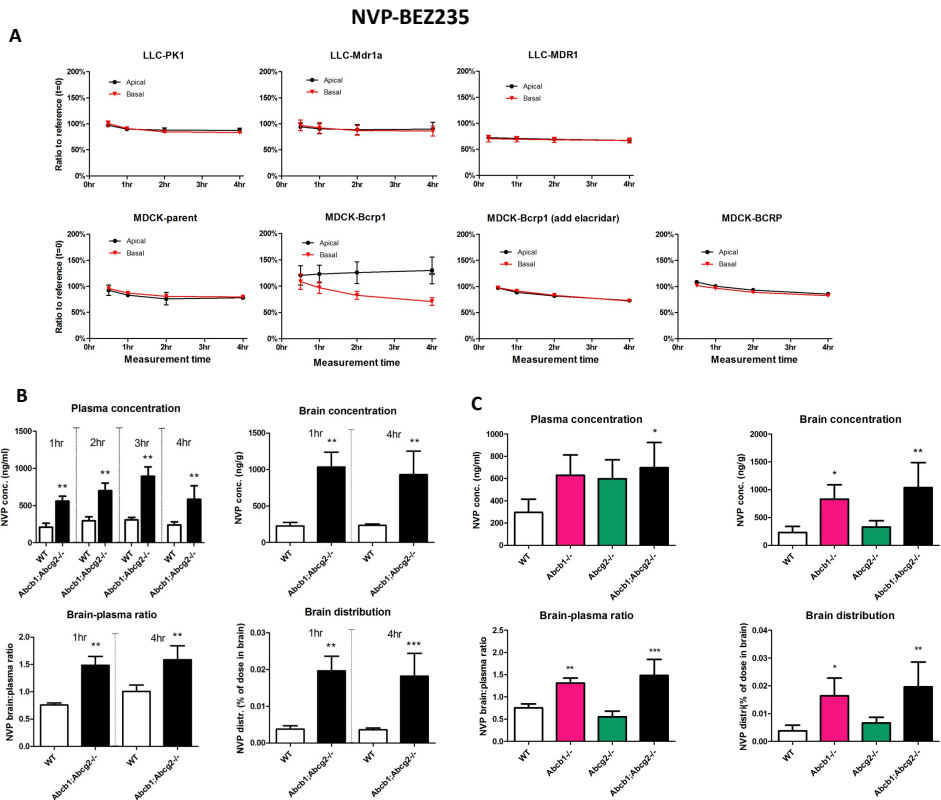


**Fig. 2.** *In vitro* transport and *in vivo* pharmacokinetics of NVP-BE235. **A**, Transepithelial translocation of rapamycin was assessed using LLC-PK1 cells, LLC-Mdr1a or LLC-MDR1 (human ABCB1), or MDCK-parent, MDCK-Bcrp1 or MDCK-BCRP (human ABCG2). Elacridar (5  $\mu$ M) was added to MDCK-Bcrp1 or MDCK-BCRP cells to inhibit the transport mediated by exogenous Abcg2/ABCG2 of MDCK lines. Results are presented as the ratio of observed concentration to reference concentration. Data are means  $\pm$  SD; n = 6 per experiment. \* P < 0.05; \*\* P < 0.01; and \*\*\* P < 0.001, comparing the difference of apical vs basolateral drug concentrations at a each time point with that at the initial time point (30 min). **B and C**, NVP-BE235 plasma and brain concentrations, brain-plasma ratio and brain distribution of WT and Abcb1a/1b-/-; Abcg2-/- mice, or together with Abcb1a/1b-/-, Abcg2-/- mice following p.o. administration of a dose of 10 mg/kg of NVP-BE235. **C**, Plasma and brain samples were collected at 1 hr. Data are presented as means  $\pm$  SD, n = 5 animals per group. \* P < 0.05; \*\* P < 0.01; and \*\*\* P < 0.001, compared with WT mice. NVP: NVP-BE235.

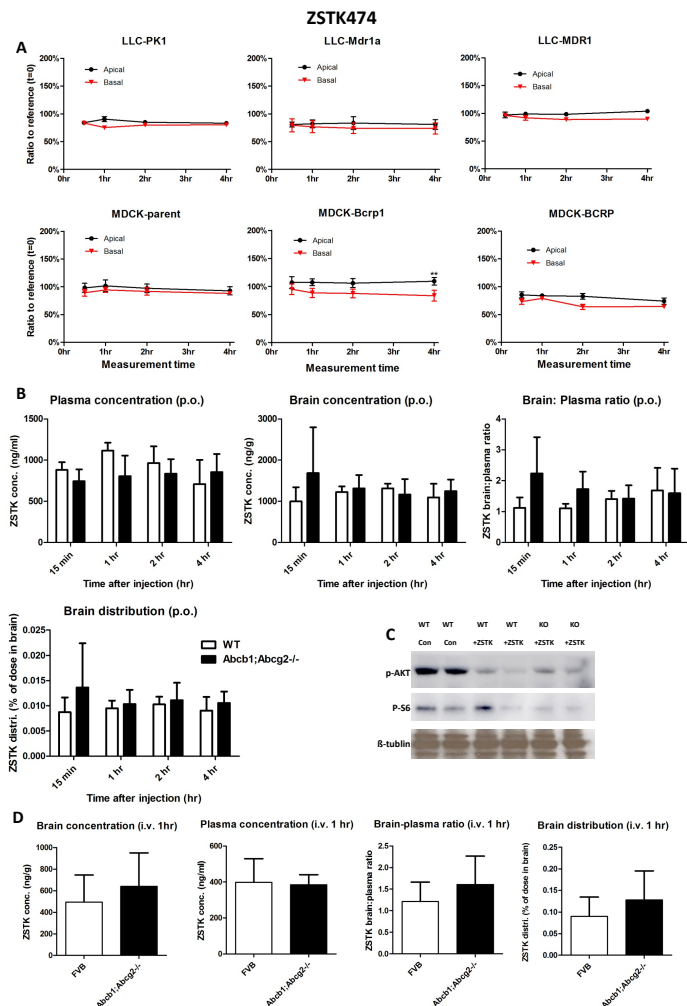


**Fig. 3.** *In vitro* transport and *in vivo* pharmacokinetics of ZSTK474.

**A**, Transepithelial translocation of ZSTK474 was assessed using LLC-PK1 cells, LLC-Mdr1a or LLC-MDR1 (human ABCB1), or MDCK-parent, MDCK-Bcrp1 or MDCK-BCRP (human ABCG2). Results are presented as the ratio of the observed concentration relative to the reference concentration. Data are means  $\pm$  SD;  $n = 6$  per experiment. \*  $P < 0.05$ , comparing the difference of apical vs basolateral drug concentrations at a each time point to that at the initial time point (30 min). **B and D**, ZSTK474 plasma, and brain concentrations in WT and *Abcb1a/1b*<sup>-/-</sup>/*Abcg2*<sup>-/-</sup> mice following p.o. administration of a dose of 200 mg/kg (**B**), or i.v. administration of a dose of 10 mg/kg (**D**). **C**, Western blot of mouse brain samples probed with antibodies against pAkt, pS6 Rb. Blots were re-probed with  $\beta$ -tubulin to confirm equal loading. Brain samples were collected from WT and *Abcb1a/1b*<sup>-/-</sup>/*Abcg2*<sup>-/-</sup> mice at 2 hr following p.o. administration of a dose of 200 mg/kg. **D**, Plasma and brain samples were collected at 1 hr following administration. Data are presented as means  $\pm$  SD,  $n = 5$  animals per group. ZSTK: ZSTK474.

Abcb1a/b;Abcg2<sup>-/-</sup> mice at a dose of 200 mg/kg. Plasma and brain concentrations and the brain-to-plasma ratio of ZSTK474 were similar between WT and Abcb1a/b;Abcg2<sup>-/-</sup> mice (Fig.3 B). The PI3K signaling pathway in brain samples collected from WT and knockout mice at two hr after drug administration was greatly suppressed as shown in Fig.3 C. Next, i.v. administration of ZSTK474 dissolved in DMSO at a relatively low dose (10 mg/kg) was employed to confirm the negligible impact of Abcb1 and Abcg2 *in vivo*. Again, we did not find any significant difference of plasma, brain concentration and brain-to-plasma ratio between WT and knockout mice, confirming that the systemic clearance and brain penetration are not limited by Abcb1 and Abcg2 (Fig.3 C).

#### ***NVP-BEZ235 and ZSTK474 inhibit the PI3K signaling and proliferation of GBM cells***

The anti-proliferative activities of both NVP-BEZ235 and ZSTK474 were assessed *in vitro* using GBM cells derived from our spontaneous transgenic high-grade glioma mouse models. These cells harbor a combination of genetic deletions that are common in human GBM, including Ink/Arf, P53 and/or Pten together with an activated Ras pathway. Both agents showed a dose-dependent growth inhibitory activity against all GBM cell lines, with an about 10-fold higher potency of NVP-BEZ235 compared to ZSTK474. No clear difference in sensitivity for these agents was found in any of the GBM cell line genotypes (Fig.4 A). In addition, the target inhibition by NVP-BEZ235 and ZSTK474 in these GBM cells was verified by Western blot analyses at different concentrations. As shown in Fig.4 B, NVP-BEZ235 ( $\geq 100$  nM) and ZSTK474 ( $\geq 1000$  nM) effectively inhibited the phosphorylation of AKT and S6 ribosomal protein, but did not affect the pERK level of MAPK signaling pathway. Lower concentrations of ZSTK474 and NVP-BEZ235 did not inhibit phosphorylation of AKT and S6 (data now shown).

#### ***Inhibition of PI3K pathway in a spontaneous GBM delays tumor onset and prolongs survival***

We recently established high-grade gliomas models using conditional mice with different genetic backgrounds: *viz.* Ink4a/Arf;K-Ras<sup>v12</sup>;LucR, Pten;Ink4a/Arf;K-Ras<sup>v12</sup>;LucR, P53;Ink4a/Arf;K-Ras<sup>v12</sup>;LucR and P53;Pten;Ink4a/Arf;K-Ras<sup>v12</sup>;LucR. All of these mice develop Grade III or IV gliomas spontaneously after intracranial CMV-Cre lentivirus injection that recapitulate many histopathological and biological features of human gliomas [17]. As shown in Fig. 5A, GBMs with a deleted PTEN gene proliferate much more rapidly *in vivo* than PTEN proficient Ink4a/Arf;K-Ras<sup>v12</sup> tumors. As a result, Ink4a/

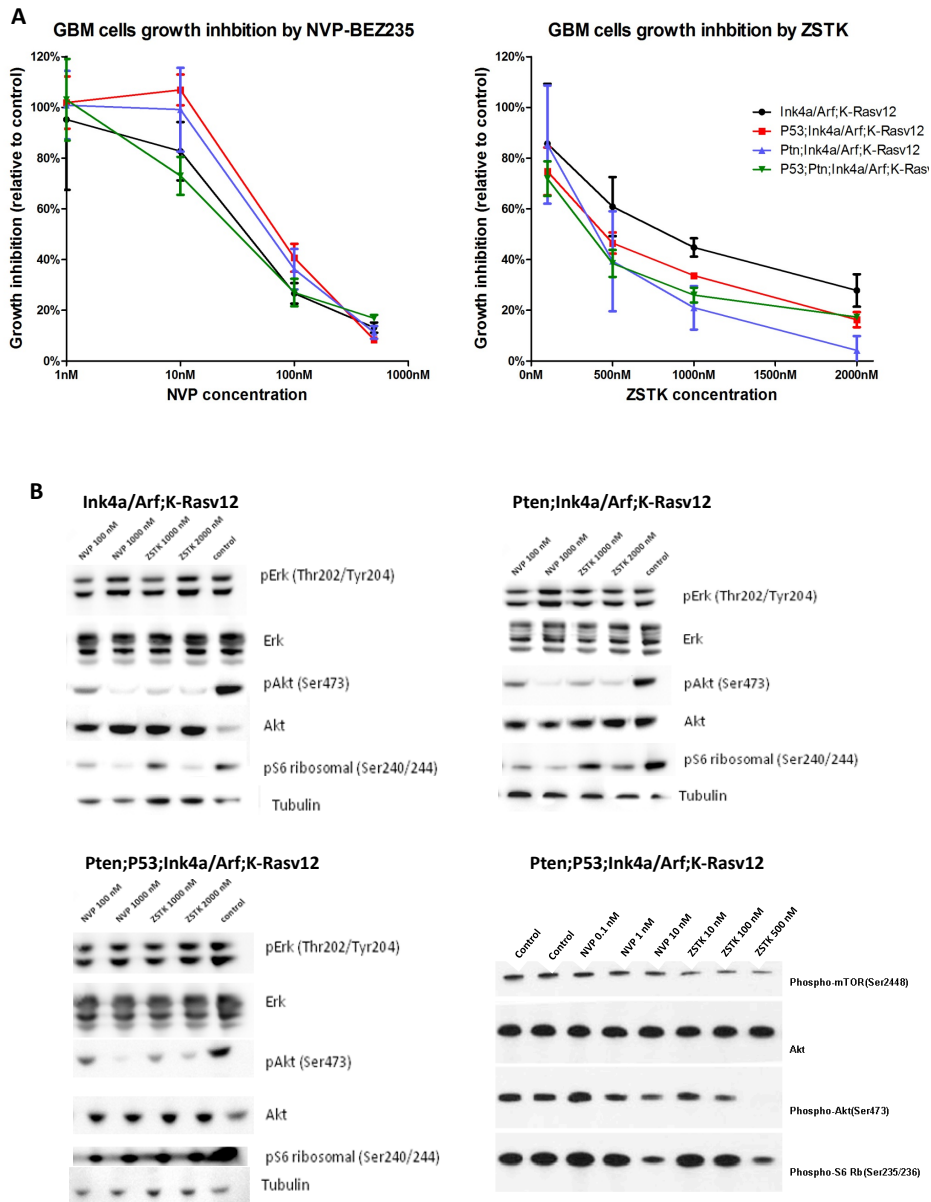


**Fig. 4.** Anti-proliferative effect and PI3K and MEK/ERK signaling inhibition of PI3K inhibitors in GBM cells. **A**, Growth inhibition of GBM cells with various genotypes treated with 1, 10, 100 or 500 ng/ml of NVP-BE235 or 100, 500, 1000 or 2000 ng/ml of ZSTK474 for two days relative to controls. Data are means  $\pm$  SD.  $n = 4$  per treatment. **B**, GBM cells for Western blotting were collected 4 hours after treatment with NVP-BE235 or ZSTK474 at indicated concentrations and probed with antibodies against pErk, total Erk, pAkt, total Akt, pS6 Rb. Blots were also probed with  $\beta$ -tubulin to confirm equal loading. NVP: NVP-BE235; ZSTK: ZSTK474.



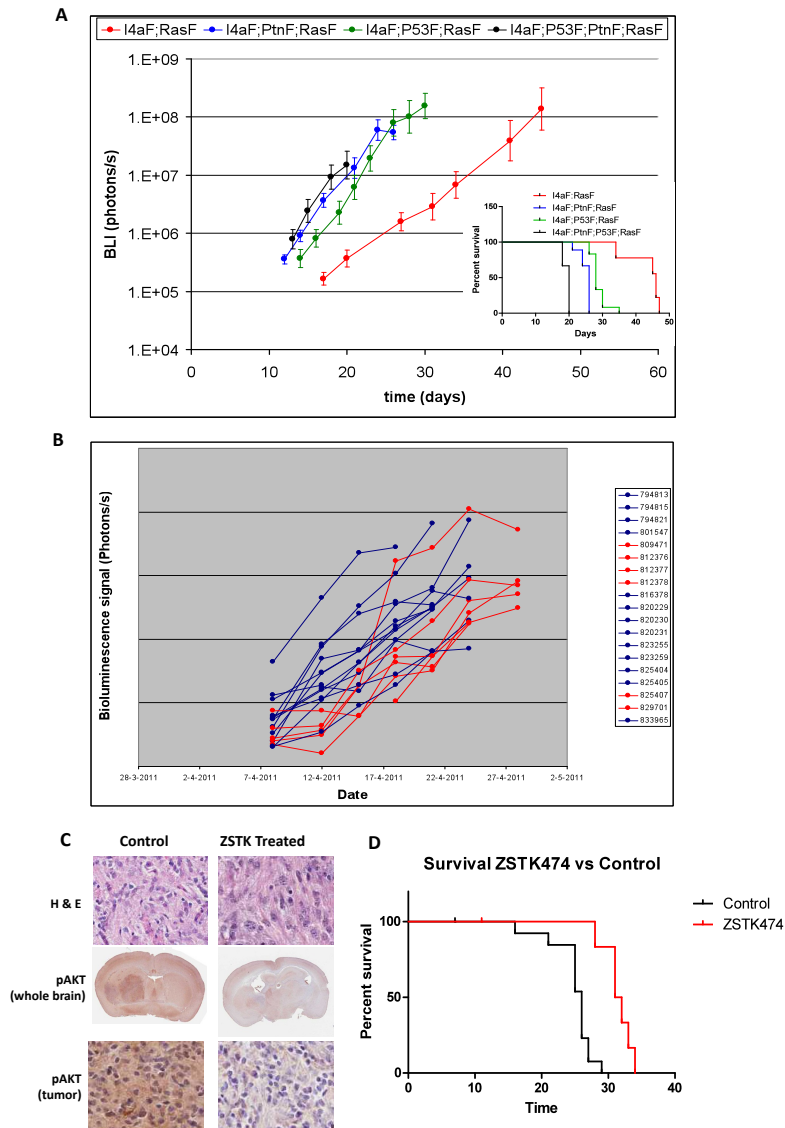


**Fig. 5.** Inhibiting the PI3K pathway in the spontaneous GBM mouse model. **A**, tumor growth ratio curves of GBM carrying mice with different genotypes: Ink4a/Arf;K-Rasv12;LucR, Pten; Ink4a/Arf;K-Rasv12;LucR, P53;Ink4a/Arf;K-Rasv12;LucR and P53;Pten; Ink4a/Arf;K-Rasv12;LucR. The embedded panel, Kaplan-Meier analysis for GBM related survival. **B**, PTEN;Ink4a/Arf;K-Rasv12 conditional mice (WT) with spontaneous GBM induced by intracranial injection of lenti-Cre virus received ZSTK474 at a dose of 200 mg/kg q.d. (n=6; red lines) or no treatment (n=13; blue) starting from day 3 after lentivirus injection. **B**, Histological sections of the intracranial grown GBM stain with H&E (upper panels) and by immunohistochemistry using anti p-Akt (middle and lower panel). **C**, Kaplan-Meier analysis for GBM related survival of control and ZSTK474 treated mice.

Arf;K-Ras<sup>v12</sup> mice that develop gliomas survived significantly longer than Pten;Ink4a/Arf;K-Ras<sup>v12</sup> mice (median survival 45 vs 26 day;  $P < 0.001$ ). Similarly, the deletion of PTEN in mice with P53-null tumors also have an accelerated tumor onset and progression (P53;Ink4a/Arf;K-Ras<sup>v12</sup> vs Pten;P53;Ink4a/Arf;K-Ras<sup>v12</sup> gliomas; 28 vs 20 day, respectively;  $P < 0.0001$ ), suggesting that activation of the PI3K by PTEN deletion signaling is important in these high-grade glioma models.

Next, we evaluated the therapeutic effect of ZSTK474 using spontaneous PTEN;Ink4a/Arf;K-Ras<sup>v12</sup>;LucR high-grade glioma model. In these tumors PI3K signaling was markedly suppressed two hr after mice received ZSTK474 treatment (Fig.5 C). ZSTK474 also delayed the onset of tumor formation as shown in Fig.5 B, although once tumors were more advanced, ZSTK474 was not able to reduce the proliferation rate of these tumors. Overall, ZSTK474 treatment increased the median survival from 26 to 32 days ( $p=0.0002$ , Fig.5 D). These results suggest that PI3K signaling is suppressed by ZSTK474 *in vivo*, but that the signaling that is triggered by the deletion of PTEN is not fully abrogated. Otherwise the tumor onset and progression in Pten;Ink4a/Arf;K-Ras<sup>v12</sup>;LucR mice would have been more similar to that observed in Ink4a/Arf;K-Ras<sup>v12</sup>;LucR mice.

**Table 1.** MS/MS and LC parameters including parent and daughter mass, tubelens off set, collision energy and retention time of rapamycin and tacrolimus.

Parameter	Rapamycin	tacrolimus
Parent mass	936.6	826.5
Daughter mass	409.2	616.2
Tube lens off set	163	136
Collision energy [V]	54	36
Retention time [min]	2.8	2.7

## DISCUSSION

Although small-molecule targeted therapies hold promise for treatment of malignant gliomas, these agents need to penetrate the BBB sufficiently and reach both the tumor cells at the center of the lesion as well as the invasive glioma cells in order to be efficacious. Using *in vitro* and *in vivo* mouse models, we determined the impacts of Abcb1 and Abcg2, two well established drug efflux transporters expressed at BBB, on brain penetrations of rapamycin, NVP-BE2235 and ZSTK474. Abcb1 severely impairs the brain penetration of rapamycin, and to some extent also of NVP-BE2235. However, ZSTK474 is not transported by Abcb1 and/or Abcg2 *in vitro*, and its brain penetration is not affected by these two transporters, indicating a good brain permeability of this agent. Both NVP-BE2235 and ZSTK474 caused efficient inhibition of proliferation and of PI3K/mTOR signaling in cell lines with different genotypes derived from our spontaneous murine high-grade glioma models. In the spontaneous PTEN deficient GBM model, ZSTK474 (200 mg/kg q.d.) delayed the tumor onset and prolonged the overall survival, although the tumor proliferation was only minimally suppressed when tumors had progressed to bigger lesions. Our results suggest that some of the currently available PI3K inhibitors may be able to reach the GBM tumor cells and cause pharmacodynamic effects (*e.g.* target inhibition). However, single PI3K inhibitor treatment alone is probably not sufficient to cause a meaningful therapeutic response against full blown GBM.

One of the critical issues for successful targeted therapy is that sufficient drug should reach the tumor cells to achieve the target inhibition. Unfortunately, many of the targeted agents are good substrates of drug efflux transporters and hence, they have a limited brain penetration. Rapamycin is the prototype inhibitor of mTOR and has been tested in clinical trial against GBM without much success [25]. Due to Abcb1 mediated brain efflux the brain concentration of rapamycin was extremely low (7 ng/g at 1 hr in the elacridar experiment) after receiving a dose that has previously been used by others in preclinical models of cancer. Importantly, the brain accumulation of rapamycin was not corrected for the amount of blood in the brain vasculature (1.4%) [26]. This, however, becomes especially important when brain-to-blood (plasma) levels are very low. In fact, with a brain-to-plasma ratio of about 0.04, the levels that we detected in the brains of Abcg2<sup>-/-</sup> mice is for a substantial part just blood borne drug that did not penetrate the BBB. In fact, Mendiburu-Elicabe et al recently showed that even in a U87

xeno graft model with leaky vessels neither target inhibition nor survival have been achieved upon administration of a dose of 3 mg/kg of rapamycin, and further increase of dose caused severe weight loss [27]. In the brains of *Abcb1* and *Abcb1;Abcg2* knockout mice the brain level was about 150 ng/g. Further investigations to see if these values are sufficient for target inhibition (pAKT/pS6RP) are pending. Elacridar significantly improves the brain penetration of rapamycin so it might provide an alternative solution to combine with rapamycin to target the PI3K pathway in brain disease.

Comparing blood levels was more difficult, because the blood levels of rapamycin in the knockout mouse models were much higher than in WT mice. Most likely this is due to a factor in blood of the knockout mice, which avidly binds rapamycin. Due to this binding, the fraction of drug that is available for distribution to the tissues is much lower than expected based on the total drug level measured by LC-MS. Presumably this binding also reduced the degradation of rapamycin in plasma from knockout mice relative to WT mice. Ferron and Jusko have reported that rapamycin is unstable in both plasma and whole blood of human, rabbit and rat [24]. The degradation of rapamycin is presumably caused by the esterase mediated hydrolysis of rapamycin providing an intermediate metabolite seco-rapamycin for further degradation [28, 29]. Further investigations into the difference between knockout and WT plasma are ongoing. In other organs, such as kidney and liver, the levels of rapamycin were much higher than in brain (Fig.1 B and C) and similar in knockout and WT mice.

*Abcb1* is the most dominant efflux transporter at the human and mouse BBB. Although the *in vitro* transwell experiments for NVP-BEZ235 did not show transport by *Abcb1*, the brain concentration was significantly increased in *Abcb1* deficient mice. In contrast, the absence of *Abcg2* alone did not statistically increase the brain concentration and brain-plasma of NVP-BEZ235 ratio in comparison with WT mice. We have found similar results with other drugs that are relatively weak substrates, such as temozolomide and Palomid 529. This result suggest that although the *in vitro* transport model is suitable to identify substrates as shown for rapamycin, the lack of transport in this assay does not always predict the impact of *Abcb1* at the BBB. Consequently, *in vivo* studies remain necessary to assess the actual role of this transporter in drug delivery to the brain.

For this reason, we also checked the effect of Abcb1 and Abcg2 on the brain penetration of ZSTK474. In this case the absence of transport in the transwell assays was in line with the results in the ABC-transporter knockout mice. Overall ZSTK474 has a very good brain penetration with a brain-to-plasma ratio of about 1.2. This characteristic would make this compound a suitable candidate for targeting in the brain.

We have created a range of neurosphere GBM cell lines from spontaneous glioma mouse models established recently [17]. Those cells were always cultured on ultra-low binding (ULB) plates in serum free medium supplemented with EGF and bFGF. Under these conditions, the tumor cells form so called neurospheres that remain in a more undifferentiated state than if they were cultured in serum medium. Furthermore, they largely maintain the geno- and phenotypic characteristics of the original glioma when re-injected back into recipient mice [30]. *In vitro* proliferation assays can be carried out with these tumor cell lines grown as neurospheres on ULB plates or as adherent cultures on laminin coated plates. To demonstrate the applicability for testing the potency of PI3K-mTOR inhibitors, we have performed a feasibility study with cell lines derived from Ink4a/Arf;K-Ras<sup>v12</sup>, Pten;Ink4a/Arf;K-Ras<sup>v12</sup>, P53;Ink4a/Arf;K-Ras<sup>v12</sup> and P53;Pten;Ink4a/Arf;K-Ras<sup>v12</sup> GBM (Fig. 4). On a molar base, NVP-BE2235 is more potent than ZSTK474 in the PTEN proficient cell line. This may partly be due to the fact that the NVP-BE2235 inhibits both PI3K and mTOR, whereas ZSTK474 inhibits predominantly PI3K. At a safe dose of 200 mg/kg, the brain concentration of ZSTK474 is, however, much higher than NVP-BE2235 in WT mice, which may compensate for this difference in potency. In fact, regarding the brain concentrations obtained from the WT mice in the pharmacokinetic studies, both of the two agents reached their effective target inhibition level in WT brain.

Although several studies with PI3K inhibitors, given as a single agent, have shown promising tumor growth inhibitory potencies by *in vitro* or *in vivo* models using established GBM cell lines such as U87-MG [27], it should be taken into account that these GBM cells have been cultured for many generations. When grown *in vivo*, they form homogenous non-invasive lesions with a relative stable genome, unlike the highly heterogeneous GBMs that are typically found in patients. Moreover, because the BBB in these non-invasively growing tumors is disrupted, all tumor cells are well accessible for substances present in blood. In this sense, the invasively growing spontaneous glioma model is a more realistic model for performing intervention studies with drugs. We have

performed a pilot experiment in *Pten;Ink4a/Arf;K-Ras<sup>v12</sup>* spontaneous tumors because PTEN deficient tumors developed much more rapidly than the PTEN proficient tumors in *Ink4a/Arf;K-Ras<sup>v12</sup>* mice. Based on this finding, we expected that the tumor growth profile of *Pten;Ink4a/Arf;K-Ras<sup>v12</sup>* spontaneous tumors may become more like *Ink4a/Arf;K-Ras<sup>v12</sup>* tumors. Indeed, we found that treatment with ZSTK474 significantly improved survival and caused inhibition of pAKT and pS6RP in tumors and surrounding brain. However, the response was much more modest than might have been expected based on the notion that PTEN is an important factor driving this model. GBM is characterized by multiple parallel disturbed signaling pathways, making it unlikely that single target treatment can be very efficacious against this disease. Very likely, a combination with other drugs targeting other pathways (RAS-MEK-ERK, CDK4/6-RB) may be necessary. Obviously, however, also these drugs will need to cross the BBB sufficiently to reach tumor cells in pharmacologically relevant levels. Our preclinical models are well suited to select the most optimal candidates for further investigation.

## Reference List

- [1] Cancer Genome Atlas Research Network. Comprehensive genomic characterization defines human glioblastoma genes and core pathways. *Nature* 2008;455:1061-8.
- [2] Parsons DW, Jones S, Zhang X, et al. An integrated genomic analysis of human glioblastoma multiforme. *Science* 2008;321:1807-12.
- [3] Kreisl TN, Lassman AB, Mischel PS, et al. A pilot study of everolimus and gefitinib in the treatment of recurrent glioblastoma (GBM). *J Neurooncol* 2009;92:99-105.
- [4] Chang SM, Kuhn J, Wen P, et al. Phase I/pharmacokinetic study of CCI-779 in patients with recurrent malignant glioma on enzyme-inducing antiepileptic drugs. *Invest New Drugs* 2004;22:427-35.
- [5] Chang SM, Wen P, Cloughesy T, et al. Phase II study of CCI-779 in patients with recurrent glioblastoma multiforme. *Invest New Drugs* 2005;23:357-61.
- [6] Galanis E, Buckner JC, Maurer MJ, et al. Phase II trial of temsirolimus (CCI-779) in recurrent glioblastoma multiforme: a North Central Cancer Treatment Group Study. *J Clin Oncol* 2005;23:5294-304.
- [7] Wang X, Yue P, Kim YA, Fu H, Khuri FR, Sun SY. Enhancing mammalian target of rapamycin (mTOR)-targeted cancer therapy by preventing mTOR/raptor inhibition-initiated, mTOR/ricor-independent Akt activation. *Cancer Res* 2008;68:7409-18.
- [8] Stoeltzing O, Meric-Bernstam F, Ellis LM. Intracellular signaling in tumor and endothelial cells: The expected and, yet again, the unexpected. *Cancer Cell* 2006;10:89-91.
- [9] O'Reilly KE, Rojo F, She QB, et al. mTOR inhibition induces upstream receptor tyrosine kinase signaling and activates Akt. *Cancer Res* 2006;66:1500-8.
- [10] Yilmaz OH, Valdez R, Theisen BK, et al. Pten dependence distinguishes haematopoietic stem cells from leukaemia-initiating cells. *Nature* 2006;441:475-82.
- [11] de Vries NA, Beijnen JH, van Tellingen O. High-grade glioma mouse models and their applicability for preclinical testing. *Cancer Treat Rev* 2009;35:714-23.
- [12] de Vries NA, Beijnen JH, Boogerd W, van Tellingen O. Blood-brain barrier and chemotherapeutic treatment of brain tumors. *Expert Rev Neurother* 2006;6:1199-209.
- [13] de Vries NA, Buckle T, Zhao J, Beijnen JH, Schellens JH, van Tellingen O. Restricted brain penetration of the tyrosine kinase inhibitor erlotinib due to the drug transporters P-gp and BCRP. *Invest New Drugs* 2010;30:443-9.
- [14] Polli JW, Olson KL, Chism JP, et al. An unexpected synergist role of P-glycoprotein and breast cancer resistance protein on the central nervous system penetration of the tyrosine kinase inhibitor lapatinib (N-{3-chloro-4-[(3-fluorobenzyl)oxy]phenyl}-6-[5-[[2-(methylsulfonyl)ethyl]amino]methyl]-2-furyl]-4-quinazolinamine; GW572016). *Drug Metab Dispos* 2009;37:439-42.
- [15] Liu TJ, Koul D, LaFortune T, et al. NVP-BE2235, a novel dual phosphatidylinositol 3-kinase/mammalian target of rapamycin inhibitor, elicits multifaceted antitumor activities in human gliomas. *Mol Cancer Ther* 2009;8:2204-10.

- [16] Kong D, Dan S, Yamazaki K, Yamori T. Inhibition profiles of phosphatidylinositol 3-kinase inhibitors against PI3K superfamily and human cancer cell line panel JFCR39. *Eur J Cancer* 2010;46:1111-21.
- [17] de Vries NA, Bruggeman SW, Hulsman D, et al. Rapid and robust transgenic high-grade glioma mouse models for therapy intervention studies. *Clin Cancer Res* 2010;16:3431-41.
- [18] Lin F, Chandrasekaran G, de Gooijer MC, Beijnen JH, van TO. Determination of NVP-BEZ235, a dual PI3K and mTOR inhibitor, in human and mouse plasma and in mouse tissue homogenates by reversed-phase high-performance liquid chromatography with fluorescence detection. *J Chromatogr B Analyt Technol Biomed Life Sci* 2012;901:9-17.
- [19] Bruggeman SW, Valk-Lingbeek ME, van der Stoop PP, et al. Ink4a and Arf differentially affect cell proliferation and neural stem cell self-renewal in Bmi1-deficient mice. *Genes Dev* 2005;19:1438-43.
- [20] Clarke MJ, Mulligan EA, Grogan PT, et al. Effective sensitization of temozolomide by ABT-888 is lost with development of temozolomide resistance in glioblastoma xenograft lines. *Mol Cancer Ther* 2009;8:407-14.
- [21] Palma JP, Wang YC, Rodriguez LE, et al. ABT-888 confers broad in vivo activity in combination with temozolomide in diverse tumors. *Clin Cancer Res* 2009;15:7277-90.
- [22] Zhang Y, Huo M, Zhou J, Xie S. PKSolver: An add-in program for pharmacokinetic and pharmacodynamic data analysis in Microsoft Excel. *Comput Methods Programs Biomed* 2010;99:306-14.
- [23] Luna-Tortos C, Fedrowitz M, Loscher W. Several major antiepileptic drugs are substrates for human P-glycoprotein. *Neuropharmacology* 2008;55:1364-75.
- [24] Ferron GM. Species differences in sirolimus stability in humans, rabbits, and rats. 1998.
- [25] Reardon DA, Desjardins A, Vredenburgh JJ, et al. Phase 2 trial of erlotinib plus sirolimus in adults with recurrent glioblastoma. *J Neurooncol* 2010;96:219-30.
- [26] Dai H, Marbach P, Lemaire M, Hayes M, Elmquist WF. Distribution of STI-571 to the brain is limited by P-glycoprotein-mediated efflux. *J Pharmacol Exp Ther* 2003;304:1085-92.
- [27] Mendiburu-Elicabe M, Yin D, Hadaczek P, Zhai Y, Forsayeth J, Bankiewicz KS. Systemic rapamycin alone may not be a treatment option for malignant glioma: evidence from an in vivo study. *J Neurooncol* 2012;108:53-8.
- [28] Paine MF, Leung LY, Watkins PB. New insights into drug absorption: studies with sirolimus. *Ther Drug Monit* 2004;26:463-7.
- [29] Streit F, Christians U, Schiebel HM, Meyer A, Sewing KF. Structural identification of three metabolites and a degradation product of the macrolide immunosuppressant sirolimus (rapamycin) by electrospray-MS/MS after incubation with human liver microsomes. *Drug Metab Dispos* 1996;24:1272-8.
- [30] Lee J, Kotliarova S, Kotliarov Y, et al. Tumor stem cells derived from glioblastomas cultured in bFGF and EGF more closely mirror the phenotype and genotype of primary tumors than do serum-cultured cell lines. *Cancer Cell* 2006;9:391-403.



# **CHAPTER 4**

## **COOPERATIVE BRAIN EFFLUX BY MULTIDRUG EFFLUX TRANSPORTERS**



# Chapter 4.1

Abcc4 together with Abcb1 and Abcg2 form a robust co-operative drug efflux system that restricts the brain entry of camptothecin analogs

Fan Lin, Serena Marchetti and Dick Pluim, Dilek Iusuf, Roberto Mazzanti, Jan H.M. Schellens, Jos H. Beijnen, Olaf van Tellingen

Submitted for publication

## ABSTRACT

**Purpose:** Multidrug resistance-associated protein 4 (ABCC4) shares many features with P-glycoprotein (ABCB1) and breast cancer resistance protein (ABCG2), including broad substrate affinity and expression at the blood-brain barrier (BBB). However, the pharmacological relevance of ABCC4 at the BBB is difficult to evaluate since most drugs are also substrates of ABCB1 and/or ABCG2. **Experimental Design:** We have created a mouse strain in which all these alleles are inactivated to assess their impact on brain delivery of camptothecin analogs, an important class of antineoplastic agents and substrates of these transporters. Wild-type (WT), *Abcg2*<sup>-/-</sup>, *Abcb1a/b*<sup>-/-</sup>, *Abcc4*<sup>-/-</sup>, *Abcb1a/b;Abcg2*<sup>-/-</sup>, *Abcg2;Abcc4*<sup>-/-</sup> and *Abcb1a/b;Abcg2;Abcc4*<sup>-/-</sup> mice received i.v. topotecan, irinotecan, SN-38 or gimatecan alone or with concomitant oral elacridar. Drug levels were analyzed by HPLC. **Results:** We found that additional deficiency of *Abcc4* in *Abcb1a/b;Abcg2*<sup>-/-</sup> mice significantly increased the brain concentration of all camptothecin analogs by 1.2-fold (gimatecan) to 5.8-fold (SN-38). The presence of *Abcb1a/b* or *Abcc4* alone was sufficient to reduce the brain concentration of SN38 to the level in WT mice. Strikingly, the brain distribution of gimatecan in brain of WT mice was more than 220-fold and 40-fold higher than that of SN-38 and topotecan, respectively. **Conclusion:** *Abcc4* limits the brain penetration of camptothecin analogs and teams up with *Abcb1a/b* and *Abcg2* to form a robust cooperative drug-efflux system. This concerted action limits the usefulness of selective ABC-transport inhibitors to enhance drug entry for treatment of intracranial diseases. Our results also suggest that gimatecan might be a better candidate than irinotecan for clinical evaluation against intracranial tumors.

## INTRODUCTION

The blood-brain barrier (BBB) is a complex well-organized structure that serves to protect the brain by limiting the entry of most exogenous compounds into brain (1). On the other hand, it is seen as a major obstacle for many therapeutic agents which might otherwise be effective against brain diseases, including brain cancer (2-4). The BBB is formed by the brain endothelial cells, which are closely linked to each other by tight junctions, lacking fenestrae and having low pinocytotic activity. As a consequence, the brain entry of substances requires trans-endothelial passage, thus allowing strict regulation of brain entry by a range of uptake and efflux transporters (5). ATP-binding cassette (ABC) drug efflux transporters expressed at the BBB restrict the entry of many compounds into the brain (6). The dramatic impact of P-glycoprotein (P-gp, ABCB1/Abcb1a) on the brain entry of substrate agents was first shown by Schinkel *et al.* (7) using Abcb1a deficient mice and was later shown to be important for a plethora of agents. The cooperative action of breast cancer resistance protein (BCRP, ABCG2/Abcg2) in combination with Abcb1 became clear when we used compound Abcb1a/b;Abcg2 deficient mice (8). Until then, the functionality of Abcg2 at the BBB had not been convincingly shown by results obtained with single Abcg2 deficient mice, because of the overlapping substrate affinities of Abcb1a/b and Abcg2 and because the presence of Abcb1a/b alone is sufficient to reduce the concentration of dual ABCB1/ABCG2 substrates in the brain to the level of that in WT mice.

Camptothecin and its analogs are potent topoisomerase I inhibitors and represent an important class of anti-neoplastic agents with a wide spectrum of antitumor activity. Two camptothecin analogs, topotecan and irinotecan (CPT11), have already been approved for treatment of advanced ovarian cancer, small cell lung cancer and colon cancer (9-11). Whether they could also be efficacious against brain malignancies is speculative, but CPT11 is receiving considerable attention with more than 10 ongoing or planned clinical trials involving brain cancer (source: <http://clinicaltrials.gov>). However, whether these drugs can cross the BBB in sufficient amounts to be active against intracranial tumors remains uncertain. *In vitro* studies have demonstrated that CPT11 and its active metabolite SN-38 are also substrates of ABCB1 and/or ABCG2 (12-16), which may thus exclude these compounds from the brain, as was shown for topotecan (8). Gimatecan is another camptothecin analog with different pharmaceutical properties. Relative to

topotecan and CPT11/SN-38 it is a more lipophilic compound and a weaker substrate of ABCB1 (17;18). It is also reported to have none or minimal affinity for ABCG2 (18;19) although Marchetti *et al.* (17) reported that gimatecan is a substrate of Abcg2.

Besides ABCB1 and ABCG2, multidrug resistance protein 4 (MRP4, ABCC4/Abcc4) is also expressed at the BBB and the choroid plexus epithelium (20). ABCC4 transports a wide range of more polar endogenous molecules such as nucleotides, urate and folates, bile acids and glutathione conjugates, but is also reported to transport antiviral, antibiotic, cardiovascular and anticancer agents including topotecan, CPT11/SN-38 and gimatecan (18;20-24) *in vitro*. The initial claim (20) that the brain accumulation of topotecan is higher in single Abcc4 deficient mice could not be replicated, presumably because topotecan is also a substrate of Abcb1 and Abcg2, which dominate the restriction of its brain entry (8). More recently, however, it was shown that Abcc4 deficient mice accumulate more oseltamivir carboxylate (Ro64-0802) in their brain (25). Importantly, this relatively hydrophilic metabolite of oseltamivir is not a substrate of Abcb1 (26), explaining why the substrate functionality of Abcc4 at the BBB could be demonstrated in single Abcc4 deficient mice.

To allow more accurate assessment of the impact of Abcc4 on the BBB penetration without interference by Abcb1a/b and Abcg2, we performed a comprehensive comparison between Abcb1a/b;Abcg2;Abcc4 vs Abcb1a/b;Abcg2 deficient mice and a range of other control strains. For this purpose we used the camptothecin analogs topotecan, CPT11, SN-38 and gimatecan, which all differ to some extent in their lipophilicity and affinities towards these ABC transporters. Our results clearly demonstrate the profound impact that Abcc4 can have on the brain penetration of substrate drugs.

## MATERIALS AND METHODS

### *Chemicals and drugs*

Topotecan and elacridar were kindly provided by GlaxoSmithKline (Research Triangle Park, NC, USA). Irinotecan (Campto®) was from Pfizer (Pfizer, New York, USA); SN-38 was from Sequoia Research Products (Pangbourne, UK); and Gimatecan was provided by Novartis Pharmaceuticals Inc. (Novartis, East Hanover, NJ, USA). Blank human plasma was obtained from healthy donors (Sanquin, Amsterdam, the Netherlands). All other chemicals were purchased from Merck (Darmstadt, Germany).

### *Animals*

Mice were housed and handled according to institutional guidelines complying with Dutch legislation. All experiments with animals were approved by the local animal experiment committee. The animals used in this study were wild type (WT), *Abcg2*<sup>-/-</sup>, *Abcb1a/b*<sup>-/-</sup>, *Abcc4*<sup>-/-</sup> (20), *Abcb1a/b;Abcg2*<sup>-/-</sup> (8), *Abcg2;Abcc4*<sup>-/-</sup> and *Abcb1a/b;Abcg2;Abcc4*<sup>-/-</sup> mice, all of a >99% FVB genetic background, between 8 and 14 weeks of age. The animals were kept in a temperature-controlled environment with a 12-h dark cycle and received a standard diet (AM-II, Hope Farm B.B., Woerden, the Netherlands) and acidified water *ad libitum*.

### *Plasma and brain pharmacokinetics*

Topotecan and CPT11 were diluted to 0.5 mg/ml in 5% (w/v) glucose, whereas gimatecan and SN-38 were dissolved (2 mg/ml) in DMSO. They were administered i.v. at a dose of 2 mg/kg (for topotecan, SN-38 and gimatecan) or 5 mg/kg (for CPT11). Elacridar prepared as described earlier (8) was given p.o. at a dose of 100 mg/kg 2 h prior to camptothecins. Continuous infusion of topotecan was achieved with Alzet minipumps model 1003D (Durect Corp. Cupertino, CA, USA) filled with 2 or 10 mg/ml of topotecan in 5%(w/v) glucose. Pumps were placed in the peritoneal cavity under isoflurane anesthesia and mice were sacrificed 28 to 30 h after placement.

Mice were anesthetized by isoflurane. Blood was collected by cardiac puncture and kept on ice. The mice were sacrificed and brains were dissected. Plasma was separated by centrifugation at 10,000 g for 5 min at 4 °C. Brains were homogenized in 3 ml 1% (w/v) bovine serum albumin (BSA). Both plasma and brain homogenates were stored at -20°C

until analysis. The brain accumulation was corrected for the amount of drug in the brain vasculature (1.4%) (27).

#### *Drug analysis*

Topotecan, CPT11 and SN-38 samples were analyzed by high-performance liquid chromatography (HPLC) as described previously (28;29) but with minor modification. In brief, 100  $\mu$ l of biological sample was mixed with 200  $\mu$ l of ice-cold methanol and centrifuged at 4  $^{\circ}$ C, 20,000 g for 10 min. Next, 100  $\mu$ l of the supernatant fraction was mixed with 200  $\mu$ l of ice-cold perchloric acid (2% in water). After centrifugation at 4  $^{\circ}$ C, 20,000 g for 3 min, 100  $\mu$ l of clear supernatant was analyzed by HPLC.

For gimatecan, 50  $\mu$ l of sample was mixed with of ice-cold methanol and centrifuged at 4  $^{\circ}$ C, 20,000 g for 10 min. A volume of 200  $\mu$ l of supernatant fraction was mixed with 300  $\mu$ l 0.01 M sodium borate, centrifuged at 4  $^{\circ}$ C, 20,000 g for 5 min and 100  $\mu$ l of clear solution was injected into the HPLC system.

HPLC was performed using a DGP-3600A pump with SRD-3600 Solvent Rack, a model WPS-3000TSL autosampler (Dionex, Sunnyvale, CA, USA) and a model FP-1520 fluorescence detector (Jasco, Hachioji City, Japan) operating at 380/527 nm (excitation/emission). Separation of topotecan, CPT11 and SN-38 was performed using a Zorbax SB-C<sub>18</sub> column (75  $\times$  4.6 mm i.d., Rockland Technologies Inc, Newport, DE, USA) and for gimatecan a Symmetry C<sub>18</sub> column (2.1  $\times$  150 mm i.d. Waters, Milford, MA, USA). The mobile phase for topotecan consisted of methanol, 0.1 M hexane-1-sulfonic acid, and 0.01 M TEMED adjusted to pH 6.0 with phosphoric acid (25:10:65, v/v/v). The mobile phase for CPT11 and SN-38 consisted of 0.1 M ammonium acetate buffer pH 6.4 containing 5 mM tetrabutylammonium bromide, tri-ethylamine and acetonitrile (790:1:210, v/v/v). The mobile phase for gimatecan consisted of acetonitrile, 50 mM ammonium acetate buffer adjusted to pH 6.8 (30:70, v/v). Chromatographic data analysis was performed using Chromeleon software v6.8 (Dionex). The lower limit of quantitation was 0.05 ng/ml (plasma) and 0.5 ng/g (brain) for topotecan and SN38 and 0.2 ng/ml (plasma) and 2 ng/g (brain) for CPT-11 and gimatecan.



*Ex vivo carboxylesterase activity measurement*

Carboxylesterase activity in mouse plasma was measured by monitoring *ex vivo* conversion of CPT11 into SN-38 using previously described methods with slight modification (30). In short, 20  $\mu$ l 2.5 mM CPT11 was mixed with 800  $\mu$ l 20 mM Tris-HCl buffer (pH 7.5) and incubated at 37 °C for 30 min to reach equilibrium between the lactone and carboxylate forms of CPT11. Next, 200  $\mu$ l fresh plasma collected from WT, *Abcg2*<sup>-/-</sup> or *Abcb1a/1b*<sup>-/-</sup>; *Abcg2*<sup>-/-</sup> mice (n=3) was added (final CPT11 concentration is 50  $\mu$ M) and the mixtures were kept at 37 °C with shaking. At 0 min, 1, 2 and 4 h 100  $\mu$ l samples were collected for the determination of CPT11 and SN-38 concentrations.

## RESULTS

### Role of *Abcc4* in topotecan brain delivery

The novel *Abcg2;Abcc4*<sup>-/-</sup> and *Abcb1a/b;Abcg2;Abcc4*<sup>-/-</sup> strains were obtained by cross-breeding of the *Abcc4*<sup>-/-</sup>, *Abcg2*<sup>-/-</sup> and *Abcb1a/b;Abcg2*<sup>-/-</sup> mice. These mice are viable, fertile and do not display any overt phenotype.

To investigate the role of *Abcc4* in the brain penetration of topotecan without the interference by *Abcg2* and *Abcb1a/b*, we determined the topotecan concentrations in brain and plasma from WT, *Abcg2*<sup>-/-</sup>, *Abcb1a/b;Abcg2*<sup>-/-</sup> and *Abcb1a/b;Abcg2;Abcc4*<sup>-/-</sup> mice after i.v. administration of 2 mg/kg topotecan. In line with our previous results (8), the absence of *Abcg2* alone caused a marked 5-fold increased plasma concentration of topotecan in comparison with *Abcg2* proficient WT mice (Fig. 1A), whereas it caused only a small (2-fold) and non-significant higher brain concentration. As a consequence, the brain-to-plasma ratio was lower in *Abcg2*<sup>-/-</sup> mice relative to WT controls. In order to understand this counter-intuitive result we also determined the brain and plasma levels at 5 min post drug administration and found that the differences between the strains were much smaller at this very early time point (Fig. 1D), implicating that the absence of *Abcg2* alone has little effect on the distribution to the brain. At 1 h the plasma levels were reduced by about 20 and 6-fold in WT and *Abcg2*<sup>-/-</sup> mice, respectively, whereas the brain levels were reduced by only 5 and 3-fold. Thus it appears that efflux from the brain cannot keep up with the much more rapid elimination from plasma and the reduced brain-to-plasma ratio in *Abcg2*<sup>-/-</sup> vs. WT mice is a consequence of the more rapid decay in the plasma concentration in WT mice.

At both 1 and 4 h, the plasma concentration of topotecan in *Abcb1a/b;Abcg2*<sup>-/-</sup> and *Abcb1a/b;Abcg2;Abcc4*<sup>-/-</sup> mice was similar, whereas the concentration in brains of *Abcb1a/b;Abcg2;Abcc4*<sup>-/-</sup> mice was significantly higher than in brains of *Abcb1a/b;Abcg2*<sup>-/-</sup> mice (Fig. 1B). Overall, this resulted in a 2.0-fold and 1.9-fold elevated brain-to-plasma ratio of topotecan at 1 and 4 h, respectively, in *Abcb1a/b;Abcg2;Abcc4*<sup>-/-</sup> mice vs. *Abcb1a/b;Abcg2*<sup>-/-</sup> mice (Fig. 1C).

Because topotecan is relatively good water soluble, we decided to perform a similar experiment where topotecan (2 mg/kg/day) was delivered by Alzet minipumps in order to achieve steady-state plasma concentrations. The difference in systemic exposure in

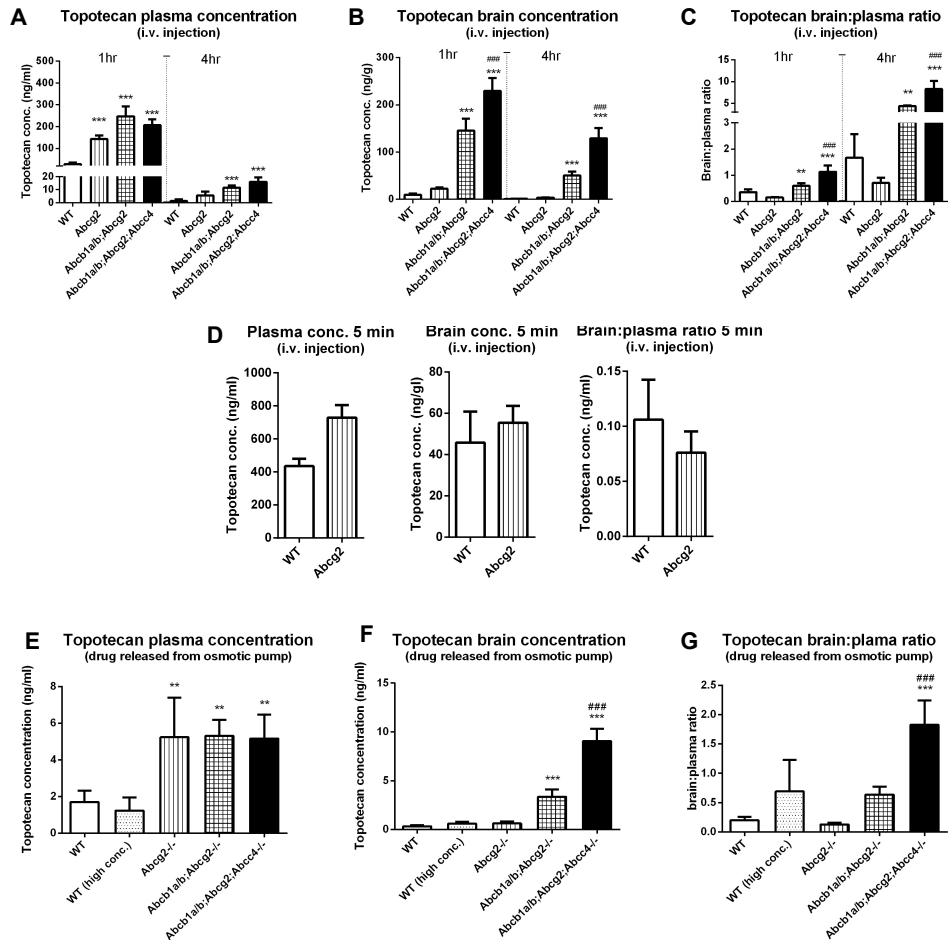


**Figure 1.** Topotecan brain and plasma pharmacokinetics. Plasma concentrations, brain concentrations and brain-to-plasma ratios of topotecan in WT (wild type), *Abcg2*<sup>-/-</sup>, *Abcb1a/b;Abcg2*<sup>-/-</sup> and *Abcb1a/b;Abcg2;Abcc4*<sup>-/-</sup> mice 1 and 4 h (A-C) and 5 min (D) after i.v. administration of 2 mg/kg topotecan or 28-30 h after implantation of an Alzet minipump delivering 2 or 10 (high dose) mg/kg/day (E-G). Data are means  $\pm$  SD;  $n = 8, 5, 10, 5$  (1 hr) and  $5, 5, 5, 5$  (4 hr) for WT, *Abcg2*<sup>-/-</sup>, *Abcb1a/b;Abcg2*<sup>-/-</sup> and *Abcb1a/b;Abcg2;Abcc4*<sup>-/-</sup> mice (A, B and C);  $n = 5$  and  $5$  for WT and *Abcg2*<sup>-/-</sup> mice (D);  $n = 5, 4, 5, 5$  and  $5$  for WT, WT (high dose), *Abcg2*<sup>-/-</sup>, *Abcb1a/b;Abcg2*<sup>-/-</sup> and *Abcb1a/b;Abcg2;Abcc4*<sup>-/-</sup> mice (E, F and G). \*  $P < 0.05$ ; \*\*  $P < 0.01$ ; and \*\*\*  $P < 0.001$ , compared with WT mice. ###  $P < 0.001$ , compared with *Abcb1a/b;Abcg2*<sup>-/-</sup> mice.

WT and *Abcg2*<sup>-/-</sup> strains at this dose was modest as steady-state plasma levels differed only by about 3-fold. The brain concentration was significantly higher in *Abcb1a/b;Abcg2;Abcc4*<sup>-/-</sup> mice than in *Abcb1a/b;Abcg2*<sup>-/-</sup> mice (Fig 1E-G) confirming the impact of *Abcc4*. We also included a cohort of WT mice that received a 5-fold higher dose level (10 mg/kg/day) in an attempt to compensate for the higher clearance in WT mice; however, the plasma levels were not proportionally higher. We have no clear explanation for this finding.

Together these result show that *Abcc4* restricts the brain penetration of topotecan in the absence of *Abcb1a/b* and *Abcg2*, but has no effect on the plasma level of topotecan.

### **Roles of *Abcb1a/b*, *Abcg2* and *Abcc4* in brain delivery of CPT11 and its active metabolite SN-38**

*Abcb1a/b;Abcg2*<sup>-/-</sup> mice had significantly higher plasma levels of CPT11 and SN-38 than *Abcg2*<sup>-/-</sup> mice, whereas there was no difference between *Abcb1a/b;Abcg2*<sup>-/-</sup> and *Abcb1a/b;Abcg2;Abcc4*<sup>-/-</sup> mice receiving CPT11 (Fig. 2A). Interestingly, the CPT11 level in plasma of all *Abcg2*<sup>-/-</sup> mice was markedly lower than that of WT mice, whereas the plasma level of SN-38 was significantly higher than that of WT mice. Given the fact that the sum of concentrations (SUM[CPT11+SN-38]) in plasma of WT and *Abcg2*<sup>-/-</sup> mice were similar, the reduction in CPT11 levels are probably not due to elimination (efflux) by *Abcg2*. Since carboxylesterase(s) are principally involved in the conversion of CPT11 to its active metabolite SN-38, an increased expression of carboxylesterase(s) in *Abcg2* deficient mice might underlie this accelerated conversion of CPT11 into SN-38. We evaluated the *ex vivo* conversion rate of CPT11 into SN-38 using freshly collected plasma of WT, *Abcg2*<sup>-/-</sup> and *Abcb1a/b;Abcg2*<sup>-/-</sup> mice. Following the incubation of CPT11 in *Abcg2*<sup>-/-</sup> murine plasma for only 1 h, more than 20% of the parent drug was already converted into SN-38, whereas only 1% of CPT11 was converted to SN-38 after 4 h incubation in WT plasma. A similar conversion rate to that in *Abcg2*<sup>-/-</sup> mice was observed in plasma of *Abcb1a/b;Abcg2*<sup>-/-</sup> mice.

The marked elevation of the CPT-11 to SN-38 conversion in all strains that are deficient in *Abcg2* relative to *Abcg2* proficient strains makes it more difficult to interpret the role of the ABC transporters on the brain penetration. It is clear, however, that *Abcb1a/b* plays a pivotal role in brain penetration of CPT11 given the 10.2-fold and 15.9-fold higher brain

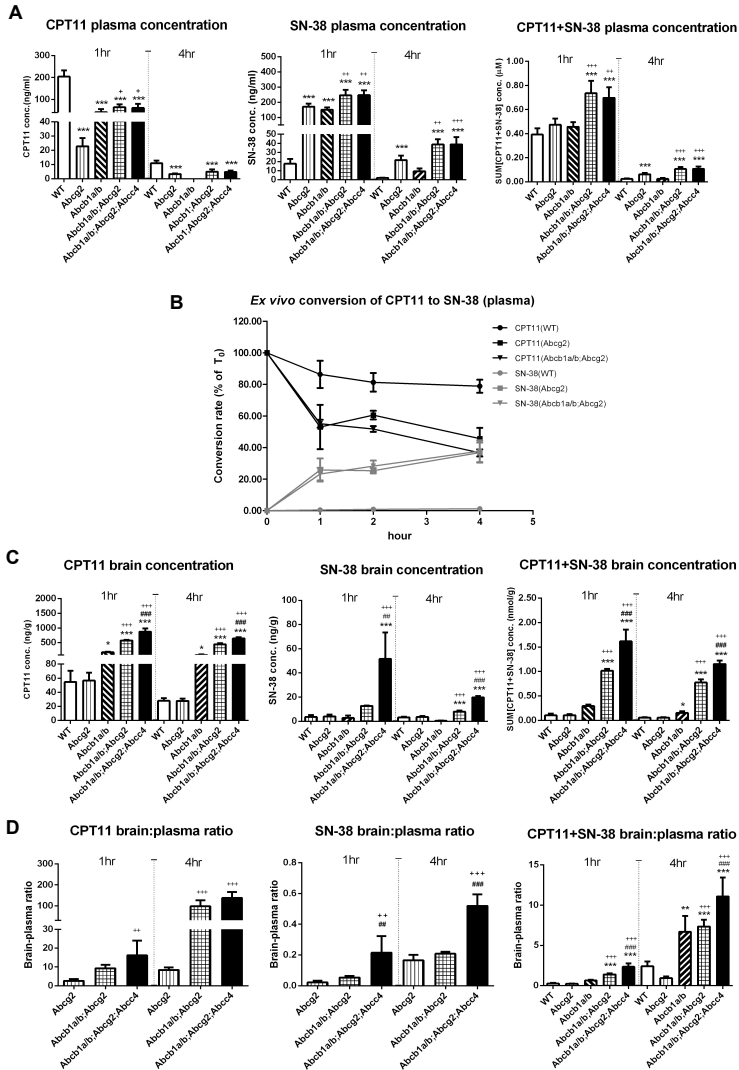


**Figure 2.** Irinotecan (CPT11) and SN-38 brain and plasma pharmacokinetics. Plasma concentrations (A), brain concentrations (C), brain-to-plasma ratios (D) of CPT11, SN-38 and SUM[CPT1+SN-38] (sum of molarities of CPT11 and SN-38) in WT, *Abcg2*<sup>-/-</sup>, *Abcb1a/b*<sup>-/-</sup>, *Abcb1a/b;Abcg2*<sup>-/-</sup> and *Abcb1a/b;Abcg2;Abcc4*<sup>-/-</sup> mice 1 and 4 h after i.v. administration of 5 mg/kg CPT11. The conversion rate of CPT11 to SN-38 during 4 h ex vivo incubation of plasma from WT, *Abcg2*<sup>-/-</sup> and *Abcb1a/b;Abcg2*<sup>-/-</sup> mice with 50  $\mu$ M CPT11 in buffer (B). For panel A, C and D, data are means  $\pm$  SD, n = 5, 5, 5, 5, 6 (1 hr) and 5, 5, 5, 5, 5 (4 hr) for WT, *Abcg2*<sup>-/-</sup>, *Abcb1a/b*<sup>-/-</sup>, *Abcb1a/b;Abcg2*<sup>-/-</sup> and *Abcb1a/b;Abcg2;Abcc4*<sup>-/-</sup> mice (A, C and D). \*  $P < 0.05$ ; \*\*  $P < 0.01$ ; and \*\*\*  $P < 0.001$ , compared with WT mice. +  $P < 0.05$ ; ++  $P < 0.01$ ; and +++  $P < 0.001$ , compared with *Abcg2*<sup>-/-</sup> mice. #  $P < 0.05$ ; ##  $P < 0.01$ ; and ###  $P < 0.001$ , compared with *Abcb1a/b;Abcg2*<sup>-/-</sup> mice. Note break in Y axes of the CPT11 and SN-38 plasma concentrations.. For panel B, data are means  $\pm$  SD, n = 3 per strain.

CPT11 levels at 1 and 4 h, respectively in *Abcb1a/b;Abcg2<sup>-/-</sup>* mice vs. *Abcg2<sup>-/-</sup>* mice (Fig. 2C). *Abcb1a/b* also limits the brain penetration of SN-38, although the difference between *Abcg2<sup>-/-</sup>* and *Abcb1a/b;Abcg2<sup>-/-</sup>* mice was smaller (about 2.5-fold). Importantly, however, the additional deletion of *Abcc4* in the absence of *Abcb1a/b* and *Abcg2* resulted in a further 3.4-fold higher brain concentration of SN-38 at 1 h. Similarly, the CPT11 levels

**Table 1.** Increase (fold change) of the brain concentrations, brain-to-plasma ratios and percentages of dose in brain after administration of topotecan, irinotecan (SUM[CPT11 and SN-38]), SN38 and gimatecan caused by deficiency in *Abcb1a/b*, *Abcg2* and/or *Abcc4*. Comparison of *Abcg2;Abcb1a/b;Abcc4<sup>-/-</sup>* and WT mice shows the overall impact from *Abcg2*, *Abcb1a/b* and *Abcc4*. Comparison of *Abcg2;Abcb1a/b;Abcc4<sup>-/-</sup>* and *Abcg2;Abcb1a/b<sup>-/-</sup>* mice shows the impact of *Abcc4*. Comparison of *Abcg2;Abcb1a/b<sup>-/-</sup>* and *Abcg2<sup>-/-</sup>* mice shows the impact of *Abcb1a/b*. Unit, fold. N/A, not assessed.

	Time point	Topotecan	SUM [CPT11+SN38]	SN-38	Gimatecan
<b>Brain concentration</b> ( <i>Abcg2;Abcb1a/b;Abcc4</i> vs. WT)	1 hour	24	15	6.6	4.1
	4 hour	94	21	N/A	4.4
<b>Brain concentration</b> ( <i>Abcg2;Abcb1a/b</i> vs. <i>Abcg2</i> )	1 hour	6.5	9.1	1.2	2.1
	4 hour	14	14	N/A	2.4
<b>Brain concentration</b> ( <i>Abcg2;Abcb1a/b;Abcc4</i> vs. <i>Abcg2;Abcb1a/b</i> )	1 hour	1.6	1.6	5.8	1.4
	4 hour	2.6	1.5	N/A	1.2
<b>Brain-plasma ratio</b> ( <i>Abcg2;Abcb1a/b;Abcc4</i> vs. WT)	1 hour	3.2	8.8	0.7	3.4
	4 hour	4.2	4.5	N/A	3.8
<b>Brain-plasma ratio</b> ( <i>Abcg2;Abcb1a/b</i> vs. <i>Abcg2</i> )	1 hour	3.8	5.9	1.3	1.7
	4 hour	6.2	7.6	N/A	1.8
<b>Brain-plasma ratio</b> ( <i>Abcg2;Abcb1a/b;Abcc4</i> vs. <i>Abcg2;Abcb1a/b</i> )	1 hour	1.9	1.7	2.7	1.3
	4 hour	1.9	1.5	N/A	1.5
<b>Percentage of the dose in brain</b> ( <i>Abcg2;Abcb1a/b;Abcc4</i> vs. WT)	1 hour	23	16	7.5	3.8
	4 hour	81	23	N/A	3.9
<b>Percentage of dose in brain</b> ( <i>Abcg2;Abcb1a/b</i> vs. <i>Abcg2</i> )	1 hour	6.1	8.1	1.1	2.1
	4 hour	12.7	13	N/A	2.2
<b>Percentage of the dose in brain</b> ( <i>Abcg2;Abcb1a/b;Abcc4</i> vs. <i>Abcg2;Abcb1a/b</i> )	1 hour	1.5	1.6	5.6	1.3
	4 hour	2.4	1.5	N/A	1.2

were higher but the difference was only 1.5-fold. Overall, the SUM[CPT-11+SN-38] in brain and the brain-to-plasma ratio of *Abcb1a/b;Abcg2<sup>-/-</sup>;Abcc4<sup>-/-</sup>* mice were significantly higher than those of *Abcb1a/b;Abcg2* mice (Fig. 2F and Table 1)

### Roles of *Abcb1a/b*, *Abcg2* and *Abcc4* in brain delivery of gimatecan

Gimatecan is a relatively new camptothecin analog and little is known about the impact of drug efflux transporters of this analog *in vivo*. Therefore, we evaluated the roles of *Abcb1a/b*, *Abcg2* and *Abcc4* in gimatecan plasma and brain pharmacokinetics using our knockout mice. Unlike topotecan and CPT11, the plasma concentration of gimatecan was not different across all strains on i.v. administration of 2 mg/kg gimatecan, except there was a 1.5-fold elevation of the gimatecan plasma level in *Abcb1a/b;Abcg2<sup>-/-</sup>* at 4 h (Fig. 3A). Moreover, the plasma levels of all strains were much higher than those of topotecan or CPT11/SN-38.

Interestingly, there were also smaller differences in the brain concentration of gimatecan across all strains, relative to topotecan and CPT11/SN-38 (Fig. 3B). However, there were clear differences between *Abcb1a/b* deficient strains (*Abcb1a/b;Abcg2<sup>-/-</sup>* and *Abcb1a/b;Abcg2;Abcc4<sup>-/-</sup>*) and *Abcb1a/b* proficient strains (WT, *Abcg2*, *Abcc4<sup>-/-</sup>* and *Abcg2;Abcc4<sup>-/-</sup>*). Deletion of *Abcb1a/b* alone caused a small but significant 1.9-fold

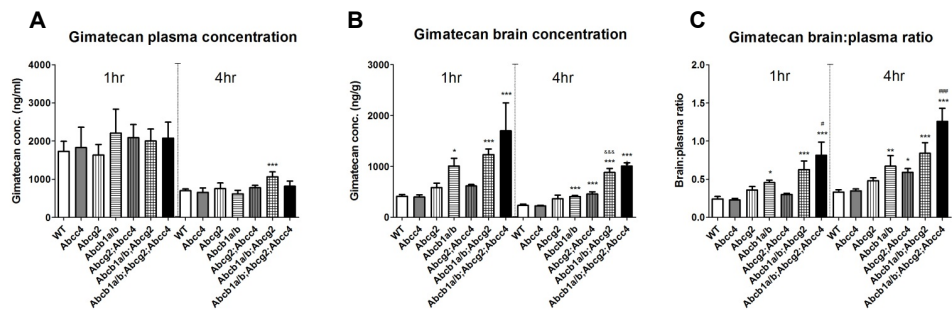


**Figure 3.** Gimatecan brain and plasma pharmacokinetics. Plasma concentrations (A), brain concentrations (B) and brain-to-plasma ratios (C) of gimatecan in WT, *Abcc4<sup>-/-</sup>*, *Abcg2<sup>-/-</sup>*, *Abcb1a/b<sup>-/-</sup>*, *Abcg2;Abcc4<sup>-/-</sup>*, *Abcb1a/b;Abcg2<sup>-/-</sup>* and *Abcb1a/b;Abcg2;Abcc4<sup>-/-</sup>* mice 1 and 4 h after i.v. administration of 2 mg/kg gimatecan. Data are means  $\pm$  SD, n = 5, 5, 5, 4, 6, 5, 5 (1 hr) and 5, 4, 5, 5, 5, 5 (4 hr) for WT, *Abcc4<sup>-/-</sup>*, *Abcg2<sup>-/-</sup>*, *Abcb1a/b<sup>-/-</sup>*, *Abcg2;Abcc4<sup>-/-</sup>*, *Abcb1a/b;Abcg2<sup>-/-</sup>* and *Abcb1a/b;Abcg2;Abcc4<sup>-/-</sup>* mice (A, B and C). \*  $P < 0.05$ ; \*\*  $P < 0.01$ ; and \*\*\*  $P < 0.001$ , compared with WT mice. &  $P < 0.05$ ; &&  $P < 0.01$ ; and &&&  $P < 0.001$ , compared with *Abcb1a/b<sup>-/-</sup>* mice. #  $P < 0.05$ ; ##  $P < 0.01$ ; and ###  $P < 0.001$ , compared with *Abcb1a/b;Abcg2<sup>-/-</sup>* mice.

increase relative to WT mice. *Vice versa*, the brain penetration in Abcb1a/b proficient Abcg2;Abcc4 mice was similar to that in WT mice and much lower than in Abcb1a/b;Abcg2;Abcc4<sup>-/-</sup> mice. Consequently, Abcb1a/b appears to be the most important factor limiting the brain penetration of gimatecan. Although the difference in the brain concentration of gimatecan between Abcb1a/b;Abcg2<sup>-/-</sup> and Abcb1a/b;Abcg2;Abcc4<sup>-/-</sup> mice was small, the brain-to-plasma ratio in the latter was significantly higher at both 1 and 4 h, indicating that Abcc4 also contributes to limiting the brain penetration of gimatecan. The same was seen for Abcg2 by comparing Abcb1a/b<sup>-/-</sup> vs. Abcb1a/b;Abcg2<sup>-/-</sup> mice. Overall, however, the impact of these drug efflux transporters on gimatecan brain penetration is not as strong as for topotecan or CPT11.

#### **Effect of the dual ABCB1 and ABCG2 inhibitor elacridar on brain penetration of SN-38 and gimatecan**

We previously reported that co-administration of the dual ABCB1 and ABCG2 inhibitor elacridar together with topotecan markedly increased the brain penetration of topotecan (8). Because our present findings demonstrate that Abcc4 also impairs the brain penetration of camptothecin analogs, we investigated the effect of elacridar on the brain penetration of SN-38 in various Abcc4 deficient strains. SN-38 was used because the previous experiments clearly indicated that this compound was one of the best Abcc4 substrates. Co-administration of elacridar markedly enhanced the plasma SN-38 concentration across all strains, with the most dramatic increase in WT and Abcc4<sup>-/-</sup> mice (Fig. 4A). Presumably, the impact of elacridar on the plasma level of SN-38 is mainly due to the inhibition of Abcg2 mediated elimination because: 1), the plasma level of SN-38 in Abcg2<sup>-/-</sup> mice was markedly higher than that of WT mice; 2), the plasma level of SN38 was only moderately increased in Abcg2;Abcc4<sup>-/-</sup> mice upon concomitant elacridar; 3) the SN-38 plasma level did not differ between Abcg2<sup>-/-</sup> and Abcb1a/b;Abcg2<sup>-/-</sup> mice, or between Abcg2;Abcc4<sup>-/-</sup> and Abcb1a/b;Abcg2;Abcc4<sup>-/-</sup> mice, suggesting that Abcb1a/b is not actively involved in the elimination of SN-38. Intriguingly, elacridar also substantially increased the plasma level of SN-38 in Abcb1a/b;Abcg2;Abcc4<sup>-/-</sup> mice by a yet unknown cause.

Similar to what we found for topotecan, the brain-to-plasma ratio cannot be compared when the plasma elimination is very different, such as between Abcg2 proficient and deficient strains.



Therefore, we focused on the actual brain concentration of SN-38. *Abcb1a/b;Abcg2;Abcc4<sup>-/-</sup>* mice lacking all three transporters had a 6.6-fold higher brain concentration of SN-38 relative to WT mice. Strikingly, there was no difference between

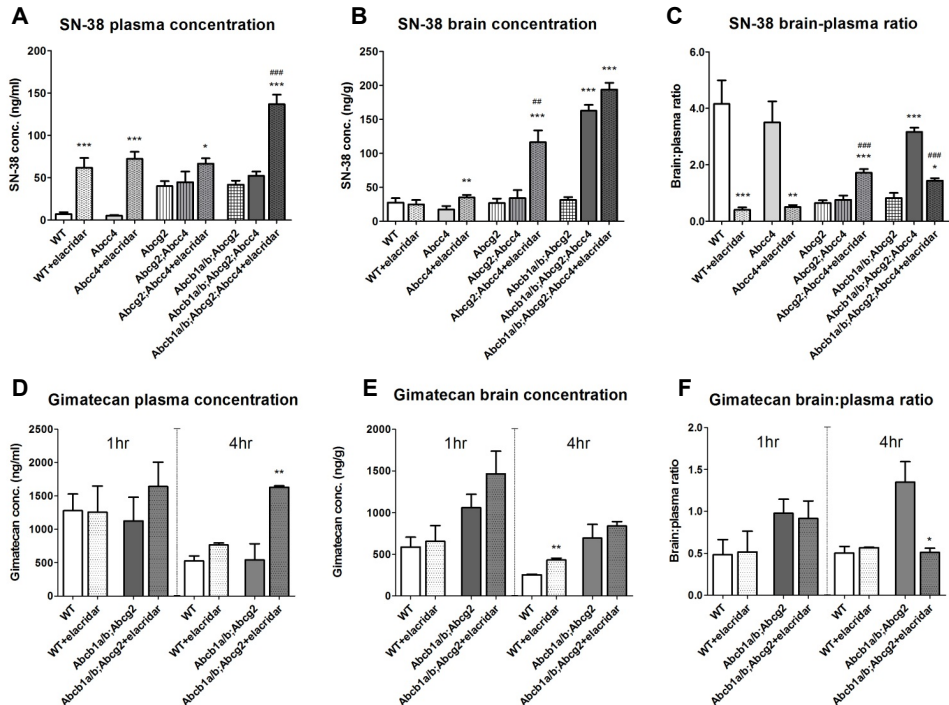


**Figure 4.** Effect of elacridar on the brain and plasma pharmacokinetics of SN-38 and gimatecan. Plasma concentrations (A), brain concentrations (B) and brain-to-plasma ratios (C) of SN-38 in WT, *Abcg2<sup>-/-</sup>*, *Abcc4<sup>-/-</sup>*, *Abcg2<sup>-/-</sup>*, *Abcg2;Abcc4<sup>-/-</sup>*, *Abcb1a/b;Abcg2<sup>-/-</sup>* and *Abcb1a/b;Abcg2;Abcc4<sup>-/-</sup>* mice 1 h after i.v. administration of 2 mg/kg SN-38 with or without co-administration of elacridar (2 h before the SN-38 administration, oral 100 mg/kg). Data are means  $\pm$  SD,  $n = 5, 5, 4, 5, 5, 4, 5, 5, 4$  and  $5$  for WT, WT+elacridar, *Abcc4<sup>-/-</sup>*, *Abcc4<sup>-/-</sup>*+elacridar, *Abcg2<sup>-/-</sup>*, *Abcg2;Abcc4<sup>-/-</sup>*, *Abcg2;Abcc4<sup>-/-</sup>*+elacridar, *Abcb1a/b;Abcg2<sup>-/-</sup>*, *Abcb1a/b;Abcg2;Abcc4<sup>-/-</sup>*, *Abcb1a/b;Abcg2;Abcc4<sup>-/-</sup>*+elacridar groups (A, B and C);  $n = 3, 3, 3, 4$  (1 hr) and  $3, 3, 3, 3$  (4 hr) for WT, WT+elacridar, *Abcb1a/b;Abcg2<sup>-/-</sup>* and *Abcb1a/b;Abcg2<sup>-/-</sup>*+elacridar groups (D, E and F) \*  $P < 0.05$ ; \*\*  $P < 0.01$ ; and \*\*\*  $P < 0.001$ , compared with the first column of the same sub-group. #  $P < 0.05$ ; ##  $P < 0.01$ ; and ###  $P < 0.001$ , compared with the second column of the same sub-group. Plasma concentrations (D), brain concentrations (E) and brain-to-plasma ratios (F) of gimatecan in WT, *Abcg2<sup>-/-</sup>* and *Abcb1a/b;Abcg2<sup>-/-</sup>* mice 1 and 4 h after i.v. administration of 2 mg/kg gimatecan with or without co-administration of elacridar (2 h before the SN-38 administration, oral 100 mg/kg). Data are means  $\pm$  SD,  $n = 3$ . \*  $P < 0.05$ ; \*\*  $P < 0.01$ , compared with the first column of the same sub-group.

the concentrations of SN-38 in brains of *Abcb1a/b;Abcg2<sup>-/-</sup>* and WT mice (Fig. 4B). In line with this result, administration of elacridar did not increase the SN-38 concentration in brain of WT mice as well. These results suggest that *Abcc4* alone is sufficient to maintain a similar brain level of SN-38 as achieved in WT mice. Similarly, the brain concentrations in *Abcg2<sup>-/-</sup>*, *Abcc4<sup>-/-</sup>* and *Abcg2;Abcc4<sup>-/-</sup>* mice were also not different compared with WT mice, suggesting that the presence of *Abcb1a/b* alone is also enough to reduce the brain concentration of SN-38 to the level of WT.

Because *Abcb1a/b;Abcc4<sup>-/-</sup>* mice do not exist, we could not evaluate the role of *Abcg2* by a similar genetic analysis. However, with the help of elacridar to inhibit *Abcb1a/b* and (partially) *Abcg2* we can make an estimation of the relative importance of *Abcg2*. The brains of *Abcg2;Abcc4<sup>-/-</sup>* mice that receive elacridar accumulate to about 70% of the level observed in *Abcb1a/b;Abcg2;Abcc4<sup>-/-</sup>* mice, indicating that *Abcb1a/b* is substantially, albeit not completely, inhibited by elacridar (Fig. 4). When we compare the brain penetration of SN-38 in *Abcc4<sup>-/-</sup>* mice vs. *Abcc4;Abcg2<sup>-/-</sup>* mice both receiving elacridar and assume that *Abcb1a/b* is inhibited to the same extent in both strains, the difference in brain penetration between these two strains will be mainly due to the activity of *Abcg2*.

We also investigated the effect of elacridar on gimatecan, as gimatecan appears to be a weaker substrate of *Abcc4*. Surprisingly, co-administration of elacridar did not increase the brain-to-plasma ratio of gimatecan. The brain concentration of gimatecan in mice receiving elacridar did not differ at 1 h and was 1.7-fold increased at 4 h ( $p < 0.05$ ) relative to mice not receiving elacridar. However, when corrected for the plasma concentration, the brain penetration of gimatecan was not significantly different in WT mice in the presence or absence of elacridar (Fig 4E and F), suggesting that the increased brain penetration at 4 h is mainly a reflection of the higher gimatecan plasma levels. Also, no significant additional effect of elacridar was found on brain concentration of gimatecan in *Abcb1a/b;Abcg2<sup>-/-</sup>* mice. Similar to SN-38, elacridar increased the plasma levels in *Abcb1a/b;Abcg2<sup>-/-</sup>* mice by a yet unidentified mechanism.

### **Impact of *Abcb1a/b*, *Abcg2* and *Abcc4* on brain distributions of camptothecins**

For all tested camptothecin analogs, their brain distributions (rendered as the percentage of total dose present in brain) were significantly increased when *Abcb1a/b*, *Abcg2* and *Abcc4* were simultaneously deleted. Loss of these transporters caused a profound

increase of percentage of total dose of topotecan in brain (22-fold and 84-fold at 1 and 4 h, respectively), slightly less profound for CPT11 (16 and 23-fold), and only a moderate increase for gimatecan (3.8 and 3.9-fold, Table 1), suggesting that the brain distributions of all camptothecins are affected by the drug efflux transporters but to differing extents depending on their unique structures.

We also compared the brain distributions of all camptothecins (Fig. 5). The brain distributions of the camptothecin analogs show a wide variation between WT and *Abcb1a/b;Abcg2;Abcc4<sup>-/-</sup>* mice. Strikingly, even in WT mice in which all these efflux transporters are present, up to 0.40% of total gimatecan dose was present in the brain at 1 h and 0.21% at 4 h. These values are more than 40-fold and 220-fold higher than those found for topotecan and for SN-38 at 1 h, respectively, and 160-fold and 140-fold at 4 h, respectively. In contrast, the percentage of CPT11 that was converted to SN-38 and detected in brains of *Abcb1a/b;Abcg2;Abcc4<sup>-/-</sup>* mice was exceptionally low (0.026% and 0.010% at 1 h and 4 h, respectively) and was even lower in WT mice (0.002% and 0.001% at 1 h and 4 h, respectively). At 1 h after drug administration, this was only 9% of the total SN-38 and CPT11 level in brain.

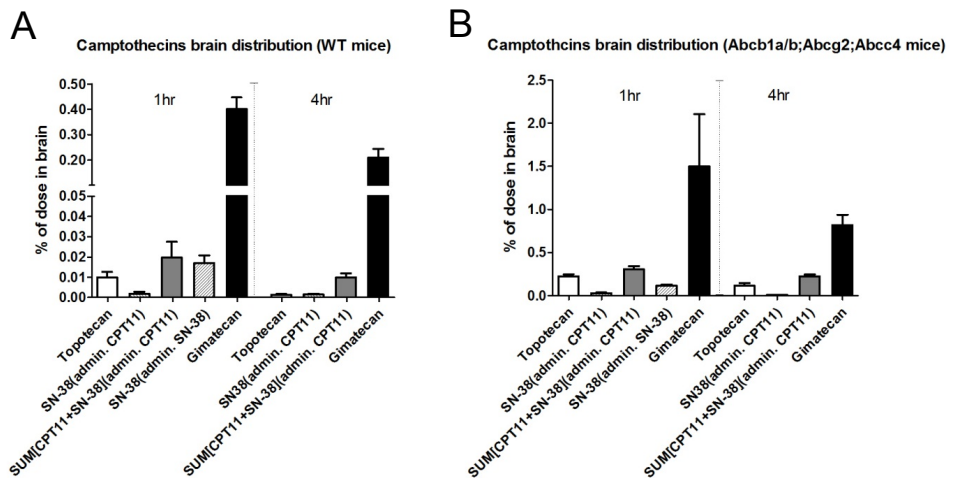


**Figure 5.** Brain distributions (represented by percentage of dose in brain) of topotecan, SN-38 after administration of CPT11 or SN-38, and gimatecan in WT and *Abcb1a/b;Abcg2;Abcc4<sup>-/-</sup>* mice 1 and 4 h after i.v. administration of 2 mg/kg topotecan, 5 mg/kg CPT11, 2 mg/kg SN-38 (only with data of 1 h) and 2 mg/kg gimatecan, respectively. Note break in Y axes of the % of dose in brain.

## DISCUSSION

The present study shows that Abcc4 is an important factor limiting the brain penetration of the camptothecin analogs topotecan, CPT11, SN-38 and gimatecan. However, due to the overlapping affinities of Abcb1a/b and Abcg2 (two other dominant drug efflux transporters at the BBB), the actual contribution of Abcc4 to the elimination of camptothecins in brain can only be assessed when the two other transporters are absent. Together, this co-operative drug-efflux system of functionally overlapping transporters constructs a robust protective barrier against molecules entering the brain. Unfortunately, however, this protection may also lead to inadequate exposure of brain malignancies when treated with camptothecin analogs or other triple-substrate drugs. Due to the presence of Abcc4, co-administration of the dual ABCB1 and ABCG2 inhibitor elacridar is unable to enhance the brain penetration of SN-38. In contrast to SN-38, the more lipophilic analog gimatecan has itself much more favorable brain distribution properties and, from that perspective, may be a more useful candidate for treatment of intracranial tumors than any of the other camptothecin analogs.

Abcc4 is well known for its ability to transport a range of endogenous molecules and drugs, including camptothecin analogs (18;20-22;24;31). Abcc4 was first found by RT-PCR in the microvessel enriched fraction of bovine brain (32). Its presence in the apical membranes of mouse brain microvessels and in the basolateral membranes of choroid plexus epithelium was shown by Leggas *et al.* (20) using Abcc4 knockout mice. The absence of Abcc4 in the choroid plexus in Abcc4<sup>-/-</sup> mice resulted in about 10-fold higher topotecan levels in the cerebrospinal fluid. Similarly, they observed a higher brain concentration of topotecan in Abcc4<sup>-/-</sup> mice vs. Abcc4 proficient WT mice (20). This latter result, however, could not be confirmed when we compared Abcc4<sup>-/-</sup> and WT mice, even when looking into multiple strain backgrounds, gender, dose levels and sampling times (8). The lack of an increased brain penetration of topotecan in the Abcc4<sup>-/-</sup> mice can now be explained by the presence of Abcb1a/b and Abcg2 at the BBB. The relative importance of each of the transporters at the BBB is demonstrated using our Abcb1a/b;Abcg2;Abcc4<sup>-/-</sup> mice as a reference. In most earlier studies comparing WT and ABC transporter knockout mice, the WT has been taken as reference (e.g. stating that absence results in an x-fold increase of compound y). This makes sense when looking at single knockouts, but becomes much more complex when analyzing compound

knockouts. Instead, by taking the mouse model in which all of the studied transporters have been deleted as reference, we can now add in one of each ABC transporter at a time. Thus, by comparing *Abcb1a/b;Abcg2;Abcc4<sup>-/-</sup>* mice vs. *Abcb1a/b;Abcg2<sup>-/-</sup>* mice, we can assess the role of *Abcc4* and it turns out that *Abcc4* alone is sufficient to reduce the SN38 levels (following SN38 administration) to those achieved in WT mice. It also follows that *Abcc4* is an important factor for topotecan, gimatecan and CPT11, albeit in a decreasing order (Table 1). A similar analysis was done for SN38 and *Abcb1a/b* by comparing *Abcb1a/b;Abcg2;Abcc4<sup>-/-</sup>* and *Abcg2;Abcc4<sup>-/-</sup>* mice, showing that *Abcb1a/b* alone is also sufficient to reduce the brain level of SN38 to that of WT mice.

Taking the most extensive combination knockout mouse as reference also provides a different view on what is frequently referred to as synergistic interaction between *Abcb1a/b* and *Abcg2* in restricting the brain penetration of substances (33;34). This claim of synergy is based on the finding that the absence of both *Abcb1a/b* and *Abcg2* together results in a much greater brain accumulation than the absence of only *Abcb1a/b* or *Abcg2*, as was first described for topotecan (8). However, synergy implicates that two or more factors (*e.g.* drug transporters) together are more efficient in their action (*i.e.* reducing brain entry) than each of these factors by themselves. Obviously, this is not the case, as the presence of *Abcb1a/b* or *Abcc4* alone was sufficient to reduce the brain concentration of SN38 to the level in WT mice. True synergy would have implied that the presence/action of a single transporter would have had only a very minor effect on the brain accumulation, whereas only the combined presence would result in a profound reduction in the brain accumulation. Therefore, it is more appropriate to use the term cooperative drug efflux or concerted efflux, rather than synergy, to describe the interaction of these ABC transporters at the BBB. Following the SN-38 example, this expression of multiple transporters with overlapping affinities for substrates probably not only limits the entry of camptothecins in brain, but also serves as a general defense mechanism protecting brain from potentially harmful substances. Inactivation or inhibition of one or even two transporters may challenge the transport capacity of the remaining transporter(s) but would not jeopardize the co-operative protection that is offered by the combination. This should be kept in mind when trying to modulate ABC-transporter mediated efflux at the BBB for pharmacological purposes. Moreover, it is also important to realize that besides the drug efflux transporters ABCC4, ABCB1 and ABCG2 examined

here, the relevance of other drug transporters (such as ABCC5 and ABBC10) still needs to be addressed.

Camptothecin analogs, in particular CPT11, are frequently applied in clinical trials in glioma patients (35-38). Our work here calls into question whether CPT11 would be the most appropriate candidate. CPT11 is a prodrug that needs conversion into the active metabolite SN38, which is 100-fold to 1000-fold more potent. However, the brain accumulation of SN38 is the lowest of this panel of camptothecin analogs. The amount of SN-38 found in the brain was less than 0.002% of the total dose (after administration of CPT11) and this is only about 9% of the SUM[CPT11+SN-38] in brain. Importantly, mice express the carboxyl-esterases that are responsible for the CPT11 to SN38 conversion more abundantly than humans (39;40). As a result, humans have even lower plasma levels of SN38, which may further diminish its brain accumulation.

On the other hand, gimatecan has a much more favorable brain penetration. A key difference between gimatecan and topotecan and CPT11 is the substitution of a lipophilic chain in position 7 of the planar aromatic five-ring structure, making this compound more lipophilic and therefore probably more cell membrane permeable (18;19). Gimatecan has demonstrated significant efficacy in a number of experimental tumor models, including orthotopic brain tumors (41). Moreover, it was shown that the *in vitro* cytotoxicity to gimatecan was not affected by the over-expression of ABCB1 or ABCG2, although transwell experiments showed that this compound is a substrate of Abcg2 (17;18). The negligible transport by ABCB1 in the *in vitro* transwell assays is not in line with the significant effects of Abcb1a/b on the brain penetration. This may be due to species differences in substrate affinity; or, the ABC transporter knockout model may be a more stringent test than the *in vitro* assays to establish whether a compound is an ABCB1/Abcb1a/b substrate. Taking Abcb1a/b;Abcg2;Abcc4<sup>-/-</sup> as reference (Fig. 3), Abcb1a/b alone appears to be capable of reducing the brain levels of gimatecan almost to those found in WT mice, whereas Abcg2 and Abcc4 together were less efficient. Importantly, however, together these three ABC transporters cooperatively reduce the brain penetration of gimatecan by about 4-fold (Table 1).

Elacridar is an inhibitor of ABCB1 and ABCG2 and has been successfully used to increase the brain penetration of many substrate drugs, *e.g.* gefitinib and sunitinib (42;43), and

also to some extent topotecan (8). Unfortunately, co-administration of elacridar to WT mice did not improve the brain penetration of SN-38 or gimatecan. The lack of effect on SN-38 brain penetration can be explained by the fact that Abcc4 alone was already sufficient to achieve low brain levels similar to those in WT mice, and that elacridar does not inhibit Abcc4. Due to the concerted action by these three ABC transporters, it will be a challenging task to increase the brain penetration of SN-38 by modulation of ABC transporter activity at the BBB.

On the other hand, the BBB penetration of gimatecan was much less affected by the ABC transporters, although also in this case elacridar did not result in any improvement. A possible explanation could be that gimatecan is in fact a good substrate of Abcb1a/b and/or Abcg2, but the high cell membrane permeability of the gimatecan masks this property thus making the partial inhibition of Abcb1a/b and Abcg2 by elacridar unnoticeable.

In conclusion, using a collection of compound ABC transporter knockout mice we have shown that the cooperative action by Abcc4 with Abcb1a/b and Abcg2 at the BBB restricts the brain penetration of triple-substrate drugs. This work underscores the importance of preclinical models, as such information can not be obtained from clinical studies in patients. Importantly, patients may benefit from these animal models as they may assist in selecting the most appropriate BBB-penetrable candidates of drugs that have to act inside the brain for clinical trial.

## Reference List

- (1) de Boer AG, Gaillard PJ. Drug targeting to the brain. *Annu Rev Pharmacol Toxicol* 2007;47:323-55.
- (2) Agarwal S, Sane R, Oberoi R, Ohlfest JR, Elmquist WF. Delivery of molecularly targeted therapy to malignant glioma, a disease of the whole brain. *Expert Rev Mol Med* 2011;13:e17.
- (3) Muldoon LL, Soussain C, Jahnke K, Johanson C, Siegal T, Smith QR et al. Chemotherapy delivery issues in central nervous system malignancy: a reality check. *J Clin Oncol* 2007;25:2295-305.
- (4) de Vries NA, Beijnen JH, Boogerd W, van Tellingen O. Blood-brain barrier and chemotherapeutic treatment of brain tumors. *Expert Rev Neurother* 2006;6:1199-209.
- (5) Urquhart BL, Kim RB. Blood-brain barrier transporters and response to CNS-active drugs. *Eur J Clin Pharmacol* 2009;65:1063-70.
- (6) Deeken JF, Loscher W. The blood-brain barrier and cancer: transporters, treatment, and trojan horses. *Clin Cancer Res* 2007;13:1663-74.
- (7) Schinkel AH, Smit JJ, van Tellingen O, Beijnen JH, Wagenaar E, van Deemter L et al. Disruption of the mouse *mdr1a* P-glycoprotein gene leads to a deficiency in the blood-brain barrier and to increased sensitivity to drugs. *Cell* 1994;77:491-502.
- (8) de Vries NA, Zhao J, Kroon E, Buckle T, Beijnen JH, van Tellingen O. P-glycoprotein and breast cancer resistance protein: two dominant transporters working together in limiting the brain penetration of topotecan. *Clin Cancer Res* 2007;13:6440-9.
- (9) Devore R, III, Johnson D, Crawford J, Dimery I, Eckardt J, Eckhardt SG. Irinotecan plus cisplatin in patients with advanced non-small-cell lung cancer. *Oncology (Williston Park)* 1998;12:79-83.
- (10) Gershenson DM. Irinotecan in epithelial ovarian cancer. *Oncology (Williston Park)* 2002;16:29-31.
- (11) Hurwitz H, Fehrenbacher L, Novotny W, Cartwright T, Hainsworth J, Heim W et al. Bevacizumab plus irinotecan, fluorouracil, and leucovorin for metastatic colorectal cancer. *N Engl J Med* 2004;350:2335-42.
- (12) Chu XY, Suzuki H, Ueda K, Kato Y, Akiyama S, Sugiyama Y. Active efflux of CPT-11 and its metabolites in human KB-derived cell lines. *J Pharmacol Exp Ther* 1999;288:735-41.
- (13) Nakatomi K, Yoshikawa M, Oka M, Ikegami Y, Hayasaka S, Sano K et al. Transport of 7-ethyl-10-hydroxycamptothecin (SN-38) by breast cancer resistance protein ABCG2 in human lung cancer cells. *Biochem Biophys Res Commun* 2001;288:827-32.
- (14) Smith NF, Figg WD, Sparreboom A. Pharmacogenetics of irinotecan metabolism and transport: an update. *Toxicol In Vitro* 2006;20:163-75.
- (15) Maliepaard M, van Gastelen MA, de Jong LA, Pluim D, van Waardenburg RC, Ruevekamp-Helmers MC et al. Overexpression of the BCRP/MXR/ABCP gene in a topotecan-selected ovarian tumor cell line. *Cancer Res* 1999;59:4559-63.



- (16) Hendricks CB, Rowinsky EK, Grochow LB, Donehower RC, Kaufmann SH. Effect of P-glycoprotein expression on the accumulation and cytotoxicity of topotecan (SK&F 104864), a new camptothecin analogue. *Cancer Res* 1992;52:2268-78.
- (17) Marchetti S, Oostendorp RL, Pluim D, van Eijndhoven M, van Tellingen O, Schinkel AH et al. In vitro transport of gimatecan (7-t-butoxyiminomethylcamptothecin) by breast cancer resistance protein, P-glycoprotein, and multidrug resistance protein 2. *Mol Cancer Ther* 2007;6:3307-13.
- (18) Gounder MK, Nazar AS, Saleem A, Pungaliya P, Kulkarni D, Versace R et al. Effects of drug efflux proteins and topoisomerase I mutations on the camptothecin analogue gimatecan. *Invest New Drugs* 2008;26:205-13.
- (19) Perego P, De Cesare M, De Isabella P, Carenini N, Beggiolin G, Pezzoni G et al. A novel 7-modified camptothecin analog overcomes breast cancer resistance protein-associated resistance in a mitoxantrone-selected colon carcinoma cell line. *Cancer Res* 2001;61:6034-7.
- (20) Leggas M, Adachi M, Scheffer GL, Sun D, Wielinga P, Du G et al. Mrp4 confers resistance to topotecan and protects the brain from chemotherapy. *Mol Cell Biol* 2004;24:7612-21.
- (21) Borst P, de Wolf C, van de Wetering K. Multidrug resistance-associated proteins 3, 4, and 5. *Pflugers Arch* 2007;453:661-73.
- (22) Tian Q, Zhang J, Chan SY, Tan TM, Duan W, Huang M et al. Topotecan is a substrate for multidrug resistance associated protein 4. *Curr Drug Metab* 2006;7:105-18.
- (23) Tian Q, Zhang J, Tan TM, Chan E, Duan W, Chan SY et al. Human multidrug resistance associated protein 4 confers resistance to camptothecins. *Pharm Res* 2005;22:1837-53.
- (24) Russel FG, Koenderink JB, Masereeuw R. Multidrug resistance protein 4 (MRP4/ABCC4): a versatile efflux transporter for drugs and signalling molecules. *Trends Pharmacol Sci* 2008;29:200-7.
- (25) Ose A, Ito M, Kusuhara H, Yamatsugu K, Kanai M, Shibasaki M et al. Limited brain distribution of [3R,4R,5S]-4-acetamido-5-amino-3-(1-ethylpropoxy)-1-cyclohexene-1-carboxylate phosphate (Ro 64-0802), a pharmacologically active form of oseltamivir, by active efflux across the blood-brain barrier mediated by organic anion transporter 3 (Oat3/Slc22a8) and multidrug resistance-associated protein 4 (Mrp4/Abcc4). *Drug Metab Dispos* 2009;37:315-21.
- (26) Morimoto K, Nakakariya M, Shirasaka Y, Kakinuma C, Fujita T, Tamai I et al. Oseltamivir (Tamiflu) efflux transport at the blood-brain barrier via P-glycoprotein. *Drug Metab Dispos* 2008;36:6-9.
- (27) Dai H, Marbach P, Lemaire M, Hayes M, Elmquist WF. Distribution of STI-571 to the brain is limited by P-glycoprotein-mediated efflux. *J Pharmacol Exp Ther* 2003;304:1085-92.
- (28) Schoemaker NE, Rosing H, Jansen S, Schellens JH, Beijnen JH. High-performance liquid chromatographic analysis of the anticancer drug irinotecan (CPT-11) and its active metabolite SN-38 in human plasma. *Ther Drug Monit* 2003;25:120-4.
- (29) de Vries NA, Ouwehand M, Buckle T, Beijnen JH, van Tellingen O. Determination of topotecan in human and mouse plasma and in mouse tissue homogenates by reversed-phase high-performance liquid chromatography. *Biomed Chromatogr* 2007;21:1191-200.

- (30) Guemei AA, Cottrell J, Band R, Hehman H, Prudhomme M, Pavlov MV et al. Human plasma carboxylesterase and butyrylcholinesterase enzyme activity: correlations with SN-38 pharmacokinetics during a prolonged infusion of irinotecan. *Cancer Chemother Pharmacol* 2001;47:283-90.
- (31) Tian Q, Zhang J, Tan TM, Chan E, Duan W, Chan SY et al. Human multidrug resistance associated protein 4 confers resistance to camptothecins. *Pharm Res* 2005;22:1837-53.
- (32) Zhang Y, Han H, Elmquist WF, Miller DW. Expression of various multidrug resistance-associated protein (MRP) homologues in brain microvessel endothelial cells [In Process Citation]. *Brain Res* 2000;876:148-53.
- (33) Kodaira H, Kusuhara H, Ushiki J, Fuse E, Sugiyama Y. Kinetic Analysis of the Cooperation of P-Glycoprotein (P-gp/Abcb1) and Breast Cancer Resistance Protein (Bcrp/Abcg2) in Limiting the Brain and Testis Penetration of Erlotinib, Flavopiridol, and Mitoxantrone. *J Pharmacol Exp Ther* 2010;333:788-96.
- (34) Polli JW, Olson KL, Chism JP, John-Williams LS, Yeager RL, Woodard SM et al. An unexpected synergist role of P-glycoprotein and breast cancer resistance protein on the central nervous system penetration of the tyrosine kinase inhibitor lapatinib (N-{3-chloro-4-[[3-fluorobenzyl]oxy]phenyl}-6-[5-{{[2-(methylsulfonyl)ethyl]amino }methyl}-2-furyl]-4-quinazolinamine; GW572016). *Drug Metab Dispos* 2009;37:439-42.
- (35) Reardon DA, Friedman HS, Powell JB, Jr., Gilbert M, Yung WK. Irinotecan: promising activity in the treatment of malignant glioma. *Oncology (Williston Park)* 2003;17:9-14.
- (36) Reardon DA, Quinn JA, Rich JN, Gururangan S, Vredenburgh J, Sampson JH et al. Phase 2 trial of BCNU plus irinotecan in adults with malignant glioma. *Neuro Oncol* 2004;6:134-44.
- (37) Reardon DA, Quinn JA, Rich JN, Desjardins A, Vredenburgh J, Gururangan S et al. Phase I trial of irinotecan plus temozolomide in adults with recurrent malignant glioma. *Cancer* 2005;104:1478-86.
- (38) Reardon DA, Quinn JA, Vredenburgh J, Rich JN, Gururangan S, Badruddoja M et al. Phase II trial of irinotecan plus celecoxib in adults with recurrent malignant glioma. *Cancer* 2005;103:329-38.
- (39) Rivory LP, Haaz MC, Canal P, Lokiec F, Armand JP, Robert J. Pharmacokinetic interrelationships of irinotecan (CPT-11) and its three major plasma metabolites in patients enrolled in phase I/II trials. *Clin Cancer Res* 1997;3:1261-6.
- (40) Zamboni WC, Houghton PJ, Thompson J, Cheshire PJ, Hanna SK, Richmond LB et al. Altered irinotecan and SN-38 disposition after intravenous and oral administration of irinotecan in mice bearing human neuroblastoma xenografts. *Clin Cancer Res* 1998;4:455-62.
- (41) De Cesare M, Pratesi G, Veneroni S, Bergottini R, Zunino F. Efficacy of the novel camptothecin gimatecan against orthotopic and metastatic human tumor xenograft models. *Clin Cancer Res* 2004;10:7357-64.
- (42) Agarwal S, Sane R, Gallardo JL, Ohlfest JR, Elmquist WF. Distribution of gefitinib to the brain is limited by P-glycoprotein (ABCB1) and breast cancer resistance protein (ABCG2)-mediated active efflux. *J Pharmacol Exp Ther* 2010;334:147-55.
- (43) Tang SC, Lagas JS, Lankheet NA, Poller B, Hillebrand MJ, Rosing H et al. Brain accumulation of sunitinib is restricted by P-glycoprotein (ABCB1) and breast cancer resistance protein

(ABCG2) and can be enhanced by oral elacridar and sunitinib coadministration. *Int J Cancer* 2012;130:223-33.



## Chapter 4.2

Sildenafil is not a useful modulator of ABCB1 and ABCG2 mediated drug resistance *in vivo*

Fan Lin, Lisette Hoogendijk, Levi Buil, Jos H. Beijnen, Olaf van Tellingen

European Journal of Cancer 2013. In press

## ABSTRACT

**Aim:** Recently, sildenafil was reported to be an inhibitor of P-glycoprotein (P-gp / ABCB1) and breast cancer resistance protein (BCRP / ABCG2) *in vitro*. We have now investigated the *in vivo* potency of sildenafil.

**Methods:** By using wildtype and Abcb1;Abcg2 knockout mice we have investigated the effect of sildenafil on the brain penetration of two substrate drugs (docetaxel and topotecan). Next we have investigated if sildenafil was able to improve the efficacy of doxorubicin against P-glycoprotein expressing CT26 colon cancer cells in syngeneic Balb/c mice.

**Results:** Sildenafil administered orally at a dose of 50 mg/kg did not improve the brain penetration of docetaxel and topotecan, although the plasma level of sildenafil was already much higher than can be achieved in humans. On the other hand, sildenafil increased the plasma levels of the cytotoxic drugs, but not by inhibition of Abcb1 or Abcg2, since this effect was also seen in Abcb1;Abcg2 knockout mice. The brain penetration of sildenafil was more than 20-fold higher in Abcb1;Abcg2 mice vs. wild-type mice, indicating that sildenafil is a good substrate of the two transporters. Sildenafil was also not able to improve the efficacy of doxorubicin against subcutaneous CT26 tumors. The doxorubicin level in tumor tissue did increase, but so did the concentration of doxorubicin in plasma and heart.

**Conclusion:** These results demonstrate that the potency and specificity of sildenafil as an inhibitor of ABCB1 and ABCG2 is not sufficient to warrant further clinical testing of this agent in combination with anticancer drugs.

**Keywords:** Multidrug resistance; P-glycoprotein; BCRP protein; brain penetration; sildenafil; docetaxel; topotecan; doxorubicin.

## INTRODUCTION

Sildenafil (Viagra) is an inhibitor of cyclic guanosine monophosphate (cGMP)-specific phosphodiesterase type 5 (PDE5) and used to treat male erectile dysfunction. For more or less similar purposes, it is also commonly used as “under-the-counter” drug that is conveniently available via the internet, making it probably one of the most widely but secretly used drugs.

Sildenafil has also been reported as a candidate drug for treatment of cancer patients. Serafini et al (1) reported that sildenafil boosts the endogenous antitumor immunity in a syngeneic colon tumor model and this finding was recently confirmed in a transgenic mouse model for melanoma (2). Black et al (3) reported that sildenafil potentiated the efficacy of doxorubicin in rats bearing 9L gliosarcoma, which was presumed to be due to an opening of the blood brain tumor barrier by a selective increase in tumor cGMP levels. Das et al (4) reported that sildenafil increased the efficacy of doxorubicin in prostate cancer and at the same time reduced cardiac dysfunction. Recently in two papers, Shi et al (5,6) reported that sildenafil inhibits ABCB1 (P-glycoprotein/P-gp) and ABCG2 (Breast Cancer Resistance Protein /BCRP) and advocated its potential usefulness to enhance the efficacy of substrate anticancer drugs. Indeed, ABCB1 and ABCG2 are two important members of the ABC-transporter family, involved in the disposition of a wide variety of drugs, including many anticancer agents (7). These ATP-binding cassette transporters (ABC transporters) can be expressed in tumor cells causing multidrug resistance and they are expressed in many barrier tissues restricting the penetration of drugs into pharmacological sanctuary sites, such as the brain. Consequently, these authors concluded that sildenafil might be useful to enhance the distribution and potentially the efficacy of anticancer drugs by combining this clinically approved drug with a known safety profile. It is certainly true that safe and potent inhibitors of these drug transporters may be valuable tools in the treatment of cancer patients. Besides the more classical use to combat multidrug resistant tumors, our lab is also very interested in such inhibitors to improve drug delivery to the brain with the aim of treating brain cancer. Consequently, we were intrigued by the reports on sildenafil. However, a major concern was that the conclusions on the potential of sildenafil for this purpose were solely grounded on *in vitro* models. We therefore performed a set of experiments to assess the potency and usefulness of sildenafil using *in vivo* models.

## MATERIALS AND METHODS

### *Compounds*

Sildenafil (pure compound) was purchased from Sigma Aldrich. We used sildenafil 20 mg (Revatio) tablets (Pfizer, New York, NY, USA) for the *in vivo* experiments. Docetaxel (pure compound was from Sequoia Research Products (Pangbourn, UK). We used the clinical formulation of docetaxel (Hospira, Benelux, Brussels, BE) for *in vivo* studies. Topotecan (pure compound was kindly provided by GlaxoSmithKline (Middlesex, UK). Zosuquidar (was a gift from Eli Lilly (Indianapolis, IN, USA) and Palomid 529 from Paloma Pharmaceuticals (Jamaica Plain, MA, USA).

### *Tumor cell line*

The CT26p cell line was kindly provided by Dr IJ Fidler (MD Anderson, Houston, TX, USA). Stocks stored in liquid nitrogen were thawed and cultured in Modified Eagles Medium (Life Technologies, Inc., Breda, The Netherlands), supplemented with L-glutamine, sodium-pyruvate, penicillin, streptomycin, non-essential amino acids and 10% fetal calf serum (all from Life Technologies, Breda, The Netherlands) and maintained in 5% CO<sub>2</sub> in humidified air at 37°C. *In vitro* toxicity of doxorubicin in CT26 cells was analyzed by MTT assay in 96-well plates seeded with 300 cells per well being incubated with drugs for 72 h. IC50 curves were plotted using Graphpad Prism (v5.0).

### *Animals*

Animals used for pharmacokinetic studies were wild-type (WT) and Abcb1a/b;Abcg2 knockout (TKO) mice backcrossed to FVB background between 10 and 14 weeks of age. Animals used for efficacy experiments using the CT26 cell line were Balb/c mice. All animals were housed and handled according to institutional guidelines complying with Dutch legislation. Animals were kept in a temperature-controlled environment with a 12-hours light/12-hours dark cycle and received a standard diet (AM-II; Hope Farms, Woerden, The Netherlands) and acidified water *ad lib*. All experiments involving animals were approved by the local animal ethics committee of our institute.

### *Pharmacokinetic studies*

Sildenafil tablets (20 mg) were powdered using a mortar and then dissolved in acidified water: ethanol (75:25; v/v). The final concentration (5 mg/ml) was checked by HPLC (see



below). To determine the exposure to sildenafil after oral administration of 50 mg/kg, 6 mice received sildenafil p.o. and serial blood samples were collected from the tails. To determine the brain penetration of docetaxel and topotecan, WT and TKO mice received 50 mg/kg of sildenafil p.o., followed 30 min later by an i.v. dose of docetaxel (33 mg/kg) or topotecan (2 mg/kg). Each cohort consisted of at least 5 mice per time point. After 1 hour animals were anaesthetized with isoflurane, their blood was collected by cardiac puncture and kept on ice until centrifugation (10 min, 4000g, 4°C). The supernatant plasma fractions were stored at -20°C until HPLC analysis. Immediately after cardiac puncture, the mice were killed by cervical dislocation and brain, liver, kidney, lung and heart were dissected. Tissues were collected on dry ice. They were stored at -20°C until homogenization and subsequent HPLC analysis. To determine the doxorubicin concentration in plasma, tumors and other tissues, tumor bearing Balb/c mice were used at 4, 24 and 48 h after doxorubicin administration. Doxorubicin (5 mg/kg) was given at t=0 h. Sildenafil (10 or 50 mg/kg) was given at -15 min, 3h and 6h.

#### *Drug analyses*

Topotecan was measured by HPLC-fluorescence detection using an established method (8). Doxorubicin was also measured by HPLC-fluorescence detection {van Asperen J., 1998 9 /id}. Docetaxel in brain by HPLC-MS/MS (10) and in plasma and other tissues by HPLC-ultraviolet detection (11). Sildenafil was measured by HPLC (12,13) with some modifications. In brief, samples (50 µl) were mixed with Palomid 529 (5 µg/ml; Internal Standard) and 150 µl of 0.01 M NaOH. After adding 1 ml of diethyl ether (Sigma Aldrich), the vials were shaken for 5 min and centrifuged (5 min 10,000 g). The lower aqueous layer was frozen on dry-ice and the organic phase transferred to a clean tube and dried by vacuum. The residue was dissolved in 50 µl acetonitrile: water (30:70; v/v) and 20 µl was subjected to HPLC separation on a Symmetry C18 3.5 µm column (2.1 x 150 mm) Waters, Milford, MA, USA. The mobile phase A was 0.05 M phosphate buffer pH 6.0 containing 10 mM tetrabutyl ammonium bromide (Merck, Darmstadt, Germany) and mobile phase B was a mixture of acetonitrile : water (80:20; v/v). The gradient conditions were 0-7 min: fixed at 50%B; 7-12 min: linear gradient 50-80%B; 12-17 min: fixed at 80%B; 17-17.5 min: back to 50%B and equilibration for 12 min. Effluent was monitored by UV detection at 300 nm.

*Antitumor efficacy*

Cells for *in vivo* injection were trypsinized, washed twice with saline and 25,000 cells in 50  $\mu$ l were injected bilateral into the flanks of syngeneic Balb/c mice. Tumors size was measured biweekly by calipers in two directions and the volume was calculated by the formula:  $0.5 \times A \times B^2$ , where A is the long and B the short diameter. Animals were stratified when tumors had reached a mean size of 200  $\text{mm}^3$ . Doxorubicin (5 mg/kg) was given at t=0 h. Sildenafil (10 or 50 mg/kg) was given at -15 min, 3h and 6h.

## RESULTS

First, we established the potency of sildenafil to inhibit Abcb1 and/or Abcg2 at the blood-brain barrier using ABC-transporter knockout mice as reference. Wild-type (WT) and Abcb1a/b;Abcg2 deficient (TKO) mice received 50 mg/kg of sildenafil, 30 min later followed by i.v. topotecan or docetaxel. Whereas the brains of TKO mice accumulated significantly more of each drug (Fig. 1 A), conforming to the previous findings (8,11), the effect of sildenafil on the brain penetration of both drugs was insignificant. Sildenafil, profoundly increased the plasma level of both agents, but mainly by interactions unrelated to Abcb1/Abcg2, since this effect was also observed in TKO mice (Fig. 1 B). This lack of potency to enhance the brain penetration was not due to insufficient exposure to sildenafil. Following oral administration of 50 mg/kg, the plasma level of sildenafil peaked at 7  $\mu\text{g/ml}$  and remained above 2  $\mu\text{g/ml}$  for 3 hours (Fig. 1 C). Such concentrations are considerably higher than previously reported in humans receiving safe doses (13). The brain penetration of sildenafil itself was more than 20-fold higher in TKO vs. WT mice demonstrating that sildenafil is an excellent Abcb1 and/or Abcg2 substrate (Fig. 1 D).

In a second set, we established the potency of sildenafil (10 or 50 mg/kg) to enhance the antitumor efficacy of doxorubicin (5 mg/kg) and tumor accumulation using s.c. grafted CT26 tumors in syngeneic Balb/c mice. This non-drug selected cell line endogenously expresses a moderate level of P-gp (14) and adding the established P-gp inhibitor zosuquidar at a concentration of 5  $\mu\text{M}$  reduces the *in vitro* IC50 of doxorubicin by 7-fold (Fig. 2A). Likewise a concentration of 5 to 25  $\mu\text{M}$  of sildenafil significantly reduced the IC50 values to a similar level as zosuquidar. When doxorubicin was administered to mice alone or in combination with 10 and 50 mg/kg of sildenafil, the  $\text{AUC}_{0-48\text{h}}$  of doxorubicin in tumors increased significantly from  $40.3 \pm 2.2$  to  $50.3 \pm 3.3$  and  $62.0 \pm 4.0$   $\text{nM}\cdot\text{h}$ , in a dose dependent fashion (Fig 2 B). However, this increased drug accumulation was not translated into an improved response on tumor growth rate (Fig 2 C). Moreover, concomitant administration of 50 mg/kg of sildenafil also significantly increased the  $\text{AUC}_{0-48\text{h}}$  of doxorubicin in heart from  $148.4 \pm 7.4$  to  $200.8 \pm 7.9$   $\text{nM}\cdot\text{h}$  and in plasma from  $1010 \pm 50$  to  $1210 \pm 50$   $\text{nM}\cdot\text{h}$ .

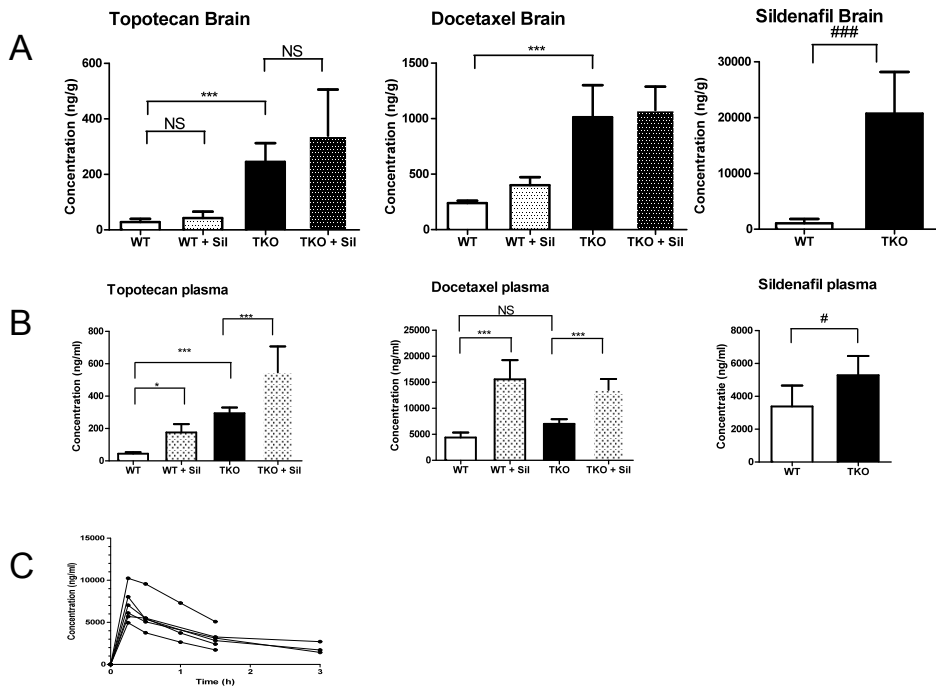


**Figure 1. Brain penetration of topotecan, docetaxel and sildenafil**

Wild-type (WT) and *Abcb1;Abcg2* knockout mice (TKO) received 50 mg/kg sildenafil (Sil) p.o., followed 30 min later by 2 mg/kg topotecan iv or docetaxel iv administration. Blood and tissues were collected 1 h after administration of the cytotoxic agent. Sildenafil did not increase the brain penetration of topotecan (A: left panels) or docetaxel (A: right panels), but did increase the plasma concentrations of both (B). The brain penetration of sildenafil was significantly increased in TKO mice. The plasma concentration of sildenafil was also significantly increased. The plasma concentration – time curves in 6 individual WT animals receiving 50 mg/kg of sildenafil is depicted in the lower right panel (C). Statistical analysis by Bonferroni (\*) or T-test (#) using Graphpad Prism: \*, # =  $P < 0.05$ ; \*\*\*, ### =  $P < 0.001$ ; NS = not significant.

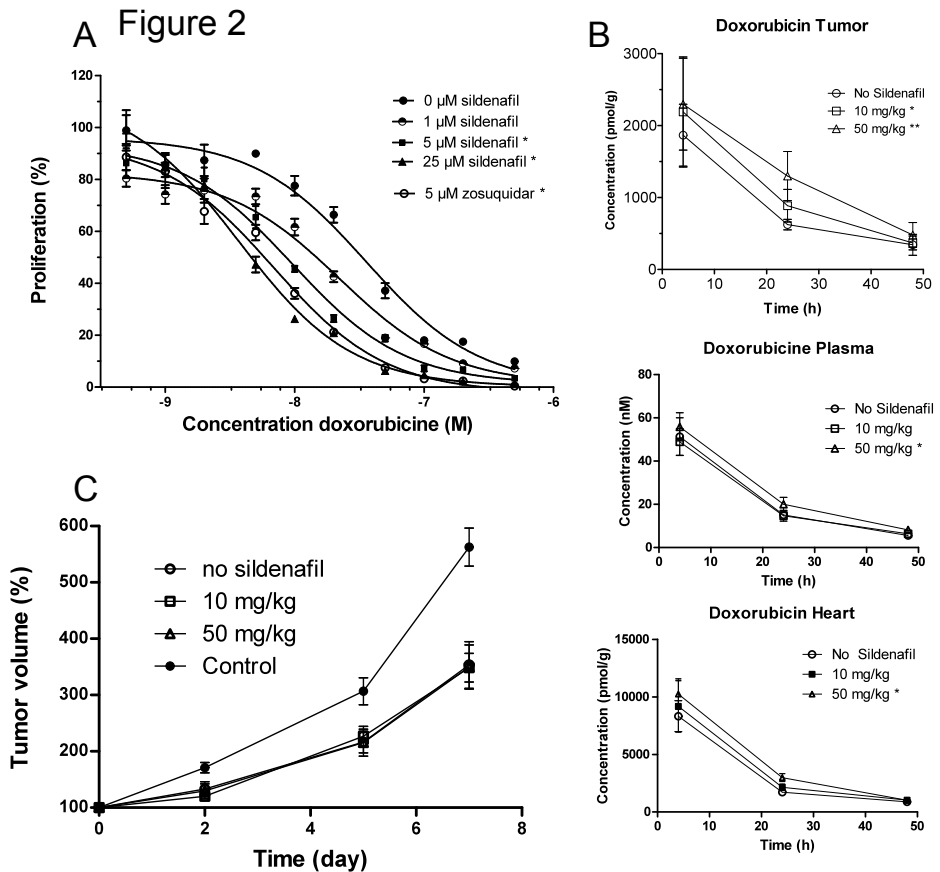


**Figure 2. Potency of sildenafil to boost the efficacy of doxorubicin against CT26 cells**

Sildenafil at 5 and 25  $\mu\text{M}$  significantly potentiated the *in vitro* toxicity of doxorubicin by the same extent as 5  $\mu\text{M}$  of zosuquidar (A: upper left panel). IC<sub>50</sub> curves in Graphpad Prism: \* $P < 0.05$  relative to doxorubicin only, \*\* $P < 0.01$ . Sildenafil 10 and 50 mg/kg p.o. increased the i.v. doxorubicin AUC in a dose dependent fashion in CT26 tumors and heart tissue (B: right panels; \* $P < 0.05$ , \*\* $P < 0.01$  relative to no sildenafil). Doxorubicin (5 mg/kg) significantly reduced the tumor growth relative to controls receiving saline. Unfortunately, the efficacy of doxorubicine was not improved by sildenafil (C: lower left panel).

## DISCUSSION

This study shows that sildenafil is unfortunately neither potent nor selective enough to be a therapeutically useful inhibitor of ABC-transporters. ABCB1 and ABCG2 are important factors in drug disposition and in multidrug resistance. ABCB1 is a membrane-associated efflux transporter with a broad substrate affinity and was first discovered in 1976 by Juliano and Ling (15) by its ability to confer multidrug resistance to cultured tumor cells. The finding that a membrane-associated efflux transporter was responsible for causing multidrug resistance by reducing intracellular drug levels created the hope that multidrug resistance could be managed by using inhibitors of this efflux pump and was at the basis of a new and rapidly expanding area of research (7). Initially, of-the-shelf agents such as verapamil and cyclosporin were tested in clinical studies, which failed mainly because of their drug-related side effects. Importantly, however, many of the major pharmaceutical companies initiated drug discovery programs aimed to find potent and selective ABCB1 inhibitors, ultimately resulting in the generation of zosuquidar (16), elacridar (17) and tariquidar (18). In the meantime, a range of other ABC transporters such as ABCC1 (MRP1) and ABCG2 (BCRP) were discovered, making clear that more than just one drug efflux pump might be at the basis of clinical multidrug resistance (7).

Sildenafil was reported to be an inhibitor of ABCB1, ABCG2 (5,6), ABCC4 (19) and very recently also ABCC10 (20). This presumed combined inhibitory activity of multiple relevant ABC transporters drew our attention and we decided to investigate the *in vivo* potency of this agent, as this was not included in the previous reports. For this purpose we used a set of established *in vivo* tests, but unfortunately we were unable to demonstrate *in vivo* potency of sildenafil in any of these models. First, by using TKO mice as reference, we were unable to demonstrate an effect of sildenafil on the BBB penetration of the Abcb1 substrate docetaxel or the dual Abcb1/Abcg2 substrate topotecan, whereas our previous studies using the dual Abcb1/Abcg2 inhibitor elacridar did result in a significant effect on the brain penetration of these agents (8,11). Secondly, we used the CT26 colon carcinoma model in syngeneic Balb/c mice to investigate if sildenafil was able to potentiate the efficacy of the Abcb1 substrate doxorubicin, but again without success. Notably, this is the same model that Serafini et al (1) have used to show that sildenafil is active as single agent, due to its beneficial effect on the host antitumor immunity. Because we focused on the inhibitory effects of sildenafil on ABC

transporters in this study, we did not include a sildenafil-only arm in our study design. However, it may be that these indirect immune-mediated antitumor effects of sildenafil are annulled by the immune suppressive effects of the chemotherapeutic agent. Moreover, sildenafil was reported to boost the effects of doxorubicin against prostate cancer (4) and, concurrently, reduce the cardiac toxicity of doxorubicin. Apparently, the boosting of doxorubicin did not work in this CT26 colon carcinoma model. Moreover, the pharmacokinetic interaction and enhanced accumulation of doxorubicin in the heart calls for caution when considering this combination in the clinic.

These negative findings with sildenafil in our *in vivo* study panel are disappointing. Apparently, on the one hand, the exposure to sildenafil is not sufficient to cause a meaningful interaction with these drug transporters *in vivo*. This may be due to a high protein binding of this drug. On the other hand, however, the systemic exposure that was achieved in our models was already much higher than clinically achievable. Consequently, further dose increments are not a realistic option.

Because sildenafil is a relatively easy to purchase, self-medication by cancer patients who have read about the potential beneficial effects of sildenafil on the internet (<http://www.foxnews.com/health/2011/11/28/cancer-fighting-cells-get-boost-from-viagra/>), without consulting or informing their physician is not inconceivable. This, however, may pose a serious risk, considering the observed pharmacokinetic interaction with the two anticancer agents that we have tested.

In conclusion, claims on the potency of ABC transporter inhibitors require *in vivo* validation. Our experiments demonstrate that the potency and specificity of sildenafil as an inhibitor of ABCB1 and ABCG2 is not sufficient to warrant further clinical testing of this agent in combination with anticancer drugs.

**Acknowledgements:**

We would like to thank J. Hendriks and B. Thijssen for performing the LC-MS assay for docetaxel.

## Reference List

1. Serafini P, Meckel K, Kelso M, Noonan K, Califano J, Koch W, Dolcetti L, Bronte V, and Borrello I. Phosphodiesterase-5 inhibition augments endogenous antitumor immunity by reducing myeloid-derived suppressor cell function. *J Exp Med* 2006; 203: 2691-702.
2. Meyer C, Sevko A, Ramacher M, Bazhin AV, Falk CS, Osen W, Borrello I, Kato M, Schadendorf D, Baniyash M, and Umansky V. Chronic inflammation promotes myeloid-derived suppressor cell activation blocking antitumor immunity in transgenic mouse melanoma model. *Proc Natl Acad Sci U S A* 2011; 108: 17111-6.
3. Black KL, Yin D, Ong JM, Hu J, Konda BM, Wang X, Ko MK, Bayan JA, Sacapano MR, Espinoza A, Irvin DK, and Shu Y. PDE5 inhibitors enhance tumor permeability and efficacy of chemotherapy in a rat brain tumor model. *Brain Res* 2008; 1230: 290-302.
4. Das A, Durrant D, Mitchell C, Mayton E, Hoke NN, Salloum FN, Park MA, Qureshi I, Lee R, Dent P, and Kukreja RC. Sildenafil increases chemotherapeutic efficacy of doxorubicin in prostate cancer and ameliorates cardiac dysfunction. *Proc Natl Acad Sci U S A* 2010; 107: 18202-7.
5. Shi Z, Tiwari AK, Shukla S, Robey RW, Singh S, Kim IW, Bates SE, Peng XX, Abraham I, Ambudkar SV, Talele TT, Fu LW, and Chen ZS. Sildenafil reverses ABCB1- and ABCG2-mediated chemotherapeutic drug resistance. *Cancer Res* 2011; 71: 3029-41.
6. Shi Z, Tiwari AK, Patel AS, Fu LW, and Chen ZS. Roles of Sildenafil in Enhancing Drug Sensitivity in Cancer. *Cancer Res* 2011; 71: 3735-8.
7. Shukla S, Ohnuma S, and Ambudkar SV. Improving Cancer Chemotherapy with Modulators of ABC Drug Transporters. *Curr Drug Targets* 2010; 12: 621-30.
8. de Vries NA, Zhao J, Kroon E, Buckle T, Beijnen JH, and van Tellingen O. P-Glycoprotein and Breast Cancer Resistance Protein: Two Dominant Transporters Working Together in Limiting the Brain Penetration of Topotecan. *Clin Cancer Res* 2007; 13: 6440-9.
9. van Asperen J, van Tellingen O, and Beijnen JH. Determination of doxorubicin and metabolites in murine specimens by high-performance liquid chromatography. *J Chromatogr B Biomed Sci Appl* 1998; 712: 129-43.
10. Kuppens IE, van Maanen MJ, Rosing H, Schellens JH, and Beijnen JH. Quantitative analysis of docetaxel in human plasma using liquid chromatography coupled with tandem mass spectrometry. *Biomed Chromatogr* 2005; 19: 355-61.
11. Kemper EM, Verheij M, Boogerd W, Beijnen JH, and van Tellingen O. Improved penetration of docetaxel into the brain by co-administration of inhibitors of P-glycoprotein. *Eur J Cancer* 2004; 40: 1269-74.
12. Lee M and Min DI. Determination of sildenafil citrate in plasma by high-performance liquid chromatography and a case for the potential interaction of grapefruit juice with sildenafil citrate. *Ther Drug Monit* 2001; 23: 21-6.
13. Al Ghazawi M, Tutunji M, and Aburuz S. Simultaneous determination of sildenafil and N-desmethyl sildenafil in human plasma by high-performance liquid chromatography



- method using electrochemical detection with application to a pharmacokinetic study. *J Pharm Biomed Anal* 2007; 43: 613-8.
14. Fan D, Beltran P, Wang Y, Bucana C, Yoon S, Deguzman A, and Fidler I. Cell density-dependent regulation of mdr-1 gene expression in murine colon cancer cells. *Int J Oncol* 1996; 9: 865-78.
  15. Juliano RL and Ling V. A surface glycoprotein modulating drug permeability in Chinese hamster ovary cell mutants. *Biochim Biophys Acta* 1976; 455: 152-62.
  16. Dantzig AH, Law KL, Cao J, and Starling JJ. Reversal of Multidrug Resistance by the P-Glycoprotein Modulator, LY335979, from the Bench to the Clinic. *Curr Med Chem* 2001; 8: 39-50.
  17. Hyafil F, Vergely C, Du VP, and Grand-Perret T. In vitro and in vivo reversal of multidrug resistance by GF120918, an acridonecarboxamide derivative. *Cancer Res* 1993; 53: 4595-602.
  18. Mistry P, Stewart AJ, Dangerfield W, Okiji S, Liddle C, Bootle D, Plumb JA, Templeton D, and Charlton P. In vitro and in vivo reversal of P-glycoprotein-mediated multidrug resistance by a novel potent modulator, XR9576. *Cancer Res* 2001; 61: 749-58.
  19. Reid G, Wielinga P, Zelcer N, de Haas M, van Deemter L, Wijnholds J, Balzarini J, and Borst P. Characterization of the Transport of Nucleoside Analog Drugs by the Human Multidrug Resistance Proteins MRP4 and MRP5. *Mol Pharmacol* 2003; 63: 1094-103.
  20. Choi MK and Song IS. Characterization of efflux transport of the PDE5 inhibitors, vardenafil and sildenafil. *Journal Pharm Pharmacol* 2012; 64: 1074-83.



# Chapter 5

SUMMARY  
NEDERLANDSSTALIGE SAMENVATTING  
LIST OF PUBLICATIONS  
CURRICULUM VITAE

## Summary

Malignant gliomas including glioblastoma multiforme (GBM) and anaplastic astrocytoma are devastating and lethal malignant primary brain tumor in humans. Especially, GBM, the most common and aggressive malignant primary subtype, is associated with rapid and aggressive disease progression and short survival. Because of its invasive nature, GBM can be considered a disease of the entire brain and usually cannot be completely eradicated by conventional local treatments including surgical resection and adjuvant stereotactic radiotherapy. The spreading of GBM cells (deep) into surrounding healthy brain tissue enables rapid recurrence/re-growth after resection and results into a short overall survival of GBM patients. Since the brain is a well-perfused organ, systemic delivery of chemotherapeutic drugs via the blood stream are expected to exert their antitumor effect on the remnant tumor cells that migrated to parts distant from the original lesion. However, except for temozolomide, the only agent showing significant improvement of the median survival of GBM patients of about 2 months, most chemotherapeutics are inactive in GBM.

Targeted therapy holds the promise for the new generation of chemotherapy due to their effects in selective inhibition of deregulated signaling pathways that are more critical in cancer cells than normal cells. In the past decade, encouraging results have been obtained in preclinical and clinical studies with application of small molecules or antibodies in various types of cancers, leading to the approval of several promising agents by the Food and Drug Administration (FDA) and/or the European Medicines Agency (EMA) (*e.g.* imatinib for acute myeloid leukemia, vemurafinib for melanoma and crizotinib for non-small cell lung cancer). Nevertheless, efforts applying these successful drugs to the treatment of GBM received only disappointing outcomes.

Considerable evidence suggests that the blood-brain barrier (BBB), restricting the brain delivery of most traditional chemotherapies, is also an important factor for limiting the therapeutic effects of targeted agents. This not only includes large molecules, such as for example antibodies directed against epidermal growth factor receptor (*i.e.* cetuximab) but, importantly, also of most of the small molecule inhibitors (*e.g.* erlotinib, lapatinib), since these are substrates of the ABC (ATP-binding cassette) multidrug efflux transporters which are expressed at the BBB as well as in the membranes of tumor cells. Therefore, ABC-transporters like ABCB1 (P-glycoprotein) and ABCG2 (BCRP) may

severely compromise the ability of small drugs to reach and inhibit their intracellular target in brain tumor cells.

**Chapter 1.1** is a review article where we discuss two important factors that may limit the efficacy of small molecule targeted therapeutics, namely, drug efflux transporters and intrinsic resistance of glioma tumor cells. Both of them may be responsible for the failures encountered in recent clinical trials employing targeted therapeutics in treatment of GBM. Ideal drugs for GBM should be designed to have a low affinity for ABC transporters such as ABCB1 and ABCG2 to reduce the impacts of these transporters on the brain (tumor) penetration of drugs. Alternatively, co-administration of targeted agents together with inhibitors of these drug efflux transporters (e.g. elacridar) may be a useful strategy to increase the BBB penetration of currently available drugs and should be considered. In addition, the tumorigenesis and progression of GBM is usually driven by several deregulated pathways acting in parallel. Therefore, targeting one single, prevalent target might be insufficient to achieve significant efficacy. Consequently, a more successful approach for the use of targeted therapies might be to focus on applying smart combinations of targeted agents directed against all the involved core pathways.

**Chapter 2.1 and 2.2** describes the development of bio-analytic assays for determining two targeted agents, Palomid 529, a dual mTORC1 and mTORC2 inhibitor, and NVP-BE2235, a dual PI3K and mTORC1 inhibitor in plasma, brain and other tissues. In these two assays we applied liquid-liquid extraction for sample pretreatment and reversed-phase high-performance liquid chromatography (HPLC) for sample separation. UV and fluorometric detection were used for quantification of Palomid 529 and NVP-BE2235, respectively. Methodological validations demonstrated that both of the two assays are accurate, selective and reproducible. These methods have been applied to study the pharmacokinetics of Palomid 529 and NVP-BE2235 in mouse plasma and brain samples (**Chapter 3.1 and 3.3**) and may also be applied for drug analyses of clinical samples in the future.

**Chapter 3.1** reports on the plasma pharmacokinetics and brain penetration of a novel targeted agent, Palomid 529. Palomid 529 is a dual mTORC1 and mTORC2 inhibitor, which prevents the activation of the feedback loop leading to upstream activation of AKT signaling, a phenomenon that was typical for the first generation of mTOR inhibitors

(e.g. rapamycin and other rapalogs) that solely inhibit mTORC1. Interestingly, we found that this compound lacks affinity for ABCB1/ABCG2 both *in vitro* and *in vivo*. As a single agent treatment, Palomid 529 significantly inhibited intracranial U87 GBM growth in mouse recipients relative to controls that did not receive treatment. Furthermore, oral application of this drug has been explored, and an acceptable oral availability (>50%) could be achieved by optimization of the formulation. Overall, the pharmacokinetic features of Palomid 529 are favorable for the potential application of this drug against intracranial disease, including malignant gliomas, and make it an interesting candidate to be tested in combination with conventional chemo- and/or radiotherapy, or another targeted therapy.

**Chapter 3.2** explores the potential benefit to combine the potent Poly (ADP-ribose) polymerase (PARP) inhibitor ABT-888 (veliparib) with temozolomide, the standard drug for treatment of GBM. PARP inhibitors enhance the activity of DNA damaging therapies by impeding the base excision repair pathway, thus providing a potential strategy to improve the efficacy of chemo-radiotherapy. Unfortunately, we found that ABT-888, is a dual substrate of Abcb1 and Abcg2. Consequently, Abcb1 and Abcg2 not only impaired the *in vitro* anti-proliferative effect of ABT-888 and temozolomide in cell cultures, but also caused a 4.9-fold reduction of the brain accumulation of this drug. Using several clinically more relevant *in vivo* high-grade glioma mouse models, we further confirmed that Abcb1 and Abcg2 are important for the outcome of temozolomide and PARP inhibitor ABT-888 combination therapy. Importantly, the dual Abcb1 and Abcg2 inhibitor elacridar could inhibit Abcb1 and Abcg2 mediated efflux, leading to an elevated brain penetration and anti-proliferative effect of ABT-888 when combined with temozolomide. Ultimately, co-administration of elacridar enhanced tumor response and survival of mice treated with temozolomide and ABT-888 therapy. Next to the impact of Abcb1 and Abcg2, we also found that the therapeutic benefit of ABT-888 in WT mice was only significant in PTEN deficient tumors. This is probably due to the fact that PTEN deficient tumors have a defect homologues recombination. DNA repair pathway which serves as a back-up for the inhibited base-excision repair pathway. This finding suggests that a subgroup analysis in patients whose tumors are deficient in PTEN would be informative, as patients in this subgroup may benefit mostly from this treatment.

**Chapter 3.3** describes the different impacts of Abcb1 and Abcg2 on the brain penetration and anti-glioma effects of three different PI3K-mTOR pathway inhibitors, namely,

rapamycin, the prototype mTORC1 inhibitor; NVP-BE2235, a dual mTOR and PI3K inhibitor and ZSTK474, a PI3K inhibitor. *In vitro* transport experiment showed that rapamycin is transported by Abcb1. Its brain penetration and distribution was about 10-fold lower in wild type mice relative to Abcb1 deficient mice, which may partly explain the failures of previous clinical trials using rapamycin and rapalogs in treatment of GBM. By *in vitro* assays, NVP-BE2235 was identified as a substrate of Abcg2, but interestingly its brain penetration was still mainly hindered by Abcb1 but not Abcg2 *in vivo*. Nevertheless, in spite of the impaired brain penetration by Abcb1, the concentration that was achieved in the brain upon oral administration of a relevant dose (10 mg/kg) was still sufficient for target inhibition. We also found that ZSTK474 was not a substrate of Abcb1 and a poor or non-substrate of Abcg2. No significant impact by Abcb1 and Abcg2 has been observed on the brain penetration of ZSTK474. In a clinically more relevant spontaneous GBM model, ZSTK474 (200 mg/kg q.d., p.o) delayed the tumor onset and prolonged the overall survival, although the tumor proliferation rate in more advanced tumors was not eventually suppressed. Overall, this chapter demonstrates the potential impact of Abcb1 and Abcg2 in the brain penetration of PI3K/mTOR inhibitors. Optimal candidates for clinical trial in GBM patients may be selected from those agents with a low affinity for these two transporters such as ZSTK474.

**Chapter 4.1** demonstrates that another ABC drug efflux transporters expressed at BBB, *viz.* Abcc4 (Multidrug resistance protein 4; Mrp4) also actively contributes to the brain efflux of camptothecin analogs together with Abcb1 and Abcg2. This could only be demonstrated by using a newly developed mouse model carrying an additional deficiency of Abcc4, next to Abcb1a/b and Abcg2. These Abcb1;Abcg2;Abcc4 deficient mice have a significantly increased brain penetration of all camptothecin analogs over Abcb1;Abcg2 deficient mice. This ranged from 1.2-fold for gimatecan to 5.8-fold for SN-38. Importantly, the three transporters teamed up to form a robust co-operative drug efflux system that restricts the brain entry of these camptothecin analogs. The presence of Abcb1a/b or Abcc4 (and probably also Abcg2) alone was sufficient to reduce the brain concentration of SN38 to the level observed in wild type mice. Therefore, co-administration of elacridar failed to significantly increase the brain penetration of SN-38 in WT mice since it does not inhibit Abcc4. Moreover, we also observed that the distribution of gimatecan in the brain of wild type mice was more than 40-fold and 220-fold higher than that of topotecan and SN-38, respectively, which is likely due to the more lipophilic nature of

gimatecan. Together, this chapter demonstrates that the concerted action of Abcc4, Abcb1 and Abcg2 limits the usefulness of selective ABC-transport inhibitors to enhance drug entry for treatment of intracranial diseases. Furthermore, our data suggest that gimatecan might be a better candidate than irinotecan for clinical evaluation against intracranial tumors.

**Chapter 4.2** demonstrates that sildenafil (Viagra®) is not a useful ABCB1 and ABCG2 inhibitor *in vivo*. Recently, sildenafil has been reported to be an inhibitor of ABCB1 and ABCG2 inhibitor *in vitro*. Because ABCB1 and ABCG2 are expressed in tumor cells as well as barrier tissues such as the BBB, the authors concluded that sildenafil –as a clinically approved drug with a known safety profile- might be useful to enhance the distribution and thereby the efficacy of anticancer drugs by combining this. However, by using several *in vivo* models we could demonstrate that such claim were unwarranted. We found that sildenafil was not capable to improve the brain penetration of docetaxel and topotecan, whereas it did increase the plasma levels of the cytotoxic drugs. This latter finding did not result from the inhibition of Abcb1 or Abcg2, since the same effect was also seen in Abcb1;Abcg2 knockout mice. Sildenafil was also not able to improve the efficacy of doxorubicin against subcutaneous CT26 tumors that are known to express Abcb1. The doxorubicin level in tumor tissue did increase marginally, but so did the concentration of doxorubicin in plasma and heart. These drug-drug interactions pose a risk for cancer patients receiving chemotherapeutic drugs. Based on these results, we advise against the use of sildenafil in combination with anticancer drugs.

In conclusion, our *in vitro* and *in vivo* models are useful tools to evaluate the impact of drug efflux transporters on the BBB penetration and potential activity of targeted therapeutics for treatment of GBM. Importantly, our work demonstrates that Abcb1/ABCB1 and Abcg2/ABCG2 could have a marked impact on the efficacy of targeted therapies against malignant gliomas. The dual ABCB1 and ABCG2 inhibitor elacridar was very effective to enhance the brain penetration and efficacy of ABCB1 and/or ABCG2 substrate drugs such as ABT-888, but it appeared to be less or not useful for camptothecin analogs which are also substrates of ABCC4. However, the ideal candidates for malignant glioma therapy would be drugs that lack affinity for the major efflux transporters at the BBB. We therefore recommend that clinical evaluation of targeted agents for GBM trials should give the priority to agents that are not substrates of the ABC-transporters.



## Nederlandsstalige samenvatting

Het maligne glioom (glioblastoma multiforme en anaplastisch astrocytoma) is een ongeneeslijke primaire hersentumor met een vaak uiterst agressief en verwoestend verloop. Dit geldt in het bijzonder voor het glioblastoma multiforme (GBM), dat van de maligne gliomen de meest voorkomende variant is.

Aangezien GBM een zeer invasief karakter heeft, moet het als een ziekte door het gehele brein worden beschouwd. Het kan daarom nooit volledig worden verwijderd middels lokale conventionele therapieën, zoals operatie en adjuvante (stereotactische) radiotherapie. De invasie van tumorcellen diep in het omliggende normale hersenweefsel biedt de tumor na verwijdering de kans op een snelle hergroei en leidt tot een zeer korte gemiddelde overlevingsduur voor GBM patiënten. Omdat de hersenen een zeer goed doorbloed orgaan is, zou men kunnen verwachten dat systemisch gegeven chemotherapeutica via het bloed wel alle overgebleven tumorcellen zou moeten kunnen bereiken (en doden). Echter, afgezien van het middel temozolomide, dat de gemiddelde overlevingsduur van GBM patiënten met ongeveer 2 maanden kan verlengen, is er geen enkel ander middel dat een significant effect heeft op de overlevingsduur.

Doelgerichte therapieën worden verondersteld een nieuw tijdperk van anti-kanker behandeling in te luiden, aangezien deze hun effect behalen door een selectieve remming van de ontspoorde signaleringsroutes die vooral actief zijn in tumorcellen, maar niet of minder van belang zijn voor gezonde cellen. Het afgelopen decennium zijn er bemoedigende resultaten bereikt met dit type middelen in bijv. acute myeloïde leukemie (imatinib), melanoom (vemurafinib) en specifieke vormen van niet-kleincellig longcarcinoom (crizotinib), en deze hebben al geleid tot goedkeuring door de Food and Drug Administration (FDA) en de European Medicines Agency (EMA). Echter, pogingen om deze aanpak ook toe te passen voor een meer succesvolle behandeling van maligne glioma hebben tot dusverre alleen nog maar teleurstellende resultaten opgeleverd.

Er zijn veel aanwijzingen dat de bloed-hersen barrière (BHB), die de hersendistributie van veel klassieke (chemo)therapeutica beperkt, ook een belangrijke factor is m.b.t. het verminderen van de effectiviteit van de doelgerichte therapeutica. Dit betreft niet alleen grote moleculen, zoals antilichamen gericht tegen epidermal growth

factor receptor (cetuximab), maar ook de meeste klein moleculaire therapeutica (bv. Erlotinib en lapatinib), omdat deze substraat zijn van ABC (ATP-Bindings Cassette) geneesmiddelen efflux transporteiwitten, die tot expressie komen in de BHB en in de celmembraan van tumorcellen. Hierdoor kunnen ABC-transporteiwitten, zoals ABCB1/Abcb1 (P-glycoproteïne) en ABCG2/Abcg2 (BCRP), in ernstige mate de toegankelijkheid van dit type geneesmiddelen verminderen, waardoor deze niet in staat zijn om hun intracellulaire doel te bereiken en te remmen.

Hoofdstuk 1.1 is een overzichtsartikel en behandelt twee belangrijke factoren die de effectiviteit van klein moleculaire geneesmiddelen kan beperken, nl. geneesmiddelen efflux transporteiwitten en de intrinsieke resistentie van glioma tumorcellen. Beide factoren kunnen hebben bijgedragen aan het mislukken van recente klinische trials met doelgerichte therapeutica voor de behandeling van GBM. Efflux systemen beperken de bereikbaarheid van tumorcellen in de hersenen voor therapeutica. Idealiter zouden therapeutica voor de behandeling van GBM zo moeten worden ontworpen, dat zij niet of nauwelijks een substraat zijn voor de ABC-transporteiwitten. Als alternatief kunnen de doelgerichte therapeutica worden toegediend samen met een remmer van deze efflux transportsystemen (bv. elacridar). Daarnaast is het ontstaan en de progressie van GBM het gevolg van een deregulatie van meerdere signaal-transductie routes, waardoor het selectief remmen van slechts een van deze routes niet voldoende zal zijn om een goed behandelingseffect te bereiken. Dientengevolge zou een meer succesvolle behandeling met doelgerichte therapeutica wellicht kunnen worden bereikt door slimme combinaties van middelen, om zodoende alle cruciale signaaltransductie routes tegelijkertijd te remmen.

Hoofdstuk 2.1 en 2.2 beschrijven de ontwikkeling van bioanalytische bepalingsmethodes voor twee doelgerichte therapeutica, t.w. Palomid 529, een gecombineerde mTORC1 en mTORC2 remmer, en NVP-BE235, een gecombineerde PI3K en mTOR1 in plasma, hersenen en andere weefsels. Beide bepalingsmethodes berusten op monstervoorbehandeling middels vloeistof-vloeistof extractie en scheiding d.m.v. hoge-druk vloeistof chromatografie. Detectie middels UV en fluorescentie werd gebruikt voor Palomid 529, respectievelijk NVP BE235. Deze methodes zijn vervolgens gebruikt om

de farmacokinetiek in plasma en weefsel-homogenaten van muizen te bestuderen en kunnen ook worden gebruikt voor de analyse van deze middelen in patiëntenmonsters.

Hoofdstuk 3.1 beschrijft de plasma farmacokinetiek en hersenpenetratie van het nieuwe doelgerichte therapeuticum Palomid 529. Palomid 529 is een gecombineerde remmer van zowel het mTOR1 als het mTOR2 complex en voorkomt daarmee de activatie van AKT via mTORC2, een fenomeen dat typisch was voor de eerste generatie van mTOR remmers (rapamycine e.a. zgn. rapalogs), die alleen mTORC1 remden. Van belang is dat we hebben gevonden, dat dit middel niet of nauwelijks affiniteit heeft voor ABCB1/Abcb1 en ABCG2/Abcg2, zowel *in vitro* als *in vivo*. Toegediend als enig middel was Palomid 529 in staat om de intracraniale groei van U87 GBM cellen te remmen t.o.v. onbehandelde controlemuizen. Daarnaast hebben we de mogelijkheid om dit middel oraal toe te dienen onderzocht en een acceptabele (>50%) biologische beschikbaarheid kon worden bereikt na optimalisatie van de formulering. Deze twee kenmerken zijn gunstig voor een evt. toepassing bij hersentumoren en maken dit middel tot een potentiële kandidaat voor combinatiebehandeling van hersentumoren met de conventionele radio-chemotherapie en/of andere doelgerichte therapeutica.

Hoofdstuk 3.2 beschrijft het onderzoek naar het mogelijk toepassen van combinaties van de krachtige PARP remmer ABT-888 (veliparib) en temozolomide, het standaard chemotherapeuticum voor behandeling van hersentumoren. PARP remmers versterken de activiteit van DNA beschadigende therapieën door het remmen van het zgn. “base-excision” DNA reparatiemechanisme, wat dus een potentiële strategie kan zijn om de effectiviteit van chemo-radiatietherapie te versterken. Echter, wij hebben vastgesteld dat ABT-888 een goed substraat is van zowel ABCB1/Abcb1 als ABCG2/Abcg2. Als gevolg hiervan hebben wij gevonden, dat deze efflux transporters niet alleen *in vitro* de anti-proliferatieve effecten van ABT-888 reduceren, maar ook de distributie van ABT-888 in de hersenen met een factor 4.9 verminderen. Door gebruik te maken van verscheidene klinisch meer relevante hoog-gradige glioma muismodellen hebben we bevestigd, dat ABCB1 en ABCG2 belangrijke factoren zijn voor de uitkomst van temozolomide en ABT-888 combinatietherapie. Belangrijk is verder, dat de ABCB1/ABCG2 remmer elacridar in staat is, om efflux van ABT-888 door ABCB1 en ABCG2 grotendeels te blokkeren. Dit leidde tot een betere hersenpenetratie van ABT-888 en een verbeterde *in vitro* anti-proliferatie door ABT-888 i.c.m. temozolomide. Uiteindelijk leidde de combinatie-therapie met

elacridar tot een verbeterde response en langere overleving van muizen behandeld met temozolomide en ABT-888. Naast deze invloed van ABCB1 en ABCG2 hebben we ook gevonden, dat de therapeutische bijdrage van ABT-888 alleen significant was in tumoren die deficiënt waren voor PTEN. Dit is waarschijnlijk het gevolg van het feit dat PTEN deficiënte tumoren een verstoring hebben van het zgn. homologe recombinatie DNA reparatiemechanisme, zodat dit minder goed als back-up voor de door ABT-888 geremde base-excision reparatieroute kan fungeren. Het potentiële belang van de PTEN status van de tumor op de effectiviteit van ABT-888 suggereert, dat het informatief zou zijn om een subgroepanalyse uit te voeren op GBM patiënten die nu in klinische trials worden behandeld met dit middel, aangezien het hier mogelijk een subgroep betreft, die het meeste baat zou kunnen hebben bij deze behandeling.

Hoofdstuk 3.3 beschrijft het belang van ABCB1 en ABCG2 op de hersenpenetratie en de anti GBM effectiviteit van drie verschillende remmers van de PI3K-mTOR signaal-transductie route, t.w. rapamycine, het prototype remmer van het mTOR1 complex, NVP BEZ235, een gecombineerde PI3K en mTOR1 remmer en ZSTK474, een PI3K remmer. D.m.v. *in vitro* transportproeven hebben we aangetoond, dat rapamycine een substraat is voor Abcb1. De hersenpenetratie van dit middel was ca. 10-voudig lager in wildtype muizen t.o.v. muizen die deficiënt zijn voor Abcb1, wat een (gedeeltelijke) verklaring kan zijn voor het falen van rapamycine (e.a. soortgelijke rapalogs) in klinische trials in GBM patiënten. Uit *in vitro* modellen is gebleken, dat NVP-BEZ235 vooral een substraat van Abcg2 is. Echter, de hersenpenetratie bleek toch vooral te worden verminderd door Abcb1 en niet zozeer door Abcg2. Niettemin, ondanks de verminderde hersenpenetratie door Abcb1, bleek de concentratie die in de hersenen kon worden bereikt, na een relevante dosis (10 mg/kg), voldoende voor remming van het doel-eiwit. We hebben tevens aangetoond, dat ZSTK geen substraat is voor Abcb1 en niet of nauwelijks voor Abcg2. Deze twee transporteiwitten hadden ook geen impact op de hersenpenetratie van dit middel. In een meer klinisch relevant geacht spontaan hersentumormodel bleek ZSTK474 in staat om het ontstaan van deze tumoren te vertragen en de overleving te verlengen, hoewel de uiteindelijke groeisnelheid in een meer vergevorderd tumorstadium, niet werd verlaagd. Dit hoofdstuk laat het belang van Abcb1 en Abcg2 op de hersenpenetratie van PI3K-mTOR remmers zien. Selectie van de meest optimale kandidaat-middelen voor klinische testen zou gemaakt kunnen worden aan de hand van de affiniteit van deze middelen voor Abcb1 en Abcg2.

Hoofdstuk 4.1 toont aan, dat naast Abcb1 en Abcg2 nog een andere ABC efflux transporter in de BHB, t.w. Abcc4 (multidrug resistentie proteïne 4; Mrp4), actief bijdraagt aan de efflux van camptothecine analoga uit de hersenen. Dit kon worden aangetoond m.b.v. een nieuw-ontwikkeld muismodel, dat naast Abcb1 en Abcg2, ook deficiënt is voor Abcc4. Deze Abcb1;Abcg2;Abcc4 muizen hadden t.o.v. Abcb1;Abcg2 muizen een significant hogere hersenpenetratie van de verschillende camptothecine analoga. Het verschil bedroeg 1.2-voudig in geval van gimatecan tot 5.8-voudig voor SN38. Van belang is, dat deze drie transportproteïnes als een team samenwerken en zo een robuust efflux-systeem vormt dat de hersenpenetratie van de camptothecine analogen beperkt. De aanwezigheid van slechts één van deze transporteiwitten (Abcb1, Abcg2 of Abcc4) blijkt al voldoende om de concentratie van SN38 in de hersenen te verlagen tot de spiegels die in wildtype muizen worden gevonden. Hierdoor was elacridar ook niet in staat de hersenpenetratie van SN38 te verhogen in wildtype muizen, want elacridar remt Abcc4 niet. Bovendien hebben we gevonden, dat gimatecan een meer dan 40 en 220-voudige hogere spiegel in de hersenen van wildtype muizen bereikt t.o.v. topotecan, respectievelijk SN38, wat vermoedelijk komt doordat gimatecan een veel meer lipofiele verbinding is. Dit hoofdstuk laat zien, dat de samenwerking van Abcc4, Abcb1 en Abcg2 de toepasbaarheid van selectieve remmers van ABC-transportproteïne om de doorlaatbaarheid van de BHB te verhogen kan beperken. Bovendien blijkt uit onze resultaten, dat gimatecan wel eens een beter middel dan irinotecan zou kunnen zijn voor de behandeling van intracraniale tumoren.

Hoofdstuk 4.2 beschrijft experimenten waaruit blijkt, dat sildenafil (Viagra®) geen bruikbare remmer van ABCB1 en ABCG2 *in vivo* is. Recentelijk is op basis van *in vitro* experimenten beschreven, dat sildenafil een remmer van ABCB1 en ABCG2 zou zijn. Omdat ABCB1 en ABCG2 tot expressie komen in tumorcellen en in barrièreweefsels zoals de BHB, hebben de auteurs de conclusie getrokken, dat sildenafil -een voor andere indicaties reeds goedgekeurd en dus veilig geacht middel- mogelijk gebruikt zou kunnen worden, om de distributie en daarmee de werkzaamheid van antikanker middelen te versterken. Echter op basis van ons onderzoek, waarbij wij gebruik hebben gemaakt van diverse *in vivo* modellen, bleek deze claim niet gerechtvaardigd. We vonden dat sildenafil geen enkel effect heeft op de hersenpenetratie van ABCB1 en ABCG2 substraatmiddelen (docetaxel en topotecan), terwijl het middel wel de plasmaspiegels verhoogde. Dit laatste effect was overigens niet het gevolg van het remmen van Abcb1 en/of Abcg2, want

dezelfde effecten werden waargenomen in *Abcb1;Abcg2* deficiënte muizen. Sildenafil was ook niet in staat de effectiviteit van doxorubicine tegen subcutaan groeiende CT26 tumoren te verbeteren, terwijl hiervan bekend is, dat deze cellen *Abcb1* tot expressie brengen. Sildenafil verhoogde wel in enige mate de doxorubicinespiegels in de tumoren, maar hetzelfde gebeurde in plasma en het hart. Deze interacties kunnen risico's vormen voor patiënten. Op basis van deze experimenten adviseren wij om sildenafil niet te gebruiken in combinatie met antikanker middelen.

Concluderend, onze *in vitro* en *in vivo* modellen zijn zeer geschikte gereedschappen voor het bestuderen van de impact die geneesmiddelen-efflux transportsystemen kunnen hebben op de BHB penetratie en mogelijke werkzaamheid van doelgerichte therapeutica voor de behandeling van GBM. Belangrijk is, dat wij hebben aangetoond dat *Abcb1* en *Abcg2* een belangrijke impact kunnen hebben op de effectiviteit van doelgerichte farmaca tegen maligne gliomen. De duale *Abcb1/Abcg2* remmer elacridar was zeer effectief in het verhogen van de hersenpenetratie en effectiviteit van *Abcb1* en/of *Abcg2* substraatmiddelen, zoals ABT-888, maar bleek veel minder effectief in geval van de camptothecine analoga. Dit geldt waarschijnlijk ook voor andere middelen, die naast ABCB1 en ABCG2 ook nog worden herkend door Abcc4. Hoewel het remmen van deze systemen dus een mogelijke optie is, zou het nog beter zijn, als middelen die moeten worden toegepast voor de behandeling van maligne gliomen, niet of nauwelijks affiniteit hebben voor deze efflux transportsystemen in de BHB. De kans dat een klinisch onderzoek leidt tot een teleurstellend resultaat, wordt uitermate groot indien het middel wel een goed substraat is. Daarom bevelen wij aan bij de klinische evaluatie van doelgerichte farmaca in klinische trials voor GBM, prioriteit te geven aan die middelen die niet herkend worden door geneesmiddelen-efflux transportsystemen.

## LIST OF PUBLICATIONS

- (1) **Lin F**, de Gooijer MC, Roig EM, Christner S, Beumer JH, Beijnen JH, van Tellingen O. High-grade glioma mouse models identify ABCB1, ABCG2 and PTEN as important factors for response to temozolomide and ABT-888 combination therapy. To be submitted.
- (2) **Lin F**, de Gooijer MC, Hanekamp D, Chandrasekaran G, Weijer R, Buil L, Sparidans R, Beijnen JH, van Tellingen O. Optimize the therapeutic effect of PI3K/mTOR inhibitor in high-grade gliomas by selecting Blood-brain Barrier permeable agents. To be submitted.
- (3) **Lin F**, de Gooijer MC, Hanekamp D, Beijnen JH, van Tellingen O. Targeting on Core (Mutated) Pathways of High-grade Gliomas: Challenges of Intrinsic Resistance and Drug Efflux Transporters. Invited review. Submitted.
- (4) **Lin F**, Marchetti S, Pluim D, Iusuf D, Mazzanti R, Schellens JHM, Beijnen JH, van Tellingen O. Abcc4 together with Abcb1 and Abcg2 form a robust co-operative drug efflux system that restricts the brain entry of camptothecin analogs. Submitted.
- (5) **Lin F**, Hogendijk H, Beijnen JH, van Tellingen O. Sildenafil is not a useful inhibitor of ABCB1 and ABCG2 *in vivo*. European Journal of Cancer. 2013. In press.
- (6) **Lin F**, Buil L, Sherris D, Beijnen JH, van Tellingen O. Dual mTORC1 and mTORC2 inhibitor Palomid 529 penetrates the Blood-Brain Barrier without restriction by ABCB1 and ABCG2. International Journal of Cancer. 2013. In press.
- (7) **Lin F**, Chandrasekaran G, de Gooijer MC, Beijnen JH, van Tellingen O. Determination of NVP-BEZ235, a dual PI3K and mTOR inhibitor, in human and mouse plasma and in mouse tissue homogenates by reversed-phase high-performance liquid chromatography with fluorescence detection. J Chromatogr B Analyt Technol Biomed Life Sci 2012;901:9-17
- (8) **Lin F**, Sherris D, Beijnen JH, van Tellingen O. High-performance liquid chromatography analysis of a novel small-molecule, anti-cancer drug, Palomid 529, in human and mouse plasma and in mouse tissue homogenates. J Chromatogr B Analyt Technol Biomed Life Sci 2011;879:3823-31.
- (9) Lagas JS, **Lin F**, Wagenaar E, Vlaming ML, van Tellingen O, Beijnen JH, et al. P-glycoprotein (P-gp/Abcb1), Abcc2, and Abcc3 determine the pharmacokinetics of etoposide. Clin Cancer Res 2010;16:130-40.





## CURRICULUM VITAE

The author of this thesis, Fan Lin, was born on June 28, 1978 in Huzhou, China. His first research experience was obtained from a student research project named “Exploring the optimal *in vitro* culture conditions for *Zantedeschia aethiopica*” in Life Sciences Institute of Zhejiang University where he also studied Biology for 4 years and received his bachelor diploma in 2000. After graduation, he worked in the Beijing Genomics Institute first as a genome sequencing analyst and later as an independent lab researcher. From 2004 to 2006 he worked as Java and J2EE developer in Zhejiang supcon software co. ltd, China. In 2006, he moved to Amsterdam and started the Master’s program in Medical Biochemistry at the University of Amsterdam. During this study his first internship was performed in the lab of SILS-Mass Spectrometry of Biomacromolecules of University of Amsterdam under supervision of Dr. Piet. de Groot. His second internship was performed in the lab of Dr. Alfred H. Schinkel in the Netherlands Cancer Institute/Antoni van Leeuwenhoek Hospital under supervision of Dr. Jurjen Lagas. In August 2009, Fan Lin obtained his Master’s degree in Science. In January 2010, he started his PhD project in at the Department of Clinical Chemistry (or Preclinical Pharmacology) in the Netherlands Cancer Institute under supervision of Prof. Dr. Jos H. Beijnen and Dr. Olaf van Tellingen at the Netherlands Cancer institute. The results of this research are described in this thesis. Since March 2013, he works as a postdoctoral researcher in the lab of Dr. Lim Yoon Pin at Department of Biochemistry of National University of Singapore.



## Acknowledgements

In spite of hard work, big stress, and countless repeats of the “experimenting-writing-submitting-revision” cycles, working on the PhD is also a joyful, exciting, often overwhelming and certainly unforgettable experience. One of the joys is such as now, upon a point very close to the end, to look over the journey past and remember all the people who have helped and supported me along this long but fulfilling road.

First of all I would like to express my heartfelt gratitude to my promotor Prof. Dr. Jos Beijnen and co-promotor Dr. Olaf van Tellingen. Thank you for giving me this great opportunity to perform my doctoral research in this interesting topic which combines pharmacology and oncology perfectly. Dear Jos, thanks for your critical reading of my manuscripts, valuable advices and of course, continuous concern and supports during my PhD. Dear Olaf, it is a real pleasure to work in your lab under your daily supervision. You set a great example for me as a highly motivated researcher, a passionate scientist, a handy lab expert, a critical thinker and writer. I sincerely thank you for your patience and cordiality in the numerous discussions we have had. Even though not all our discussions led to agreements, I cannot be more sure that what I received from you has been the most important source of inspiration and motivation for my PhD studies and perhaps also for my future career. Without your supervision, guidance and assistance this PhD would not have been achievable.

Furthermore, I am very grateful to my colleague Levi Buil and all the highly motivated, talented and enthusiastic students, Mark, Gayathri, Ruud, Diana, Eloy, Nishita and Stephan, who have been worked or are working in the ‘lab of Olaf’. Dear Levi, thanks for all the assistance and administrative work you did. Although most of them were ‘invisible’, such as genotyping, they were certainly indispensable. More importantly, thanks for the great time we had together and the jokes, talks and laughter we have shared. Mark, you were the very important contributor to my research and to our lab, as being illustrated in the picture hanging in the corridor or the co-authorships present in my papers. Gayathri, you are my first master student and I am not sure that I showed you everything correct at that moment, but anyway you achieved your success in developing an analytic assay of NVP-BEZ235 which ended up in publication. Good luck with your PhD study in Cambridge Research Institute! Stephan and Nishita, thanks for

your contributions to the ABT-888 and PI3K inhibitors projects and your company in my last stage in NKI. I hope that your current internships can provide you more than enough (both expertise and experience) for your career plans of the next stage. I wish you all the best.

Next I want to thank all the other co-authors of our papers published or to be published. Dr. Dieta Brandsma, thanks for your reading and comments on our review article; Prof. Dr. Jan Schellens and Dr. Serena Marchetti, thanks for your contribution to our paper about camptothecin analogs. Dr. David Sherris, thanks for providing Palomid 529 for two of our studies. Dr. Jan-Hendrik Beumer and Susan Christner, thanks for your help of measurement of ABT-888 samples.

I am also greatly indebted to the 'Alfred's group' for all of your helps. Dear Dr. Alfred Schinkel, thanks for your advices and you helps of many times. I have benefited a lot from the Wednesday's morning work discussions of your group, and particularly from your incisive comments. Els, I am not sure that I got all your humor in our conversations, but I would like to thanks for your great help in providing me mice for experiments. Without them I would have missed many bars in my figures. Anita, also thanks for your help, especially when Els was not in service. My special thanks go to Seng, Selvi and Dilek. You are not only my peer group, my friends, but also literally my soulmates in research. We had so many common topics about life, research and future shared or to be shared as exotic PhD student studying ABC drug transporters in NKI. And of course, thanks for all your helps and supports. I was very lucky to meet all of you and we should one day complete our 'song of transporters'.

I would also like to thank all the people from animal department from whom I received enormous helps for my animal experiments. Dear Bjorn and Tania, even though G2Zuid might be a horrible place for mice, but your optimistic attitude and helpfulness constructively make it a place with pleasant working environment. And of course, thanks for your caring of my sick mice for numerous times. Many thanks also go to G3 and G1 colleagues, Yvonne, Marissa, Adrie, klaas, Sjaak, Henk... In addition, I would like to thank Ji-Ying and Martin and other colleagues from the department of animal pathology department, for your critical analyses for my animal tissue samples as well as your professional advices.

I also want to thank Dr. Sven and members in your group, Serge, Charlotte, Guotai, Janneke, Ariena and Wendy for all the pleasant talks we had (most of them were during animal experiments), and the agents I borrowed from you.

Working in the department of Clinical Laboratory, I was sometimes confused about the fact that I was located in this department although our researches have nothing to do with patients or any clinical samples. However, the confusion and incompatibility was soon replaced by all the friendly, joyful and lovely faces in this floor. I would like to thank all of you for all the conversations, cakes and coffees we had together. Particularly, I want to thank Tiny, Dorothé, Marian, and Arianne, for your concerns and helps for my research and daily life, for the interesting talks we had during lunch or coffee time.

Last but not least, I want to express my special gratitude for my families and the Chinese friends working in the NKI. Esther and Shuyang, my small family, thanks for your company all the way. Your presence is certainly the most important source of motivation for me to accomplish this doctoral study. SunCong, Liqing, Xuezhen, Yanlin, Baoxu, Guotai, Chenwei, Zhanghua and Chenchun, thank you for all the agents I borrowed from you, and all the great time we had here. All the best for you!

Certainly this is not a complete list including all the names I want to express my acknowledgement. Therefore I would like to express my sincere gratitude to all of you who have contributed to the researches described in this thesis. Without you, accomplishment of my PhD study and this thesis would never be possible!